Investigations on Nanocrystalline ZnO Thin Film Based Heterojunctions for Electronic and Photonic Device Applications

Doctoral Thesis

Submitted by

Shashi Kant Sharma
Research Scholar
ID: 2012REC9532

Under Supervision of

Dr. C. Periasamy
Assistant Professor, Dept. of ECE, MNIT Jaipur

Department of Electronics & Communication Engineering
Malaviya National Institute of Technology, Jaipur, India
November 2016

Investigations on Nanocrystalline ZnO Thin Film Based Heterojunctions for Electronic and Photonic Device Applications

Submitted by

Shashi Kant Sharma
Research Scholar
ID: 2012REC9532

Under Supervision of

Dr. C. Periasamy
Assistant Professor, Dept. of ECE, MNIT Jaipur

Submitted in fulfillment of the requirements of the degree of Doctor of Philosophy

to the

Department of Electronics & Communication Engineering
Malaviya National Institute of Technology, Jaipur, India
November 2016

Certificate

This is to certify that the thesis entitled "**Investigations on Nanocrystalline ZnO Thin Film Based Heterojunctions for Electronic and Photonic Device Applications**" being submitted by **Shashi Kant Sharma** is a bonafide research work carried out under my supervision and guidance in fulfillment of the requirement for the award of the degree of **Doctor of Philosophy** in the Department of Electronics & Communication Engineering, Malaviya National Institute of Technology, Jaipur. The matter embodied in this thesis is original and has not been submitted to any other University or Institute for the award of any other degree.

Dr. C. Periasamy
Assistant Professor
Department of ECE
MNIT, Jaipur

Declaration of Authorship

I, Shashi Kant Sharma, declare that this thesis titled, ‘Investigations on Nanocrystalline ZnO Thin Film Based Heterojunctions for Electronic and Photonic Device Applications’ and the work presented in it are my own. I confirm that:

- This work was done wholly or mainly while in candidature for a research degree at this University.
- Where any part of this thesis has previously been submitted for a degree or any other qualification at this University or any other institution, this has been clearly stated.
- Where I have consulted the published work of others, this is always clearly attributed.
- Where I have quoted from the work of others, the source is always given. With the exception of such quotations, this thesis is entirely my own work.
- I have acknowledged all main sources of help.
- Where the thesis is based on work done by myself jointly with others, I have made clear exactly what was done by others and what I have contributed myself.

Signed: ____

Date: ____

Everything that is really great and inspiring is created by the individual who can labor in freedom.

-- Albert Einstein

Acknowledgements

It seems like yesterday when I enrolled for my PhD program and see, this beautiful journey is reaching towards a delightful end. This is a wonderful opportunity for me to acknowledge the people without whom it would not have been possible to complete my doctoral degree. Truly, words are not enough to express my gratitude to all of them.

First of all, I would like to express my deep and sincere gratitude to my supervisor, Dr. C. Periasamy, Assistant Professor, Department of Electronics & Communication Engineering, Malaviya National Institute of Technology, Jaipur, India. His painstaking guidance despite of very busy schedule, inspiring supervision, invaluable and tireless devotion, scientific approach and brilliant technological acumen has been a source of tremendous help and motivation throughout my research period.

I also express my sincere gratitude to Departmental Research Evaluation Committee (DREC) members, Prof. Vineet Sahula, Prof. D. Boolchandani and Dr. Lava Bhargava for their scholarly guidance, encouragement, and constructive criticisms that contributed immensely to the successful completion of this work. I am thankful to Prof. K.K. Sharma, Head, Department of Electronics & Communication Engineering, MNIT, Jaipur and all other faculty members for their kind support during entire period of my work. I am also thankful to all the office staff of the department for their help and co-operation.

I feel immense pleasure to acknowledge Prof. P. Chakrabarti, Director, MNNIT, Allahabad, India for his valuable suggestions, inspiring guidance and consistent encouragement without which, this thesis could have never been materialized. I would also like to thank Dr. K. Asokan (Scientist F, IUAC-New Delhi), Dr. Viera Skakalova (Faculty of Physics, University of Vienna), Dr. Bernhard C. Bayer (Post Doctoral Fellow, University of Vienna), Dr. A.D.D. Dwiwedi (Post Doctoral Fellow, University of Bordeaux, France), Dr. Shaivalini Singh (International Research Professor, Yeungnam University, South Korea), Dr. Amar Patnaik (Co-ordinator, Centre for Tribology, MNIT) and Mr. Sumit Vyas (Research Scholar, MNNIT Allahabad) for their kind co-operation and valuable suggestions.

I am really thankful to Prof. M. K. Banerjee, Dr. Kanupriya Sachdeva and Technical Staff (Mr. Sachin Surve, Mr. Mohtashim Reza, Mr. Sandeep Kher, Mr. Atul Sharma, Mr. Ramesh Prajapati, Shubham Gautam, Deepak Sharma and Anand), Materials Research Centre (MRC), MNIT, Jaipur for their kind co-operation and support at different stages of my experimental work.

It is my pleasure to acknowledge my senior mates and colleagues in the department: Dr. Sanjeev Kumar Metya, Dr. Vipin Pal, Mr. Lokesh Garg, Ms. Sapna Khandelwal, Mrs. Lintu Rajan, Mr. Vinay Kanungo, Mr. Mukesh Gupta, Mr. Nikhil Deep Gupta and Mr. Anup Sharma for their guidance, encouragement and support. My heartfelt thanks to my loving juniors: Shailendra, Hemant, Amit, Nitesh, Komal, Teena, Niketa, Rama, Yogendra, Ashish Tyagi, Sourabh, Asif Sir, Bharat, Ashish Chaudhary and Upendra with whom I spent countless relaxing, hilarious and pleasant moments. The discussions, experiments, evening tea at Annapurna, paper acceptance celebrations, birthday parties and all other cherishable moments which we all spent together will always remain memorable for me. !! I Will Miss You All !!

It is my pleasure to mention some colleagues and friends from MNIT: Saumya Jain, Kuldeep Tiwari, Rishi Sir, Vikas Sir, Jitendra Sir, Ornav Sir, Akshay Sir, Arun Vinod, Dinesh and Mahendra for their help, guidance and nice company.

The people, who instilled inspiring in my life are those who bought me up, nurtured and imparted me the real virtues of humanities, empathy and kindness. They are my real motivators to bring me at the present position and blessed me with their grace and affection. I record my deep and utmost gratitude to my father *Mr. Sajjan Kumar Sharma* and my mother *Mrs. Sunita Sharma*, for their devotion, sacrifices, encouragement, support, and prayers for my whole life. I can say, this small space is not enough to acknowledge your contributions in my life. Endless thank to my lovely sister *Surabhi*, my brother-in-law *Ashish* and my dearest bhanji *Anvi* for their love and affection in every aspect of my life.

This acknowledgement would be incomplete without thanking “Almighty God”. Without his blessing, it would not have been possible to complete this endeavour.

Abstract

Znic Oxide's peculiar properties such as wide bandgap (3.37eV), large exciton binding energy (60 meV), high thermal conductivity, low temperature processing, high electron mobility and good transparency have drawn a great interest of researchers in recent years. ZnO offer a diverse range of nanostructures with large surface to volume ratio that can play a key role to improve luminescence, absorption, photo-detection properties of various devices. Based on all these fascinating properties, ZnO has emerged as a potential candidate for optoelectronic, photonic, piezoelectronic and transparent electronics device applications. Undoubtedly, among all p-type substrates, the commercial silicon has drawn a significant attention for ZnO based devices due to its lower cost and mature fabrication process. Therefore, our objective in this study was to investigate the potentiality of n-ZnO/p-Si heterojunctions for optoelectronic and photonic devices that can be very useful in a variety of civil and military applications.

This work presents a systematic study on simulation, fabrication and characterization of n-ZnO/p-Si heterjunctions and their application in ultraviolet light detection. First, electrical and optical properties of n-ZnO/p-Si based UV detector have been studied using ATLAS simulator from silvaco international so that the performance of the detector can be optimized over the tool itself with reduced fabrication cost and efforts. This simulation study presents a systematic investigation on various important detector parameters such energy band diagrams, dark current, quantum efficiency, responsivity and noise equivalent power. Effect of parameter variations (such as thickness, light intensity, operating wavelength and applied reverse bias voltage) on the performance of the photodetector has also been studied.

Then, high quality ZnO thin films have been grown using RF sputtering technique. Various physical and growth parameters such as film thickness, annealing temperature, RF power and gas flow rate have been optimized in order to achieve the high quality films. Effect of all these parameters over structural and optical properties of RF sputtered ZnO thin films have been investigated in detail. The structural properties such as crystallographic orientations, grain size, lattice constant, stress, strain and surface roughness have been studied using X-Ray Diffraction (XRD), Scanning Electron Microscope (SEM) and Atomic Force Microscope (AFM) respectively. The various optical properties such as optical bandgap, transmittance, absorbance, refractive index, dielectric constant, urbach energy and photoluminescence have also been investigated.

The optimization of ZnO thin films was followed by temperature dependent electrical study of n-ZnO/p-Si heterojunction diodes. The results confirmed the high thermal stability of fabricated diodes for a temperature range of 25-120°C. Effect of temperature over various electrical parameters such as series resistance, reverse saturation current, ideality factor and Richardson constant have also been investigated in detail. Gaussian distribution function with standard deviation of σ_0 around the mean barrier height has been used to solve the problem of barrier inhomogeneity at n-ZnO/p-Si interface. Results also confirm that the temperature dependent I-V characteristics of n-ZnO/p-Si heterojunction obey the theory of thermionic emission with Gaussian distribution.

Finally n-ZnO/p-Si heterojunction ultraviolet detector was fabricated using RF sputtering technique. The structural and surface morphological properties have been investigated using XRD, AFM, SEM, TEM and Raman spectroscopy. The various electrical parameters such as ideality factor, barrier height, doping concentration, built-in potential and depletion width have been derived from current-voltage and capacitance-voltage measurements. The performance of the fabricated diode towards ultraviolet light was tested using current-voltage characteristics. Various performance parameters of the detector such as responsivity and detectivity have also been evaluated.

In this work, demonstration of cost effective n-ZnO/p-Si heterojunction ultraviolet detectors suggest that ZnO/Si heterojunction based devices and technologies do have a promising potential to get extended from research labs to commercial future market.

Table of Contents

List of Figures

List of Tables

Dedicated to my parents
for their love, endless support and encouragement. . .

CHAPTER 1

Introduction

In this chapter, general background of contributed work has been presented. The basic structural, optical and electrical properties of ZnO as a semiconductor material have been explained. The different applications of ZnO thin films in optoelectronic and nanoelectronic devices have been presented. The objectives and organization of the thesis have been elaborated at the end.

1.1 General Background

The invention of semiconductor transistor by Bell Laboratories in 1947 has brought incredible pace in semiconductor industry [1]. Fabrication of smaller, faster and highly efficient devices with large volume manufacturing at lower cost is advancing day by day. In continuation, thin film metal oxide based devices have witnessed a phenomenal development in the area of semiconductor science and technology. Nanostructure based thin films are supposed to have a revolutionalised impact on semiconductor industry.

In last decade, ZnO has drawn a significant research interest of researchers due to its excellent properties as a wide bandgap semiconductor material. The wide and direct bandgap (3.37 eV), high electron mobility, large exciton binding energy (60 meV), good transparency, high thermal conductivity and easiness of growing different nanostructures (nanorods, nanoflowers, nanbelts and nanowires etc.) with different low cost deposition methods make it a potential candidate for a variety of nanoelectronic and optoelectronic device applications [2]. The large exciton binding energy of ZnO results in an intense near-band-edge excitonic emission which ensures its application in lasers [3]. ZnO is easily etchable in all acids and alkalis which can be very useful in the fabrication of nano-dimension devices. The high optical transparency of ZnO provides an opportunity to use it in UV detection and solar cell applications [4]. Recent reports also confirm that ZnO is also a promising material for gas sensing, spintronics, flat panel displays, thin film transistor and piezoelectronic nanogenerator applications [5].

However, ZnO is not a new material and several reports on ZnO are available since 1935 [6]. But in last decade, it has emerged as the second most popular material after silicon. Its popularity in semiconductor industry is increasing day by day. One important problem that is required to overcome before commercialization of ZnO based devices in optoelectronic world is: "The reliable and reproducible growth of p-doped ZnO films". However, several reports on p-doped ZnO films with various group-V doping elements such as P, N, As and Sb etc. are available in literature [7] but still, the stable and high quality p-type conductivity of ZnO films have not been achieved yet. A lot of sincere research efforts by various research groups across the globe are going on to grow high quality p-type ZnO films. Alternatively, other efforts to deposit n-type ZnO over various p-type substrates have also been done so that potentiality of ZnO in many advanced device applications can be explored. Some reports where n-ZnO was deposited over various p-type substrates such as Si, GaN, NiO, AlGaN, SiC, CdTe, CuO and ZnTe etc. are available in literature [8].

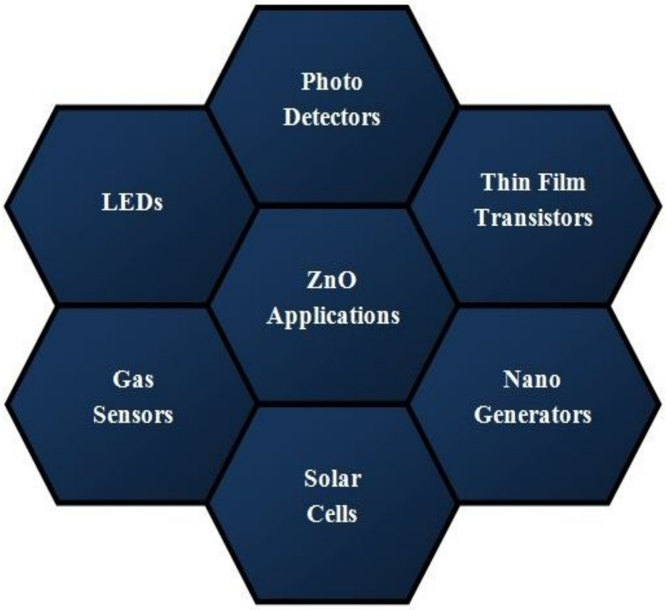

Fig.1.1 Different applications of ZnO in electronics.

1.2 Material Properties of ZnO

All the applications of ZnO mentioned in above section originate from its material properties. Therefore, it is important to discuss the structural, optical and electrical properties of ZnO. This section explains the various properties of ZnO that makes it a popular candidate for variety nanoelectronic and optoelectronic device applications.

1.2.1 Structural Properties

ZnO is one of the widely studied material, and in most of the cases it crystallizes either in cubic zinc blend or hexagonal wurtzite form where each anion is surrounded by four cations at the corner of a tetrahedron and vice versa [9]. The nature of this tetrahedral coordination is sp^3 covalent bond. A substantial ionic character also exists in these kind of materials that can increase the bandgap beyond the one expected from covalent bonds. ZnO is the II-VI group compound semiconductor whose ionicity lies between ionic and covalent semiconductors. Fig.1.2 (a) and (b) shows hexagonal wurtzite and zinc blend structures of ZnO. Among all structures of ZnO, hexagonal wurtzite structure is the most stable one under ambient conditions. The wurtzite structure consists of hexagonal unit cell with lattice constants varying in the range of 3.2475-3.2501 Å and 5.2042-5.2075 Å for a-parameter and c-parameter respectively. Various point defects such as oxygen vacancies, Zn interstitials and threading dislocations are the probable reasons for the deviation of lattice constants from their ideal values [10].

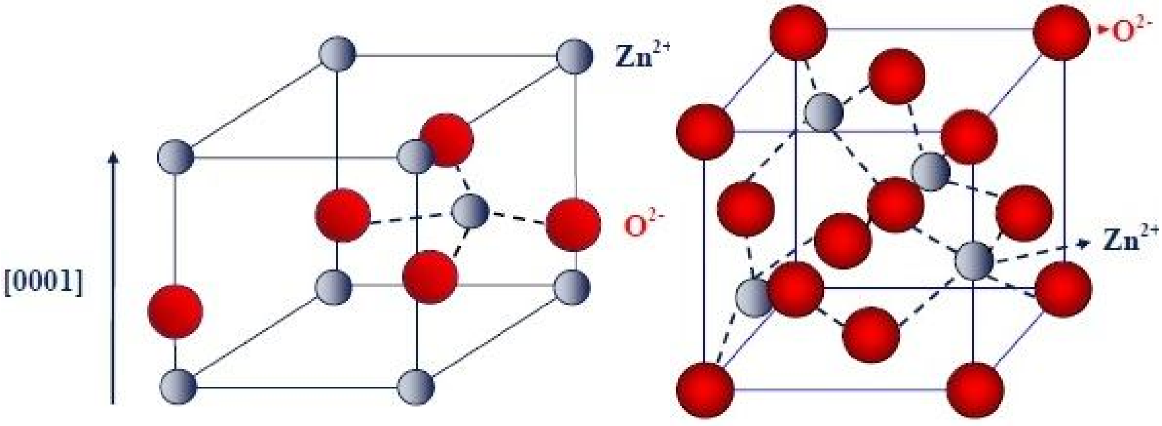

(a) **(b)**

Fig.1.2 (a) Hexagonal wurtzite structure of ZnO (b) Cubic zinc blende structure of ZnO.

1.2.2 Optical Properties

The direct and large bandgap of ZnO i.e. 3.37 eV with high exciton binding energy (60 meV) makes ZnO a promising material for photonic and optoelectronic applications at room temperature. ZnO thin films behave as transparent layers for visible wavelength range (400-700 nm) that can be very advantageous in solar cell and transparent electronics applications. Large bandgap of ZnO ensures its usability in ultraviolet applications whereas large exciton binding energy which is sufficiently higher than that of GaN (~25 meV) allows efficient excitonic emission even at the room temperature. The large exciton binding energy is an indication of efficient radiative recombination of photo-generated carriers that makes ZnO a potential alternate to GaN in optoelectronic applications. There exists a variety of optical characterization techniques through which various optical parameters such as transmittance, reflectance, refractive index, dielectric constant, cathodoluminescence and photoluminescence for ZnO thin films can be obtained. Table 1.1 shows various important properties of ZnO [1-10].

1.2.3 Electrical Properties

It is really important to understand the electrical properties of ZnO thin films to ensure its potentiality for nanoelectronic device applications. The basic current transport mechanism for semiconductors depends upon low and high electric fields [10]. When the electric field is sufficiently low, the energy gained by electrons due to electric field is very small as compared to the thermal energy of electrons which makes the electron mobility independent of electric field and obeys Ohm’s law. When the electric field is sufficiently high, the external field is no longer negligible as compared to thermal energy of electrons and the electron mobility becomes field dependent.

The current-voltage measurement is the key parameter to investigate the performance of various devices like sensors, solar cells and thin film transistors. Various electrical parameters such as ideality factor, barrier height and Richardson constant that are important to analyze the performance of different devices can be derived from I-V measurements. The capacitance-voltage (C-V) measurement is a powerful experimental technique to investigate charge distribution and depletion region potential of heterojunction based devices. When two semiconductor materials with different Fermi level comes in contact, the charge transfer between the two semiconductors take place until the equilibrium state is achieved. This results in the formation of depletion regions in both sides of the junction. Various important electrical parameters such as built-in potential, barrier height, donor concentration, depletion width and position of fermi levels can be derived from C-V measurement of the fabricated devices.

Table 1.1: Material Properties of ZnO [1-10]

Molecular formula	ZnO
Molar mass	81.40 g/mol
Appearance	Yellowish white/Amorphous white
Crystal structures	Wurtzite, Zinc blende, Rock salt
Density	5.606 g/cm^3
Solubility in water	0.16 mg/100mL
Boiling point	2360^{o}C
Melting point	1975^{o}C
Intrinsic carrier concentration (per cm^3)	10^{16} to 10^{20}
Effective mass of electrons	$0.24m_o$
Effective mass of holes	$0.59m_o$
Electron mobility (at 300 K)	200 cm^2/V.sec.
Hole mobility (at 300 K)	5-50 cm^2/V.sec
Lattice constants	a=b=3.25 Å, c= 5.20 Å
Energy gap	3.37 eV (Direct Bandgap)
Exciton binding energy	60 meV
Refractive index	2.0041
Relative dielectric constant	8.66
Typical impurities	Ga, Al, H, In, Mg, Cd.
Typical defects	Zinc vacancies, Zinc interstitials, Oxygen vacancies.

1.3 Basics of ZnO Thin Film Based Devices

1.3.1 Electrical Contacts

Metal-Semiconductor (M-S) contacts play a key role in current injected semiconductor devices [11]. Their properties govern the current transport mechanism of these electrical contacts. The M-S contacts can realize many characteristics of p-n junctions with comparatively higher switching speed with much simpler fabrication steps. However, poor quality of these contacts may result in large leakage current under reverse bias conditions. Ideally, a metal-semiconductor contact will be called as ohmic if the barrier formed by metal-semiconductor is zero. In such ohmic contacts, the carriers are free to move in or out of the semiconductor so that contact resistance is minimum across the metal semiconductor interface. The schottky diodes exhibit rectifying nature and the work function of metal remains higher than the semiconductor. In n-type metal-semiconductor system, the following different current transport mechanisms may exist:

(i) For moderately doped semiconductors (e.g. donor concentration $<10^{17}cm^{-3}$), thermionic emission will be the dominating current transport mechanism due to sufficiently large barrier height. In this mechanism, the electrons with kinetic energy larger than the potential barrier will move from one side to the other in order to contribute the current.

(ii) For highly doped semiconductors where barrier height is sufficiently small due to larger doping, quantum mechanical tunneling is the dominating carrier transport mechanism. In this mechanism, the electrons with energy in the vicinity of the fermi energy level tunnels through the barrier due to the small barrier height at high energy levels.

(iii) Recombination of the carriers in the depletion region can also contribute the current in metal semiconductor contacts.

(iv) Injection of holes from metal to semiconductor which is equivalent to the recombination of electrons-holes in the neutral region, can also contribute the current in these M-S systems.

A. Ohmic Contacts

Ohmic and schottky contacts represent the basic metallization techniques for semiconductor device fabrication. When metal and semiconductor makes a contact, the ohmic and schottky nature of the contact depends upon two parameters (i) work function and (ii) electron affinity [12]. As the dimensions of the devices are scaling down, getting good ohmic contacts has become more and more important. It is evident from the experimental results that the strong dependence of barrier height on metal work function is only valid for ionic semiconductors. In the case of III-V compounds, the barrier height remains independent of the work function of the metal. Since most of the II-VI semiconductor compounds have ionic bonding with large $\Delta\chi$, ohmic nature of these materials can be realized based on metal work function and semiconductor electron affinity. A good ohmic contact should have negligible contact resistance with linear current versus voltage characteristics [14]. If the semiconductor is n-type, the metal work function should be close to or less than the electron affinity of the semiconductor in order to get ohmic contact. For p-type semiconductor, the metal work function must be close to or higher than the sum of bandgap and electron affinity of the semiconductor. Fig. 1.3 shows the energy band diagram of a metal semiconductor contact before junction formation and at thermal equilibrium.

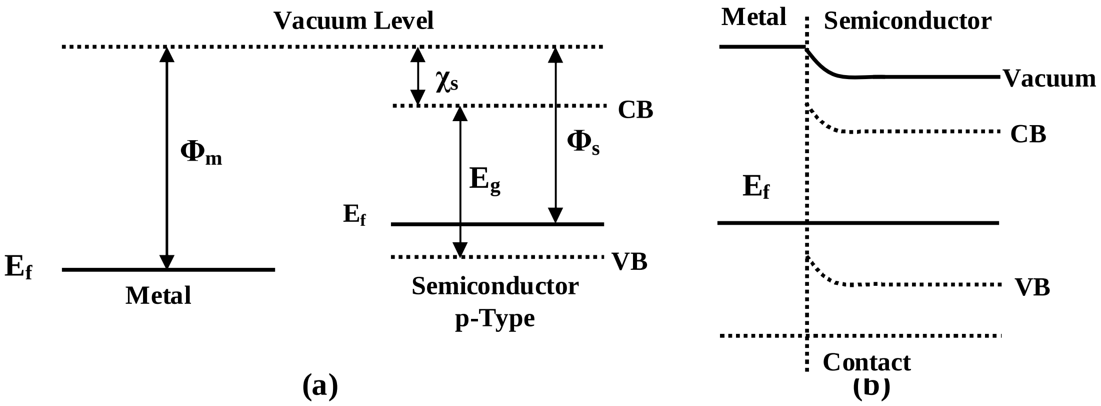

Fig. 1.3 Energy band diagram of a metal semiconductor contact (a) before junction formation and (b) at thermal equilibrium.

B. Schottky Contacts

The study of schottky diodes started in early 1960’s to understand the role of surface states and fermi level pinning, regardless of metal work function. C.A. Mead reported the first schottky contact in 1965 [15]. W. Schottky and N. F. Mott reported the first model in 1935 to describe the formation of such junctions over n-type semiconductors [12]. Therefore, these types of contacts are called as schottky-mott diodes or schottky contacts. In metal-semiconductor systems, metals do have higher work functions than semiconductors (refer Fig. 1.4). It is clear from the band diagram of metal schottky contacts that the electrons in the semiconductor will flow towards metal until the fermi levels of the two materials will get aligned.

Fig. 1.4 shows the energy band diagram of a metal-semiconductor schottky contact where the work-function of the metal is larger than that of n-type semiconductor. The values $q\varphi_s$, $q\varphi_m$ and $q\chi$ represents semiconductor work function, metal work function and semiconductor electron affinity respectively. In equilibrium stage, $qV_{bi}\ (=q(\varphi_m-\varphi_s))$ and $q\varphi_B\ (=q(\varphi_m-\chi_s))$ represents the band bending and schottky barrier height respectively. Under forward bias condition, the resultant potential difference faced by semiconductor side becomes $q(V_{bi}-V_F)$, which results in lager flow of electrons from semiconductor to metal side. On the other hand, under reverse bias conditions the barriers height becomes $q(V_{bi}+V_R)$, which reduces the electron flow drastically across the junction due to higher barrier potential. As a result, in schottky diodes the net current flow dominates only in one direction i.e. forward bias.

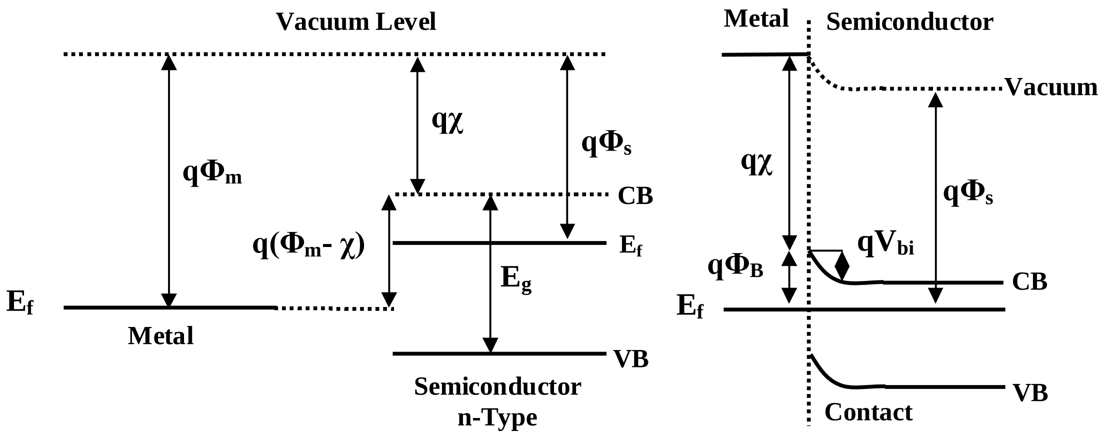

(a) (b)

Fig. 1.4 Energy band diagram of a schottky contact (a) before junction formation and (b) at thermal equilibrium

1.3.2 p-n Heterojunction Diodes

A p-n heterojunction is formed by combining two dissimilar semiconductor materials. The band discontinuity or band offset formed at the interface due to different band gaps of two semiconductors is the unique feature of heterojunction diodes. The band offset also plays an important role in the current transport mechanism of semiconductors diodes. Based on the alignments of energy bands, the semiconductor heterojunctions can be classified in three types [16] (refer Fig.1.5): (i) Type-I (Straddled Type) (ii) Type-II (Staggered Type) (iii) Type-III (Broken Gap Alignment).

Anderson reported first heterojunction of Ge/GaAs in 1960 [17]. The electron affinity model proposed by him helped to predict the energy band diagrams of heterojunctions at the interface. This model assumes the ideal performance of heterojunction diodes with no interface states present at the junction. The current transport is considered to be entirely dominated by injection of carriers over the band offsets into the quasi-neutral region of the diode. This ideal case rarely exists in typical heterojunctions but generally used as the basic model to evaluate the performance of the heterojunctions.

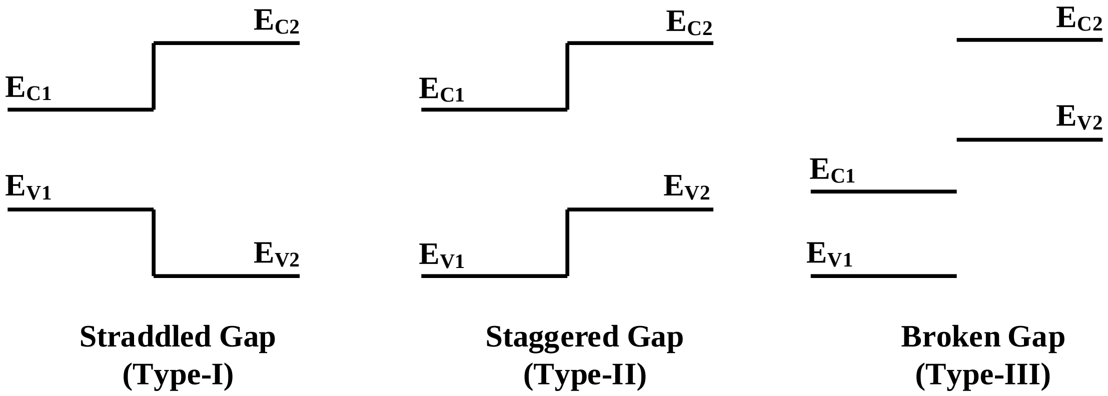

Fig. 1.5 Types of energy band alignments in heterojunction diodes.

Fig. 1.6 demonstrates the equilibrium energy band diagram of an abrupt n-ZnO/p-Si heterojunction. ΔE_C and ΔE_V represents the conduction and valence band discontinuities respectively.

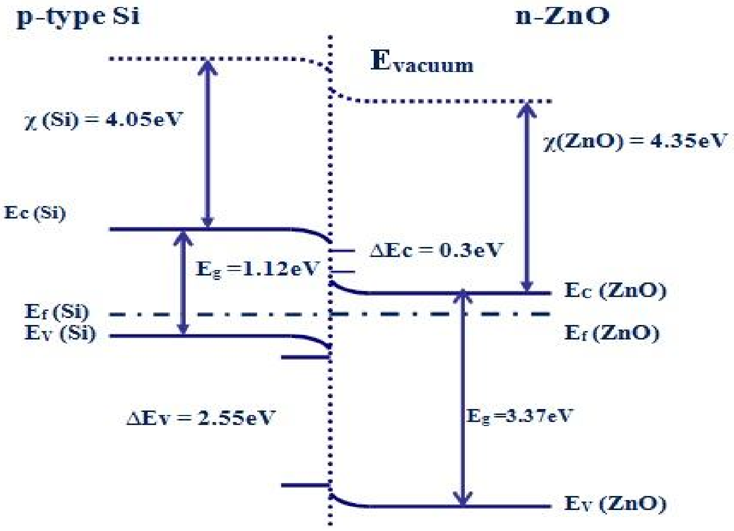

Fig. 1.6 Energy band diagram for abrupt n-ZnO/p-Si heterojunction diode.

Eq. 1.5 presents the ratio of band bending at the interface of the semiconductor heterojunction [18].

$$\frac{V_{b1}}{V_{b2}} = \frac{N_2\varepsilon_2}{N_1\varepsilon_1} \tag{1.1}$$

Where V_{b1}, V_{b2} represents the band bending and N_1 and N_2 represents doping densities in n and p regions of the heterojunction interface at thermal equilibrium. It has been observed that the Anderson model stands good in predicting the band discontinuities of heterojunctions but the current-voltage behavior obtained from experimental data has not shown good relevance with this model.

This is due to the absence of interface states and abrupt heterojunction interfaces which are not possible to achieve during the fabrication of the heterojunction. In practical heterojunction diodes, the current transport mechanism generally includes (i) recombination of carriers in the depletion region (ii) carrier injection over band offsets (diffusion or thermionic emission) and (iii) tunneling of carriers into interface states. There exist no definite model which can predict the exact current transport mechanism in heterojunctions because it is strongly influenced by quality of the fabricated heterojunctions.

1.3.3 Basic Working Principle of Photodiodes

Generally, two terminal based metal-semiconductor photodetectors can be classified into four categories [19]: (i) photoconductors (ii) schottky photodiodes (ii) metal-semiconductor-metal (MSM) photodiodes and (iv) metal-insulator-semiconductor (MIS) photodiodes. Fig. 1.7 shows the schematic diagrams of different photodiodes. The basic working principle of all semiconductor based photodetectors includes two basic steps: (i) The wavelength that needs to be detected should be allowed to get absorbed on the active area of the photodetector. (ii) A suitable electric field should be applied across the device by choosing appropriate biasing voltages so that the resultant current due to electron-hole pair generation in active region can be obtained in the external circuit. The bandgap of the semiconductor material decides that which wavelength will be detected by the fabricated detector. Some important parameters which are required to be evaluated for measuring the performance of the photodetector are as follows:

Quantum Efficiency: Quantum efficiency is the measure of number of electron-hole pairs generated per unit photons.

Responsivity: Responsivity of a photodetector can be described as the ratio of photocurrent generated to the optical power in linear region of response. Generally in phototodetectors, responsivity is highest for the wavelength region in which photon energy is somewhat higher than the bandgap energy.

Detectivity: Detectivity allows different photodetectors to be compared independent of detector bandwidth and area. High value of detectivity ensures the suitability of heterojunction photodetectors for low noise applications.

Noise Equivalent Power: Noise equivalent power is the minimum detectable power for a photodetector.

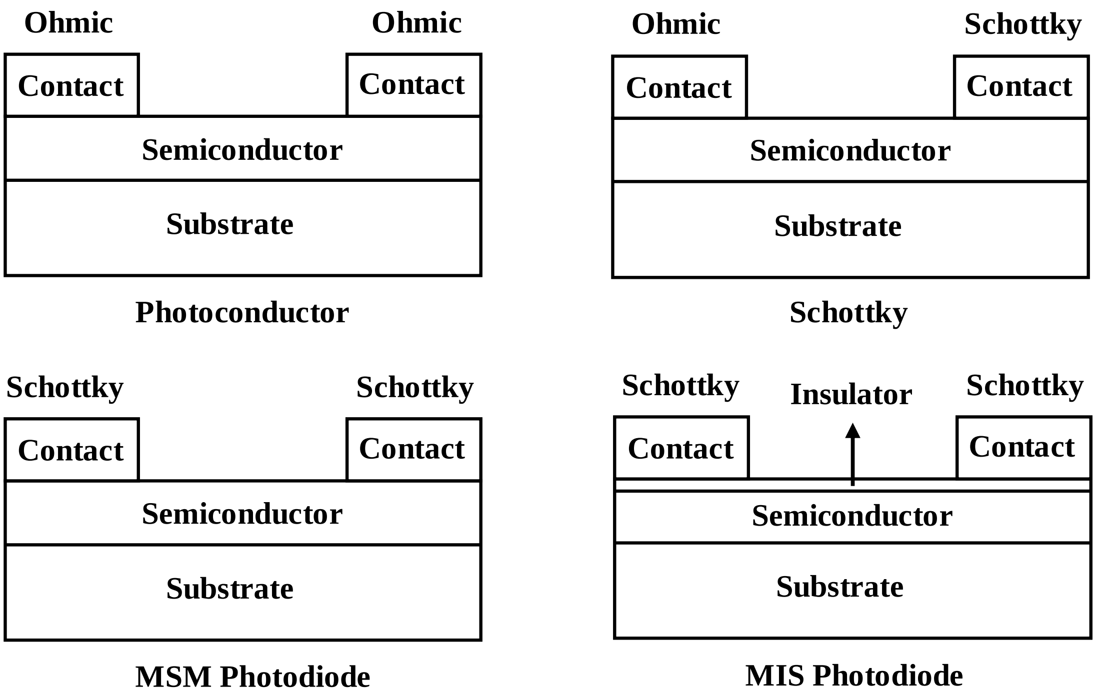

Fig. 1.7 Schematic structures of different semiconductor photodetectors.

1.4 Applications of ZnO Thin Films

1.4.1 UV Photodetector

As mentioned earlier, ZnO has drawn a substantial attention of researchers for UV detection applications. Large and direct bandgap, high surface to volume ratio and other superior properties of ZnO has made it a promising choice for ultra violet light detection with high selectivity and sensitivity. Mollow observed the ultraviolet response of ZnO films first time in 1940s [20]. However, the work on ZnO films based photodetectors have got significant attention in 1980s. In the beginning, the results obtained from ZnO based detectors were not very good. But the improvement in fabrication process for growing high quality nanostructured ZnO thin films has improved the performance of these detectors significantly. In past decade, Different ZnO based UV photodetectors such as metal-semiconductor-metal photodiode, schottky photodiode and p-n heterojunction photodiode have been reported by researchers [16-17]. All the reports available in the literature suggests that RF sputtering, pulsed laser deposition, molecular beam epitaxy, metal organic chemical vapor depositions and vacuum coating are the suitable methods to fabricate ZnO thin films based UV photodetectors. High responsivity, good UV/visible contrast ratio and low noise characteristics of ZnO thin film based detectors has ensured their usability in a variety of applications.

1.4.2 Light-Emitting Diodes (LEDs)

In past, many wide bandgap materials such as GaN [21], SiC [22] and ZnO [23] have been studied for light emitting diodes and other optoelectronic applications. In recent years, ZnO has emerged as a promising candidate among all these materials. Many favorable properties such as wide and direct band gap, high exciton binding energy (60 meV), inexpensive nature with good safety and stability has made ZnO one of the most suitable choice for LED applications. ZnO can be grown with many novel structures such as nanowires, nanowalls, nanorods and nanoribbons that can be very useful building block in LED applications. Many efforts have been made to fabricate ZnO based LEDs using different deposition techniques on different substrates such as SiC, $SrCu_2O_2$, GaN and Si etc. Recent reports on ZnO based homojunction and heterojunction LEDs has confirmed the potentiality of ZnO thin films in light emitting diode (LED) applications [24-26].

1.4.3 Thin Film Transistors and Transparent Electronics

TFTs for transparent electronics need all the device components such as substrate, gate, channel and electrodes to be transparent. High transparency of ZnO in visible wavelength region has made it a potential candidate for all transparent electronic applications. ZnO thin film based transparent TFTs can be very useful in many transparent electronics applications such as touch display panels, flat panel displays and optical coatings. For polymer based flexible substrates also ZnO is a suitable oxide material, because it can be processed at lower temperature. Nomura *et al.* demonstrated first transparent ZnO TFT in 2003 [27]. Recently, many studies on ZnO based TFTs have been reported by researchers [28-30]. The main advantage of ZnO thin film based TFT is the magnitude of the electron channel mobility which leads to faster operating speeds and high driver currents.

1.4.5 Piezoelectric Nanogenerator

Among the known nanomaterials, ZnO provides three key advantages for piezoelectric device applications: (i) ZnO exhibits a diverse range of nanostructures such as nanowires, nanosprings, nanobelts, nanoflowers, nanowalls, nanorods, nanobows and nanohelics which is very much needed for piezoelectronic device applications. (ii) ZnO is relatively non-toxic and bio-compatible so that it can be used for medical applications with less toxicity. (iii) It exhibits both piezoelectronic and semiconducting properties which is the necessary requirement for sensor and transducer applications. The first ZnO nanowire array based piezoelectric nanogenerator which converts the mechanical energy to electricity was demonstrated by Wang *et al.* [31]. They demonstrated the conversion of nanomechanical energy into electrical energy by using coupled semiconducting and piezoelectric properties of ZnO nanowire arrays. The fabrication of ZnO nanostructures over flexible substrates to enhance the conversion efficiency of nanogenerators has attracted a wide attention of researchers in recent years. Such nanogenerators can provide flexible power sources with their potential applications in sensors, actuators and nanoelectromechanical systems.

1.4.6 Gas Sensors

Semiconductor oxide based nanostructures have drawn a substantial attention of researchers for gas sensing applications. High thermal/chemical stability, wide bandgap and large surface to volume ratio of ZnO have made it a suitable candidate for gas sensing applications. The larger surface to volume ratio of ZnO thin films/nanostructures results in a variety of advantages such as faster sensing response and high sensitivity. In addition to this, excellent surface charge-transfer properties and high surface-adsorption ability also ensures the suitability of ZnO thin films for gas sensing applications. Several reports are available in literature which demonstrates the sensitivity of ZnO towards different gases such as methane [32], hydrogen [33], oxygen [34], NO_x [35] and CO [36] etc.

1.5 Scope of the Thesis

The fundamental objective of this thesis is to make a systematic investigation on ZnO thin film based heterojunctions and devices for electronic/optoelectronic applications. First, the simulation study of ZnO/Si heterojunction photodiode have been presented using

ATLAS simulator from SILVACO International. In best of our knowledge, no simulation reports for ATLAS simulation of ZnO based photodetectors are available in literature. So these simulation studies can be very helpful to reduce the fabrication cost and efforts by optimizing various device parameters over the simulation tool itself before moving for the actual device fabrication. Then, ZnO thin films were grown over silicon and glass substrates using thin film deposition techniques. Various physical and growth parameters were optimized during the deposition in order to achieve high quality ZnO thin films. A detailed investigation on structural, optical and electrical properties of n-ZnO/p-Si heterojunctions has been done and the stability of these fabricated diodes at high temperature ranges has also been tested. The scope of the work has further been extended to investigate the ultraviolet light detection properties of these ZnO based heterojunctions for a variety of civil and military applications. The thesis consists of eight chapters including the present one entitled as “Introduction”. The remaining chapters are organized as follows:

Chapter -2 compiles some important state-of-the-art work in this area. The major work done in this field by various research groups is presented in brief. A detailed review on latest trends in the field of ZnO thin films, n-ZnO/p-Si heterojunctions and their applications in UV detectors have been reviewed in detail. Based on the literature survey, various research gaps in this area have been identified. Finally, the motivation behind this study has been outlined at the end of the chapter.

Chapter-3 presents the working principles of RF sputtering and thermal vapor deposition techniques to grow high quality ZnO thin films for optoelectronic device applications. The basic working mechanisms of various structural, optical and electrical characterization techniques such as XRD, AFM, SEM, TEM, Ellipsometery, I-V and C-V etc. have also been presented.

Chapter-4 presents simulation study and performance analysis of n-ZnO/p-Si heterojunction based photodetector. Different electrical and optical parameters such as energy band diagram, electric field profile, dark current, quantum efficiency, responsivity, detectivity and noise equivalent power of ZnO/Si heterojunction based photodetector have been simulated as a function of device thickness, operating wavelength and applied reverse bias voltage. The simulation software ATLAS™ in SILVACO package has been used to describe the effect of n-ZnO/p-Si interface properties on its photodetection.

Chapter-5 is devoted to the preparation, characterization and optimization of nanocrystalline ZnO thin films using RF sputtering technique. High quality ZnO thin films were grown over p-Si (100) and glass substrates by RF magnetron sputtering technique. Effect of various physical and growth parameters such as thickness, annealing temperature, sputtering power and gas flow rate on structural and optical properties of ZnO thin films have been investigated in detail so that high quality ZnO thin films for a variety of optoelectronic and photonic devices can be achieved. Surface morphology, structural properties and quality of thin film have been studied using X-Ray Diffraction (XRD), Atomic Force Microscopy (AFM), Scanning Electron Microscopy (SEM) and Energy-Dispersive X-ray (EDX). The micro structural parameters for the film such as grain size, lattice parameters, defect density, stress and strain have been studied in detail. Optical properties such as transmittance, reflectance, absorption coefficient, refractive index and dielectric constant for a spectral range of 300 nm to 800 nm have been evaluated. Photoluminescence (PL) spectra for ZnO thin films have also been investigated.

Chapter-6 deals with fabrication and characterization of n-ZnO/p-Si heterojunction diodes. Nanostructured zinc oxide (ZnO) thin film were deposited on p-type silicon (Si) substrate using vacuum coating technique for fabricating n-ZnO/p-Si heterojunction diodes. Structural properties, surface morphology and quality of thin film have been studied using XRD, AFM and Energy Dispersive X-ray Spectroscope (EDX) measurements. The temperature dependent electrical junction properties were investigated by Current-Voltage-Temperature (I-V-T) measurements. Effect of temperature variation on various electrical parameters of the fabricated p-n junction diode such as series resistance, reverse saturation current, ideality factor, barrier height and Richardson constant have been studied. Gaussian distribution function with standard deviation of σ_0 around the mean barrier height has been used to solve the problem of barrier inhomogeneity at n-ZnO/p-Si interface.

Chapter-7 presents ultraviolet light detection properties of n-ZnO/p-Si heterojunction diodes. ZnO nanocrystalline thin films were deposited over p-Si (100) substrates using RF sputter deposition. The structural and surface morphological properties of the deposited films were studied using XRD, AFM, SEM, TEM and Raman spectroscopy. The junction properties of n-ZnO/p-Si heterojunction diodes were investigated using current-voltage and capacitance-voltage measurements. Various important electrical parameters such as ideality factor, barrier height, built-in potential, donor concentration and depletion width have also been evaluated. The UV detection properties of the fabricated diodes were investigated using a UV lamp of 365 nm wavelength.

Chapter-8 concludes some major findings and outcomes of the thesis. The chapter summarizes all the results presented in Chapter 4-7 of the thesis. Finally, the future scope of the work is outlined in the end.

CHAPTER 2

ZnO Thin Films for Optoelectronic Devices: A General Review

This chapter presents a review on some important state-of-the-art work reported by various research groups in the area of ZnO thin film based optoelectronic devices.

2.1 Introduction

Literature survey plays a significant role in any kind of research. A thorough knowledge of the state of the art work in any research area can only be predicted by the future trends in that particular research area. Therefore, this chapter is dedicated to present some important state of the art work reported by different research groups in the area of ZnO thin films. This chapter primarily focuses on some important investigations that have been done in the area of ZnO thin film based optoelectronic devices over the last decade. Structural, optical and electrical properties of ZnO thin films, n-ZnO/p-Si heterojunctions and their applications in UV detection have been reviewed in detail.

2.2 ZnO Thin Films

Thin films can be defined as the layers whose thickness varies from nanometers to few micrometers. They exhibit better properties than bulk materials for a variety of applications. Thin film technology has emerged as very potential candidate for optical coatings and electronic device applications. The nanostructured thin film reduces the material loses, enhances the efficiency for solar cells, improves the sensitivity of gas sensors due to larger surface area to volume ratio and can be very useful in wide variety of applications. The pivot influence of thin film technology in diverse and challenging frontiers such as optical coatings, metallurgical coatings, micro magnetism, surface science, superconductivity mechanism and microelectronics is now a part of literature survey.

In recent years, different ZnO based nanostructures such as nanowires, nanotubes, nano flowers, nanowalls and nanobelts etc. have attracted a significant research interest because of their potential applications in next generation sensor and molecular technology. ZnO can be grown with a wide variety of nanostructures which makes it one of the most popular nanomaterial. Different techniques such as spin coating, thermal evaporation, metal organic chemical vapor deposition (MOCVD), pulsed laser deposition (PLD) and RF sputtering have been employed in past to grow different ZnO nanostructures. This section presents some recent state-of-the-art work to grow high quality ZnO thin films using different deposition techniques.

2.2.1 Spin Coating Technique

The synthesis of ZnO thin films using spin coating technique includes three principle steps: (i) solution preparation (ii) coating and (iii) heat treatment. Various research groups have reported the preparation and characterization of ZnO thin films using spin coating technique in past.

Smirnov *et al.* [37] investigated the structural and optical properties of ZnO thin films using spin coating technique. The precursor solution of ethanol, zinc acetate and ammonium hydroxide was used to deposit ZnO films over glass substrates. The nature of deposited films was found to be polycrystalline, and transparency of the thin films was more than 75% in the spectral range of 450-130 nm. They also investigated the effect of spinning speed and heat treatment over structural and optical properties of deposited ZnO thin films.

Tsay *et al.* [38] studied the effect of Sn doping on crystallinity, structural and optical properties of sol-gel derived ZnO thin films. They varied the Sn doping from 1 to 5 at .% and found that the doping of Sn in ZnO film improves the surface roughness. They also observed that the film doped with 2 at.% Sn concentration have exhibited best results with a transmittance, roughness and resistivity of 90%, 1.92 nm and 9.3×10^2 Ω-cm respectively.

Brien *et al.* [39] prepared ZnO thin films using zinc acetate, isopropanol and monoethanolamine. The prepared films were post annealed in a temperature range of 500-650°C in order to achieve high crystallinity. The transmittance for deposited films was found to be more than 85% with absorption edge around ~378 nm. The optical bandgap was found to be varied in the range of 3.298-3.306 eV. They also investigated the effect of Zn concentration, thickness and annealing temperature on structural and optical properties of the deposited films.

Srinivasan *et al.* [40] deposited zinc oxide thin films over sapphire substrate using spin coating technique. They studied the effect of annealing temperature on ZnO thin films and concluded that annealing improves the crystallinity of deposited films. Photoluminiscense spectra of deposited films exhibited two line structure which attributes to UV emission and defect related emission. AFM study also confirmed that the annealing temperature have improved the surface morphology of the deposited films.

Kim *et al.* [41] investigated the effect of pre heating on structural and optical properties of ZnO thin films. They observed a high transparency of more than 85% for pre-heated films. The optical bandgap was found to be varied in the range of 3.24-3.26 eV. The PL spectra exhibited the UV emission in near band edge with a broad green-yellow emission at 490 - 620 nm.

2.2.2 Pulsed Laser Deposition

Pulsed laser deposition is one of the popular technique to synthesize oxide and nitride materials. In pulsed laser deposition, a high energy laser pulse is focused over the bulk target to evaporate the source material. When energy density of laser beam is sufficient enough, each laser beam can easily vaporize the material which is required to be deposited.

Gondoni *et al.* [42] investigated structural and functional properties of aluminium doped ZnO thin films using pulsed laser deposition in oxygen ambient. They varied the deposition pressure from 0.01 to 10 Pa to analyze the effect of defect formation and oxygen vacancies over various properties of ZnO thin films. They obtained best results for a deposition pressure of 2 Pa and the transparency of deposited films was found to be increased with increasing working pressure.

Drmoshb *et al.* [43] studied the properties of cu doped ZnO thin films using PLD technique. In order to obtain ZnO-Cu composites, pure Zn and Cu targets were irradiated with 248 nm KrF laser in a special geometric arrangement. They also observed a shift in XRD spectra peak due to Cu doping. The photoluminescence spectra also revealed a red shift in the emission peak with decreased bandgap at higher doping concentration. They concluded that PLD can give good quality films without pre and post heating treatment.

Doping in semiconductor materials can be very useful to change the bandgap of the deposited films. **Jiang *et al.* [44]** deposited Cd doped ZnO thin film using pulsed laser deposition technique. The bandgap of ZnO thin films with 9.6% cadmium content was found to be 2.88 eV. They also investigated the effect of fluorine doping on structural, optical and electrical properties of PLD deposited ZnO thin films. They varied the oxygen pressure from 0.1-0.5 Pa. At oxygen pressure of 0.1 Pa, the optimum values of resistivity, carrier concentration and hall mobility were found to be 4.83×10^{-4} Ωcm, 5.43×10^{20} cm^{-3} and 23.8 $cm^2V^{-1}S^{-1}$ respectively.

Variation in deposition parameters also affects the quality of deposited films considerably. **Cracium *et al.* [45]** reported how all these parameters affect the quality of deposited films in pulsed laser deposition. **Zhaoyang *et al.* [46]** investigated the impact of laser repetition frequency over surface morphological and optical properties of ZnO thin films. The results conclude that the film deposited at 5 Hz frequency have exhibited high crystallinity with excellent UV emission.

2.2.3 Molecular Beam Epitaxy

Ting *et al.* [47] studied the impact of MgO and GaN buffer layers over structural, electrical and optical properties of ZnO thin films grown over sapphire substrate using MBE technique. They reported that GaN and MgO buffer layer reduces the lattice mismatch between ZnO and GaN that improves the crystalline quality of deposited ZnO film. The X-Ray diffraction analysis revealed that the introduction of buffers layers between ZnO and GaN reduces the film strain whereas the nature of stress got changed from tensile to compressive with the introduction of buffer layer. They also reported that the GaN as buffer layer improves the surface morphology whereas the MgO as buffer layer improves the surface roughness significantly.

Iwata *et al.* [48] used molecular beam epitaxy technique to grow ZnO thin films over silicon substrate. Their study revealed that lower H_2/O_2 ratio using RHEED pattern exhibits a streaky pattern for nitrogen doped ZnO films. The concentration of nitrogen in deposited films was found to be 1×10^{19} cm^{-3}. However no type conversion from n-type to p-type has been observed due to nitrogen induced trap states.

Chen *et al.* [49] used plasma assisted molecular beam epitaxy technique to grow high quality ZnO thin films. They used Mg as buffer layer between ZnO and sapphire substrate so that lattice mismatch between the two layers can be minimized. The value of rectification ratio for the fabricated schottky diode was found to be 104. They suggested that the low electron concentration of undoped ZnO layers can be a good choice for p-doping.

Liu *et al.* [50] fabricated ZnO thin film based UV photoresistor using molecular beam epitaxy technique. Two Knudsen cells with zinc (7N) and magnesium (5N) have been used to evaporate the metal. The values of dark resistance and ratio of dark to light resistance were obtained as 1010 Ω and 2.3×10^5 respectively. The responsivity of the fabricated detector was found to be 1 $\Omega^{-1}W^{-1}$. A linear relation between photoresistance and reciprocal optical power density has also been observed for the fabricated structure.

Przezdziecka *et al.* [51] demonstrated fabrication and characterization of p-ZnO:As/n-GaN ultraviolet detector using MBE technique. The fabricated detector exhibited high ultraviolet response with faster response time of less than 2 ms.

Pietrzyka *et al.* [52] used plasma assisted molecular beam epitaxy technique to fabricate ZnO:N/ZnMgO:N/i-ZnO/ZnMgO/ZnO heterojunction. Conventional Knudsen cells (Mg (6N) and Zn (6N)) were used to evaporate the metal. The photoluminescence spectra confirmed high quality of grown ZnO thin films. In order to investigate the defects present into the films, temperature dependent current-voltage and capacitance-voltage measurements have also been done. The existence of persistence photo-capacitance upto 280 K has ensured the presence of metastable centers at relatively higher barrier heights.

Asghar *et al.* [53] investigated surface morphological and interface properties of Au/ZnO schottky contact. ZnO and Au films were grown over Si substrates using MBE and E-Beam techniques respectively. The values for barrier height and ideality factor were obtained as 0.61 eV and 2.15 respectively for the fabricated structure which confirmed the presence of barrier inhomogeneties at the heterojunction interface. They also reported frequency dependent capacitance-voltage study to investigate the density of interface.

2.2.4 Metal Organic Chemical Vapor Deposition

Wang *et al.* [54] investigated fabrication and characterization of ZnS/ZnO heterojunction properties using MOCVD technique. Thermal evaporation and MOCVD techniques have been used to deposit ZnS and ZnO layers respectively. They observed that different orientations of ZnS nanobelts may result in different surface morphologies of the fabricated ZnS/ZnO heterojunctions. The fabricated structure has shown a strong emission peak in green and weak violet regions.

Biswas *et al.* [55] fabricated ZnO based humidity sensor using MOCVD method. ZnO nanostructures were obtained over r-sapphire substrates using horizontal reactor MOCVD method without any catalyst. The recovery and response time were found to be 12 sec. and 3 sec. respectively with high stability and repeatability. They observed that the fabricated device has given a quick response to relative humidity changes due to quantum side effects. Results concluded that ZnO nanostructures grown by MOCVD method can have potential applications in preparation of highly sensitive humidity sensors.

Wang *et al.* [56] investigated UV electroluminescence properties of n-ZnO/NiO/p-GaN diode prepared using MOCVD method. The device has shown a diode like behavior with a turn voltage of 7.5 V. The use of NiO as blocking layer between ZnO and GaN resulted in high resistance state. The values of conduction band offsets for ZnO/NiO and ZnO/GaN heterojunctions were found to be 2.93 eV and 0.15 eV respectively. They also observed a strong electroluminescence emission peak at 381 nm which suggests that Ni layer sandwiched between ZnO and GaN can confine the electrons in n-ZnO side which will be very effective in ultra violet emission.

Lie *et al.* [57] reported fabrication and characterization of InGaN/GaN multiple quantum well LEDs using MOCVD method. The fabricated quantum well consists of total nine layers. The contacts for electrical characterization were obtained from Ti/Al/Au to achieve high conductivity. The study confirms that high quality GaN films can be achieved using MOCVD method.

Biethan *et al.* [58] investigated photoluminescence properties of ZnO nanostructures grown over Si substrate using MOCVD technique. Different samples with ZnO nanostructures varying in the range of 20-100 nm at different temperatures ranges (500-800 °C) were prepared using MOCVD technique. They observed a decrease in nanostructure sizes with increasing growth temperature. The emission peaks for prepared samples were observed at 368 nm, 370 nm, 373 nm, 383 nm and 391 nm respectively at different growth temperatures. The shift in these peaks is attributed to quantum confinement effects. An improvement in crystalline quality of ZnO nanostructures with increasing growth temperatures has also been observed.

Addonizio *et al.* [59] deposited double textured ZnO:B film plasma etched polymer using MOCVD technique. They developed a method to produce highly textured TCO surfaces by growing ZnO:B on a buffer layer consisting of UV curved highly transparent acrylic polymer (IBA) with modified surface using RIE process. It is seen that the surface properties of double textured ZnO thin films also depend upon etched polymer properties. Double textured ZnO:B films have exhibited excellent scattering properties with good electrical properties.

Kim *et al.* [60] used MOCVD technique to fabricate ZnO based hybrid LEDs over p-GaN substrate. They used MOCVD technique with vertical wall reactor to fabricate n-ZnO film/n-ZnO nanorods/p-GaN structure. The fabricated structure has exhibited high crystallographic properties. The turn-on voltage of the fabricated structure was found to be 11V.

2.2.5 RF Sputtering

RF sputtering is one of the popular technique for growing ZnO thin films. Sputtering involves removal of surface atoms from the sputtering target due to bombardment of high energy particles. Generally, two type of sputtering methods (i) RF magnetron sputtering (ii) DC sputtering are used to deposit ZnO thin films. Among these, RF magnetron sputtering is more popular due to its simplicity, low cost and lower operating temperature. The growth of the films in sputtering is generally carried out in Ar/O_2 ambient. The argon enhances the sputtering rate and, oxygen acts as reactive gas during the deposition. The RF power can be tuned to control the sputtering yield from ZnO target.

Dang *et al.* [61] used RF sputtering to deposit ZnO thin films. Zinc target with O_2/Ar gas mixture was used for the deposition. Effect of plasma power, O_2/Ar ratio and substrate temperature variation on quality of ZnO films have also been studied. They concluded that the post annealing has improved the quality of deposited films. Gas flow rate and RF power can also be used to control the quality of the deposited films.

Kumar *et al.* [62] deposited ZnO thin films over silicon substrate using RF sputtering technique. RF power, deposition pressure and annealing temperature were maintained at 150 W, 9×10^{-3} mbar and 500-700 °C during the deposition. Influence of substrate porosity over surface morphological and optical properties have also been studied. They found that the deposition of ZnO on mesoporous substrates can have potential applications in development of gas sensors.

Hardan *et al.* [63] prepared ZnO/Si structure for photodetection applications using RF sputtering technique. Deposition pressure, sputtering power and post annealing temperature were maintained at 2×10^{-2} mbar, 200 W and 900 °C respectively during the deposition. They observed a significant enhancement in photocurrent under UV illumination for the fabricated structure. Impedance spectroscopy revealed that the basing voltage and ultraviolet light affects the grain boundary resistance considerably.

Bhavanasi *et al.* [64] studied the substrate temperature dependent light scattering properties of RF sputtered ZnO:Al thin films. The values of argon flow rate, deposition pressure, RF power and annealing temperature were 15 sccm, 8×10^{-3} mbar, 100 W and 300 °C respectively at the time of deposition. They also observed that the light scattering capability of the fabricated structure has increased with substrate temperature.

Jouane *et al.* [65] deposited ZnO thin films over ITO coated flexible substrate using sputtering technique. The post annealing temperature was varied in the temperature range of 140-180 °C. The RF power and deposition pressure was maintained at 100 watt and 8×10^{-3} mbar respectively during the deposition. The optimal performance of device was achieved for annealing temperature of 160 °C. The power conversion efficiency achieved at this annealing temperature was highest.

Effect of grain size over ethanol sensing properties of RF sputtered ZnO thin films have been reported by **Tanvaskos *et al.* [66].** ZnO thin films with different thicknesses where grain size varies from 60-130 nm have been deposited using RF sputtering technique. The deposited ZnO films have shown highest sensitivity with low ethanol concentration (10-50 ppm). The sensitivity of the deposited structure was found to be increased with operating temperature. They reported that the films with smaller grain size needs longer time to respond ethanol, but its recovery is faster than large grain size samples.

Duan *et al.* [67] deposited ZnO:Ag thin film over silicon substrate using RF sputtering technique. Firstly, a thin buffer layer of ZnO thin film was deposited over Si at 40 watt RF power. Then, ZnO:Ag thin film was deposited over the buffer layer at 100 watt sputtering power. It was observed that the ZnO thin film deposited over the buffer layer has shown larger grain size, good rectification and high carrier mobility with deep level emission. It has also been observed that the buffer layer reduces the lattice mismatch which helps to improve the surface quality of the deposited film.

2.2.6 Thermal Vapor Evaporation

Thermal evaporation technique uses resistive heating to vaporize the source material. It is a simple and low cost method to evaporate various materials. It does not require any high temperature growth and catalyst to grow thin films. High quality films can be grown using this method. This section presents some recent reports for deposition of ZnO thin films using thermal evaporation technique.

Liu *et al.* [68] demonstrated the growth and characterization of ZnO nanowires over silicon substrate using RF sputtering technique. The structural characterization of deposited films has shown high crystallinity of deposited films. The diameter and length of the grown nanowires were found to be in the range of 10-100 nm and ~10 micron respectively. They suggested that high throughput of this technique can be very advantageous in variety of nano-device applications.

Abdulgafour *et al.* [69] prepared low cost Pd/ZnO structure using thermal evaporation method. The value of load resistance for Pd/ZnO heterojunction diode under dark and illumination were found to be 80.4 KΩ and 23.5 kΩ respectively. The responsivity and quantum efficiency of the fabricated structure were found to be 0.106 A/W and 43.8 % respectively at a biasing voltage of 5 V.

Nguyen *et al.* [70] studied the infrared emission properties of ZnO nanostructures grown over Si/SiO_2 substrate using thermal evaporation technique. They observed a strong ultra violet emission with a broad emission from red to near infrared region for the grown nanostructure. The near ultra violet emission is attributed to carrier transition between ZnO and O_2 interstitials.

Feng *et al.* [71] reported the preparation and characterization of ZnO nanoflowers using thermal evaporation technique. A strong UV emission at 386 nm wavelength for grown ZnO nanoflowers has been observed. In addition to that, weak yellow-green emission has also been observed. Growth mechanism of ZnO nano flowers have also been discussed in detail.

Zaier *et al.* [72] studied the effect of post annealing temperature over surface morphological, optical and electrical properties of ZnO thin films grown by thermal evaporation. The optical bandgap of prepared ZnO thin films was found to be increased from 3.13-3.25 eV with temperature varying in the range of 200-500 °C. The variation in resistivity from 2×10^{-3}- 4×10^{-2} Ωcm has also been observed with varying annealing temperature.

Singh *et al.* [73] investigated various optical properties of ZnO thin films grown by thermal oxidation of pure metallic zinc. They grown Zn thin films by thermal evaporation and then deposited samples were oxidized at different temperatures varying in the range of 300-500°C. The films annealed at 500°C have shown highest cyrstallinity with a bandgap of 3.32 eV. The study revealed that high quality ZnO thin films can be achieved by thermal evaporation provided that annealing has been done at optimum temperature.

Ahmad *et al.* [74] grown catalyst/seed free ZnO thin films over graphene by thermal evaporation of Zn in oxygen ambient. They investigated the effect of substrate position over the surface quality of ZnO thin films. They observed that the films grown at 600 °C have shown less structural defects. They concluded that both growth temperature and substrate position plays an important role in the preparation of high quality ZnO thin films.

Periasamy *et al.* [75] investigated the time dependent degradation of Pt/ZnO based piezoelectronic generator using vacuum coating unit. They demonstrated conversion of nanomechanical energy into electrical energy by exploiting the piezoelectronic properties of ZnO nano-needles. They observed that nanogenerator performance degrades with time which is attributed to tip abrasion by repeated scanning. Table 2.1 summarizes some recent reports on ZnO nanostructures grown using different deposition techniques.

Table 2.1: Summary of studies done on growth of ZnO thin films from previously published work.

Structure Type	**Matrix**	**Technique**	**Growth Reagent**	**Growth Condition**	**Ref.**
ZnO	Au coated Si	Carbo-thermal reduction	ZnO & graphite	900°C, 30 min	[76]
ZnO nano-Tetrapods	Silicon	Vapour-Phase transport	Zn & $Zn(CH_3COO)_2$	650°C, 15 min	[77]
ZnO Nanaowires 500°C	MWCNT/Si	Thermal Vapour Evaporation	Zn	700°C, 3h	[78]
ZnO Nanaowires	Silicon	Thermal Vapour Evaporation	Zn	450°C	[79]
ZnO Nanoflakes & ZnO Nanowires	Glass	Localized Oxidation	Zinc film	300°C, 5 min	[80]
ZnO Nanaowires	Silicon at 700°C	Vapour-Phase Transport	ZnO & graphite	1100°C, 30 min	[81]
ZnO Thin Film	SiO_2	MOCVD	Diethylzinc, O_2	350°C	[82]
ZnO Nanostructures	MWCNTs/PG	Vapour-Phase Self-catalysis	Zn, ZnO & graphite	750°C, 15–30 min	[83, 84]
ZnO Nanotips	SiO_2, glass, c-sapphire	MOCVD	Diethylzinc, O_2	350–475°C, 50 Torr	[85,86, 87]
ZnO Nanowire/belts	Sapphire	Thermal evaporation	ZnO	< 1150°C	[88]
Nanoporus ZnO Film	Au coated glass	RF magnetron sputtering	Zinc	300 W, 50 mTorr	[89, 90]
n-ZnO Thin Film	Borosilicate glass	RF magnetron sputtering	Zinc	75 W, 1Pa, 200°C	[91]
n-ZnO Thin Film	Glass	PLD	ZnO	1.5–3 Jcm^{-2} at 3×10^{-7}torr,	[92]
n-ZnO NR	Au/Al_2O_3	VLS growth	ZnO & graphite	950°C, 20–30 min, 300–400 mbar	[93]
n-ZnO Nanocombs	Si Silicon	Vapour-Phase Transport	ZnO & Graphite	900°C, 30 min, 8×10^{-1}Torr	[94]
n-ZnO Nanostructures	ZnO-$Ga/SiO_2/Si$	CVD	Zinc	600°C, 30 min	[95]
n-ZnO Nanotetrapods	Quartz plate	Thermal Evaporation	Zinc	900°C	[96,97]
n-ZnO Nanaowires	Silicon	Thermal Evaporation	ZnO & Gold Catalyst	900–950°C	[98]

2.3 n-ZnO/p-Si Heterojunctions

As discussed earlier, ZnO has many potential advantages over other large bandgap materials (such as SiC and GaN), including large electron binding energy, high quantum efficiency, larger resistance at high energy radiations and possibility of wet etching. ZnO has ensured its potentiality for many optoelectronic applications such as UV detector, LEDs, gas sensors, solar cells and piezolectronic nanogenerators etc. Both n and p doped ZnO is required to develop various ZnO based devices. Since, It is really difficult to grow high quality, stable and reproducible p-type ZnO thin films, a wide attention have been given to grow n-ZnO over various p-type substrates such as Si, p-GaN and p-polymer to fabricate p-n heterojunctions. For next generation nanoelectronic devices, it is highly desirable to fabricate high quality p-n heterojunctions with lower processing temperature at larger area. In present scenario, it is important to integrate ZnO thin films with silicon technology in order to develop practical applications of ZnO thin films for a wide range of optoelectronic device applications. Silicon is having central position in semiconductor industry. Large area availability of Si with low cost and excellent quality has provided a unique opportunity to integrate Si with a variety of ZnO based optoelectronic devices. However a little progress has taken place so far in the area of electrical characterization of n-ZnO/p-Si heterojunctions. The electrical performance of n-ZnO/p-Si heterojunctions depends upon a variety of parameters such as lattice mismatches, p-n junction interfacial characteristics, built-in potential, band offsets, film thickness, operating temperature and post annealing temperature etc. This section presents some studies reported by various research groups in the area of n-ZnO/p-Si heterojunctions.

Cho et al. **[99]** fabricated n-ZnO/p-Si heterojunction using RF sputtering technique. The RF power and sputtering time was maintained at 70 watt and 1 hour respectively. To avoid inter diffusion of Si and Zn atoms, rapid annealing at 600 °C was done for fabricated samples. They observed that the post annealing has improved the crystalline quality of deposited film which also results in enhanced rectification ratio of fabricated p-n heterojunction diode. The barrier height of the fabricated structure was found to be decreased from 0.078-0.033 eV. This abrupt reduction in barrier height with increased annealing temperature is attributed to diffusion of boron into n-ZnO.

It is important to investigate the electrical characteristics of n-ZnO/p-Si heterojunction to ensure their potentiality in variety of optoelectronic device application. **Aksoy *et al.* [100]** studied the effect ambient temperature on electrical characteristics of n-ZnO/p-Si heterojunction device using sol-gel technique. They varied the ambient temperature from 296-383 K to investigate the effect of temperature over ideality factor and barrier height of the fabricated heterojunction. The value of ideality factor was found to be decreased with increasing ambient temperature whereas barrier height was found to be increased with ambient temperature. The value of open circuit voltage and short circuit current were found to be 0.19 V and 8.03×10^{-8} A at 100 Wcm^{-2} intensity.

Lee *et al.* [101] optimized n-ZnO/p-Si heterojunction for photodiode applications. n-ZnO thin films were sputter deposited over p-Si substrate. The deposition temperature was taken as 300 °C, 400 °C, 480 °C and 550 °C during the deposition. Ar/O_2 ratio was maintained at 6:1 during the deposition. The photoelectric properties of the fabricated diode have also been tested using monochromatic red light of 670 nm wavelength. The diode fabricated at the substrate temperature of 480 °C have shown maximum photocurrent and responsivity whereas ZnO film deposited at 550 °C have exhibited best crystalline quality and schotiometery. They concluded that the quality of diode junction plays an important role for fabricating efficient photodiode.

Kim *et al.* [102] investigated the photoresponse of n-ZnO/p-Si and n-ZnO/n-Si heterojunctions using RF sputtering technique. They observed that all n-ZnO/p-Si heterojunctions have exhibited a strong rectification whereas the rectification of n-ZnO/n-Si heterojunction was found to be weak. The photoelectric effect of the fabricated heterojunctions has been tested using 670 nm red light. Kim *et al.* concluded that photoelectric properties of the fabricated structure also depend upon stoichiometry and crystalline quality of deposited films. High quality of ZnO thin films can pass the visible light in p-Si more effectively under reverse bias condition which can generate high density photocurrent.

Solylu *et al.* [103] investigated the effect of Mg doping on electrical and optical properties of n-ZnO/p-Si heterojunction prepared by spin coating technique. The AFM study of the deposited ZnO films revealed the nano-particle growth of deposited film. Electrical characterization shows that the fabricated n-ZnO/p-Si heterojunction have exhibited the non ideal behavior with ideality factor more than 1 which is probably due to interface states, interfacial layer and series resistance. A strong influence of Mg doping over R_S versus V characteristics have also been observed. They concluded that electrical performance of n-ZnO/p-Si heterojunction can be controlled by Mg doping.

Urgessa *et al.* [104] grown self aligned ZnO nanorods over p-Si seeded substrate using chemical bath deposition at 80°C. The I-V characteristic exhibited very high rectification for the fabricated n-ZnO/p-Si heterojunction. The capacitance-voltage characteristics have also been investigated to study n-ZnO/p-Si heterojunction properties. Based on interface states and energy band diagram, they concluded that the hopping of charge carriers through multistep tunneling could be the dominating current transport mechanism in n-ZnO/p-Si heterojunctions.

Zhang *et al.* [105] grown nanocrystalline ZnO thin films over p-Si using sol-gel process. The AFM study revealed that the ZnO thin film consist of 50-100 nm grains with hexagonal wurtzite structure. The electrical and current transport properties of ZnO/Si heterojunction have been investigated using temperature dependent I-V and C-V measurements. The temperature dependent I-V study suggested that the multi step tunneling current is the dominating mechanism for forward conduction of ZnO/Si heterojunction. The activation energy of the saturation current was found to be 0.26 eV. The capacitance-voltage analysis revealed that the nature of the heterojunction was abrupt and built-in potential of the fabricated junction was found to be 1.49 V.

Wang *et al.* [106] deposited ZnO over p-Si using atomic layer deposition technique. They observed that the use of AlN layer as buffer layer has changed the direction of growth for ZnO thin film. The buffer layer (AlN) has also improved the crystalline quality of ZnO thin films significantly. The value for valance band offset was found to be 0.83 eV, 2.95 eV and 3.06 eV respectively for AlN/Si, AlN/ZnO and ZnO/Si heterojunctions respectively. They also observed that the band alignment was modified by 0.72 eV after introduction of the buffer layer.

Buffer layer between ZnO and Si can reduce the lattice mismatch between ZnO and Si which can improve the quality of grown films. **Lu *et al.* [107]** investigated the photoelectrical properties of n-ZnO/p-Si heterojunction by inserting Al_2O_3 as buffer layer. The deposition was done using atomic layer deposition. They observed that the introduction of Al_2O_3 buffer layer has improved the crystalline quality of deposited films. They concluded that the introduction and optimization of ZnO as buffer layer can result in high quality preparation of ZnO/Si heterojunctions.

Hazra *et al.* [108] fabricated p-Si/n-ZnO heterojunction diode using thermal evaporation method. Firstly, they grown Si nanowire array over p-Si substrate using electrodeless metal deposition and etching methods. The rectification, turn-on voltage and barrier height of the fabricated p-n heterojunction diode were found to be 190 at ± 2V, 0.5 V and 0.727 eV respectively. They also investigated the ultraviolet light detection properties of n-ZnO/p-Si heterojunction diodes.

Romero *et al.* [109] studied the electrical properties of ZnO/c-Si heterojunction using chemical spray pyrolysis technique. The crystallographic orientation of ZnO thin film was found to be (001). The stability for the fabricated heterojunction for a temperature range of 20-150 °C was found to be excellent. It was observed that breakdown voltage and turn-on voltage has decreased with temperature whereas the saturation current has increased from 0.42-0.67 μA with temperature. The effect of temperature on current transport mechanism of the n-ZnO/p-Si heterojunction have also been studied and reported.

Current transport studies of n-ZnO/p-Si heterojunction was investigated by **Chen *et al.* [110]** using plasma immersion ion implantation and deposition method. They also investigated that how nitrogen doping affects the structural, optical and electrical properties of the fabricated heterojuncton. The I-V characteristics of undoped n-ZnO/p-Si junction has exhibited ohmic behavior whereas in nitrogen doped n-ZnO/p-Si heterojunction, the current was proportional to V^2 which is attributed to space charge limited current phenomenon.

Growth parameter also affects the quality of heterojunctions. **Zhang *et al.* [111]** investigated the effect of growth conditions on photovoltaic properties of ZnO/Si heterojunctions using DC reactive sputtering technique. They reported that the growth temperature and oxygen pressure plays a significant role in enhancing photovoltaic properties of the fabricated ZnO/Si heterojunctions. The values of open circuit and short circuit voltage per cm^2 were found to be 350 mV and 2.5 mA respectively. The photoconductive behavior of the fabricated n-ZnO/p-Si heterojunction has also been studied in detail.

2.4 ZnO Based UV Photodetector

Photodetector generally works in third quadrant. When absorbed photons generate electron-hole pairs, only those electron-hole pairs generated in the depletion region, or very close to that, have a chance to contribute electric current, because there is a strong electric field there to separate the two different charge carriers. The ones outside the depletion region quickly recombine and vanish.

In reverse biased p-n junction, the width of depletion region increases as we increase the applied reverse bias voltage across the diode (proportional to the square root of the voltage). So, by applying a larger voltage, more of the incident photons are converted to electric current and the efficiency increases (as long as we make sure the increased leakage current remains at a manageable level). On the other hand, in forward bias, the width of the depletion region reduces, so, only a small portion of the incident photons get converted to electric current.

As mentioned earlier, ZnO nanostructures and thin films are potential functional materials for ultraviolet light detection applications. A variety of structures such as metal-semiconductor, metal-semiconductor-metal and p-n junction have been reported in literature for UV detection applications. In photodetectors, responsivity is one of the essential parameter which measures the performance of the photodetectors. The responsivity can be defined as the ratio of photocurrent generated to the applied optical power. Generally, the photogeneration of ZnO based photodetector is governed by adsorption and desorption of oxygen. Several factors such as doping concentration, crystallographic orientation, micro-pores, thickness, grain size, annealing temperature and encapsulation of ZnO film affects the photodetection properties of photodetectors. This section presents some recent studies reported by various research groups on ZnO based photodetectors.

Hardan *et al.* [112] reported n-ZnO/p-Si heterojunction based photodiode using low temperature hydrothermal process. The fabricated detector exhibited an excellent rectification of 370 at ±10V. The highest value of responsivity was found to be 0.38 A/W at 360 nm wavelength. Furthermore, the behavior of the photodiode was found to be visible blind which ensures that n-ZnO/p-Si heterojunctions can work as a UV detector with visible blind response.

Keramatnejad *et al.* [113] investigated the effect of porous silicon substrate with various nano structures over UV detection properties of n-ZnO/p-Si photodetectors. They observed that the porosication of Si has increased the sensitivity and selectivity of the detector. Electrochemical anodic etching was used to prepare different porous substrates at different current densities, anodization times and acid concentrations. Their results concluded that the samples with highest porosity have shown highest sensitivity of 2×10^4 at -3V whereas crystalline silicon substrate has shown highest responsivity of 1109 A/W at 365 nm respectively.

Hwang *et al.* [114] studied ultraviolet response of p-Si/SiO_x/i-ZnO/n-ZnO heterojunction (p-i-n) fabricated using RF sputtering technique. They reported that the leakage current in fabricated p-i-n photodetector was three times less than the conventional p-n junction photodiode. It has also been observed that the introduction of i-ZnO has increased rejection ratio from 7 to 12.

Zhang *el al.* [115] investigated the UV detection potentiality of n-ZnO/MgO/p-Si heterojunction visible blind ultraviolet photodetector using molecular beam epitaxy technique. The rectification of the fabricated heterojunction was found to be ~10^4 at ±2 V. They reported that MgO buffer layer between ZnO and Si acts as a barrier layer for the transportation of minority carriers which improves the performance of the fabricated detector. The photoresponse spectrum of the fabricated structure reveals the visible blind detectivity of the UV detector with a sharp cutoff wavelength of 378 nm.

Xu *et al.* [116] reported fabrication and characterization of ZnO based metal-semiconductor-metal photodetector with interdigital configuration. The value of photocurrent under illumination of 365 nm wavelength was found to be 44.89 μA at the biasing voltage of 6 V. The PL analysis of the detector has shown two peaks, the one is near band edge emission and the other peak is deep level visible emission.

Vasudevan *et al.* [117] investigated that how electrode dimension and length of the nanostructures affect the ultraviolet detection capabilities of ZnO based MSM photodetectors. They fabricated MSM detector by arranging the interdigitated electrodes in square form. The length of ZnO nanostructures was varied from 20-70 nm using hydrolysis method. Their study revealed that the responsivity of the detector enhances with increasing length of the rods whereas it decreases with diameter of the rods. They also observed that the responsivity of the detector depends upon spacing and width of the fingers.

Guao *et al.* [118] reported ZnO nanowire based ultraviolet detector with different interdigital electrode distances using dielectrophoresis method. The distance between two adjacent electrodes got varied from 6.5-10 μm and the length of the electrodes was 500 μm. Results shown that the device with electrode distance of 6.5 μm have exhibited maximum responsivity of 40 A/W at 10 V. The rising and decaying stages of the photocurrent are attributed to relaxation process of deep level states and surface states. They also observed that the fabricated detector has exhibited good response at high temperature.

Somvanshi *et al.* [119] grown Pd/ZnO UV schottky diode over n-Si substrate with Sn as buffer layer using vacuum coating technique. The values of turn-on voltage, barrier height and ideality factor were found to be 0.50 V, 0.75 eV and 2.67 respectively. They investigated the UV response of the fabricated detector using UV lamp of 365 nm wavelength for a voltage range of -3 to 3 V. The value of responsivity was found to be 0.20 A/W for the fabricated photodetector.

Alkis *et al.* [120] fabricated n-ZnO/p-Si based UV/Visible photodetector using atomic layer deposition technique. They also studied the effect of growth temperature on the photodetection properties of fabricated ZnO/Si photodiode. The growth temperature was varied in the range of 80-250°C. The rectification of the ZnO photodiode was found to be 1000. The ultraviolet and visible region responsivity for the fabricated photodetector was found to be 30-37 mA/W and 74-80 mA/W respectively at a reverse bias voltage of 0.5 V. They concluded that the performance of the detector can be tuned by varying the growth temperature in atomic layer deposition.

Ko *et al.* [121] reported fabrication and characterization of ZnO nanorods based ultraviolet photodetectors using selective hydrothermal synthesis. They used shadow masking for depositing ZnO seed layer between Au/Ti electrodes to bridge the electrodes. The fabricated photodiode has exhibited a high photocurrent of 1.91×10^{-4} A for biasing voltage of 10 V under 365 nm UV illumination. They also optimized the channel width to achieve the high performance of the UV detector. For the channel width of 15 μm, they found the highest on-off ratio of 37.4.

Zhang *et al.* [122] reported modeling and characterization of ZnO based UV detector with graphene as transparent contact. They synthesized ZnO nanowires using low cost electro-deposition technique. The fabricated detector has shown a high responsivity of 10^4 A/W in near ultraviolet region. The urbach energy for fabricated detector was found to be 83 meV. They demonstrated that the responsivity of the detector has reduced with excitation power. They also proposed photoconductive mechanism which suggests that modulation of conductive surface due to variation in surface depletion layer is responsible for high photoconductive gain.

Baltakesmez *et al.* [123] grown n-ZnO films over p-Si substrate using electrochemical deposition technique. The turn-on voltage of the fabricated diode was found to be 1.2 V and 2.1 respectively. They observed an enhancement of 1000X in current with illumination wavelength of 400 nm. They concluded that the electrochemical deposition can be simple and cost effective method to develop ZnO based photodetectors. In addition, they studied various film defects which results in high ideality factor so that rectification of fabricated detectors can be improved.

Chen *et al.* [124] reported fabrication of p-ZnO/n-Si photodiodes prepared by ultrasonic spray pyrolysis technique. The nitrogen-indium doped ZnO films were deposited over Si substrate using ultrasonic spray pyrolysis technique. The fabricated photodiode exhibited high responsivity in 400-700 nm and 700-1000 nm wavelength regions. The values of responsivity and quantum efficiency were found to be 0.20 A/W and 47.7 % respectively for 530 nm wavelength.

Shichen *et al.* [125] grown ZnO nanowall based networks over silicon substrates for UV detection using plasma assisted molecular beam epitaxy technique. The thickness of the film was 10-20 nm. The values of dark current and responsivity for the fabricated detector were found to be 6 μA and 15 A/W respectively for a biasing voltage of 5 V. The detector exhibited a sharp responsivity in wavelength region of 250-360 nm with a sharp cutoff at 360 nm. The magnitude of visible rejection was found to be more than of 2 orders for the fabricated detector. Table 2.2 summarizes some of the studies reported in the area of ZnO thin film based photodetectors for ultraviolet light detection.

Table 2.2: Summary of studies done on ZnO based detectors from previously published work.

Device structure	Method	Electrodes	Detecting range	Dark current	Responsivity	Ref.
n-ZnO/p-GaN	Sputtering	Ni/Au;In	UV	-	~10^{-6} A/W at 0 V bias (370 nm)	[126]
p-NiO/ i-ZnO/n-ITO	E-Beam		UV	10 nA/cm^2 At -5V	-	[127]

Ni/n-ZnO/p-Si	RF Sputtering	Ni	UV/Vis	1 µA (at −8 V)	110 A/W (850 nm) and 210 A/W (390 nm) at −5 V bias	[128]
n-ZnO/p-SiC	MBE	Au/Al, Au/Ni	UV	2×10^{-4} A/cm^2 At -10V	0.045 A/W At -7.5V	[129]
n-ZnO/p-Si	RF Sputtering	Au-Al	UV/Vis	-	0.35 A/W (650 nm) at −5 V bias	[130]
n-ZnO/p-Si	Sol-Gel	Au	UV/Vis	7.6×10^{-5} A/cm^2 (−5 V)	-	[131]
n-ZnO/p-Si	RF Sputtering	Ni/Au, Ti/Au	UV/Vis	4.7×10^{-6} A/cm^2 (−3 V)	-	[132]
ZnO:Al/p-Si	Sol-gel	Au	UV/Vis	-	0.22 A/W at −5 V bias (420 nm)	[133]
n-ZnO/SiO_2/p-Si	Ultrasonic Spray pyrolysis	Ni/Au; Ti/Pt/Au	UV/Vis	4.98×10^{-10} A (−1 V)	0.225–0.297 A/W at −1 V	[134]
n-ZnO/i-MgO/ p-Si	MBE	Ti/Au, In	UV	<1 nA (at −2 V)	-	[135]
n-ZnO/p-Si	RF Sputtering	In , Au/Al	UV/Vis	-	0.5 A/W (310 nm) At −30 V	[136]
AlO coated n-ZnO/p-Si	RF Sputtering	Au-Al, In	UV/Vis	-	0.06 A/W at −5 V bias (310 nm)	[137]
n-ZnO/p-Si	RF Sputtering	In; Cu	UV/Vis	-	0.14–0.29 A/W at −5 V	[138, 139]

2.4 Summary and Concluding Remarks

This chapter presents some important state-of-the-art research on ZnO thin films, ZnO/Si heterojunctions and their application in UV detection applications. The literature survey presented in the above sections can be summarized as follows:

- ZnO has emerged as a potential candidate for a variety of nanoelectronic and optoelectronic devices applications. Many potential advantages of ZnO such as wide bandgap (3.37eV), high exciton binding energy, low temperature processing, abundance in nature, low cost, nontoxicity and high resistivity ensures its usability in many potential applications such as gas sensing, UV sensors, lasers, UV LEDs, Solar cells, transparent electronics &

piezoelectronic generators etc. ZnO nanostructure exhibits large surface to volume ratio, high elasticity and single crystalline nature which plays an important role in lifetime of the nano-devices. In short, ZnO thin films and ZnO based heterojunctions can be explored for variety of nano-electronic and photonic device applications.

- The advances in low cost growth of ZnO nanostructures over different substrates have made a solid foundation for ZnO to use it in the development and commercialization of many nanoscale devices at large scale. However, the quality of ZnO nanostructures and films strongly depends upon the growth conditions and deposition parameters of a specific substrate. Various ZnO based heterojunctions with different p-type substrates such as GaN, 4H-SiC, Si and PFO polymers have been reported in past. Among these, silicon is having central position in semiconductor industry with many advantages such as high quality and availability of large area p-type substrate with lower cost. ZnO nanostructures grown over p-type silicon substrates also provide a good choice to test the capability of ZnO in several optoelectronic device applications. Although many sincere efforts have been made by researchers to grow high quality ZnO thin films/nanostructures but still, there exist many significant challenges in the synthesis and growth of these films. Controlled and reliable growth of films, crystallographic orientation and density of nanostructures are some issues which needs a significant attention. In addition, different physical and growth parameters such as film thickness, substrate temperature, applied power, flow rates and annealing temperature also plays an important role in achieving high quality films. Based on previous work progress it is important to investigate the effect of all these parameters over structural, optical and electrical parameters, so that optimum performance of ZnO thin film based optoelectronic devices can be achieved. A systematic study to optimize all these physical and growth parameter using a particular deposition method is still missing in the reported literature and needs a systematic investigation.

- Difficulty in achieving reliable and reproducible p-type doping has made p-doping an unsolved problem. Low solubility of p-type dopant, spontaneous generation of donor like defects, relatively deeper acceptor states and the difficulty in impurity substitution at host atom sites are the probable reasons for this difficulty. Many efforts are going on by various research groups to improve the performance of ZnO/Si heterojunctions at room temperature. In addition to this, it is also important to study the carrier transport mechanism of n-ZnO/p-Si heterojunctions before their adoption in the fabrication of nanoelectronic devices. Temperature dependent stability of these heterojunctions also needs significant investigation in order to ensure the reliability of these heterojunction based devices at high temperature ranges. Estimation of barrier height and Richardson constant considering the barrier inhomogeneities at the interface of n-ZnO/p-Si heterojunction also needs to be investigated systematically. It is apparent that there is enough scope left for the researchers to work in this area.

- Wide bandgap (3.37 eV) and larger surface to volume ratio of ZnO nanostructures as compared to bulk ZnO results in efficient absorption of ultraviolet light. The photoconductivity of ZnO based ultraviolet detectors slightly depends upon photon absorption in active region and largely depends upon hole trapping mechanism because of adsorption and desorption of oxygen atoms at ZnO surface. The ZnO crystal quality, fabrication process, substrate quality and electrode material also plays its important role in the performance of ZnO based UV detectors. However, a little work is available on ZnO nanostructures based UV detectors in literature, it is important to investigate the ultraviolet light detection properties of n-ZnO/p-Si heterojunction devices so that the usability of these structures can be ensured in variety of civil and military applications.

Finally, the literature survey presented in this chapter concludes that there is enough scope to study ZnO thin films, n-ZnO/p-Si heterojunctions and its application in ultraviolet light detection. All these research gaps have motivated us to study ZnO thin films and ZnO thin film based heterojunctions for ultraviolet light detection applications.

CHAPTER 3

Fabrication and Characterization Techniques for n-ZnO/p-Si Heterojunctions

This chapter presents the basic working principle of the deposition techniques that has been used to prepare thin film heterojunctions. It also describes various structural, optical and electrical characterization techniques used for the characterization of ZnO thin films and heterojunctions.

3.1 Introduction

Thin film based optoelectronic devices have drawn a wide attention of researchers in recent years. Bulk materials have proved their potentiality for transparent electronic applications but, optoelectronic device application demands thin films so that the potentiality of these materials can be fully utilized in these applications. ZnO has emerged as a potential candidate for optoelectronic and microelectronic applications due to its unique and favorable properties. In order to satisfy the requirements of preparing high quality ZnO thin films, different thin film deposition techniques have been used by researchers in past. This chapter presents the working principles of RF sputtering and thermal evaporation techniques to grow high quality ZnO thin films for optoelectronic device applications. The basic working mechanisms of various structural, optical and electrical characterization techniques such as XRD, AFM, SEM, TEM, Ellipsometery, I-V and C-V etc. have also been presented.

3.2 Thin Film Deposition Techniques

3.2.1 Sputtering

Sputtering is one of the widely popular technique for depositing transparent conducting oxides. It is widely used to deposit thin films of different materials over different substrates. Its many potential advantages such as low temperature deposition, high uniformity, good adhesion of films over the substrate, ability of depositing many compounds from elemental targets and long-term stability of the process with lower deposition cost makes it highly popular technique for depositing thin films.

When a material in solid form is bombarded by high energy ions at any temperature, the surface atoms of the material may get sufficient energy so that they can come out from the target surface and this process is called as sputtering. The sputtering technique gives highly crystalline films with good uniformity over the large areas. High controllability over various deposition parameters such as sputtering power, gas flow rate and substrate temperature makes it a potential choice in semiconductor manufacturing where mass production with large area deposition is desired. Furthermore, the spitting issues that arise in thermal evaporation for high melting point materials do not occur in sputtering method. Fig.3.1 and 3.2 shows the schematic diagram and experimental setup of RF sputtering technique.

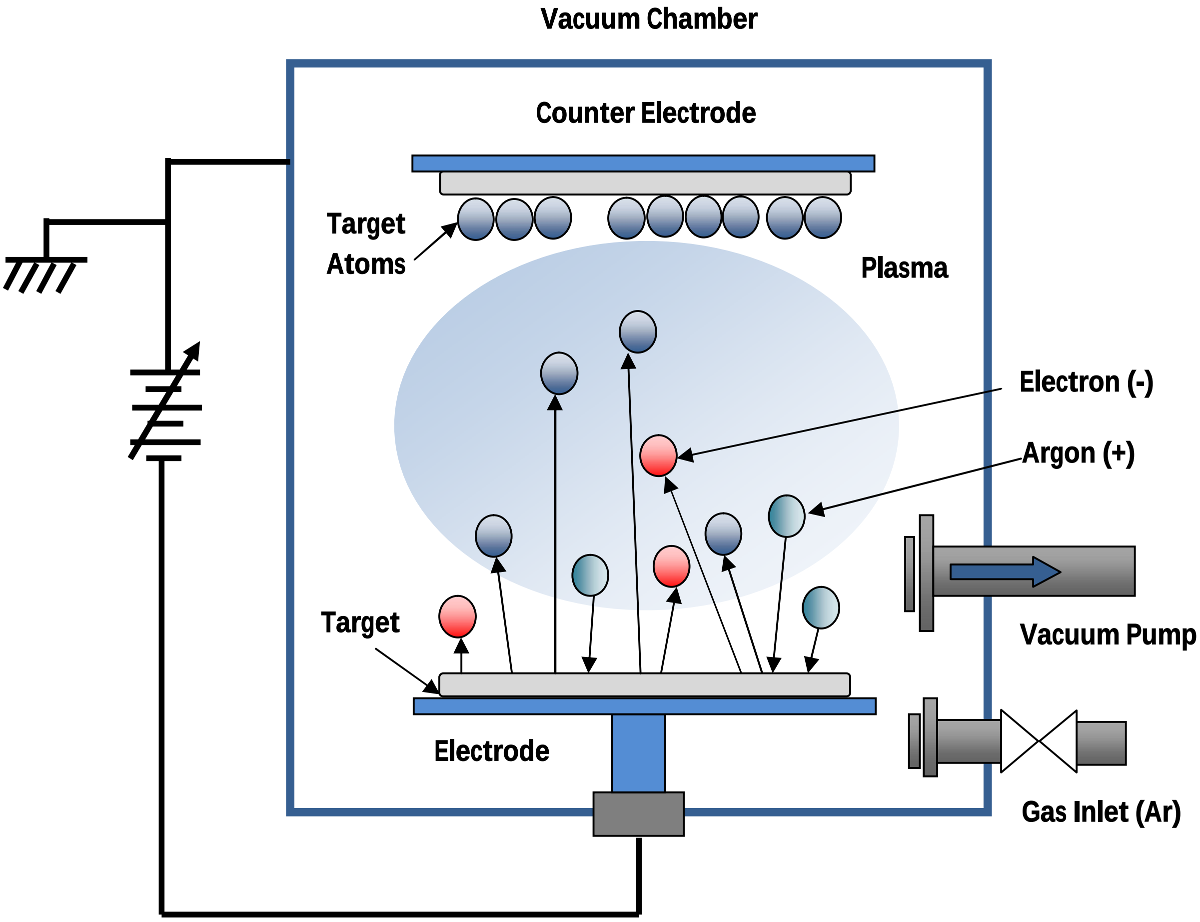

Fig.3.1 Schematic diagram of RF sputtering technique.

In sputtering process, high energy particles usually inert gases such as argon is used to withdraw the surface atoms from the source material (generally called as sputtering target). Sputtering uses controlled injection of argon in high vacuum environment (generally varying between 10^{-5}-10^{-7}mbar) in order to improve the mean free path of sputtered atoms with high purity and controllability. The high vacuum and controlled argon flow rate is sufficient to support the dense plasma between two high voltage electrodes. When the RF generator is turned on, an electric field gets stabilized between the target and substrate. In first phase of alternate supply, the biasing of the substrate is at higher potential as compared to the target. Under these conditions, any electron present in the chamber due to some background radiations or due to electron ejection from target, accelerates towards the substrate and collides with argon atoms on the way. This collision between high energy electrons and argon atoms results in positive argon ions and additional electrons. These ionized argon atoms are attracted towards the sputtering target in order to withdraw the material particles from target. The secondary electrons generated during this process again accelerate towards the substrate which leads to more collision and ionization. The argon ions which strikes the sputtering target can bounce back, can be adsorbed over the surface, can implant itself into the target or can remove the target surface ions. The argon ions accumulated over the target surface during this process increases the target potential which results in self-biasing that can hamper the acceleration of other argon ions towards the target. This accumulation of the argon ions over the target surface can be a serious issue in the case of insulating targets. However, the RF supply with quick potential reversal do not allows the ions to get buildup over the surface. In the second phase of the RF supply, the potential of the target become higher than the substrate which results in no deposition and argon ions will move away from the target which will minimize the self biasing. This self biasing is a serious issue in dc sputtering for insulating targets. As a consequence DC sputtering is generally preferred for conducting materials and RF sputtering can be used for depositing semiconductor and non-conductive materials. In RF magnetron sputtering, the magnets near the target increase the electron travel path which results in many more collisions and hence plasma density increases. In addition to this, magnetic fields near the target traps the electrons in its vicinity and keep the electrons away from the substrate which reduces substrate heating and film damage due to high energy electrons. AC current in RF range prevents the self biasing of the sputtering target which enables the deposition of the insulating films too.

Fig.3.2 Experimental setup of RF sputtering system (Company: Advanced Process Technologies, India).

3.2.2 Thermal Evaporation:

Thermal evaporation is one of the popular deposition technique in which electrical energy is used to vaporize the solid material by heating it to sufficiently high temperature. In thermal evaporation, a high current is passed through the filament/crucible which is generally made-up of metals like tungsten, molybdenum or tantalum so that it can sustain at very high temperature. The selection of filament/crucible material is dictated by the evaporation temperature and chemical reaction between the material and crucible. Fig.3.3 shows the schematic diagram of thermal evaporation system. When high electrical current is passed, the material in the crucible gets evaporated and condenses over the substrate in order to form thin film. Generally, low deposition pressure in the range of 10^{-5}-10^{-7} mbar is required to avoid the reaction between the vapor and atmosphere. At lower deposition pressure, the mean free path of evaporated material and vacuum chamber have the same order, so that these evaporated particles travel in a straight line from source to substrate. High vacuum is also necessary condition to obtain contamination free films. Fig. 3.4 shows experimental setup for thermal vapor evaporation system.

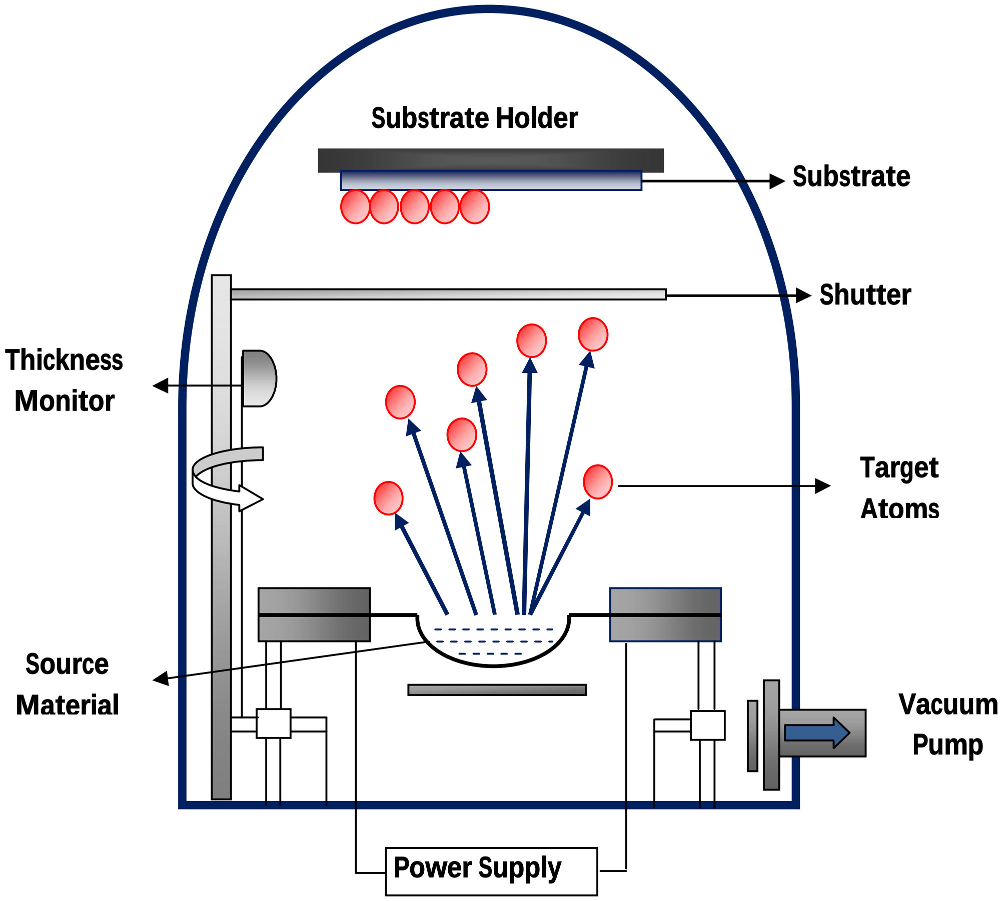

Fig.3.3 Schematic diagram of thermal vapor evaporation technique.

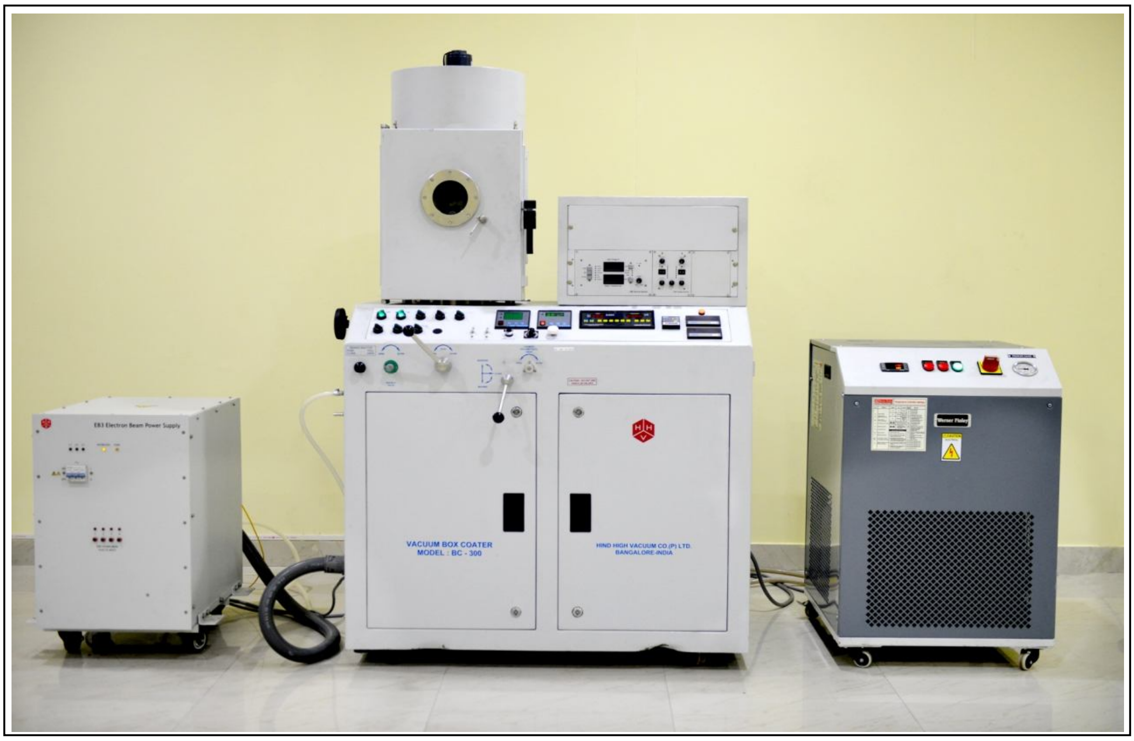

Fig.3.4 Experimental setup of thermal vapor evaporation technique (Model: BC-300 HHV).

3.3 Structural and Surface Morphological Measurement Techniques

3.3.1 X-Ray Diffraction

X-Ray diffraction is an important characterization technique to study the atomic spacing and crystal structure of deposited films [140]. A variety of micro structural parameters such as grain size, lattice constants, dislocation density, stress and strain can be derived from XRD data. X-Ray diffraction's basic working principle is constructive interference of crystalline sample and monochromatic X-rays. In XRD, cathode ray tube generates the X-rays which are filtered to produce monochromatic light. This monochromatic light is collimated and directed over the sample. The interaction of X-Ray and sample gives the constructive interference when it satisfies the Bragg's law (i.e. $n\lambda=2d\sin\theta$). Where n is integer, λ is wavelength, d is the inter-plane spacing in the crystal lattice and θ is the angle between incident beam and sample space. The inclined lines shown in Fig.3.5 shows the distance between the planes defined using miller indices h, k and l. When X-ray incidents on the sample, it gets reflected from the sample and passes through several slits such as collimator and filter before reaching to the detector. The samples are scanned through all 2θ angles so that all possible diffraction directions due to random orientation of the material can be obtained. These diffraction peaks obtained from XRD gives the identification of the desired material. The experimental setup of X-Ray diffractometer is shown in Fig. 3.6. The different microstructural parameters such as crystalline size (G), lattice constants (a,b,c), dislocation density (δ), residual stress (σ) and strain (ε) that can be derived from XRD data are as follows [141]:

$$G = \frac{0.9\lambda}{\beta\cos\theta} \tag{3.1}$$

$$\delta = \frac{1}{G^2} \tag{3.2}$$

$$a = b = \sqrt{\frac{1}{3}}\frac{\lambda}{\sin\theta} \tag{3.3}$$

$$c = \frac{\lambda}{\sin\theta} \tag{3.4}$$

$$\sigma = -233\frac{c_{film} - c_{bulk}}{c_{bulk}} \tag{3.5}$$

$$\varepsilon = \frac{\beta}{4\tan\theta} \tag{3.6}$$

Where λ is X-ray wavelength, β is full width at half maximum (FWHM), θ is Bragg's angle and c_0 (5.206 Å) is the unstrained lattice constant for bulk ZnO.

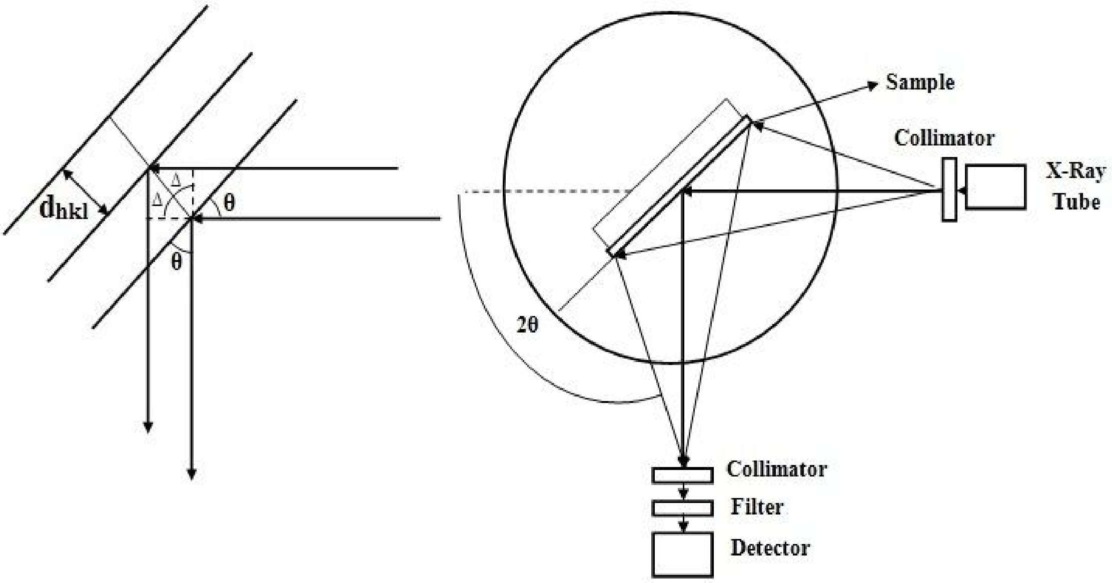

Fig. 3.5 Basic working principle of X-Ray diffraction technique.

Fig. 3.6 Experimental setup of X-Ray diffraction system (Model: PANalytical X'Pert Pro).

3.3.2 Scanning Electron Microscope (SEM)

The Scanning Electron Microscope generally produces largely magnified images of deposited films using electrons so that surface morphology of the deposited films can be analyzed [142]. Fig. 3.7 and 3.8 shows the basic working principle and experimental setup of SEM. An electron gun at the top of the microscope is used to produce high energy electron beam. The beam travels vertically through the electromagnetic fields and lenses under vacuum to fall over the sample surface. When the focused electron beam strikes the sample surface, X-Rays, secondary electrons and back scattered electrons are ejected from the sample which are collected by detectors and converted into the signals that can be seen at computer screen.

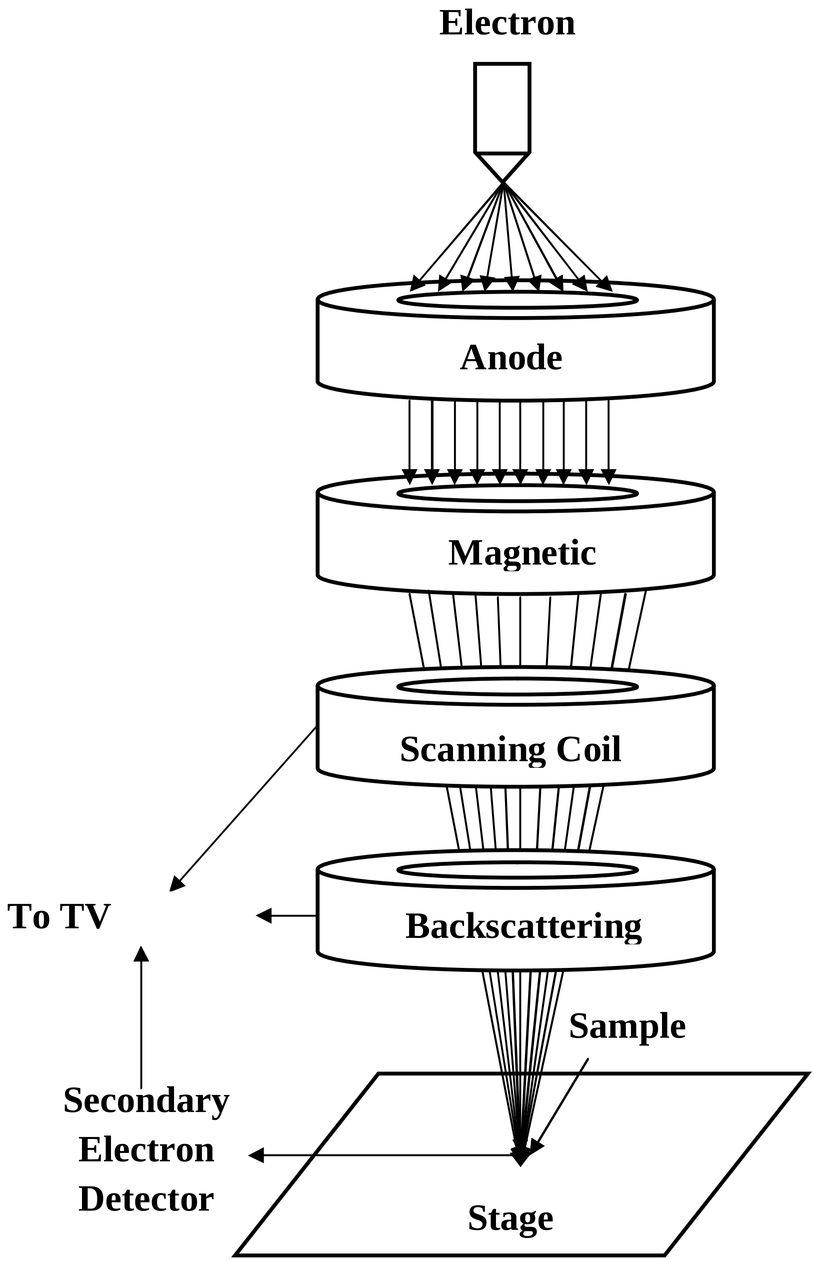

Fig.3.7 Basic working mechanism of scanning electron microscope.

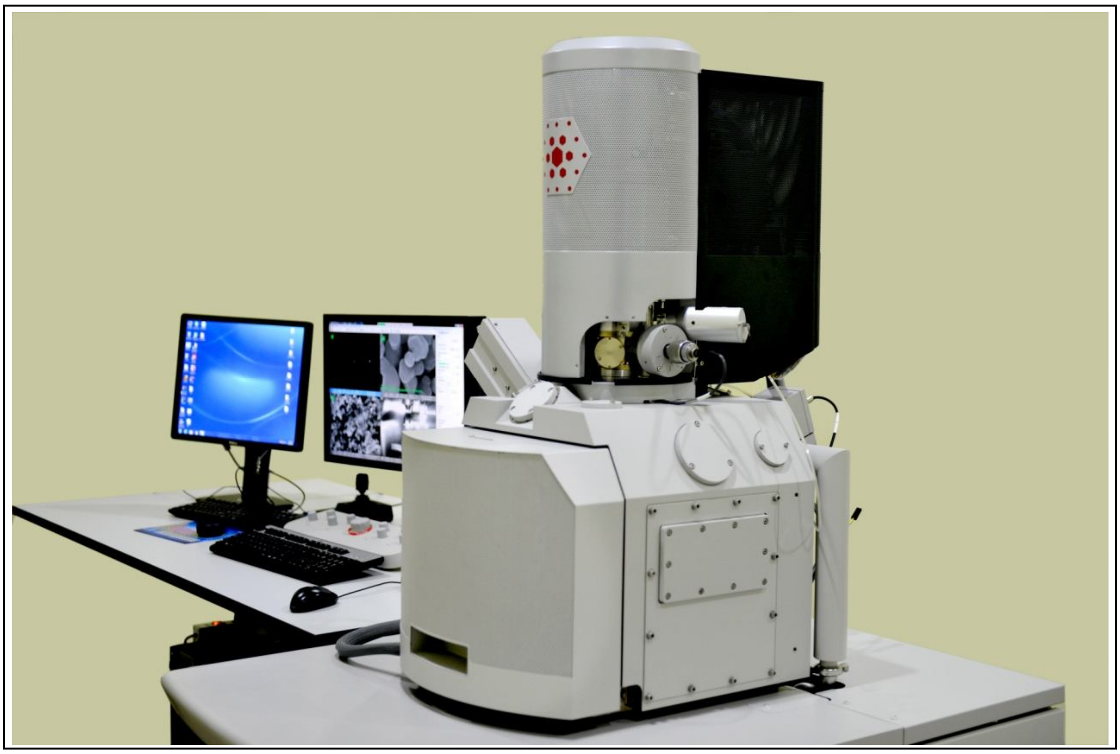

Fig.3.8 Experimental setup of scanning electron microscope (Model: Nova Nano FE-SEM 450).

3.3.3 Atomic Force Microscope (AFM)

The Atomic Force Microscope (AFM) is used to obtain surface forces and images at nano and micro level [142]. The basic working principle of AFM is shown in Fig.3.9. The cantilever spring is attached with standard microscopic tip. The basic working of AFM depends upon the bending of the cantilever spring when some external force is applied. When an adhesive interaction between tip and surface takes place, very sensitive cantilever bending due to surface and tip contact comes into picture. In order to detect this bending, a laser beam from the laser source is focused on the cantilever that reflects from cantilever and reaches towards the position sensitive detector as shown in Fig. 3.9. Depending upon the deflection of cantilever, the position of reflected laser beam changes. The position sensitive detector senses this deviation and converts this change into electrical signal. The surface imaging of the surfaces in AFM can be done using two measurement methods. (i) Contact Mode (ii) Tapping Mode. In contact mode, physical contact between sample and tip takes place. The electronic feedback maintains the resulting defletion at a constant value by changing the Z position and thus the force is measured. In tapping mode, the cantilever tip is forced to vibrate near resonant frequency. As the vibrating tip approaches the surface, the vibration amplitude of the cantilever will decrease and the interaction force between the tip and the surface will shift the resonant frequency. In tapping mode, the surface is scanned in terms of change in oscillation amplitude. The atomic force microscope can achieve a lateral resolution of 0.1-10 nm. Fig. 3.10 shows experimental setup for atomic force microscope.

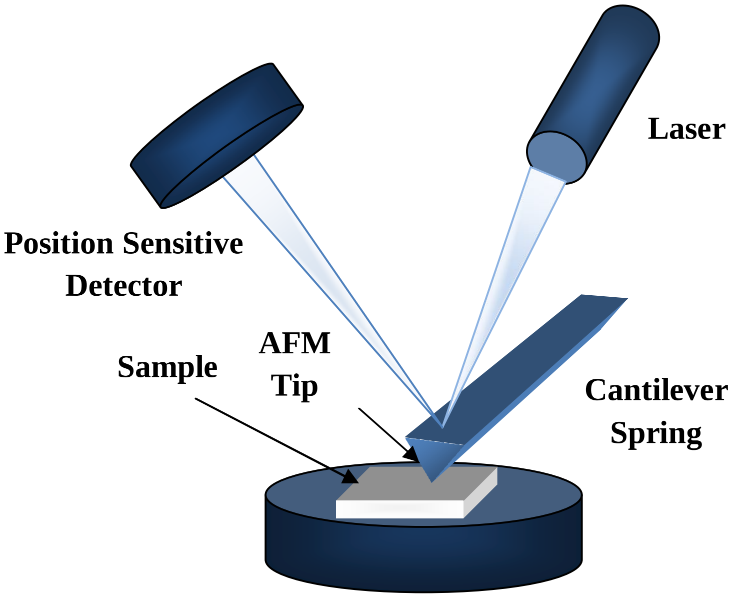

Fig.3.9 Basic working mechanism of atomic force microscope in contact mode.

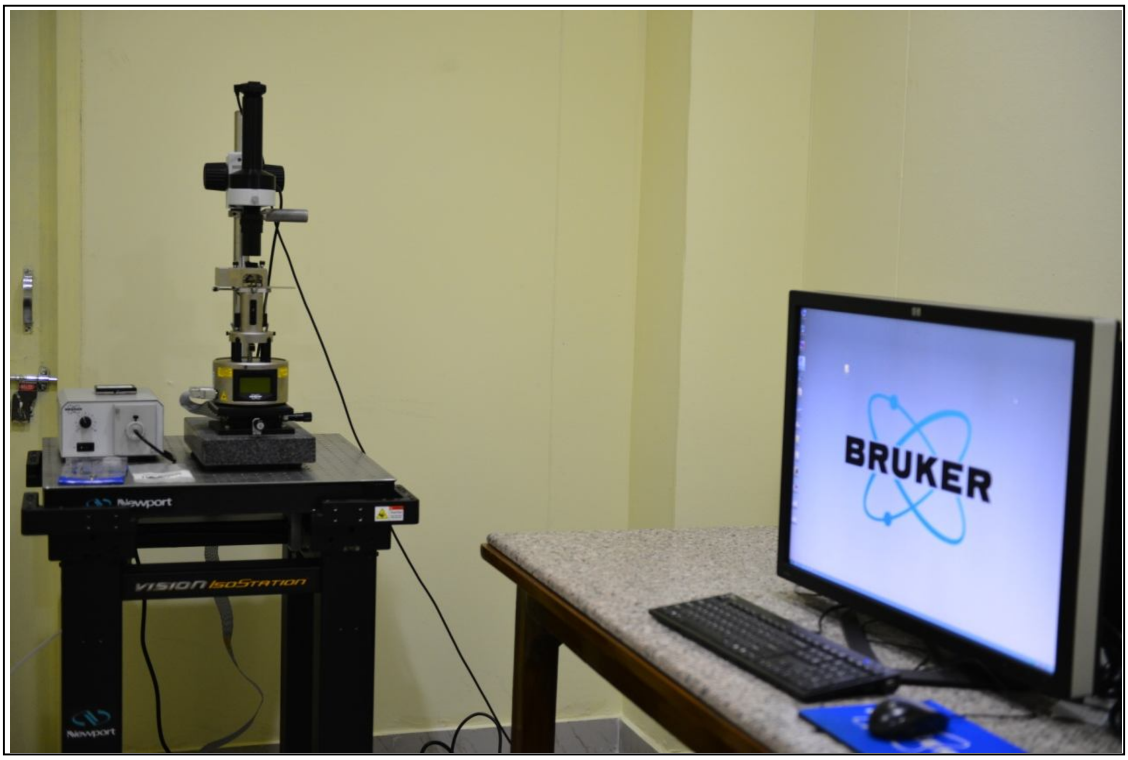

Fig.3.10 Experimental setup of atomic force microscope (Model: Multimode -8 Scanning Probe Microscope from Bruker).

2.3.4 Transmission Electron Microscope (TEM):

Transmission electron microscopy is used to obtain detailed images of extremely small areas with a magnification of about 1000 kX using electron beam. TEM can be used to analyze various features such as crystal structure, dislocations and grain boundaries etc [144]. High resolution images obtained from TEM can also be used to analyze shape, size, density and quality of the quantum wells, wires and dots. The experimental setup and basic working mechanism of transmission electron microscope is shown in Fig. 3.11 and 3.12 respectively. In TEM, the electron beam produced from electron gun is focused into a thin, small and coherent beam using condenser lenses. The condenser aperture is generally used to exclude high angle electrons. The transmitted part of condenser aperture beam strikes to the sample and passes through the sample depending upon the electron transparency and thickness of the sample. The transmitted portion is focused on the phosphor screen using objective lenses. Some optional objective lenses can also be used to improve the contrast by blocking the electron diffraction at higher angles. Further, the image is passed through intermediate and projection lenses so that higher magnification can be achieved.

Fig.3.11 Experimental setup of transmission electron microscope (Model: Tecnai G2 20 (FEI) S-Twin).

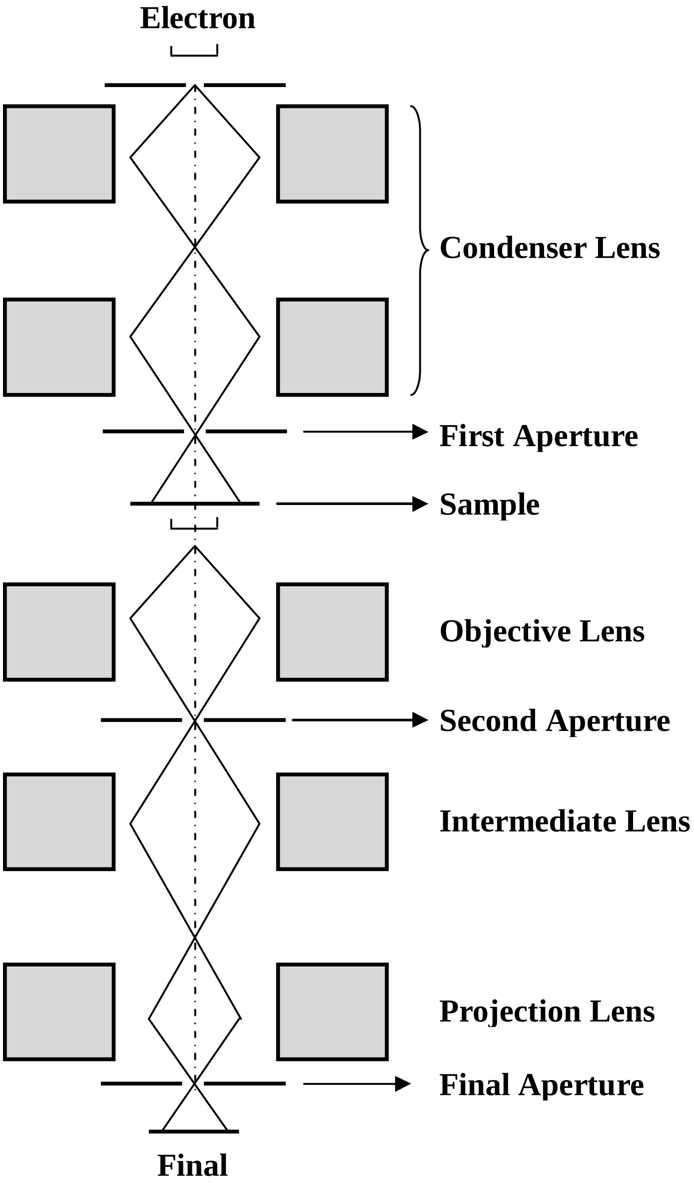

Fig.3.12 Schematic diagram for basic working mechanism of transmission electron microscope.

3.3.5 Raman Spectroscopy

Raman Spectroscopy is used to investigate rotational, vibrational and other low frequency modes in a system [145]. It relies upon monochromatic light from a laser source in near infrared, ultraviolet and visible region. The laser beam obtained from laser source interacts with phonon, molecular vibrations and other excitations in the system which shifts the energy of laser phonons up or down. This shift gives the information about vibrational modes present in the system. The basic working mechanism of Raman spectroscopy can be explained using Fig. 3.13. When the sample is exposed to monochromatic laser light, the scattered light comes out from the sample and passes through the filter to avoid any stray light. The filtered light diffracts from the diffraction grating and reaches at the detector. Fig. 3.14 shows experimental setup of Raman spectroscope.

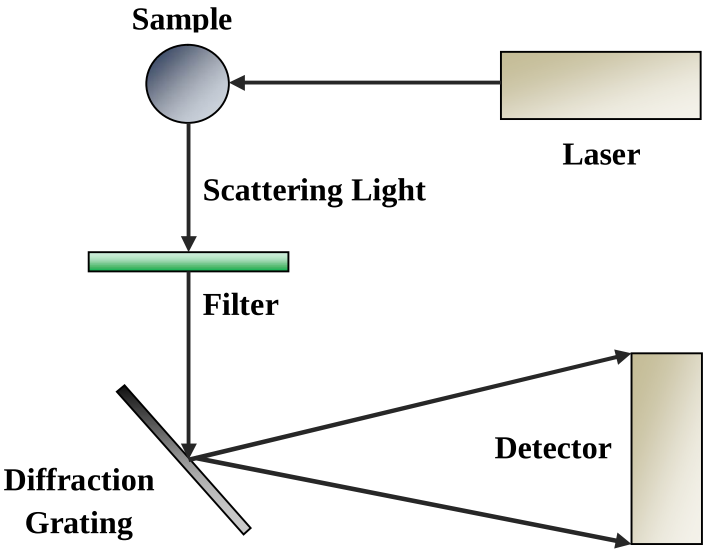

Fig.3.13 Working principle of Raman spectroscopy.

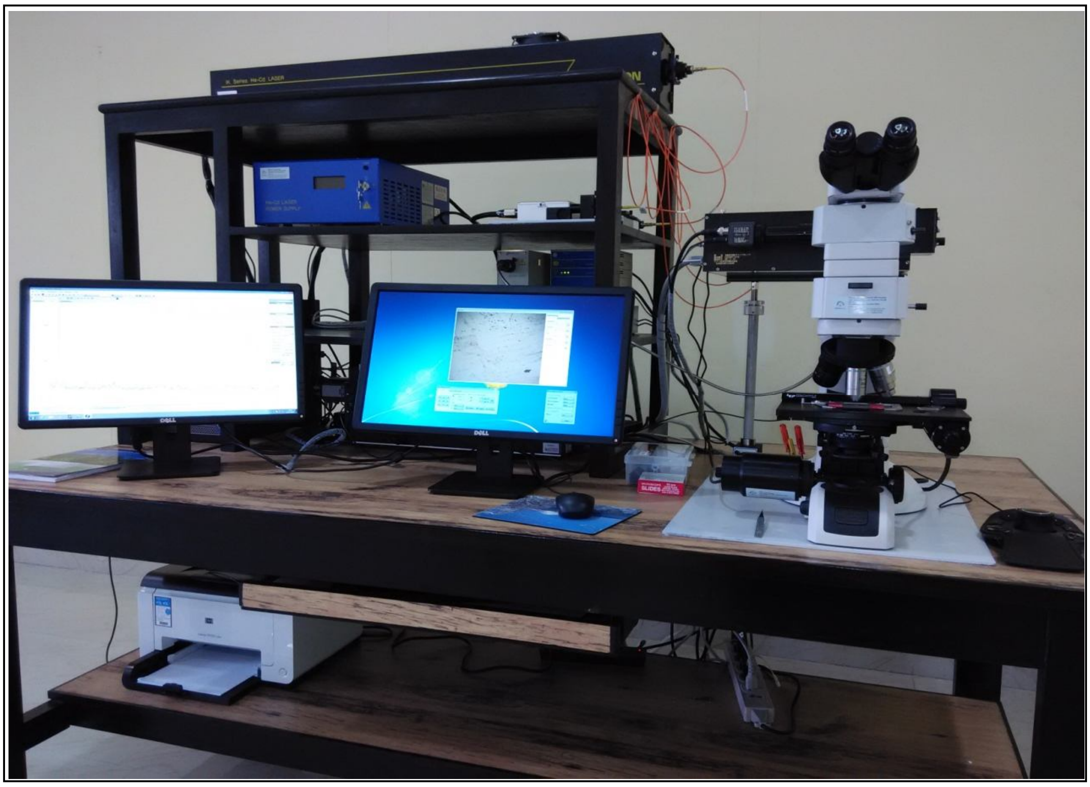

Fig.3.14 Experimental setup of Raman spectroscopy and PL spectra.

3.4 Optical Characterization Techniques

3.4.1 Ellipsometery

Elliposmetery is an accurate, simple, non invasive and non destructive method which is frequently used to obtain thickness, transmittance, absorbance and reflectance of thin films in semiconductor technology. Ellipsometery evaluates the change in polarization during transmission and reflection to compare it with a model. Fig. 3.15 and 3.16 demonstrates the basic working schematic and experimental set-up of the ellipsometer. The various other important optical parameters such as absorption co-efficient, optical bandgap, urbach energy, refractive index, dielectric constant and surface energy loss can also be derived from ellipsometery.

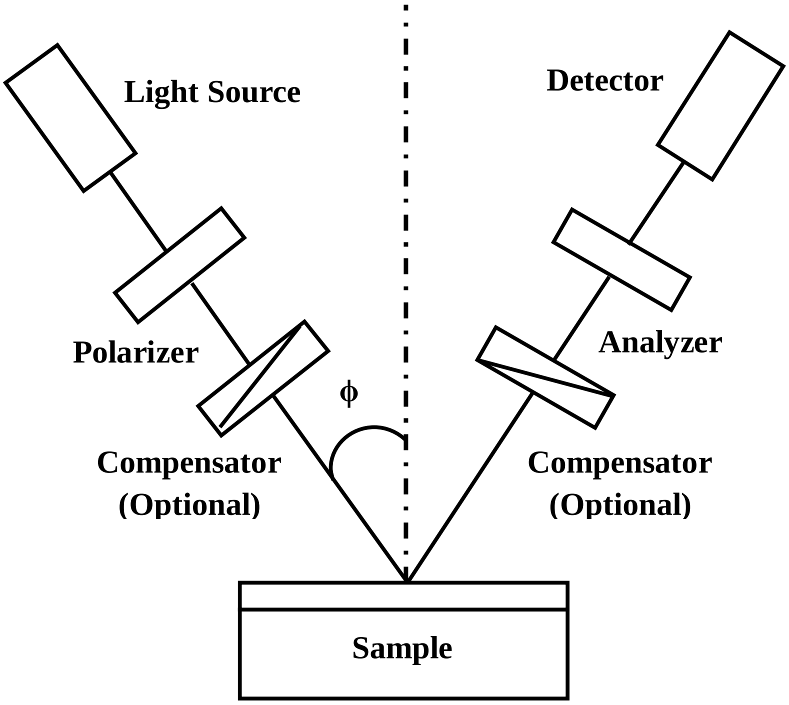

Fig.3.15 Schematic diagram for working mechanism of elliposmeter.

Fig.3.16 Experimental setup of elliposmeter (Model: VWASE VB-400 from J.A. Woollam Co.).

The absorption coefficient (α) for thin films can be calculated using Beer-Lambert's law [146]:

$$\alpha = \frac{1}{d}\ln\frac{1}{T} = \frac{2.303}{d}A \tag{3.7}$$

where d is film thickness and T is the transmittance of thin film. In addition, the relation between incident photon energy ($h\upsilon$) and absorption coefficient can be expressed as follows:

$$\alpha h\upsilon = B\left(h\upsilon - E_g\right)^n \tag{3.8}$$

where α is absorption coefficient, $h\upsilon$ is photon energy, E_g is optical bandgap and B is constant depending upon probability of absorption and refractive index of the material. Plot between $(\alpha h\upsilon)^2$ and $(h\upsilon)$ can be used to obtain the optical bandgap of the film by extrapolating the linear portion of the curve on $(h\upsilon)$ axis. The Urbach energy can be obtained by taking the reciprocal of linear region slope in $\ln(\alpha)$ versus $h\upsilon$ plot. The refractive index for thin films can be obtained using following equation [147]:

$$n = \sqrt{\frac{4R}{(1-R)^2} - k^2} + \left(\frac{1+R}{1-R}\right) \tag{3.9}$$

Where the extinction coefficient, k is given by:

$$k = \frac{\alpha\lambda}{4\pi} \tag{3.10}$$

Where α is the absorption coefficient and R is reflectivity of the thin film. The dielectric constant of thin film can be obtained using following equations:

$$\epsilon(\omega) = \epsilon_{real}(\omega) + \epsilon_{img.}(\omega) \tag{3.11}$$

where the real and imaginary parts of dielectric constant can be expressed as [148]:

$$\epsilon_{real} = n^2 - k^2 \tag{3.12}$$

$$\epsilon_{img.} = nk \tag{3.13}$$

3.4.2 Photoluminescence Spectra

Photoluminescence is a non destructive and contactless method to study the electronic structure of the material. The spectral response of PL spectra can be used to determine the optical bandgap of the deposited films. The PL spectra also provide the substantial information about the impurities and defects that strongly affects the material properties and device performance. The peak intensity of PL spectra is also helpful to analyze the qualitative changes in material quality as a function of various growth and processing parameters.

The working principle of PL is as follows: If a light particle (photon) has an energy greater than the band gap energy, then it can be absorbed and thereby raise an electron from the valence band up to the conduction band across the forbidden energy gap (See Fig. 3.17). In this process of photoexcitation, the electron generally has excess energy which it loses before coming to rest at the lowest energy in the conduction band. At this point, the electron eventually falls back down to the valence band. As it falls down, the energy it loses is converted back into a luminescent photon which is emitted from the material. Thus the energy of the emitted photon is a direct measure of the band gap energy, E_g. The process of photon excitation followed by photon emission is called photoluminescence. Experimental setup for photoluminescence spectra is shown in Fig. 3.14.

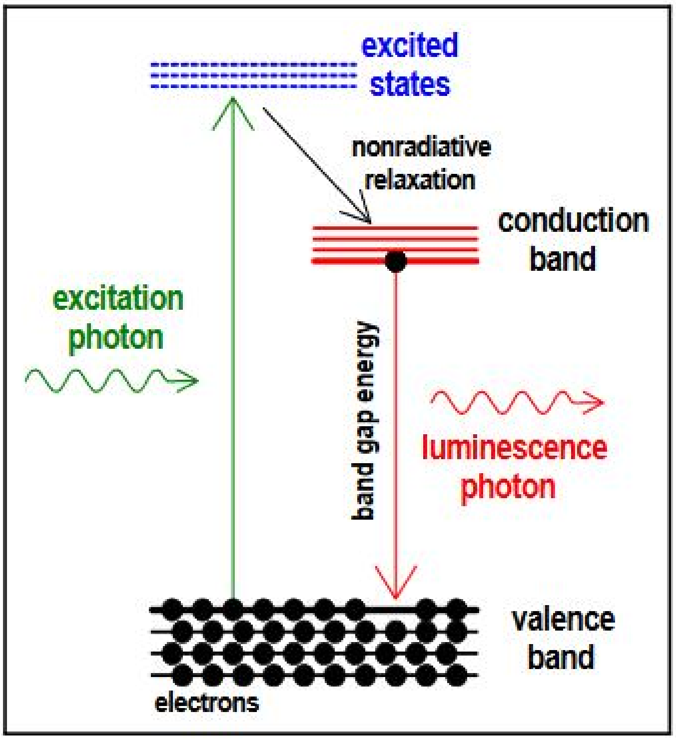

Fig 3.17. Schematic diagram for working principle of photoluminescence process.

3.5 Electrical Characterization Techniques

The electrical properties of heterojunctions are generally studied using current-voltage and capacitance-voltage measurements. Fig. 3.18 shows the experimental setup used for I-V/C-V measurements. The various important device parameters such as ideality factor, barrier height, built-in potential, donor concentration and depletion width can be derived from these measurements.

3.5.1 Current-Voltage Characteristics

Current voltage measurement plays a significant role in order to investigate the performance of various thin film based devices such as solar cells, thin film transistors and different detectors. The values of ideality factor (η) and effective barrier height ($\phi_{B,eff}$) can be obtained using following equations [149]:

$$\eta = \frac{q}{kT} \times \{\frac{dV}{d(\ln I)}\} \tag{3.18}$$

$$\varphi_{B,eff} = \frac{kT}{q} \times \ln\left(\frac{AA^{*}T^{2}}{I_{0}}\right) \tag{3.19}$$

Where k is Boltzmann constant, A is contact area, A^{*} is effective Richardson constant and I_0 is reverse saturation current.

3.5.2 Capacitance - Voltage Characteristics

In semiconductor heterojunctions, the capacitance versus voltage plot is very useful to investigate the charge distribution and depletion region potential. The capacitance versus voltage relation can be explained by conventional heterojunction theory [150]:

$$C^{2} = \frac{qN_{A}N_{D}\varepsilon_{1}\varepsilon_{2}}{2(\varepsilon_{1}N_{D} + \varepsilon_{2}N_{A})(V_{bi} - V)} \tag{3.20}$$

Where N_D is donor density, N_A is acceptor density, ε_1 and ε_2 are dielectric constants of ZnO and silicon respectively, V_{bi} is built-in potential and V is biasing voltage. Considering $V >> kT/q$ and $N_A > N_D$, the depletion region capacitance per unit area for a given reverse bias voltage as a function of permittivity can be written as follows:

$$\frac{A^{2}}{C^{2}} = \frac{2(V_{bi} - V)}{q\varepsilon_{s}N_{D}} \tag{3.21}$$

The value of built-in potential (V_{bi}) can be obtained from linear region intercept of A^2/C^2 versus voltage curve towards the biasing voltage axis. The value of donor concentration can be obtained by putting the value of slope in the following equation:

$$N_D = \frac{2}{slope * q\varepsilon_s} \tag{3.22}$$

Effective barrier height of semiconductor heterojunctions can be obtained as:

$$\varphi_{B,eff} = V_{d0} + \frac{kT}{q}\ln\left(\frac{N_C}{N_D}\right) \tag{3.23}$$

Where V_{d0} is diffusion voltage at 0V and can be expressed as $V_{d0} = V_{bi} + (kT/q)$. N_C is effective density of states in conduction band. The positions of fermi levels can be calculated using following equations [151]:

$$E_f - E_c = \frac{kT}{q} \times \ln\left(\frac{N_D}{N_C}\right) \tag{3.24}$$

$$E_V - E_f = \frac{kT}{q} \times \ln\left(\frac{N_A}{N_V}\right) \tag{3.25}$$

The depletion width of the fabricated p-n junction can be obtained as [152]:

$$W_{Dep.} = \sqrt{\frac{\varepsilon_0 \varepsilon_s (V_{bi} - V)}{qN_D}} \tag{3.26}$$

(a) (b)

Fig.3.18 Setup for I-V/ C-V measurement (a) measuring unit (Model: Agilent-B1500A) (b) probe station.

CHAPTER 4

Performance Analysis of n-ZnO/p-Si Heterojunction Photodiode: A Simulation Study

This chapter presents simulation study and performance analysis of n-ZnO/p-Si heterojunction based photodetector. Different electrical and optical parameters such as energy band diagram, electric field profile, dark current, quantum efficiency, responsivity, detectivity and noise equivalent power of n-ZnO/p-Si heterojunction based photodetector have been simulated as a function of device thickness, operating wavelength and applied reverse bias voltage. The simulation software ATLAS™ in SILVACO package is used to describe the effect of n-ZnO/p-Si interface properties on its photodetection.

4.1 Introduction

In recent years, Zinc Oxide (ZnO) has drawn a wide attention of researchers due its unique electronic and optoelectronic properties [153, 154]. Its wide band gap (3.37 eV) and high exciton binding energy (60 meV) makes it a suitable choice for a variety of optoelectronic and photonic device applications. Specifically, UV-Visible photodetectors, Light Emitting Diodes (LEDs) and piezoelectronic nanogenerators has explored the usability of ZnO due to its cheap fabrication process and enhanced optical properties. As ZnO is naturally n-type, it is very difficult to dope it with materials of p-type polarity. However, some research have been devoted to p-type ZnO films in order to fully utilize the potential of ZnO, but the difficulty in doping of ZnO with p-type polarity has led the researchers to create heterojunctions with other p-type semiconductor materials. Various ZnO based heterojunction devices have been fabricated using different p-type materials such as GaN, GaAs, Si, SiC and $SrCu_2O_2$ [155-157]. Among these, n-ZnO/p-Si heterojunction is a better choice because of its compatibility with silicon integrated circuit technology. Further, the n-ZnO/p-Si heterojunction based detectors are capable of sensing ultraviolet light efficiently that can be very useful for many advanced applications such as medicare, general illumination, military and weather-monitoring. Some work on fabrication and characterization of n-ZnO/p-Si heterojunction diodes using different deposition techniques have been reported in past but still, the performance of n-ZnO/p-Si heterojunction based photodetector with different parameter variations need to be studied and analyzed. It is desirable to study electrical and optical properties of n-ZnO/p-Si heterojunction based photodetector before their adoption in fabrication of micro/nanoscale optoelectronic devices. In this work, various important electrical and optical parameters for n-ZnO/p-Si heterojunction based photodetector have been analyzed and reported. Effect of parameter variations (such as thickness, light intensity, operating wavelength and applied reverse bias voltage) on the performance of the photodetector has also been studied. All simulation results have been obtained using ATLAS simulator from SILVACO International. In best of our knowledge, this work is probably the first report in literature which demonstrates the simulation of ZnO based detectors using TCAD tool. These kinds of studies can be very helpful to reduce the fabrication cost and efforts by optimizing the various device parameters over the simulation tool itself before moving to the actual device fabrication.

4.2 Device Description and Simulation Setup

The device structure of n-ZnO/p-Si heterojunction photodetector is illustrated in Fig. 4.1. Thickness of n-ZnO and p-Si is taken as 500 nm and 380 μm respectively. The area of the detector was taken as 50×50 μm^2 during the simulation. The light source was defined at normal incidence from top of the device. The default BEAM statement which considers the entire device area under illumination was considered to investigate the spectral response of the detector. Doping is considered to be uniform for n-ZnO and p-Si regions.

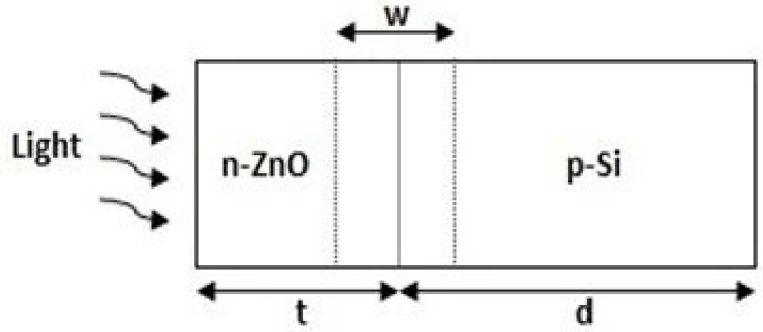

Fig.4.1. Structure of n-ZnO/p-Si heterojunction photodetector.

Different parameters required during simulation such as: conduction band discontinuity (ΔE_C), valance band discontinuity (ΔE_V) , effective density of states for electrons in the conduction band (N_C), effective density of states for holes in the valance band (N_V), separation between fermi levels and bandgap edges in p and n-type region (δ_p and δ_n) can be calculated using following equations (see Eq. (4.1-4.6)) [158].

$$\Delta E_C = \chi_{ZnO} - \chi_{Si} \tag{4.1}$$

$$\Delta E_V = \left(E_{gZnO} - E_{gSi}\right) \pm \Delta E_C \tag{4.2}$$

$$N_C = 2\left(\frac{2\pi m_e^* kT}{h^2}\right)^{\frac{3}{2}} \tag{4.3}$$

$$N_V = 2\left(\frac{2\pi m_h^* kT}{h^2}\right)^{\frac{3}{2}} \tag{4.4}$$

$$\delta_p = \frac{kT}{q} ln \frac{N_A}{N_V} \tag{4.5}$$

$$\delta_n = \frac{kT}{q} ln \frac{N_D}{N_C} \tag{4.6}$$

Where, χ_{ZnO} and χ_{Si} is the electron affinity for ZnO and Si, E_{gZnO} and E_{gSi} is the bandgap of ZnO and Si respectively, m_e^* and m_h^* is the effective mass of electron and holes , N_A and N_D is acceptor and donor concentrations in the p and n regions respectively, k is the Boltzmann constant, T is the lattice temperature and q is the charge of electron.

4.3 Simulation Results & Discussion

Simulation of n-ZnO/p-Si heterojunction photodetector has been done using ATLAS simulator from SILVACO international. Table 4.1 shows the set of parameters that have been used for ZnO during the simulation. A heterojunction photodetector program has been written in DECKBUILD interfaced with ATLAS tool from SILVACO international. Auger, Shockley-Read-Hall (SRH) and concentration dependent SRH (CONSRH) models of recombination mechanism have been taken into account for dark current evaluation [159]. Concentration dependent mobility model has been used for mobility calculation. For calculations of doping and carrier densities, fermi–dirac statistics for the parabolic shape of the conduction band have been considered in the simulation.

Table 4.1: Values of different parameters used for ZnO during ATLAS simulation

Symbol	Parameter	Values
E_{gZnO}	Bandgap [eV]	3.37
χ_{ZnO}	Electron affinity	4.35
N_D	Donor Concentration [cm^{-3}]	1×10^{19}
N_A	Acceptor Concentration [cm^{-3}]	1×10^{15}
m_n*	Effective mass of electron	0.19*m_o
m_p*	Effective mass of hole	1.21*m_o
τ	Recombination life lime [sec]	$1*10^{-9}$
ε	Dielectric constants	8.5
μ_n	Electron mobility [cm^2/V.s]	60
μ_p	Hole mobility[cm^2/V.s]	10
B	Bandwidth	1Hz

Equilibrium energy band diagram of heterojunction photodetector have been obtained using BLAZE. Fig. 4.2 shows energy band diagram for two reverse bias voltages (0V and 5V) in dark condition. It has been observed that as light falls on heterojunction photodetector, electron and hole fermi levels shift towards the conduction band. LUMINOUS tool from ALTAS device simulator has been used for optical characterization of the photodetector. Electric field profile of photodetector has been shown in Fig. 4.3. Maximum electric field of 10^5 V/cm has been observed for heterojunction photodetector. Variation of cathode current, available photocurrent and source photo current with optical wavelength is demonstrated in Fig. 4.4. Cathode current plot with wavelength shows the spectral response of the heterojunction photodetector in illumination condition and confirms UV-Visible dual-band detection capabilities of the photodetector. Other electrical and optical parameters to characterize the performance of n-ZnO/p-Si heterojunction based UV-visible photodetector are as follows:

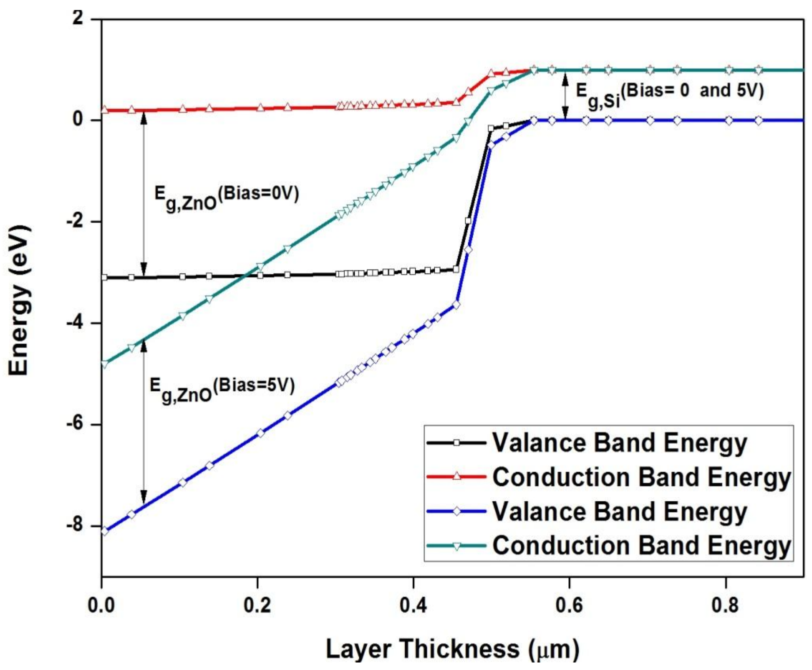

Fig.4.2. ATLAS simulated energy band diagram of n-ZnO/p-Si heterojunction photodetector (reverse bias voltage =0V and 5V, dark condition).

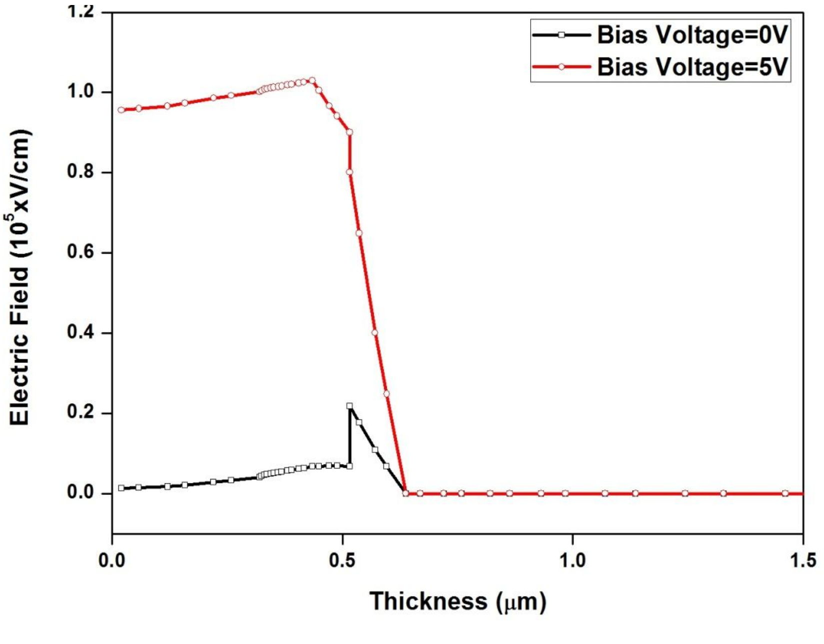

Fig.4.3. ATLAS simulated electric field profile for heterojunction photodetector (reverse bias voltage =0V and 5V, dark condition).

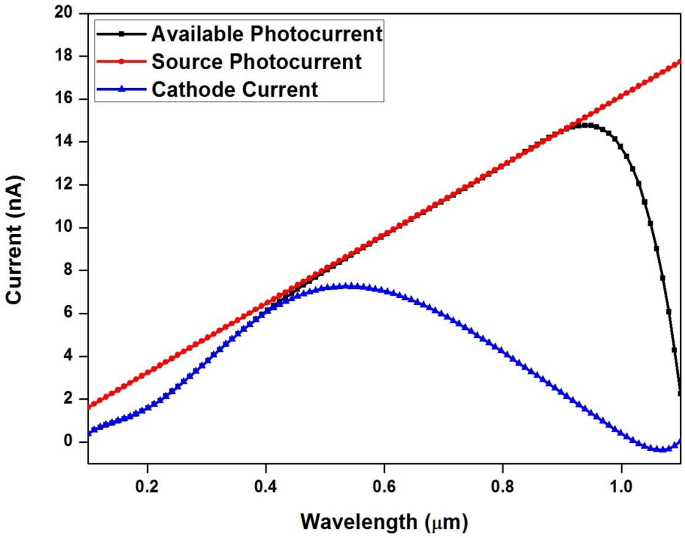

Fig.4.4. Spectral response for n-ZnO/p-Si heterojunction photodetector.

4.3.1 Dark and Illumination Current

Dark current for n-ZnO/p-Si heterojunction photodetector includes three components: (i) Tunneling Current (ii) Generation-Recombination Current (iii) Diffusion Current. Generally, narrow energy barriers and high electric field is responsible for tunneling phenomenon. At n-ZnO/p-Si interface, electrons and holes are separated by depletion region. When thickness of the barrier is thin enough, electrons and holes with energy less than the barrier height can cross the heterojunction to produce tunnelling current [160, 161]. Depletion width which is a major deciding factor for tunnelling in n-ZnO/p-Si heterojunctions can be obtained as follows [152]:

$$W_{Dep.} = \sqrt{\frac{\varepsilon_0 \varepsilon_s (V_{bi} - V)}{qN_D}} \tag{4.7}$$

Where ε_0 is the vacuum permittivity, ε_s is the dielectric constant of ZnO, V_{bi} is the built in potential , V is the biasing voltage , q is charge of electron and N_D is donor concentration respectively. The value obtained for depletion width was found to be 0.16 nm. The low value of depletion width suggests that tunneling plays a key role in current transport mechanism of n-ZnO/p-Si heterojunction diodes. Tunneling current includes two components:

A. Trap Assisted Tunneling (I_{TAT} *):*

Trap assisted tunneling (TAT) takes place due to tunnelling of minority carriers from occupied trap states on the quasi neutral side to the empty band states on other side of the junction. These trap centres are the intermediate energy levels generated by impurities present in the material. In n-ZnO/p-Si heterojunction, tunneling of electrons towards the conduction band of n side via trap levels is the major reason for trap assisted tunneling.

B. Band to Band Tunneling [I_{BTB}]:

Band to band tunneling arises due to flow of electrons from filled-in states of valance band (Si region) to partially filled states of conduction band (ZnO region) under high reverse bias voltage condition.

Diffusion current (I_{Diff}) arises due to the generation of electron hole pair in the non depleted region of n-ZnO/p-Si heterojunction photodetector. Only those electrons in ZnO region that have higher energy than the barrier (qV_{dx}) can reach the hetero-interface of the Si region. Similarly only those electrons in Si region having energy higher than the barrier $(\Delta E_c - qV_{dy})$, can reach the hetero-interface of ZnO region. Here V_{dx} and V_{dy} is potential barrier for n and p region respectively. Similar process will be followed for hole diffusion current also. In n-ZnO/p-Si heterojunction photodetector, carrier transport across the heterojunction is affected by impurities and defects in the depletion region which acts as an intermediate state for thermal generation-recombination of the carriers. This generation recombination component (I_{GR}) contributes in total current of the photodetector and, the movement of the carriers is strongly affected by n-ZnO/p-Si interface. Total dark current for n-ZnO/p-Si heterojunction photodetector can be obtained as follows [162, 163]:

$$I = I_{TAT} + I_{BTB} + I_{GR} + I_{Diff} \tag{4.8}$$

Estimation of effective recombination lifetime is also necessary to estimate the current component. Three recombination mechanisms (i) Auger recombination (τ_{AUG}) (ii) Shockley-Read-Hall Recombination (τ_{SRH}) (iii) Radiative recombination (τ_R) have been considered for carrier lifetime estimation during the simulation [164-166]. Auger recombination is the mechanism in which electron-hole recombines and energy is transferred to a third free carrier. If third free carrier is electron either it will move towards higher energy value of conduction band or it will move towards lower energy value of valance band. Auger mechanism is a three-body process because it requires one electron and two holes or two holes and one electron. In auger recombination electron-hole combines without emitting photons which reduces the quantum efficiency of the photodetector.

Shockley-Read-Hall (SRH) recombination takes place due to trapping of electrons by defect levels within the bandgap and can be reduced by lowering the concentration of foreign impurities and native defects. The recombination rate depends upon local densities of carriers in the bands of semiconductor and predominant occupation state of the charge carriers.

Radiative recombination takes place when hole in valance band directly combines with electrons in conduction band and emits the excess energy in the form of a photon. By taking all three components in consideration, effective carrier lifetime (τ) for n-ZnO/p-Si heterojunction photodetector can be evaluated as [162, 163]:

$$\frac{1}{\tau}=\frac{1}{\tau_{AUG}}+\frac{1}{\tau_{SRH}}+\frac{1}{\tau_{R}} \tag{4.9}$$

Figure 4.5 depicts dark and illumination current variation with biasing voltage. It can be seen from the graph that photocurrent has increased under the illumination. The results obtained have shown a close relevance with experimental results reported by Liu *et al.* [167]. Photodetector has shown very low dark current of the order of 10^{-14} A, which confirms the suitability of n-ZnO/p-Si heterojunction photo-detector for low noise applications. Ideality factor (η) of simulated n-ZnO/p-Si heterojunction have been derived using following equation [150].

$$\eta=\left[\frac{q}{kT}\times(\partial V/\partial \ln(I)\right] \tag{4.10}$$

Where q is the electronic charge, k is the Boltzmann constant, T is the lattice temperature. $(\partial \ln(I))/\partial V)$ have been obtained from linear region slope of $\ln(I)-V$ plot. The value of ideality factor for n-ZnO/p-Si heterojunction derived from illumination current-voltage characteristics was found to be 1.60. Fig. 4.6 shows I-V characteristics of heterojunction photodetector for different wavelengths (UV and visible). It has been observed that the variation in photocurrent for different wavelengths of light is not very significant under forward bias condition, but a considerable change in current is there for reverse bias condition. In reverse bias, as wavelength of light increased from 200 nm to 800 nm, photocurrent has also increased which shows a fair relevance with experimental results reported by Mridha *et al.* [168]

and Jeong *et al.* [169] for n-ZnO/p-Si heterojunction photodetector. It is clearly seen from Fig. 4.6 that illumination shifts the I-V curve towards positive voltage region. This behaviour may be due to unidirectional charge transport mechanism depending upon excitation wavelength [170]. Positive shift and higher value of photocurrent under illumination condition is also attributed to enhancement of band to band excitation in ZnO region. Charge interaction between ZnO and Si during illumination may tilt the bandgap of n-ZnO/p-Si heterojunction, and tunneling of charge carriers across the heterojunction could be the probable reason for this I-V shift during illumination [170, 171].

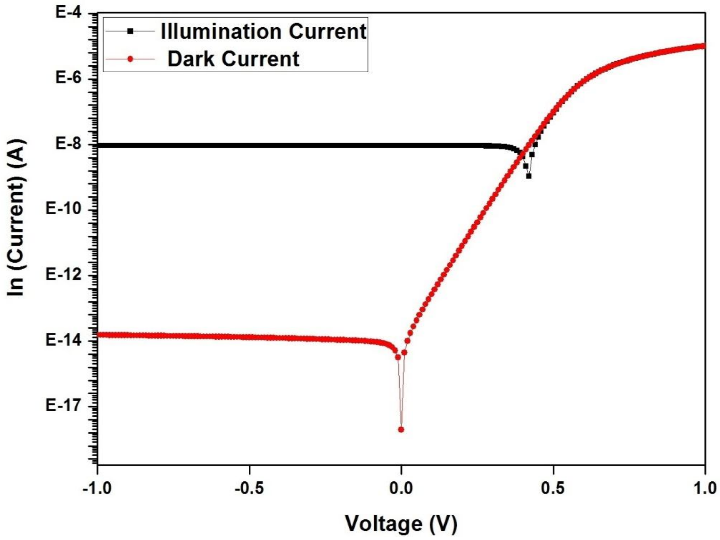

Fig.4.5. Current and voltage relationship of photodetector under dark and illumination condition (Light Intensity=0.2 W/cm^2).

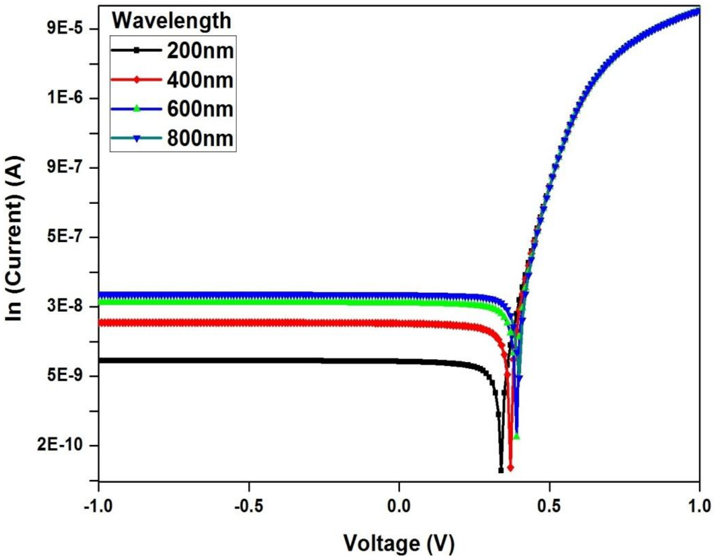

Fig.4.6. Variation of photocurrent with biasing voltage for different light wavelengths (Light Intensity=0.2 W/cm^2).

4.3.2 Quantum Efficiency

Quantum efficiency is a measure of sensitivity for n-ZnO/p-Si heterojunction photodetector. Internal quantum efficiency (IQE) and external quantum efficiency (EQE) for n-ZnO/p-Si heterojunction photodetector have been obtained as follows [172, 173]:

$$IQE = \frac{I_A}{I_S} \tag{4.11}$$

$$EQE = \frac{I_C}{I_S} \tag{4.12}$$

Where I_A, I_S and I_C are available photocurrent, source photocurrent and cathode currents respectively. Fig. 4.7 shows ATLAS simulation graph of internal and external quantum efficiency with optical wavelength for n-ZnO/p-Si heterojunction photodetector. Photodetector has shown a good internal and external quantum efficiency of ~99% and ~93% respectively for the given wavelength range. Results confirm UV detection capability of the photodetector.

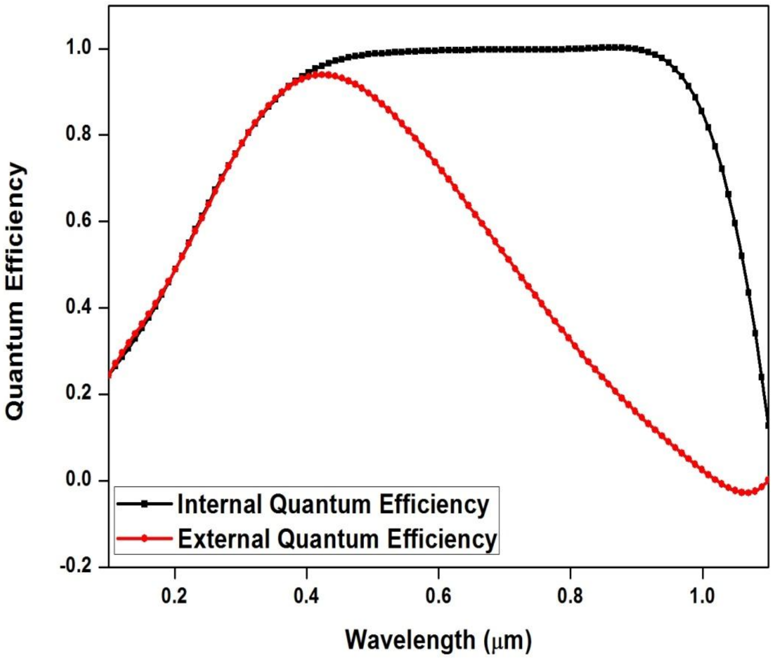

Fig.4.7. Variation of internal quantum efficiency with optical wavelength.

4.3.3 Responsivity

Responsivity of a photodetector can be described as the ratio of photocurrent generated to the optical power in linear region of response. Generally, responsivity is highest for the wavelength region in which photon energy is somewhat higher than the bandgap energy and can be obtained as [174]:

$$R = \frac{q\eta\lambda}{hc} \tag{4.13}$$

Where, λ is wavelength of light and c is velocity of light. Fig. 4.8 shows the responsivity variation of photodetector with light wavelength. Responsivity has been derived from external quantum efficiency. Photodetector has shown maximum responsivity of 0.28 A/W and 0.36 A/W for UV and visible wavelengths respectively. Results obtained for quantum efficiency and responsivity has shown a good agreement with the experimental results reported by Park *et al.* [175] and Ali *et al.* [176]. The value obtained for UV responsivity has also shown a good agreement with our experimental data which is presented in chapter 7.

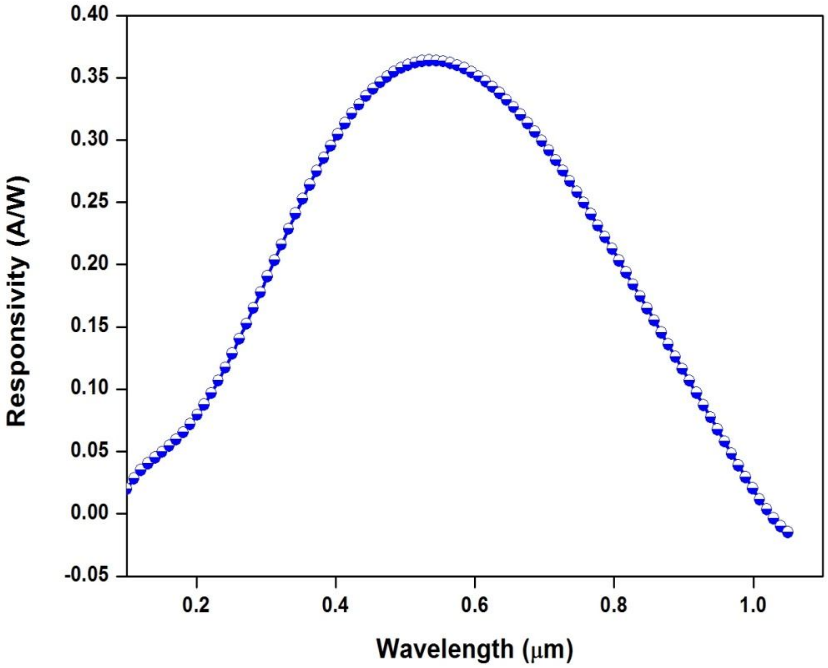

Fig.4.8. Variation of responsivity with optical wavelength for heterojunction photodetector (Biasing Voltage = -5V).

Effect of ZnO thickness variation on responsivity is shown in Fig. 4.9. It has been observed that as the thickness of ZnO layer increases, responsivity also increases.

Decrement in resistivity of ZnO layer with increasing thickness is the probable reason for increment in the responsivity of the heterojunction photodetector [177]. When thickness increases, the thicker ZnO layer will result into more electron-hole pair generation which in turn increases the photocurrent. Since responsivity depends upon the photocurrent generated, it also increases with ZnO thickness. Responsivity is the measure of the effectiveness of the detector and results demonstrated in Fig. 4.9 concludes that high gain for n-ZnO/p-Si heterojunction detector can be achieved at larger ZnO thickness.

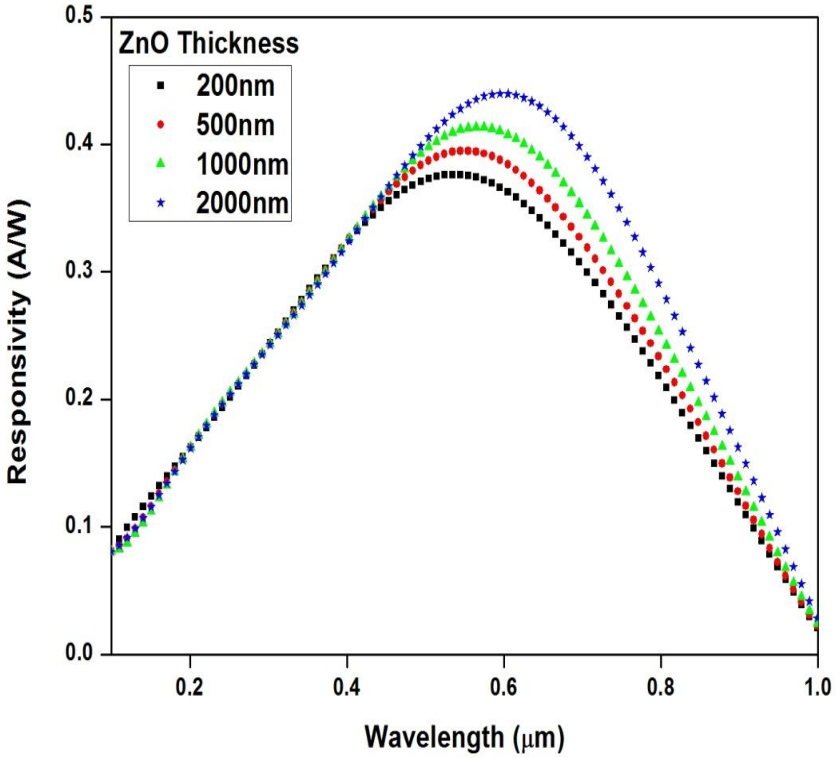

Fig.4.9. Variation of responsivity with optical wavelength for different ZnO thickness (Biasing Voltage = -5V).

It has also been observed that as intensity of light increases from 0.2 W/cm^2 to 1.0 W/cm^2, all three currents (cathode current, available photocurrent and source photocurrent (refer Fig. 4.10, 4.11 and 4.12)) for n-ZnO/p-Si heterojunction photodetector also increases but the ratio of cathode current to source photocurrent and available photocurrent to source photocurrent remains constant, hence both internal and external quantum efficiency of the n-ZnO/p-Si heterojunction photodetector remains unchanged with light intensity variation.

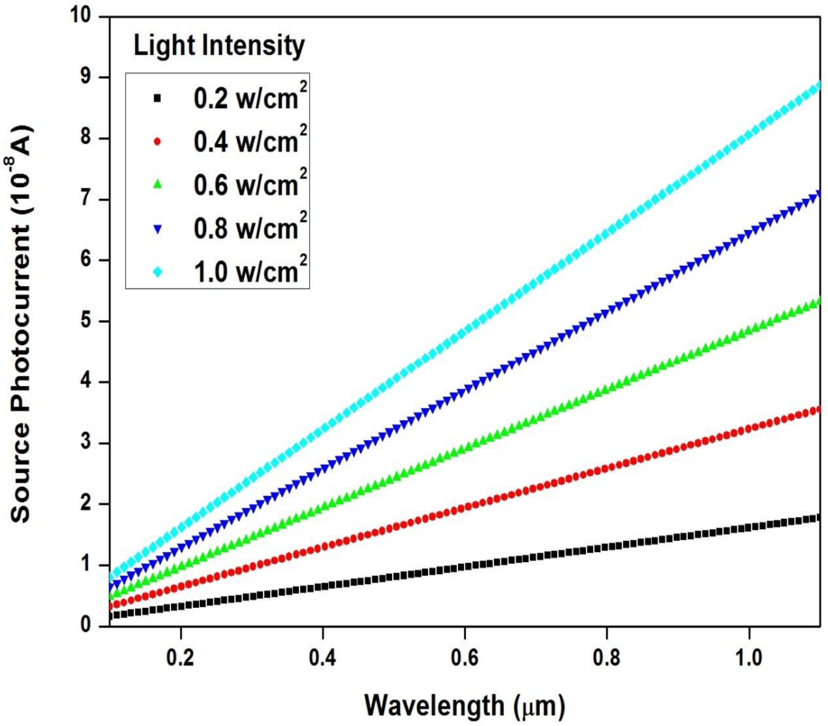

Fig.4.10. Variation of responsivity with optical wavelength for different ZnO thickness.

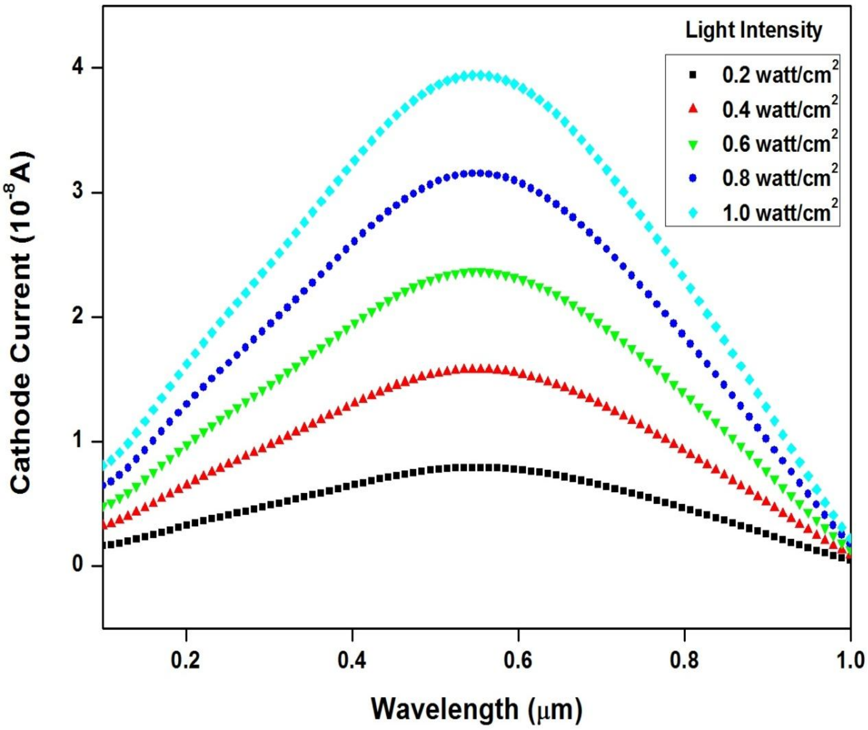

Fig.4.11. Variation of cathode current with optical wavelength for different light intensities.

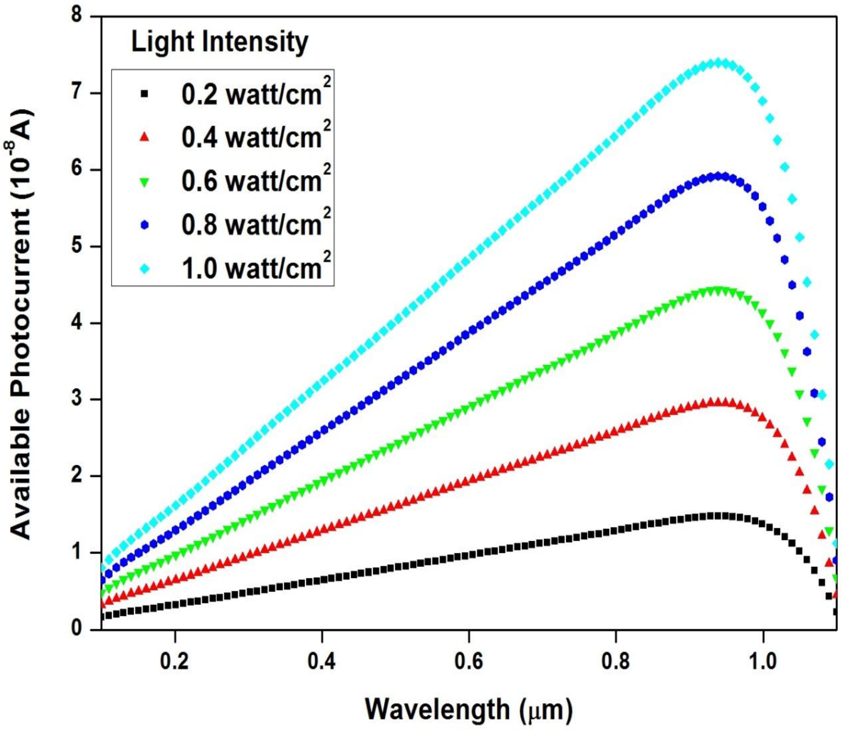

Fig.4.12. Variation of available photo current with optical wavelength for different light intensities.

4.3.4 Detectivity

Specific detectivity allows different photodetectors to be compared independent of detector bandwidth and area. High value of detectivity ensures suitability of heterojunction photodetectors for low noise applications and can be obtained as [172, 173]:

$$D^* = \frac{q\eta\lambda}{hc}\sqrt{\frac{(RA)_{net}}{4KT}} \tag{4.14}$$

where resistance area product $(RA)_{net}$ can be obtained using following equation:

$$(RA)_{net} = \left(\frac{\partial J}{\partial V}\right)^{-1} \tag{4.15}$$

Fig. 4.13 shows detectivity variation with wavelength. Good detectivity of the order of 10^{10} cm Hz ^{½} W $^{-1}$ has been observed over the given wavelength range.

4.3.5 Noise Equivalent Power

Noise equivalent power is minimum detectable power for photodetectors and can be written as:

$$NEP = \frac{A^{\frac{1}{2}} B^{\frac{1}{2}}}{D^*} \tag{4.16}$$

Where, B is bandwidth and A is the area of the detector. Relation between optical wavelength and noise equivalent power (NEP) has been shown in Fig. 4.14. Heterojunction photodetector has shown very low NEP of the order of 10^{-11} W. It can be observed that for UV and visible region, NEP is minimum which increases beyond this range.

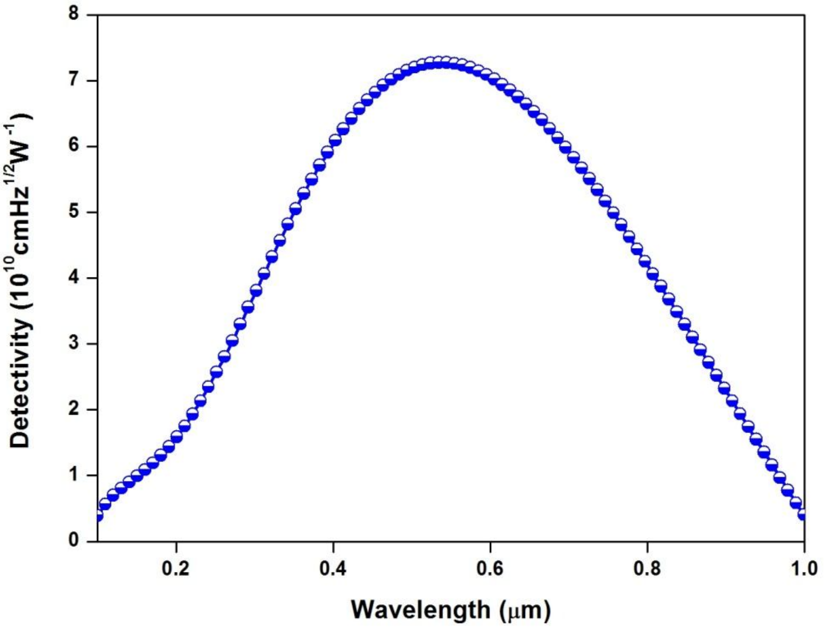

Fig.4.13. Variation of detectivity with optical wavelength (Biasing Voltage = -5V).

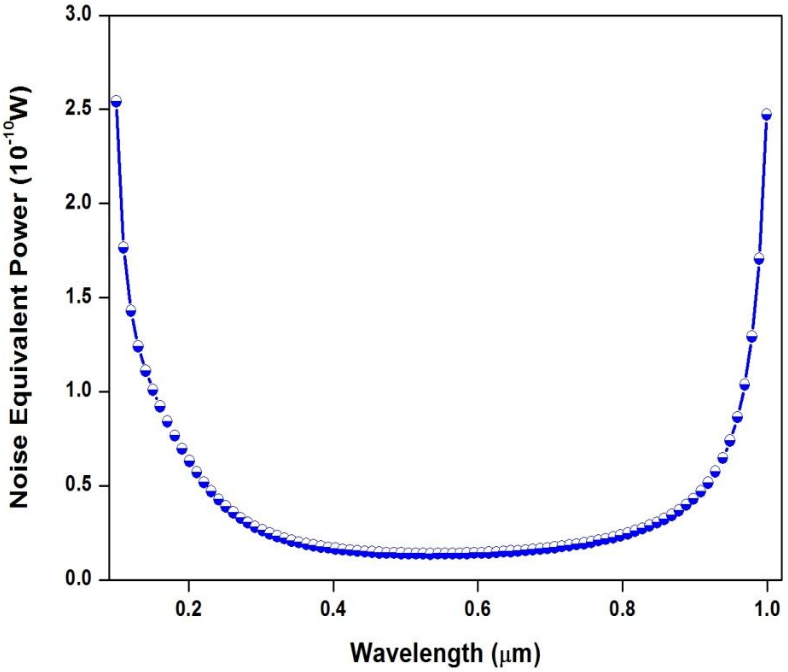

Fig.4.14. Variation of noise equivalent power with optical wavelength.

4.4 Conclusion

In this chapter, performance analysis of n-ZnO/p-Si heterojunction photodetector for different electrical and optical parameters such as dark current, quantum efficiency, responsivity, detectivity and noise equivalent power have been presented. Simulation results shows that photodetector offers a dark current, $I_D \approx 10^{-14}$ A, quantum efficiency, $\eta \approx 93$ %, responsivity $R \approx 0.36$ A/W, specific detectivity, $D^* \approx 10^{10}$ cm $Hz^{½}W^{-1}$ and NEP $\approx 10^{-11}$ W. The value obtained for UV responsivity has shown a good agreement with our experimental data which is presented in chapter 7. Results also confirm that n-ZnO/p-Si heterojunction photodetectors can detect UV wavelengths and have a great potential to become an alternative of other heterojunction based photodetectors.

CHAPTER 5

Growth and Optimization of ZnO Thin Films for Optoelectronic Device Applications

This chapter presents an intensive study on structural and optical properties of ZnO thin films prepared by RF sputtering technique. Effect of various physical and growth parameters such as thickness, annealing temperature, sputtering power and gas flow rate on structural and optical properties of ZnO thin films have been investigated in detail so that high quality ZnO thin films for variety of optoelectronic and photonic devices can be achieved.

5.1 Introduction

In recent years, ZnO has emerged as a new generation multipurpose semiconductor material for variety of optoelectronic and piezoelectronic device applications. Its high transparency in visible region, large bandgap, non-toxic nature and high exciton binding energy makes it a potential candidate for many electronic device applications such as photodetectors, LEDs, lasers, nanogenerators and transparent electrode solar cells etc. [178-180].

Difficulties in producing reproducible and reliable p-doped ZnO films have promoted an alternate approach of fabricating p-n heterojunctions with ZnO as n-type layer. Different ZnO based heterojunctions with p-type substrates such as GaN [181], SiC [182], AlGaN [157] and Si [183] have been proposed in past. Many reports on ZnO/GaN heterojunctions are available in literature due to various advantages such as similar bandgap, identical wurtzite crystal structure and less lattice mismatch (~1.8%) between ZnO and GaN. In present scenario, it is important to integrate ZnO thin films with silicon technology in order to develop practical applications of ZnO thin films for a wide range of optoelectronic device applications. Large area availability of Si with low cost and excellent quality has provided a unique opportunity to integrate Si with a variety of ZnO based optoelectronic devices.

In this context, different deposition techniques such as thermal vapour deposition, pulsed laser deposition, sol-gel, chemical vapour deposition, hydrothermal deposition and RF sputtering have been reported in past to grow thin films [184-188]. Among these, RF sputtering provides a precise control on different deposition parameters such as RF power, gas flow rate, deposition pressure, ambient atmosphere and substrate temperature which ensures repeatability and large scale stability of grown films with better controllability. Thin film device applications where c-oriented growth of the film with good controllability and conformity is important, RF sputtering is a potential choice.

New thin film devices with reduced nano dimensions has drawn a wide attention of researchers to study and understand the change in material's structural, optical and electrical characteristics with changing nano-dimensions [189-191]. Different functional properties of ZnO thin films with pressure, temperature and type of substrate have been reported in the past [192-195]. It is also important to investigate the effect of film thickness, annealing temperature, RF power and gas flow rates on structural and optical properties of RF sputtered ZnO thin films in order to ensure its suitability for a variety of optoelectronic device applications.

This chapter presents a systematic study on the effect of all these physical and growth parameters on structural and optical properties of ZnO thin films grown over p-type Si and glass substrates using RF sputtering technique. Different samples with different deposition conditions have been deposited over p-Si/glass substrates, and direct influence of thickness, annealing temperature, RF power and gas flow rates on microstructural (crystallographic orientation, roughness, grain size, lattice parameters, defect density, stress, strain) and optical parameters (transmittance, reflectance, optical bandgap, refractive index, dielectric constant, photoluminescence) of ZnO thin films have been analyzed and presented.

5.2 Experimental Details

Nanocrystalline ZnO thin films were deposited on p-Si (100) and glass substrate using RF sputtering technique. Thickness and resistivity of p-Si substrate was 380 μm and SIC Ωcm respectively. Prior to deposition, both Si wafer and glass substrates were cleaned properly. Standard RCA-1 and RCA-2 cleaning process were used for wafer cleaning. RCA-1 (Solution of NH_4OH, H_2O_2 and Deionized Water (DI)) was used for the removal of organic contamination and RCA-2 (Solution of HCl, H_2O_2 and DI water) was used for the removal of ionic contamination from the Si wafer. The Details of RCA-1 and RCA-2 method is as follows:

5.2.1 RCA-1 (Solution:- NH_4OH : H_2O_2 : Deionised (DI) Water)

25 ml NH_4OH was poured in a beaker with 180 ml of DI water. The solution was heated at 75-80°C for 5 minutes in order to increase the chemical reaction rate. Then, 50 ml of H_2O_2 (30 %) was poured in the solution and was kept for 1-2 minutes so that the solution becomes ready to use. Then, silicon wafers were soaked into this solution and the solution was heated for 6-8 minutes. The heated solution was allowed to cool for 10 minutes. In last, the silicon wafers were cleaned by rinsing in DI water and dried with dry nitrogen.

5.2.2 RCA-2 (Solution:- HCl : H_2O_2 : Deionised (DI) Water)

25 ml HCl was poured in a beaker with 180 ml of DI water. The solution was heated at 75-80°C for 5 minutes in order to increase the chemical reaction rate. Then, 50 ml of H_2O_2 (30%) was poured in the solution and was kept for 1-2 minutes so that the solution becomes ready to use. Silicon wafers were soaked into this solution and it was heated for 6-8 minutes. The heated solution was allowed to cool for 10 minutes. In last, the silicon wafers were cleaned by rinsing in DI water and dried with dry nitrogen.

Glass substrates were cleaned with acetone and isopropanol, and then rinsed in deionized water before fixing to the substrate holder. ZnO thin film was deposited over Si and glass substrate at room temperature using ZnO target (2-inch diameter) made up of 99.9% pure ZnO powder from MERCK Chemical Limited, Mumbai, India. RF/DC magnetron sputtering system from Advanced Process Technologies, India was used for depositing ZnO thin films.

For thickness dependent investigations, ZnO thin films with four different thicknesses were deposited over p-Si (100) and glass substrate using RF sputtering technique. The base pressure, deposition pressure and deposition rate were maintained at 1×10^{-6} mbar, 1×10^{-3}-3×10^{-3} mbar and 0.1-0.3 Å/sec respectively for all four samples. RF power and Ar flow rate was set as 100 watt and 15 sccm respectively during the deposition. Thickness of ZnO thin films was altered by varying the deposition time from 45 to 120 minutes. All samples were subsequently annealed for 1 hour at 400^{o}C in the argon atmosphere.

In annealing temperature dependent study of ZnO thin films, the distance between target and substrate was 12 cm. Prior to deposition, the vacuum level of sputtering system was ~5×10^{-6} mbar. Argon flow rate and deposition pressure was maintained at 10 sccm and $3\text{-}6\times10^{-3}$ mbar respectively. Deposition time was 1 hour and sputtering rate has got varied from 0.4-0.6 Å/sec during the deposition. Deposited samples were post annealed at different annealing temperatures (300°C, 400°C, 500°C and 600°C) in argon ambient to investigate the influence of annealing temperature over structural and optical properties of deposited ZnO thin films.

To investigate the effect of sputtering power over structural and optical properties of ZnO thin films, four set of ZnO thin film samples under same deposition conditions were deposited at 80 watt, 100 watt, 120 watt and 140 watt sputtering powers respectively. Vacuum level of sputtering chamber was maintained at 2-4 $\times10^{-6}$ mbar using rotary and turbo pumps. Distance between target and substrate was 13 cm. Argon flow rate and deposition pressure was maintained at 17 sccm and $3\text{-}5\times10^{-3}$ mbar respectively during the deposition. After deposition, all samples were annealed at 400 °C for 1 hour in argon ambient.

To investigate the effect of gas flow rate over structural and optical properties of ZnO thin films, the base pressure of deposition chamber was 2×10^{-6} mbar. The RF power was 100 watt during the deposition. The distance between substrate holder and target was 12 cm. Four samples of ZnO thin films at different argon gas flow rates varying from 10-40 sccm were deposited under similar deposition conditions. After deposition, deposited samples were annealed at 400°C for 1 hour in argon ambient.

5.3 Thin Film Characterization

Different type of methodologies and analytical equipments such as RF sputtering, XRD, AFM, SEM and ellipsometer (as mentioned in Chapter-3) were used to characterize the surface morphological and optical properties of deposited ZnO thin films. Detailed description of their working theory and principles is already presented in the Chapter 3

5.4 Results & Discussion

5.4.1 Effect of Thickness on Structural and Optical Properties of ZnO Thin Films

A. Structural and Surface Morphology Study

Fig. 5.1 shows XRD pattern of the ZnO thin films with different thickness. Domination of (002) oriented crystallites of hexagonal wurtzite structure for all deposited films attributes to a preferred c-axis orientation perpendicular to the surface. However a low-intensity peak with (103) crystallographic plane has also been observed with diffraction angles (2θ) 62.57°, 62.79° and 62.29° for 222 nm, 250 nm, 342 nm ZnO thin films respectively. It can be seen from Fig. 5.1 that the peak intensity has increased with increased thickness for (002) crystallographic plane. Increase in XRD peak intensity with thickness suggests that the crystalline quality of deposited films has improved with the thickness. As thickness increases; a growth competition takes place among the neighbouring crystals in accordance with their crystal orientation. When this competition leads towards the growth of same type crystal faces to form a free surface, crystalline quality of the deposited films improves. Similar behaviour has also been observed by Lin *et al.* for ZnO thin films [196]. This high quality ZnO films can be used as active layers in light emitting diode (LED) and thin film solar cell applications to improve their efficiency and lifetime. Different micro-structural parameters such as average crystalline size (D), lattice constants (a, b, c), defect density (δ), residual stress (σ) and lattice strain (η) for (002) crystallographic plane has been obtained using following equations [197,198]:

$$D = \frac{0.94\lambda}{\beta\cos\theta} \tag{5.1}$$

$$a = b = \frac{\lambda}{\sqrt{3}\sin\theta} \tag{5.2}$$

$$c = \frac{\lambda}{\sin\theta} \tag{5.3}$$

$$\delta = \frac{1}{D^2} \tag{5.4}$$

$$\sigma = -233\frac{(c - c_0)}{c_0}[Gpa] \tag{5.5}$$

$$\eta = \frac{\beta}{4\tan\theta} \tag{5.6}$$

Where λ is the wavelength of X-ray (λ = 1.5406 Å for Cu target), β is the full-width-at-half-maximum (FWHM) in radians, θ is the Bragg diffraction angle and c_0 (5.206 Å) is the unstrained lattice constant for bulk ZnO. Dependence of all important micro-structural parameters on the thickness of the deposited film is shown in Table. 5.1. It can be seen from the table that lattice constants (a, b, c) have shown good agreement with standard JCPDS data (PDF#36 – 1451(a=b=3.25 Å, c= 5.20 Å) [197]).

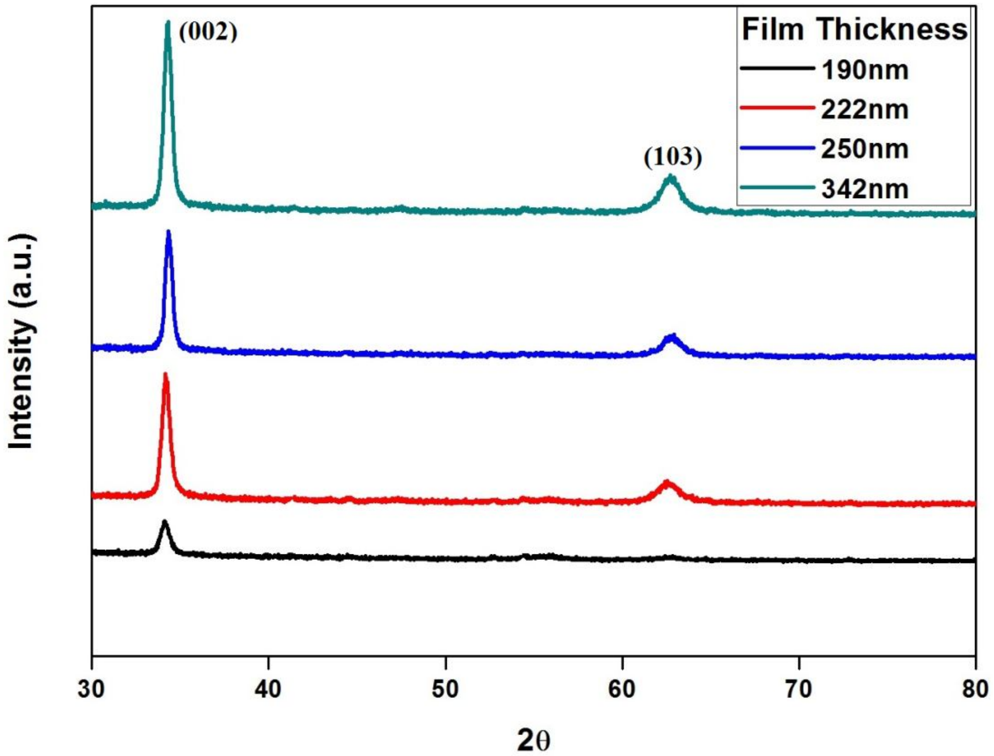

Fig.5.1. XRD spectra of ZnO thin films with thickness variation (a) 190 nm (b) 222 nm (c) 250 nm (d) 342 nm.

Table 5.1 shows that the crystalline size has increased with increase in thickness. Results obtained for crystalline size have shown a good agreement with results reported by Reddy *et al.* for RF sputtered ZnO thin films [199]. Reduction of dislocation density, stress and strain with increased thickness implies that more relaxed films with improved crystallinity have been obtained at higher thickness. Negative value of the stress obtained for deposited films signifies that the stress for the deposited films was compressive in nature. Crystal defects, lattice mismatch and difference between thermal expansion coefficient of ZnO and Si could be the probable reason for this compressive stress.

Table 5.1. Thickness dependence of different micro-structural parameters of RF sputtered ZnO thin films.

Thickness [nm]	**Peak (002) 2θ**	**a=b [Å]**	**c [Å]**	**Grain Size [nm]**	**Dislocation Density [nm^{-2}]**	**Stress**	**Strain [GPa]**
190 nm	34.12	3.031	5.251	15	4.44×10^{-3}	-2.02	8.42×10^{-3}
222 nm	34.20	3.024	5.239	17	3.46×10^{-3}	-1.49	7.25×10^{-3}
250 nm	34.33	3.013	5.220	20	2.50×10^{-3}	-0.63	6.11×10^{-3}
342 nm	34.39	3.008	5.211	49	0.41×10^{-3}	-0.23	2.49×10^{-3}

Surface morphology of deposited thin films with different thickness has been studied using AFM in contact mode. Fig. 5.2 shows AFM images of deposited ZnO thin films over an area of $5.0\times5.0\ \mu m^2$ which has shown a good agreement with the results reported by Mosquera *et al.* [200]. Root mean square roughness obtained for 190 nm, 222 nm, 250 nm and 342 nm ZnO films was 2.40 nm, 2.76 nm, 3.06 nm and 4.87 nm respectively. Large grain size and high porosity of the deposited films is responsible for this increased roughness at higher thickness. As roughness increases, surface area for gas adsorption also increases which ensures its suitability for gas sensing applications with high sensing response. High surface roughness of ZnO thin films may allow more optical absorption than flat surfaces that can be very useful in solar cell applications. It is clearly seen from Fig. 5.2 that 190 nm film has exhibited island like growth with hillocks. Careful analysis reveals that the surface homogeneity of the deposited films has improved with increased thickness. For thinner films, surface atoms are subjected to form a weak inter-atomic force in order to form a spongy loose packed structure and compactness of the deposited films increases with increased thickness due to strong inter-atomic forces at deeper layers. It can be concluded from Fig. 5.2 that films with lower thickness have no clear grain boundary, and as the thickness has increased, grains has started to develop with increasing roughness.

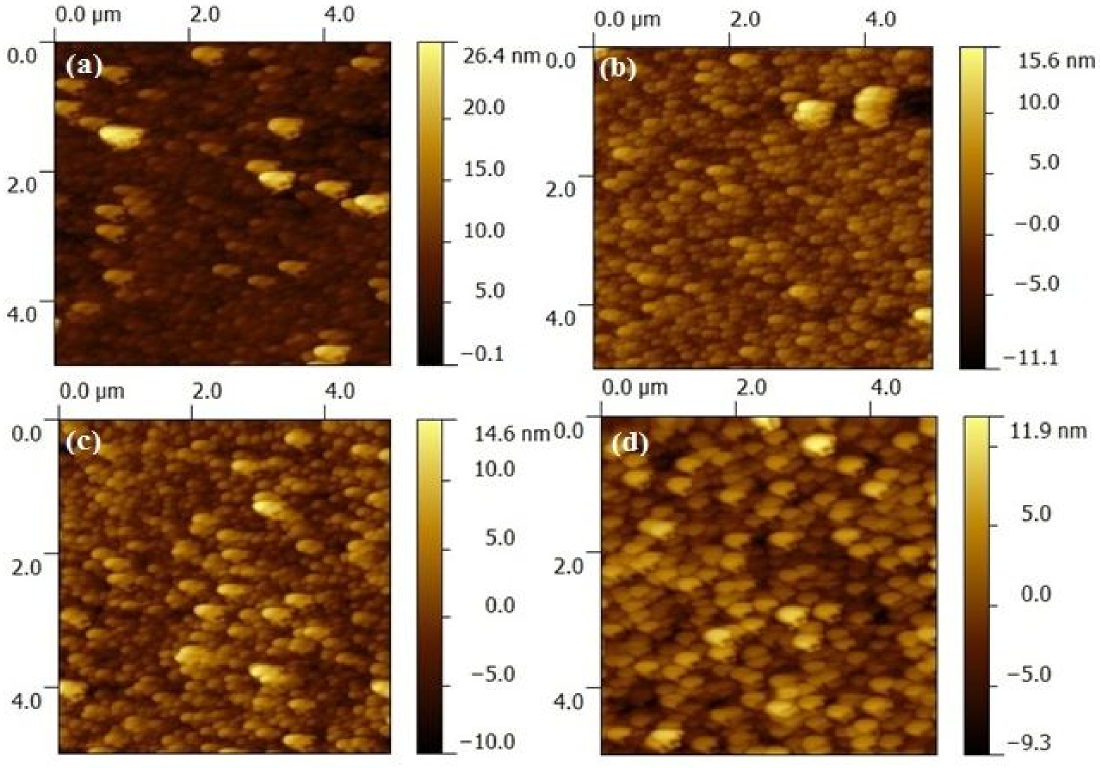

Fig.5.2. Two dimensional surface morphology images of ZnO samples obtained from AFM (a) 190 nm (b) 222 nm (c) 250 nm (d) 342 nm.

Fig. 5.3 shows SEM images of deposited ZnO thin films with different thickness at 1 μm scale with 50 kX magnification. It is evident from SEM images that surface morphology of all deposited films is almost uniform, homogenous and crack free. With increased thickness, a progressive increment in grain size has also been observed, and grain size has got varied in the range of 12-75 nm with increased thickness. These results are in good agreement with the results obtained from XRD data (refer Table 5.1). Grains shape of deposited films has also changed with increased thickness. Fig. 5.4 depicts EDX spectrum to identify the composition of deposited ZnO thin films with different thickness. It is evident from the EDX spectra that only Zn and O elements are present in the deposited films. Si peak is due to substrate. The inset in Fig. 5.4 shows atomic weight percent of Si, Zn and O elements, which implies that stoichiometry of deposited ZnO thin films strongly depends upon film thickness. The Zn and O content in the deposited films has increased with film thickness and Zn/O ratio is found to be 0.22, 0.33, 0.39 and 0.43 for 190 nm, 222 nm, 250 nm and 342 nm films respectively.

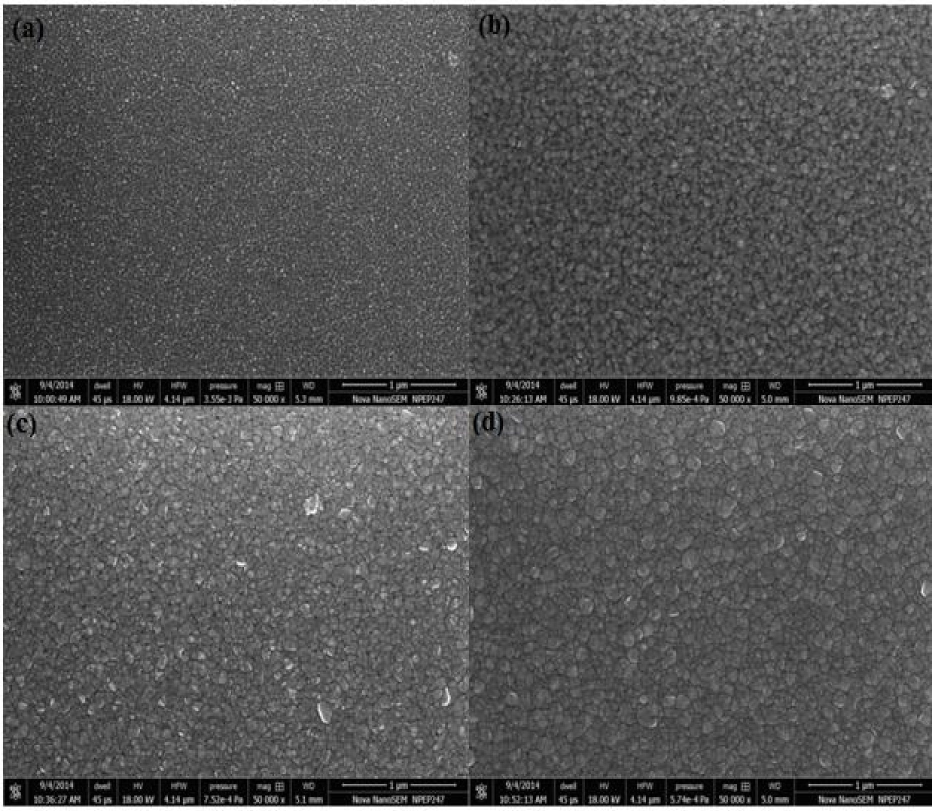

Fig.5.3. FESEM micrographs of deposited ZnO thin films with different thickness (a) 190 nm (b) 222 nm (c) 250 nm (d) 342 nm.

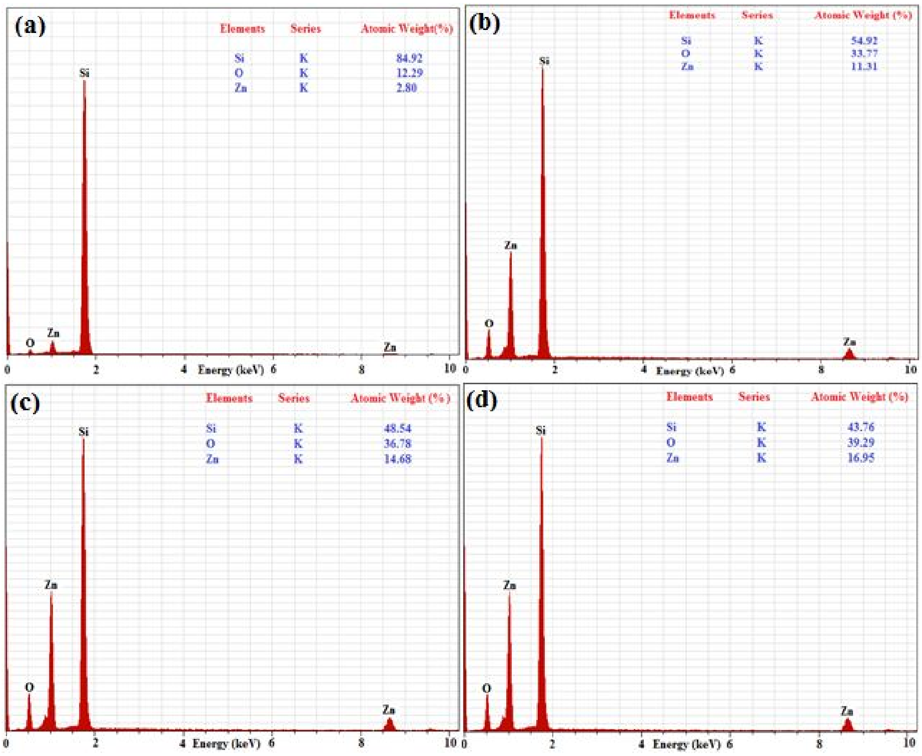

Fig.5.4. EDX spectra of ZnO thin films with corresponding atomic weight percent of elements at different thickness (a) 190 nm (b) 222 nm (c) 250 nm (d) 342 nm.

5.4.2 Optical Properties

Fig. 5.5 shows optical transmittance spectra of deposited films with different thickness. It is clearly seen that all films have shown a high transmittance of 85-90 % in the visible region with a sharp absorption edge near ~380 nm. High transmittance of deposited ZnO thin films ensures its usability as transparent window material in a variety of optoelectronic device applications. Transparent ZnO thin film coatings over the collector surface of solar cell can minimize the reflections at collector surface, which can improve the efficiency of the solar cells. Fig. 5.6 shows absorption spectra of ZnO thin films. It is evident from absorption spectra that the absorption increases with increased thickness. Reduction in the absorption beyond the band edges is attributed to the presence of impurity and lattice defects in the deposited films. Absorption coefficient (α) spectra (refer inset of Fig.5.6) which is necessary to derive optical bandgap of deposited thin films has been obtained using the following equation [202]:

$$\alpha = \frac{2.303}{d} A = \frac{1}{d} \ln \frac{1}{T} \tag{5.7}$$

Where d is the film thickness, A is the absorbance and T is the transmittance of deposited ZnO thin films. The optical bandgap of the deposited films has been evaluated using the following relation [203]:

$$\alpha h\nu = B(h\nu - E_g)^{1/2} \tag{5.8}$$

Where $h\nu$ is the photon energy, E_g is the optical bandgap and B is a constant for direct transition. The optical bandgap has been derived by extrapolating linear region of $(\alpha h\nu)^2$ versus ($h\nu$) plot (refer Fig.5.7) over ($h\nu$) axis. The linearity of $(\alpha h\nu)^2$ versus ($h\nu$) plot implies that ZnO thin films are direct transition type semiconductors. It has been observed that with increased film thickness, the optical bandgap of deposited ZnO thin films has increased from 3.24-3.26 eV. Results obtained for optical bandgap are in good agreement with those reported by Jain *et al* [203]. With increased thickness inter-atomic spacing of deposited film changes which attributes to an increase in optical bandgap. Absorption coefficient of deposited ZnO thin films varies exponentially with incident photon energy near fundamental absorption edge and obeys urbach relation which can be explained by following relation [204,205]:

$$\alpha = \alpha_0 \exp\left(\frac{E}{E_u}\right) \tag{5.9}$$

Where, E_u is the urbach energy, α_0 is the band tailing parameter and E is the photon energy. Urbach energy (E_u) has been obtained by taking the reciprocal of the slop of ln (α) versus $h\nu$ plot as shown in Fig.5.8.

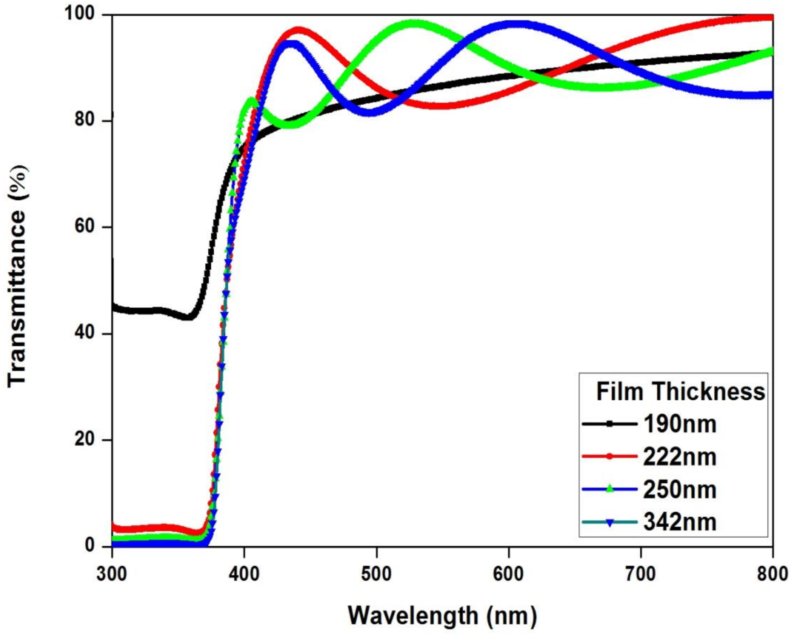

Fig.5.5. Transmittance spectra of deposited ZnO thin films with different thickness.

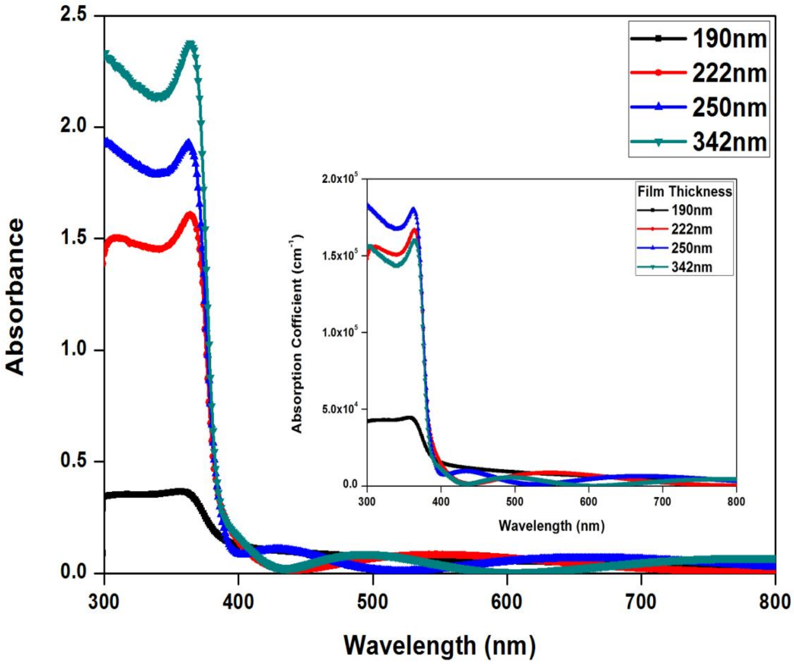

Fig.5.6. Thickness dependent absorbance spectra for ZnO thin films (inset shows absorption coefficient versus wavelength plot).

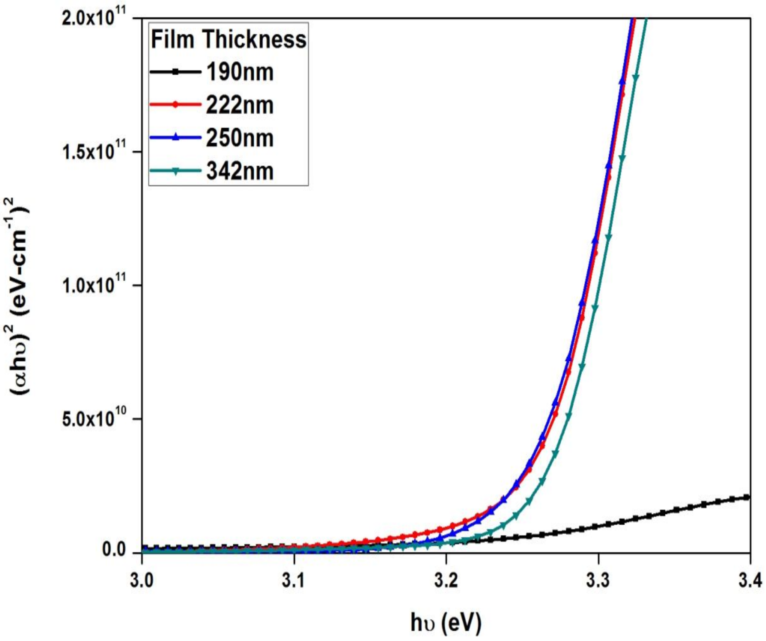

Fig.5.7. $(\alpha h\nu)^2$ versus ($h\nu$) plot for optical bandgap evaluation of ZnO thin films.

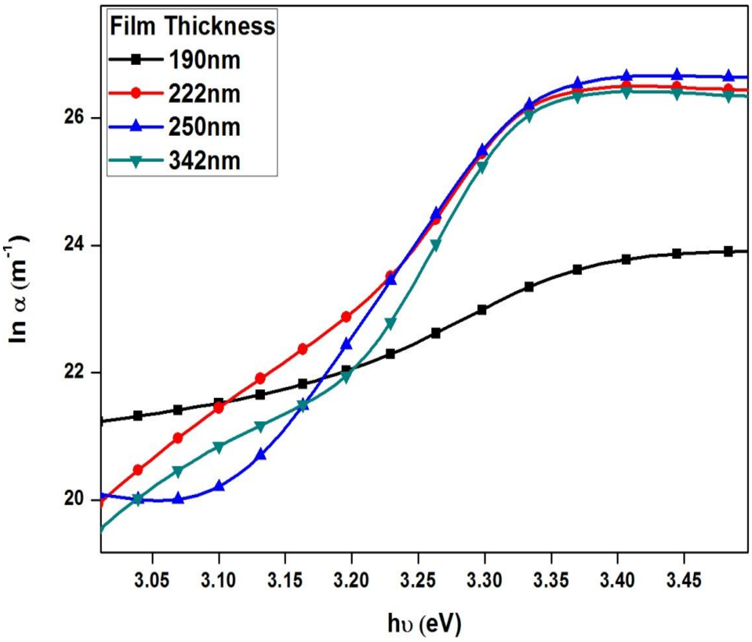

Fig.5.8. ln (α) versus $h\nu$ plot for ZnO thin films.

Table 5.2 shows the variation of the optical bandgap and urbach energy for different ZnO thickness. Urbach energy has shown an inverse relation with optical bandgap, and it is clearly seen that the urbach energy has decreased with increased film thickness. Refractive index has a significant importance in optical communication and device designing for spectral dispersion. It reflects the crystallinity and optical quality of thin films. Fig. 5.9 shows thickness dependent refractive index of ZnO thin films. It has been observed that refractive index increases as thickness increases. Transition of grains from vertical to lateral growth improves the uniformity of the deposited ZnO films which could be the probable reason for the refractive index variation with increased thickness. The typical reflectance spectra of ZnO thin films have been obtained using following relation [206].

$$R = \frac{(n-1)^2 + k^2}{(n+1)^2 + k^2} \tag{5.10}$$

Where n, k are refractive index and extinction coefficient of ZnO thin films respectively. Extinction coefficient k is given by:

$$k = \frac{\alpha\lambda}{4\pi} \tag{5.11}$$

Table 5.2. Variation of optical bandgap and urbach energy of ZnO thin films with different thickness.

ZnO Film Thickness	Optical Bandgap	Urbach Energy
190 nm	3.22 eV	94 meV
222 nm	3.24 eV	67 meV
250 nm	3.24 eV	32 meV
342 nm	3.26 eV	26 meV

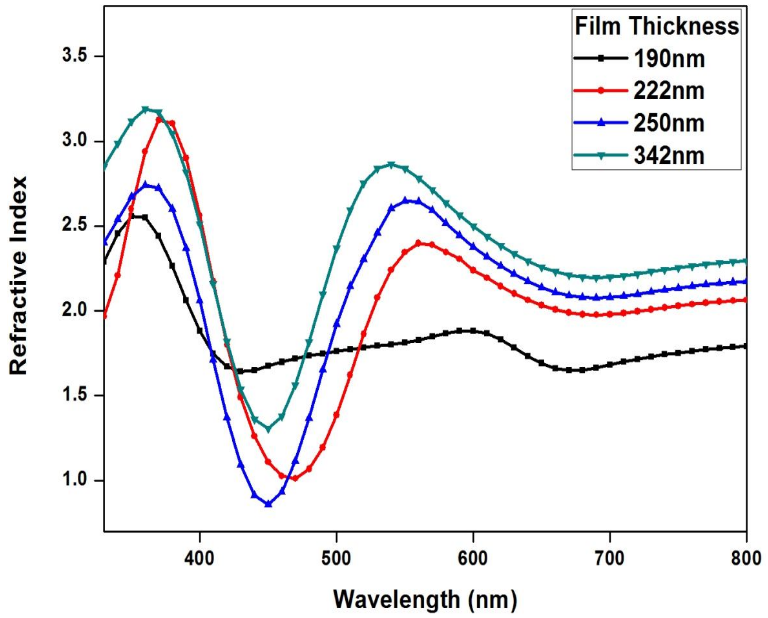

Fig.5.9. Thickness dependent refractive index variation for ZnO thin films

It is evident from reflectance spectra (shown in Fig. 5.10) that all deposited films have shown a low reflectance in the range of ~ 0-28% for a given wavelength range (300 nm - 800 nm). Low reflectance of deposited ZnO thin films suggests that ZnO can be a potential candidate for anti reflecting coating materials. Fig. 5.11 shows the extinction coefficient spectra for ZnO thin films with thickness variation. It is clear from Fig.5.11 that extinction coefficient is minimum in visible region wavelength, and it increases as wavelength decreases. Dielectric constant is also a fundamental intrinsic property of ZnO thin films. Real and imaginary part of dielectric constant tells the extent to which velocity of light slows down in deposited ZnO film. Imaginary part of ZnO thin films suggests that how the deposited films absorbs energy from the electric field due to dipole motion. Real and imaginary part of dielectric constant also gives information about loss factor, which can be obtained as the ratio of the imaginary part to the real part of dielectric constant. Real and imaginary part of dielectric constant has been obtained using following relation [207].

$$\varepsilon(\omega) = \varepsilon_R(\omega) + \varepsilon_I(\omega) \tag{5.12}$$

Where, the real ($\varepsilon_R(\omega)$) and imaginary parts ($\varepsilon_I(\omega)$) of dielectric constant can be evaluated as follows:

$$\varepsilon_R = n^2 - k^2 \tag{5.13}$$

$$\varepsilon_I = nk \tag{5.14}$$

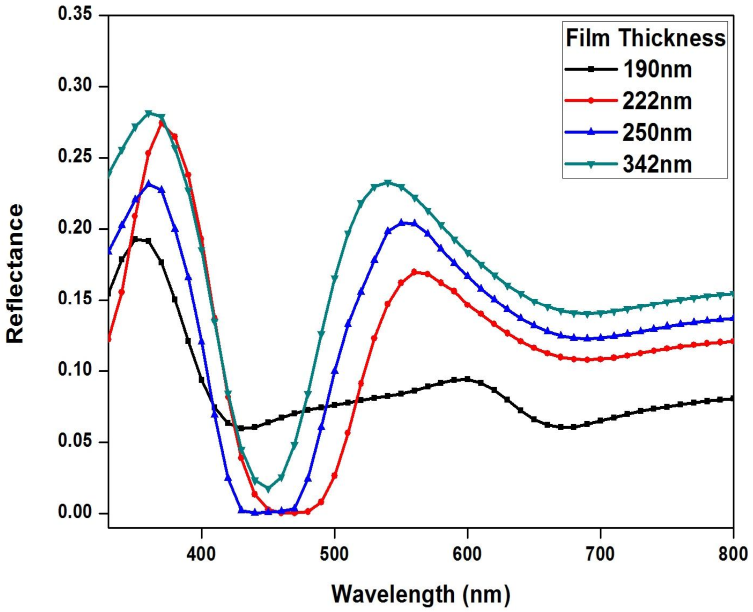

Fig.5.10. Reflectance spectra for ZnO thin films.

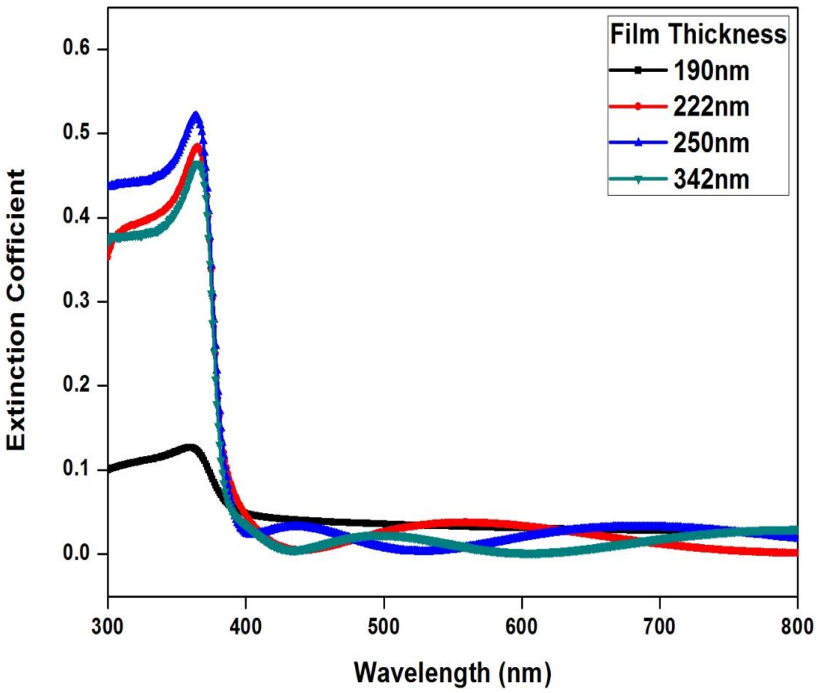

Fig.5.11. Variation of extinction coefficient with wavelength for ZnO thin films.

Fig. 5.12 and 5.13 shows the variation of real and imaginary part dielectric constant with ZnO thickness. It is clearly seen from the graph that both real and imaginary part of dielectric constant has increased with the thickness. The real and imaginary part of dielectric constant has shown the variation from 0.70-10.0 and 0-3.0 respectively for different thickness ZnO thin film.

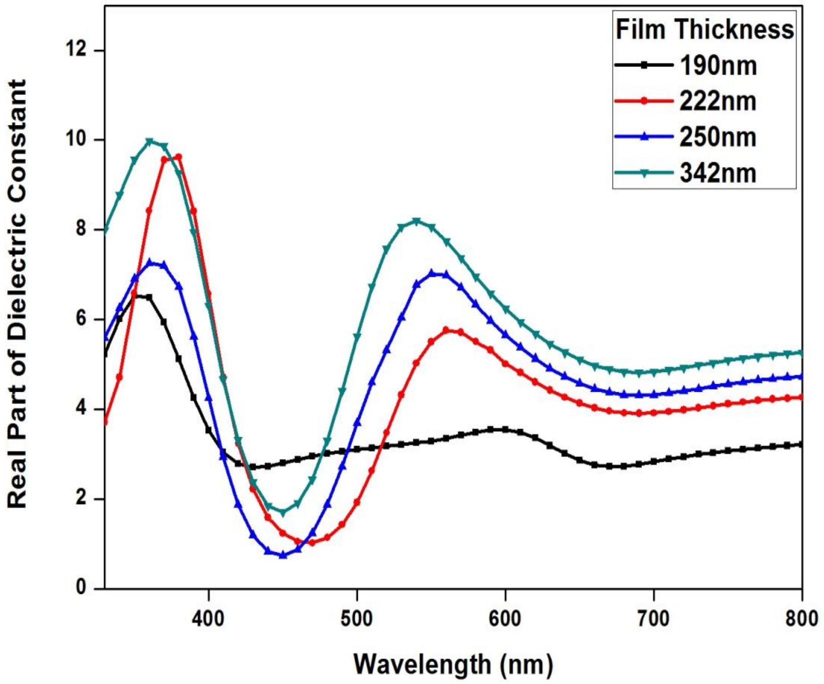

Fig.5.12. Real part of dielectric constant for different thickness ZnO thin films.

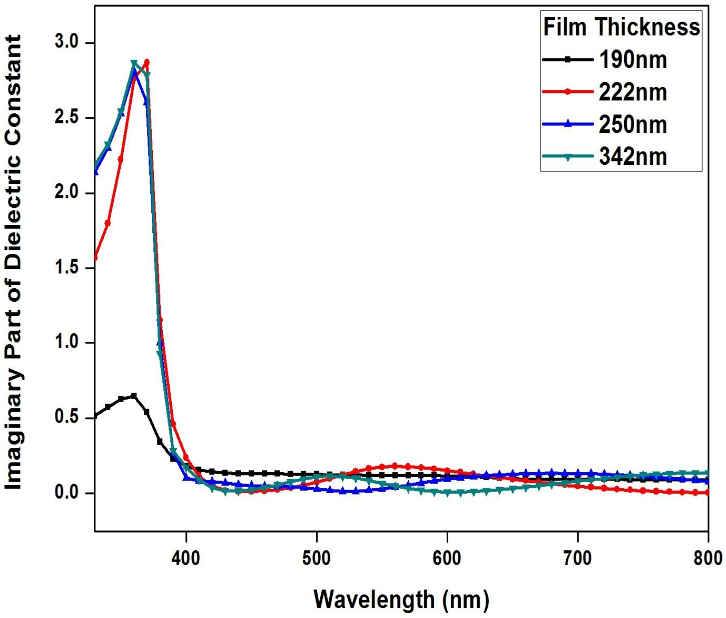

Fig.5.13. Imaginary part of dielectric constant for different thickness ZnO thin films.

Fig. 5.14 depicts thickness dependent photoluminescence spectra of ZnO thin films at room temperature. It is evident from the plot that all deposited samples have shown a strong UV emission peak attributing to the recombination of free excitons. It has been observed that RF sputtered ZnO thin films have shown a good UV emission efficiency than those prepared by molecular beam epitaxy, pulsed laser deposition and atomic layer deposition [208-210]. An increase in ultraviolet emission intensity with increased thickness has been observed. Improved crystalline quality with increased thickness that is also evident from XRD analysis is the probable reason for this increased UV emission intensity with increased thickness

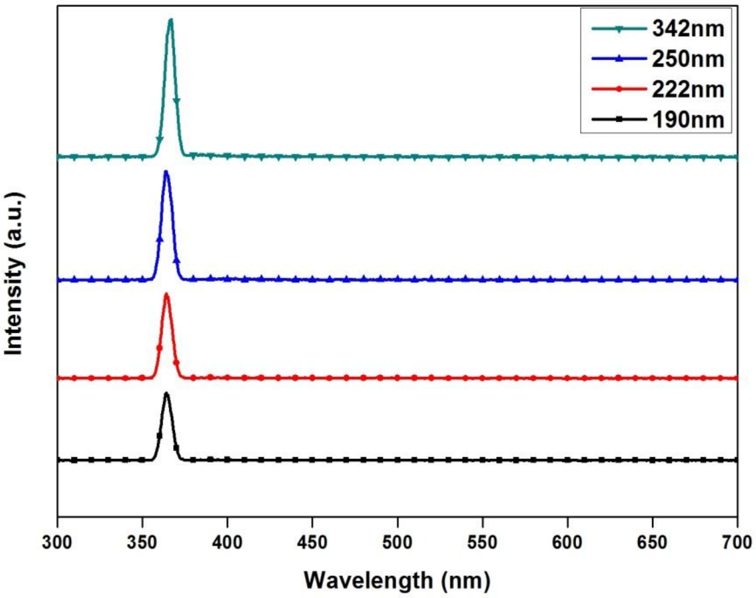

Fig.5.14. Photoluminescence spectra for thickness dependent ZnO thin films.

5.4.2 Effect of Post Annealing Temperature on Structural and Optical Properties of ZnO Thin Films

Fig. 5.15 shows XRD spectra of deposited ZnO thin films as a function of annealing temperature varied between 300 to 600 °C. All deposited films have shown polycrystalline nature with a strong (002) crystallographic orientation, indicating a preferential c-axis growth perpendicular to the substrate. Some other minor peaks with (101) and (103) orientations have also been observed. The increase in (002) diffraction peak intensity with increased annealing temperature is attributed to improved crystallinity of deposited ZnO thin films. Careful analysis reveals that the peak intensity of (101) crystallographic orientation has also increased with annealing temperature. At higher annealing temperature, some more Zn atoms may combine with oxygen to form poor crystallinity of ZnO in various directions, which could be the probable reason for enhanced peak intensity for (101) crystallographic orientation at higher annealing temperature.

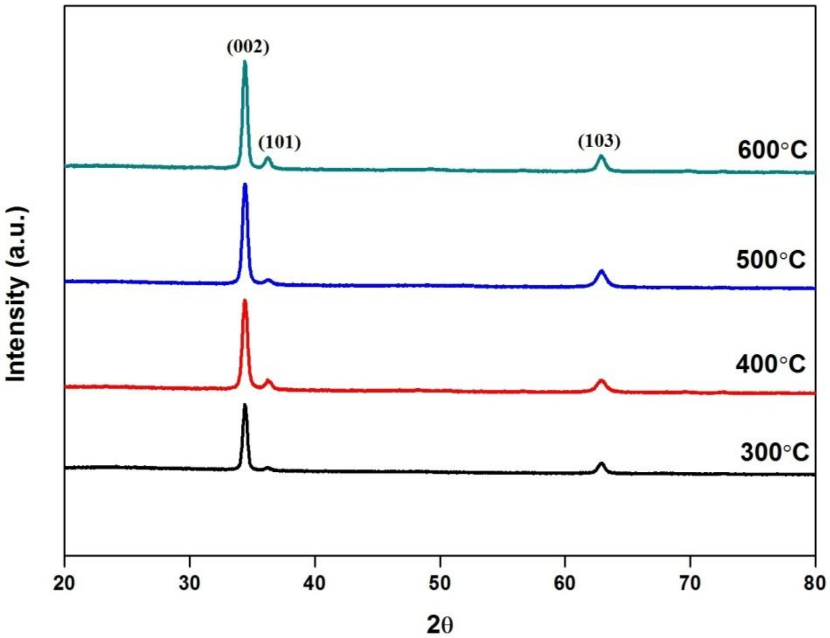

Fig.5.15. XRD diffraction patterns of ZnO thin films with post annealing temperature variation.

Fig. 5.16, Fig. 5.17 and Fig. 5.18 shows the effect of annealing temperature on various microstructural parameters such as grain size (G), dislocation density (δ), lattice constants (a,b,c), stress (η) and strain (σ) respectively. It is clear from Fig. 5.16 that the grain size has increased from 18-22 nm with increased annealing temperature. Value of lattice constants (a, b, c) (shown in Fig. 5.17) for all deposited samples have shown a good agreement with standard JCPDS data (a=b= 3.25 Å, c= 5.20 Å (PDF #36-1451)) [197]. The change in lattice constant values with increased annealing temperature is attributed to the change in nature of native imperfections. Dislocation density (Fig.5.16) and strain (Fig. 5.18) have exhibited a decreasing trend with increasing annealing temperature. Movement of Zn interstitials towards the grain boundaries which results in reduced concentration of lattice imperfections could be the probable reason for this decrement in dislocation density and strain at higher annealing temperature. High crystallinity of ZnO thin films with reduced strain ensures the usability of ZnO thin films in many optical applications. It is clear from Fig. 5.18 that the stress was compressive in nature at lower annealing temperature. As annealing temperature increases, the film has started to show tensile nature of the stress. In addition to intrinsic stress (compressive and tensile), thermal stress which arises due to lattice mismatch and difference in thermal expansion coefficient of ZnO and Si, also exists in deposited films. At lower annealing temperature, the compressive nature of the stress may be due to presence of Zn interstitials whereas the domination of oxygen vacancies in the lattice of ZnO crystallites at higher annealing temperature could be the probable reason for tensile stress.

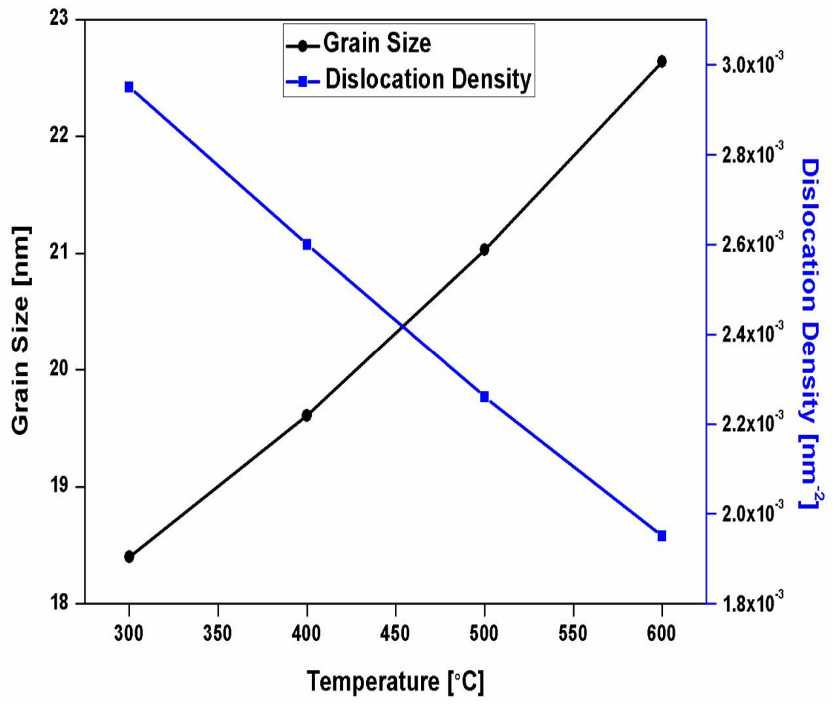

Fig.5.16. Variation of grain size and dislocation density with annealing temperature.

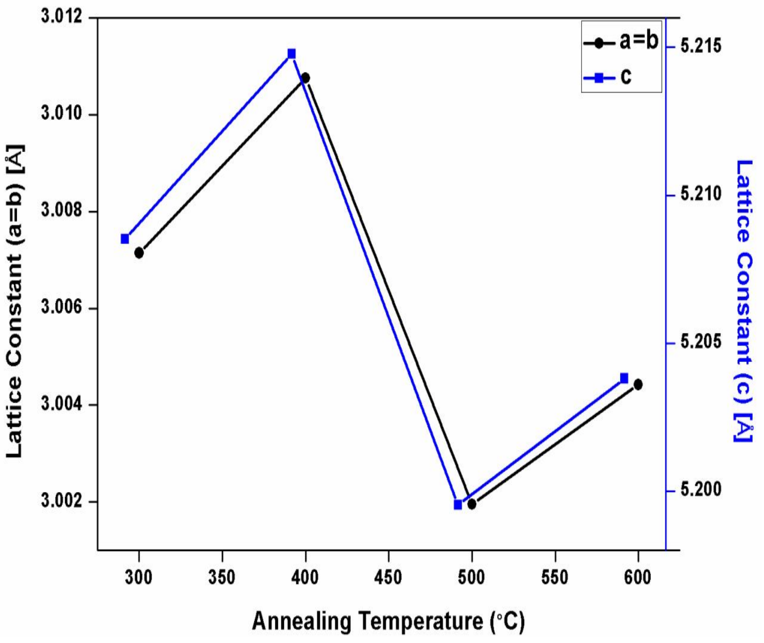

Fig.5.17. Lattice constants (a,b,c) versus annealing temperature plot.

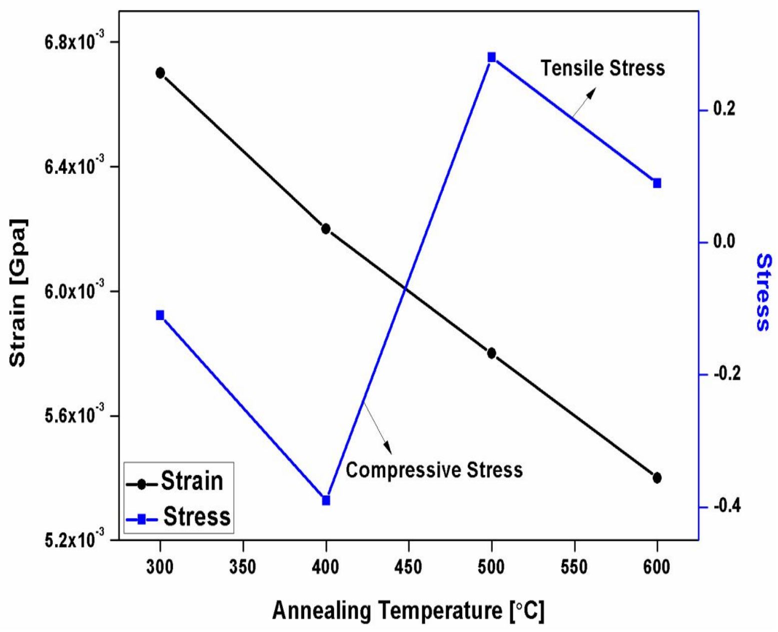

Fig.5.18. Variation of film strain and stress with annealing temperature.

Fig. 5.19 shows SEM micrographs of ZnO thin films deposited on Si substrate at different annealing temperatures. It is evident from SEM micrographs that the surface morphology of deposited ZnO thin films is dense and homogenous. It is clearly seen that grain size has increased at higher annealing temperature which may be due to coalescence process induced from thermal treatment. There may exist some frenkel defects such as Zn interstitials and oxygen vacancies at the grain boundaries of deposited films that can enhance the coalescence process to make larger grains at higher annealing temperature. High annealing temperature provides sufficient energy to the atoms of deposited film to improve the mobility that enhances the film cystallinity. Results obtained for grain size from SEM micrographs are in good agreement with XRD data and suggests that crystal growth of ZnO films can be controlled by controlling annealing temperature. SEM analysis also reveals that, at lower annealing temperature some of the grain has not grown properly and as the annealing temperature has increased, the grain growth of deposited film is more uniform.

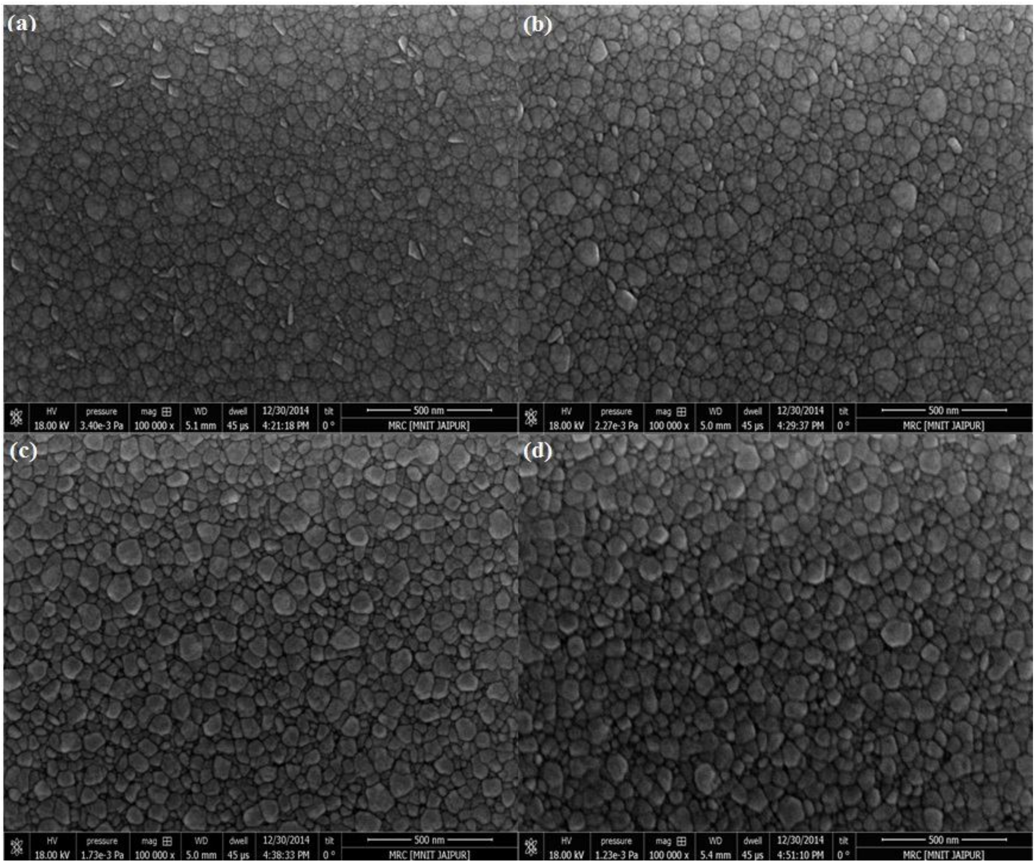

Fig.5.19. SEM micrographs of ZnO thin film samples at different annealing temperatures (a) 300°C (b) 400°C (c) 500°C (d) 600°C.

Fig. 5.20 shows the optical transmittance spectra of ZnO thin films recorded in the range of 300-700 nm. All deposited films have shown high transmittance of >85% in visible region. Fig. 5.21 shows the absorbance spectra as a function of wavelength. It is observed that the absorbance has decreased at higher annealing temperature. Inset of Fig. 5.21 shows absorption coefficient spectra of deposited ZnO samples at different annealing temperatures which have shown a good agreement with the results reported by Xue *et al.* [211].

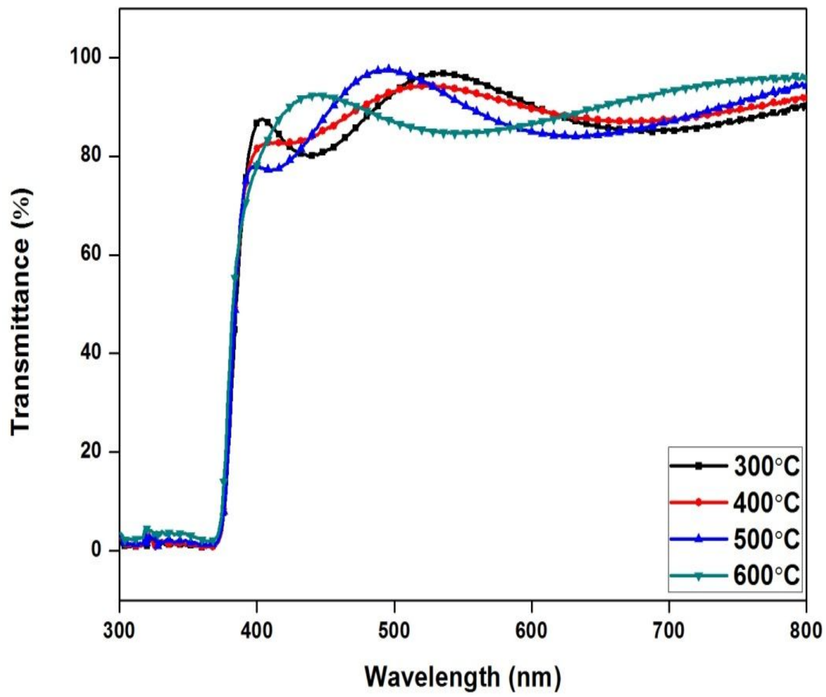

Fig.5.20. Optical transmittance plot of ZnO films at various annealing temperature.

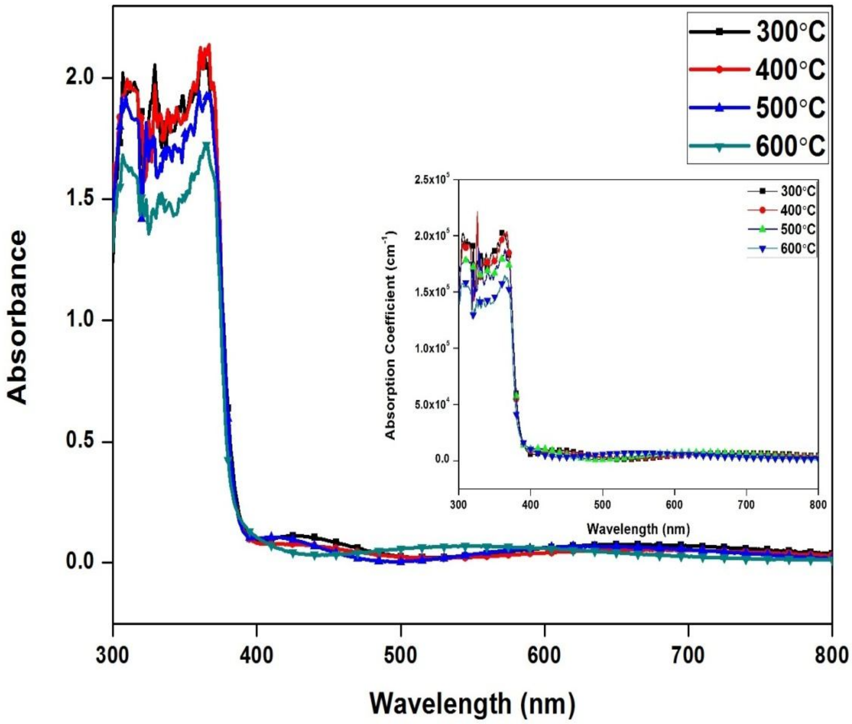

Fig.5.21. Absorbance versus wavelength spectra for ZnO thin films (inset shows variation in absorption coefficient with annealing temperature).

The optical bandgap have been obtained by extrapolating the linear region of $(\alpha h\upsilon)^2$ versus $h\upsilon$ plot, towards photon energy axis as shown in Fig. 5.22. An increase in optical bandgap from 3.26-3.28 eV is recorded with increased annealing temperature. The blue shift in absorption edge may be associated with the increased carrier concentration blocking in conduction band, also known as Burstein-Moss effect.

Urbach energy has been obtained by taking the reciprocal of linear region slop of ln (α) versus photon energy plot (refer Fig. 5.23). Inset of Fig. 5.23 shows the variation in urbach energy with annealing temperature. It is evident from the plot that the urbach energy has decreased from 59-50 meV with increasing annealing temperature which suggests that, at higher temperature film defects of deposited ZnO thin films have annealed out and hence quality of the deposited film have improved. Fig. 5.24 shows PL spectra of deposited ZnO thin films at different annealing temperature. All deposited films have exhibited a strong UV emission peak ~ 365 nm wavelength. From PL spectra, it is clear that UV emission intensity increases with increasing annealing temperature. Results obtained for PL spectra are in good agreement with the results reported by Lim *et al.* [212].

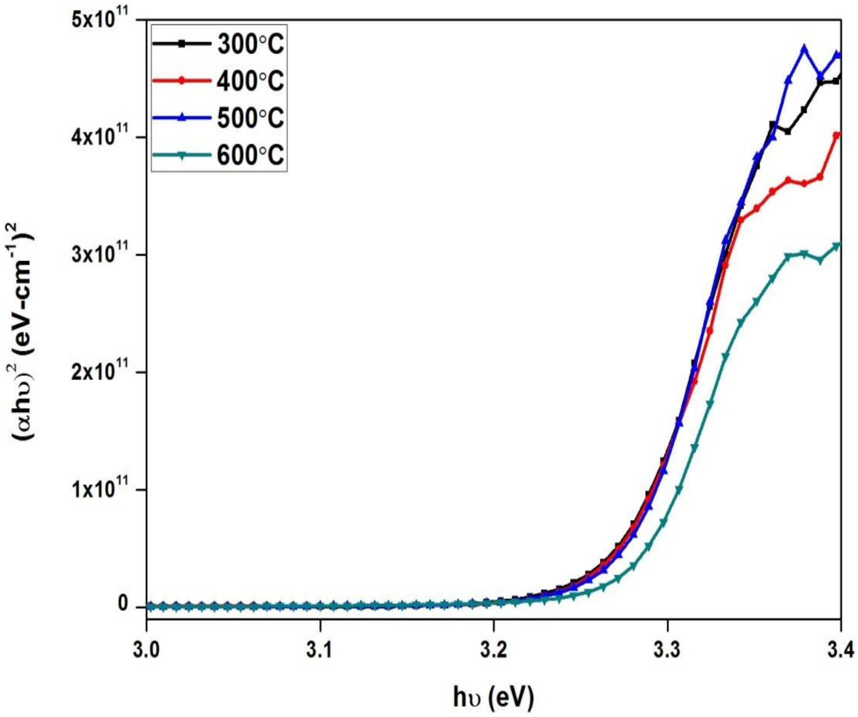

Fig.5.22. $(\alpha h\nu)^2$ versus photon energy ($h\nu$) plot for optical bandgap calculation.

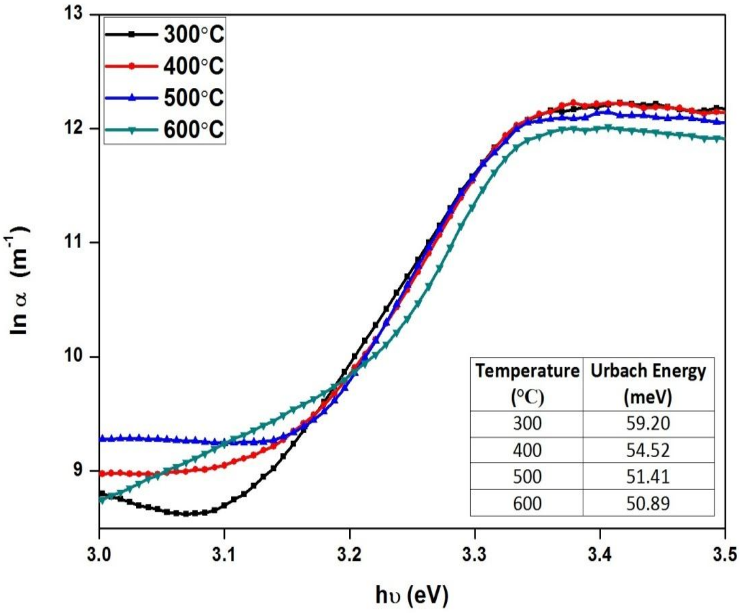

Temperature (°C)	Urbach Energy (meV)
300	59.20
400	54.52
500	51.41
600	50.89

Fig.5.23. ln (α) versus photon energy ($h\nu$) plot to obtain urbach energy relation at different annealing temperatures.

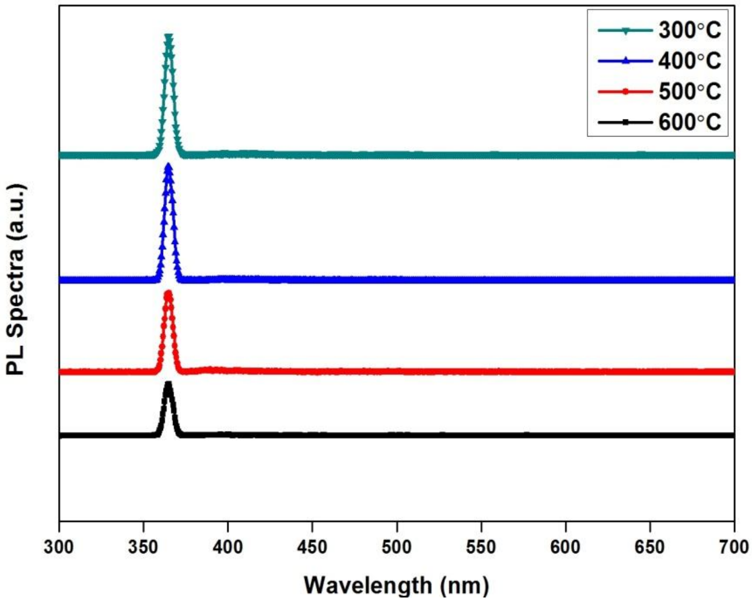

Fig.5.24. PL spectra for ZnO thin films annealed at different annealing temperatures.

5.4.3 Effect of Sputtering Power on Structural and Optical Properties of ZnO Thin Films

Fig. 5.25 shows the effect of sputtering power on growth rate. It is evident from Fig. 5.25 that growth rate has increased linearly with increasing RF power. High argon ion density and high sputtering rate is the probable reason for this enhanced growth rate. The crystallinity and microstructural properties of deposited ZnO thin films over Si and glass substrates has been studied using XRD. Fig. 5.26 shows XRD spectra of RF sputtered ZnO thin films at different sputtering powers. At lower sputtering power (80 watt), deposited film was crystalline in nature and as sputtering power increased (100-140 watt), ZnO films exhibited polycrystalline nature with one additional peak at (103) crystallographic orientation.

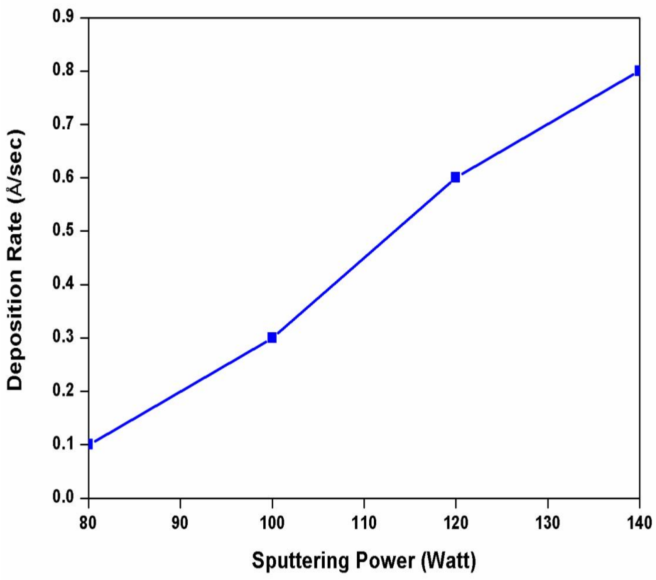

Fig.5.25. Variation of deposition rate with sputtering power.

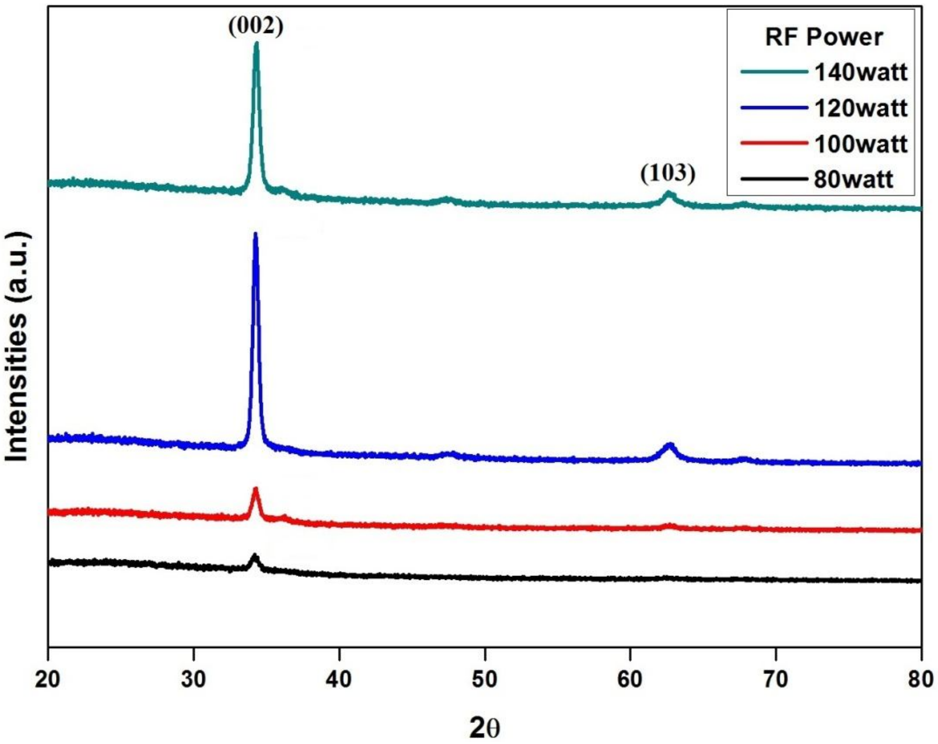

Fig.5.26. XRD spectra of ZnO thin films deposited at different sputtering powers (a) 80 watt (b) 100 watt (c) 120 watt (d) 140 watt.

Table 5.3 shows different microstructural parameters that have been derived from XRD data at different sputtering powers. It is clear from Table 5.3 that the diffraction angle (2θ) has increased with increased sputtering power. XRD analysis reveals that the peak intensity has first increased and then decreased with RF power. When sputtering power increases from 80-120 watt, the crystallinity of deposited films improves due to increased kinetic energy of the sputtering particles. Further increment in RF power accelerates the mobile energy of sputtering particles and some of them may not achieve equilibrium position, resulting in degradation of crystalline quality of deposited films.

It has been observed that grain size has increased from 12-73 nm with increasing sputtering power. Increased surface diffusion due to higher kinetic energy could be the probable reason for this increased crystalline size. Lattice constant, dislocation density, stress and strain has reduced with increased sputtering power. Values obtained for lattice constants (for all four set of samples) have shown a good agreement with standard JCPDS data (PDF#36 – 1451(a=b=3.25 Å, c= 5.20 Å)) [197]. Variation in lattice constants (a, b, c) with sputtering power is attributed to the change in the concentration of native imperfections. The negative value of stress for deposited films implies that the stress in deposited films was compressive in nature. Difference in thermal expansion coefficient of film and substrate, crystal defects and lattice mismatch between ZnO-Si heterojunction, could be the probable reason for this compressive stress.

Table 5.3. Variation of different micro-structural parameters with sputtering power.

RF Power [Watt]	**Angle (2θ)**	**Crystalline Size [nm]**	**Lattice Constant [Å]**		**Dislocation density [10^{-3}×nm^{-2}]**	**Stress [Gpa]**	**Lattice Strain**
			a=b	**c**			
80	34.1693	12.91	3.027	5.243	5.99	-1.693934311	$9.5x10^{-3}$
100	34.2605	24.52	3.019	5.230	1.66	-1.087841657	$5.0x10^{-3}$
120	34.2869	44.14	3.017	5.226	0.51	-0.913005209	$2.8x10^{-3}$
140	34.3517	73.57	3.011	5.216	0.18	-0.48501889	$1.7x10^{-3}$

Fig. 5.27 shows SEM images of ZnO thin films at 500 nm scale with 100 kX magnification. It is evident from the SEM images that the surface morphology of deposited films is almost uniform, dense and crack-free. As sputtering power increases from 80-140 watt, particle size has shown an increment of 10-85 nm. These results have shown a good agreement with XRD results (refer Table 5.3). At low

sputtering power, surface diffusion is negligible due to lower kinetic energy. As sputtering power increases, surface diffusion increases due to momentum transfer in growing surface which is attributed to increased grain size. Increased sputtering power can enhance the bombardment rate which will increase the surface mobility of the deposited films.

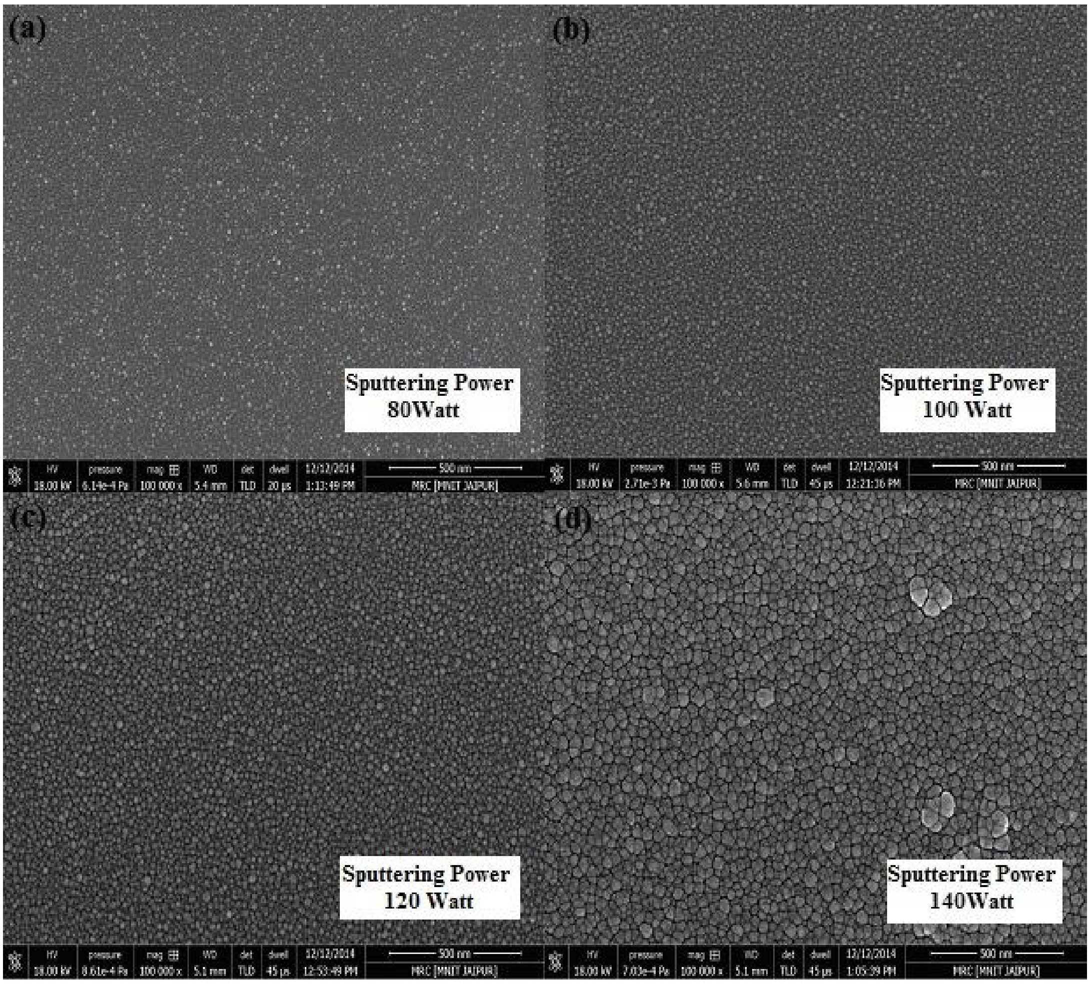

Fig.5.27. Scanning electron microscope images of ZnO thin films deposited at different sputtering powers.

Transmittance spectra of deposited ZnO thin films at different RF powers have been shown in Fig. 5.28. All films has shown high transparency with an average transmittance of >85% in visible region. High transmittance ensures good homogeneity of deposited films. The significant reduction in transmittance for wavelengths less than 400 nm (λ < 400 nm) is attributed to high absorbance characteristics of ZnO in UV region. Fig. 5.29 shows absorbance spectra of deposited films recorded in the range of 300-700 nm. It is clearly seen from absorption spectra that absorption increases with increased sputtering power. The significant fall in absorbance spectra near 375 nm wavelength is due to band edge absorption. Low absorbance in the visible region is attributed to the presence of metallic Zn interstitials.

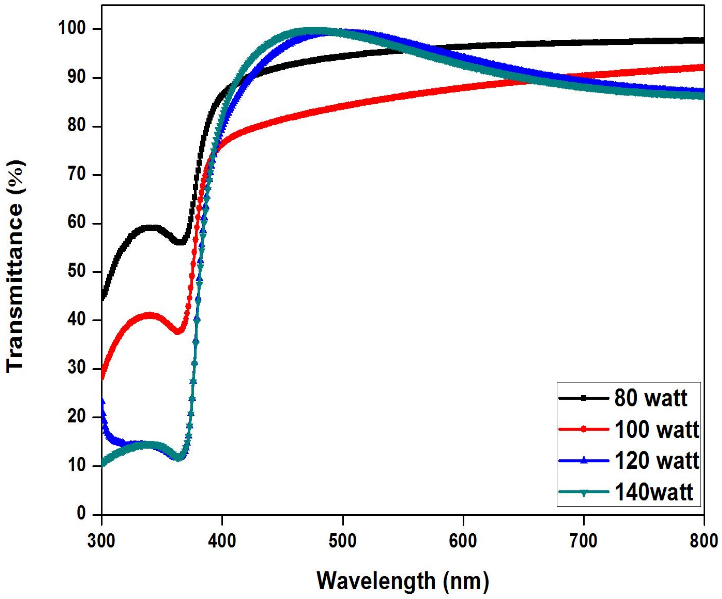

Fig.5.28. Transmittance versus wavelength plot of ZnO thin films at different sputtering powers.

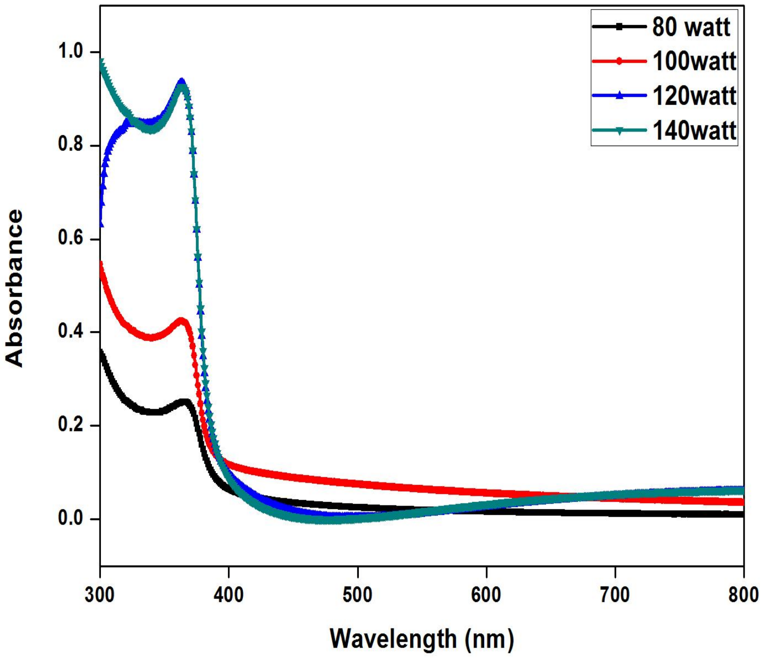

Fig.5.29. Absorbance spectra of ZnO thin films at different sputtering powers.

Photoluminescence spectra of ZnO thin films deposited at different sputtering powers is illustrated in Fig. 5.30. All deposited films have exhibited a sharp near band-edge UV emission at ~377 nm wavelength which is attributed to free exciton recombinations. Absence of other peaks except UV emission confirms high crystallinity of the deposited ZnO thin films. High crystallinity reduces the recombination centers in the film and hence radiative recombination for non equilibrium photogenerated carriers increases, which can be very beneficial in UV lasers applications. It has been observed that UV emission intensity increases as sputtering power increases from 80-120 watt and then it has decreased for 140 watt. At higher sputtering power (140 watt), energy required for surface diffusion of ZnO molecules is large enough that it can give rise to many defects, resulting in reduced UV emission intensity. UV emission intensity is strongly related to crystallization, and results obtained for PL spectra have shown good agreement with XRD results.

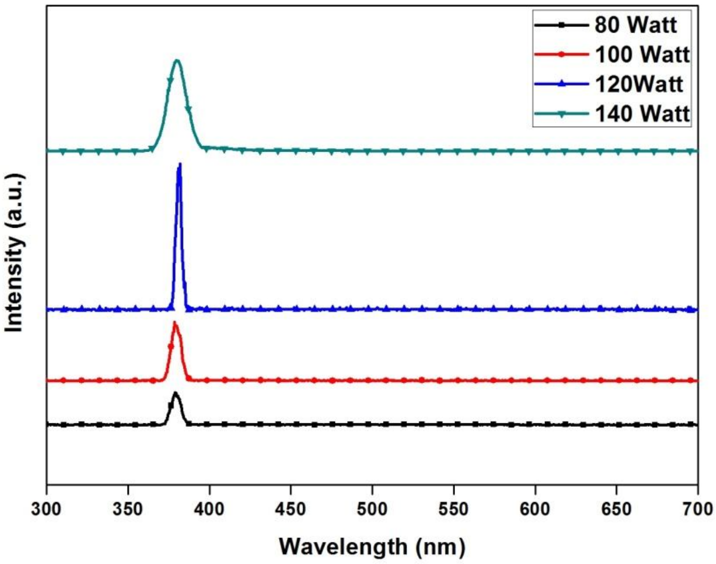

Fig.5.30. Photoluminescence spectra of ZnO thin films at different sputtering powers.

5.4.4 Effect of Gas Flow Rate on Structural and Optical Properties of ZnO Thin Films

Fig. 5.31 demonstrates the XRD pattern of deposited ZnO thin films with different argon gas flow rate varying in the range of 10-40 sccm. All deposited films have shown a strong (002) crystallographic orientation along with one additional peak at (103) orientation which confirms the polycrystalline nature of all deposited samples. It has been observed that the intensity of XRD peak was maximum at 20 sccm which has decreased considerably at higher argon flow rates (30 and 40 sccm). The XRD results indicate that the film deposited at 20 sccm has exhibited high crystallinity due to smaller FWHM value. Table 5.4 shows the effect of argon flow rate on various microstructural parameters such as grain size (D), strain, dislocation density (δ), lattice constants (a, b, c) and stress respectively.

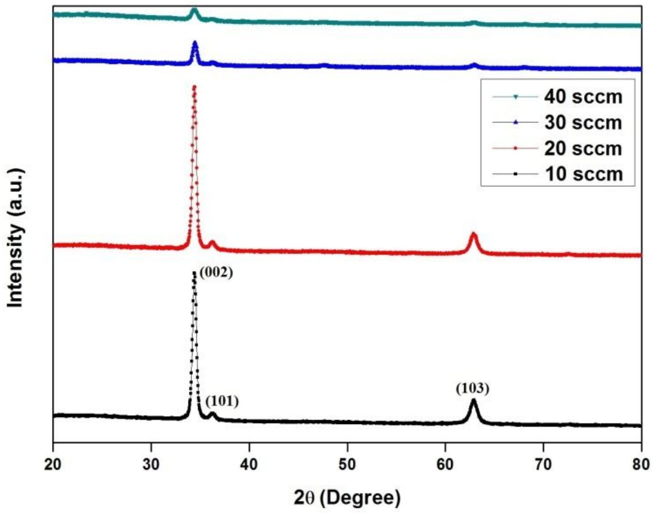

Fig.5.31. X-Ray diffraction spectra of ZnO thin films deposited at different argon flow rates.

Table 5.4. Variation of different micro-structural parameters with argon gas flow rate.

Gas Flow Rate [sccm]	**Crystalline Size [nm]**	**Lattice Strain**	**Dislocation Density [nm^{-2}]**	**Lattice Constant [Å]**		**Stress [Gpa]**
				a=b	**c**	
10	48.28	2.5×10^{-3}	0.42×10^{-3}	3.003837	5.208664	-0.11924
20	49.07	2.5×10^{-3}	0.41×10^{-3}	3.008674	5.211176	-0.23165
30	19.63	6.2×10^{-3}	2.59×10^{-3}	3.006614	5.207608	-0.07195
40	19.61	6.2×10^{-3}	2.60×10^{-3}	3.010754	5.214779	-0.3929

It is evident from Table 5.4 that the grain size has increased as the gas flow rate has increased from 10 to 20 sccm. Enhanced energetic ion bombardment with increased gas flow rate (10 to 20 sccm) promotes the mobility of adatoms, which results in increased grain size. In fact, residence time of the gas molecules play an important role in this process. Residence time is the mean time upto which the gas molecules stays in the process chamber before being pumped out and can be written as follows [213]:

$$k = \frac{V}{S} = \frac{pV}{pS} = \frac{pV}{Q} \tag{5.15}$$

Where V is the volume of the process chamber, S is the volume of the gas passing per second and Q is throughput which is equal to the pressure time of pumping speed (pS). When gas flow increases in the process chamber after a limit (30 sccm, 40 sccm in our case), the residence time of the argon atom in the process chamber reduces which results in reduced plasma density within the process chamber. This reduced plasma density slows down that deposition rate which results in reduced peak intensity and grain size at higher gas flow rates. Values obtained for lattice constants has shown a good relevance with standard JCPDS data (PDF-36 – 1451(a=b=3.25 Å, c= 5.20 Å)). Negative sign for stress signifies that the stress for all deposited films was compressive in nature. Crystal defects, difference in thermal expansion coefficients and lattice mismatch of ZnO/Si heterojunction are the probable reasons for this compressive stress. The surface morphology of ZnO thin films with argon gas flow rate variation is shown in Fig. 5.32. It is evident from SEM images that all deposited films are smooth, uniform and crack-free. It can be seen that the grain size has first increased from 10 to 20 sccm and then it has decreased at higher gas flow rate which has shown a good agreement with XRD data (refer Table 5.4).

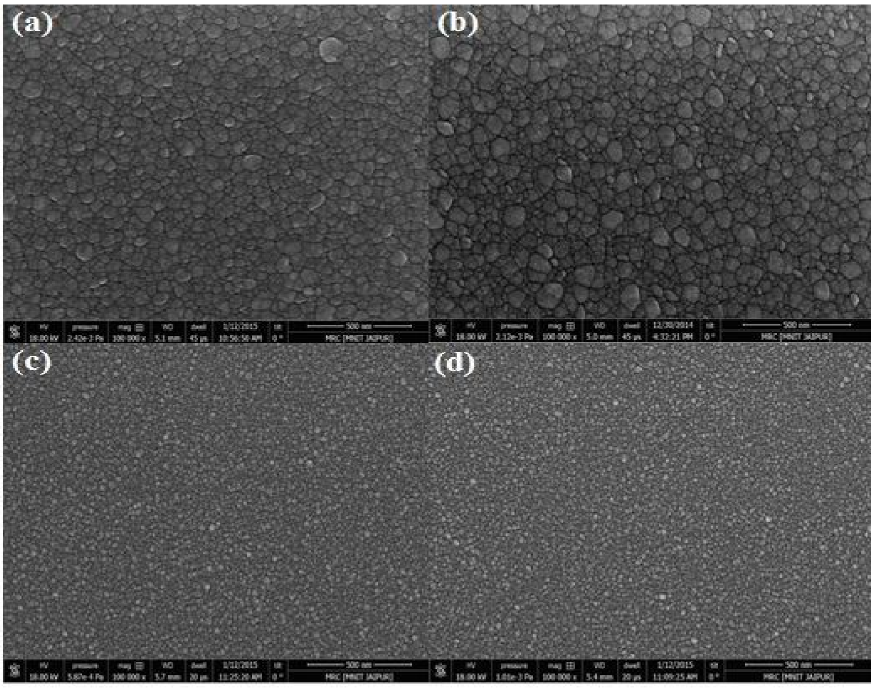

Fig.5.32. Scanning electron micrographs of ZnO thin films (a) 10 sccm (b) 20 sccm (c) 30 sccm (d) 40 sccm.

Fig. 5.33 demonstrates the effect of argon gas flow rate on the transmittance spectra of ZnO thin films for a wavelength range of 300-700 nm. The optical transmittance was about 85-98% in visible region for all deposited samples which ensures the suitability of ZnO thin films as a window material in many optoelectronic device applications. Reduced plasma density at higher gas flow rates (30 and 40 sccm) has reduced the film thickness which resulted in the absence of interference fringes in transmittance spectra at higher gas flow rates. However, the cutoff wavelength in transmittance has shown a clear shift towards shorter wavelength with increased argon flow rate. Maximum transmittance of 98.26% has been observed at 20 sccm. Fig. 5.34 shows the absorption spectra of deposited ZnO thin films at different argon gas flow rate. It is clear from the graph that absorption has first increased with gas flow rate and then it has decreased at higher gas flow rate. Absorption coefficient which is necessary to derive the optical bandgap of deposited films is shown in the inset of Fig. 5.34.

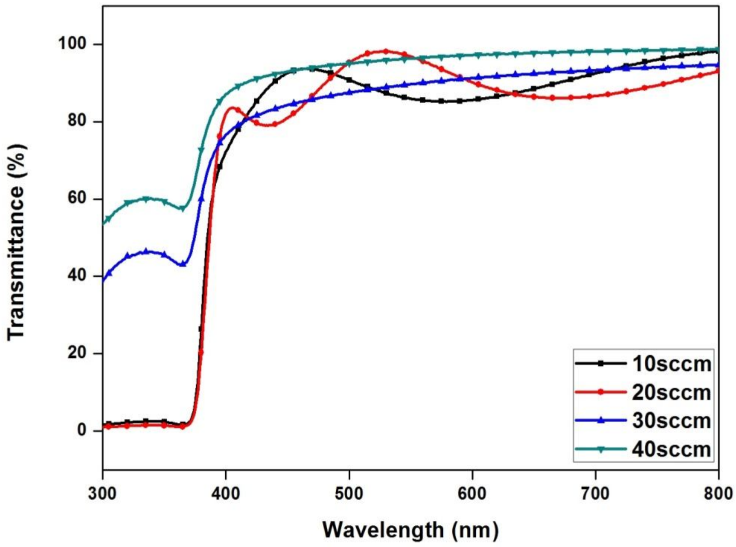

Fig.5.33. Transmittance plot of ZnO thin films at different gas flow rates.

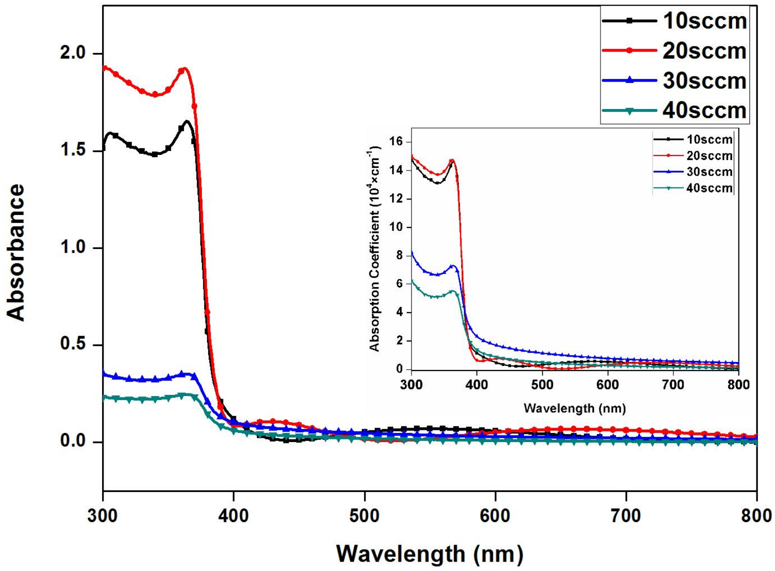

Fig.5.34. Absorbance plot of ZnO thin films at different gas flow rates. (Inset shows variation of absorption coefficient with gas flow rate).

The optical bandgap of the deposited films have been obtained from $(\alpha h\upsilon)^2$ versus $(h\upsilon)$ plot by extrapolating the linear region towards $(h\upsilon)$ axis (refer Fig. 5.35). The values obtained for optical bandgap were found to be 3.25 eV, 3.24 eV, 3.19 eV and 3.18 eV for 10 sccm, 20 sccm, 30 sccm and 40 sccm gas flow rates respectively.

Urbach energy (E_U) has been derived by taking the reciprocal of the slope of $\ln(\alpha)$ versus $h\upsilon$ plot (refer Fig. 5.36). Values obtained for urbach energy were found to be 58 meV, 66 meV, 156 meV and 155 meV for 10, 20, 30 and 40 sccm gas flow rates respectively.

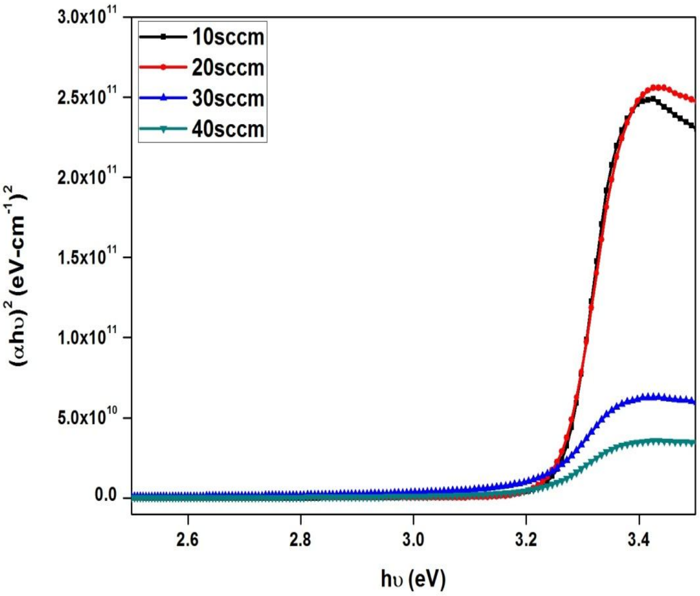

Fig.5.35. $(\alpha h\nu)^2$ versus ($h\nu$) plot for optical bandgap calculation.

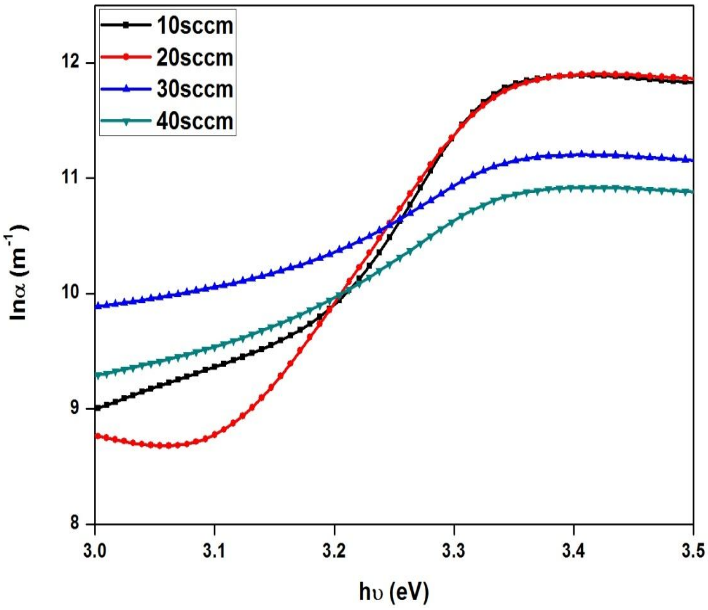

Fig.5.36. ln (α) versus $h\nu$ plot for urbach energy calculation in ZnO thin films.

5.5 Conclusion

This chapter presents preparation and optimization of ZnO thin films prepared by RF sputtering technique. In thickness dependent study of RF sputtered ZnO thin films, a detailed systematic investigation on thickness dependent structural and optical characterization of ZnO thin films have been presented which could be an important contribution for future ZnO thin film based optoelectronic devices. Four different samples of ZnO thin films with thickness varying from 190 nm to 342 nm have been deposited over p-Si and glass substrates by RF sputter at room temperature. XRD results confirmed that all deposited films were highly c-axis oriented. As thickness increases, crystalline quality of ZnO thin films has improved with increased grain size. Dislocation density, stress and strain of deposited films has decreased with increased thickness. AFM, SEM and EDX results confirm that all deposited films were almost uniform, homogenous and crack free. All deposited films have exhibited high transparency (>85%) in the visible region, and optical bandgap has shown an increment from 3.22-3.26 eV with increased thickness. Effect of thickness variation over different optical parameters such as transmittance, absorbance, optical bandgap, reflectance, absorbance, refractive index, reflectance and dielectric constant has also been investigated. Optical study shows that the refractive index, dielectric constant and UV emission intensity of deposited ZnO thin films increases with increased thickness. Results conclude that ZnO is a potential candidate for a variety of optoelectronic device applications and thickness variation in ZnO thin films do have a considerable influence over its structural and optical properties.

In annealing temperature dependent study, RF sputtered ZnO thin films were annealed at different temperatures (300°C to 600°C) in order to study the effect of post annealing temperature on deposited films. All deposited films exhibited a strong (002) crystallographic orientation and an increase in grain size with increasing annealing temperature has been observed. Nature of stress for deposited ZnO thin films got shifted from compressive to tensile as annealing temperature has increased from 300°C to 600°C. The optical transmittance was found to be more than 85 % in visible region for all deposited samples. Optical bandgap has increased at higher annealing temperature. The strong UV emission of deposited films have confirmed the usability of ZnO thin films in near UV light source applications such as next generation UV lasers.

In sputtering power dependent study, ZnO thin films were deposited over Si (100) and glass substrates at different sputtering powers (80-140 watt) using RF sputtering technique. It has been observed that the crystalline size increases with increased RF power. The ZnO films deposited at higher sputtering power has shown low defect density, stress and strain as compared to the films deposited at lower sputtering power. AFM results reveal that surface roughness has increased with increasing RF power. All films has shown high transparency (>85%) in visible region which ensures the usability of ZnO thin films in transparent electronics applications. Results confirm that the films deposited at 120 watt have shown best surface morphology and optical properties. It is believed that the balance between surface diffusion of ZnO molecules and number of ZnO molecules reaching at the substrate surface at 120 watt RF power provides optimum growth condition for high quality ZnO thin films. Effect of sputtering power on UV emission intensity has also been analyzed.

In gas flow rate dependent study, ZnO thin films with varying argon gas flow rate were deposited using RF sputtering technique. It has been observed that the peak intensity at higher gas flow rates has reduced due to reduced plasma density. A high optical transmittance of 85-98 % in visible region has been observed for all deposited samples. Some other important optical parameters such as absorption, optical bandgap and urbach energy has also been analyzed and reported. Films deposited at 20 sccm have exhibited high quality results and it has been observed that as argon gas flow rate increases from 20 scccm to 40 scccm, the plasma density degrades which reduces the deposition rate drastically.

Based on our study, the various physical and growth parameters such as thickness, sputtering power, annealing temperature and gas flow rate can lie in following range (refer Table 5.5) to achieve high quality ZnO thin films.

Table 5.5. Range of various growth parameters to achieve high quality ZnO thin films

Parameter	**Range**
Thickness	300-350 nm
Sputtering Power	100-120 watt
Annealing Temperature	400-500 °C
Gas Flow Rate	10-15 sccm

CHAPTER 6

Temperature Dependent Electrical Characteristics of Nanostructured n-ZnO/p-Si Heterojunction Diodes

This chapter presents temperature dependent electrical characteristics of n-ZnO/p-Si heterojunction diode. Estimation of series resistance, reverse saturation current, ideality factor, barrier height and Richardson constant have been done for a given temperature range of 25^0C to 120^0C. Gaussian distribution function with standard deviation of σ_0 around the mean barrier height has been used to solve the problem of barrier inhomogeneity at n-ZnO/p-Si interface.

6.1. Introduction

In recent years, ZnO has drawn a global research interest of researchers due to its unique electronic and optoelectronic properties. The wide band gap (3.37 eV), large exciton binding energy (60 meV), high electron mobility, good transparency, high thermal and mechanical stability, large saturation velocity and low growth cost ensures its suitability for different optoelectronic and nanoelectronic device applications [214]. Nanostructured ZnO is an important material for many high technological applications including diodes, solar cells, sensors, actuators, transparent conducting films, photovoltaic devices and so on. Efforts have been devoted by some researchers to produce p-type ZnO thin films in order to fully utilize the potential of ZnO. But the difficulty in producing stable and high quality p-type doping of ZnO has led the researchers to grow n-ZnO on different p-type substrates to ensure the usability of ZnO thin films in different photonic and optoelectronic devices. Different heterojunction devices such as n-ZnO/p-Si, n-ZnO/p-SiC, p-$SrCu_2O_2$/n-ZnO, p-$ZnRh_2O_4$/n-ZnO and p-NiO/n-ZnO have been reported in past [156, 215-217]. Among these, n-ZnO/p-Si heterojunction is a suitable choice due to its cost effectiveness and suitability with mature silicon ICs.

Some work on electrical and optoelectronic properties of n-ZnO/p-Si heterostructures using different fabrication methods have been reported in past [151, 218, 219]. However, no significant work for the estimation of barrier height and Richardson constant considering the barrier inhomogeneities at the interface of n-ZnO/p-Si heterojunction diode has been reported in best of our knowledge. Majumdar *et al.* reported p-ZnO/n-Si heterojunction diode using pulsed laser deposition technique [152]. They observed that barrier inhomogeneity at n-ZnO/p-Si heterojunction diode is the reason for the deviation of temperature dependent characteristics from its pure Thermionic Emission (TE) diffusion theory. In addition, Chirakkara *et al.* [151] suggested that TE theory with Gaussian distribution of barrier heights is favourable method to explain most of the electrical abnormalities of heterostructures at low and high temperatures. Al-Heniti [220] demonstrated temperature dependence of n-ZnO/p-Si p-n heterojunction diode with barrier height of 0.864 eV but estimation of Richardson constant has not been reported. Asil *et al.* investigated Richardson constant of 6.2 $Acm^{-2}K^{-2}$ which is very less than the theoretical value (32 $Acm^{-2}K^{-2}$) for ZnO [221].

This chapter presents temperature dependent I-V-T characteristics of n-ZnO/p-Si heterojunction diode using vacuum coating technique. Nanostructured zinc oxide (ZnO) thin film was deposited on p-type silicon (Si) substrate by thermal evaporation technique for fabricating n-ZnO/p-Si heterojunction diode. Estimation of series resistance, reverse saturation current, ideality factor, barrier height and Richardson constant have been done for a given temperature range of 25^0C to 120^0C. Results also confirm that the temperature dependent I-V characteristics of n-ZnO/p-Si heterojunction obey the theory of thermionic emission with Gaussian distribution.

6.2 Experimental Details

6.2.1 ZnO Thin Film Preparation

Nanostructured ZnO thin film was deposited on p-Si (100) substrate using vacuum coating method in order to fabricate n-ZnO/p-Si heterojunction diode. P-type Si (100) substrate with boron doping concentration of $\sim 7\times 10^{15}$ cm^{-3} and resistivity of 8^{-10} Ωcm was used as substrate for the fabrication of n-ZnO/p-Si heterojunction diode. ZnO powder with 99.99% purity from MERCK-Chemical limited, Mumbai, India was used as source material. Acetone, isopropyl alcohol and de-ionized water (from Milli-Q water plant of Millipore, USA, resistivity ~18 MΩcm) were used in sequence for wafer cleaning. For controlled growth of ZnO film, a 20 nm thick seed layer of Al doped ZnO (AZO with ~1% Al) was deposited on silicon wafer using vacuum coating technique. The vacuum coating unit (Model no 12A4D of HINDVAC, India) was used for AZO and ZnO layer growth in sequence. The base pressure, DC power and evaporation time was 10^{-3} mPa, 45 W and 40 minutes respectively during the deposition. The distance between source and substrate was 18 cm and deposition was done at room temperature (27°C). ZnO and Al powders were mixed with polyvinyl alcohol (PVA) in appropriate amount (by weight) for about 1 hour using agate mortar and pestle sets. ZnO and Al doped ZnO pellets were made using a hot pressure setup. Conventional molybdenum boat was used as heating filament for the evaporation of AZO/ZnO pellets during the deposition of the film. The measured thickness of ZnO thin film was ~300 nm. Then, the sample was subjected to rapid thermal annealing (RTA) at 600ºC in O_2 and Ar ambient so that the quality and conductivity of ZnO thin film nanowires can be improved. After annealing, when temperature reached at room temperature (27°C), structural and morphological properties of ZnO thin film were studied.

6.2.2 Thin Film Characterization

Detailed description of different fabrication and characterization techniques (Thermal Evaporation, XRD, AFM, EDX) to study the structural and optical properties of the fabricated n-ZnO/p-Si heterojunction is already presented in Chapter3. Subsequently, the potential of n-ZnO/p-Si heterojunction for optoelectronic device applications was also tested.

Fig.6.1 shows the schematic diagram of I-V measurement setup for n-ZnO/p-Si heterojunction diode. Ohmic contacts for I-V measurement were obtained by depositing Al dots on ZnO thin film. A ~20 nm thick Al layer was deposited on backside of p-Si substrate to obtain the ohmic contact from the back. After ensuring ohmic characteristics for Al/ZnO interface and Al/Si interface (refer Fig. 6.1), the I-V characteristics of the n-ZnO/p-Si heterojunction were studied further. The temperature dependent I-V characteristics of n-ZnO/p-Si heterojunction diode were studied using semiconductor parameter analyzers from Agilent Technologies (Model: B1500A). Temperature was varied from 25^0C to 120^0C for a voltage range of -5 to 5 V.

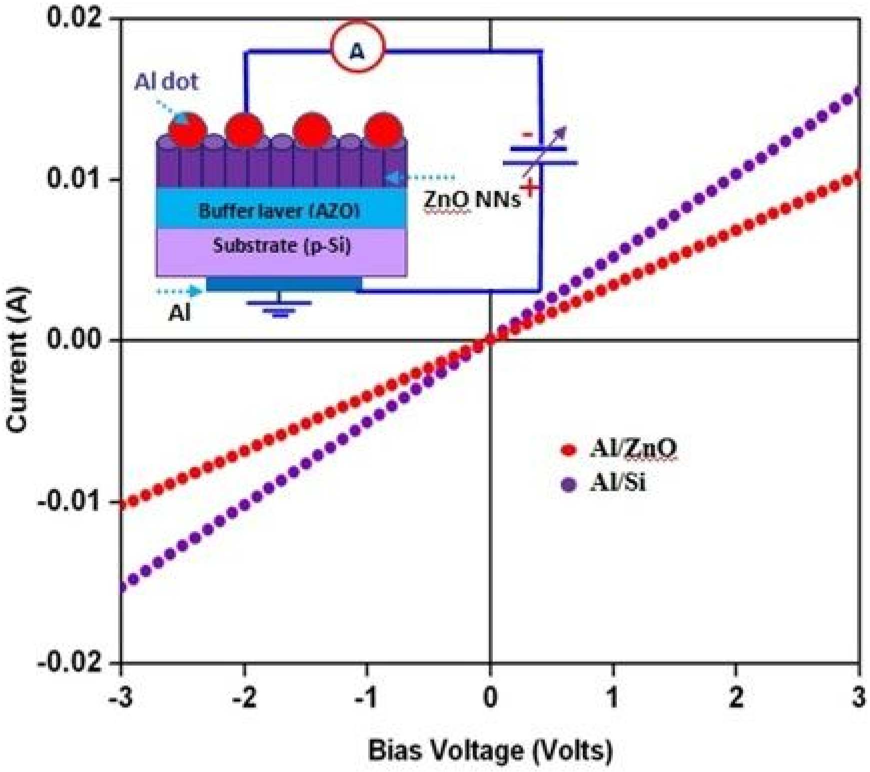

Fig.6.1. Ohmic contact plot for Al/ZnO and Al/Si interfaces (inset shows schematic diagram of heterojunction based on n-ZnO /p-Si device structure).

6.3 Results and Discussion

6.3.1 Structural and Surface Morphology Study

Figure 6.2 (a) depicts the X-ray diffraction (XRD) analysis of nanostructures n-ZnO thin film. The XRD pattern of ZnO thin film (Fig. 6.2 (a)) has shown a unique peak at $2\theta = 34.41°$ corresponding to the (002) reflexion of ZnO and confirmed a good single crystalline nature of ZnO thin film. XRD pattern indicates a preferential growth, oriented along the c-axis in accordance with previous reports available in the literature [152, 215, and 219]. The Atomic Force Microscope (AFM) image (inset Fig. 6.2 (a)) clearly demonstrates that well-aligned vertical ZnO nanoneedle arrays with excellent morphology can be grown on p-Si substrate using thermal evaporation technique.

This feature of ZnO thin film ensures its suitability for nanoelectronic device applications. Energy-Dispersive X-ray (EDX) spectra shown in Fig. 6.2 (b) confirm the presence of Zn, Al and O on the sample. The inset in Fig. 6.2 (b) shows the elements (by corresponding wt. %) present in the prepared thin film. The average diameter and length of the ZnO nanowires was found to be in the range of 20-40 nm and 3 – 4 μm respectively.

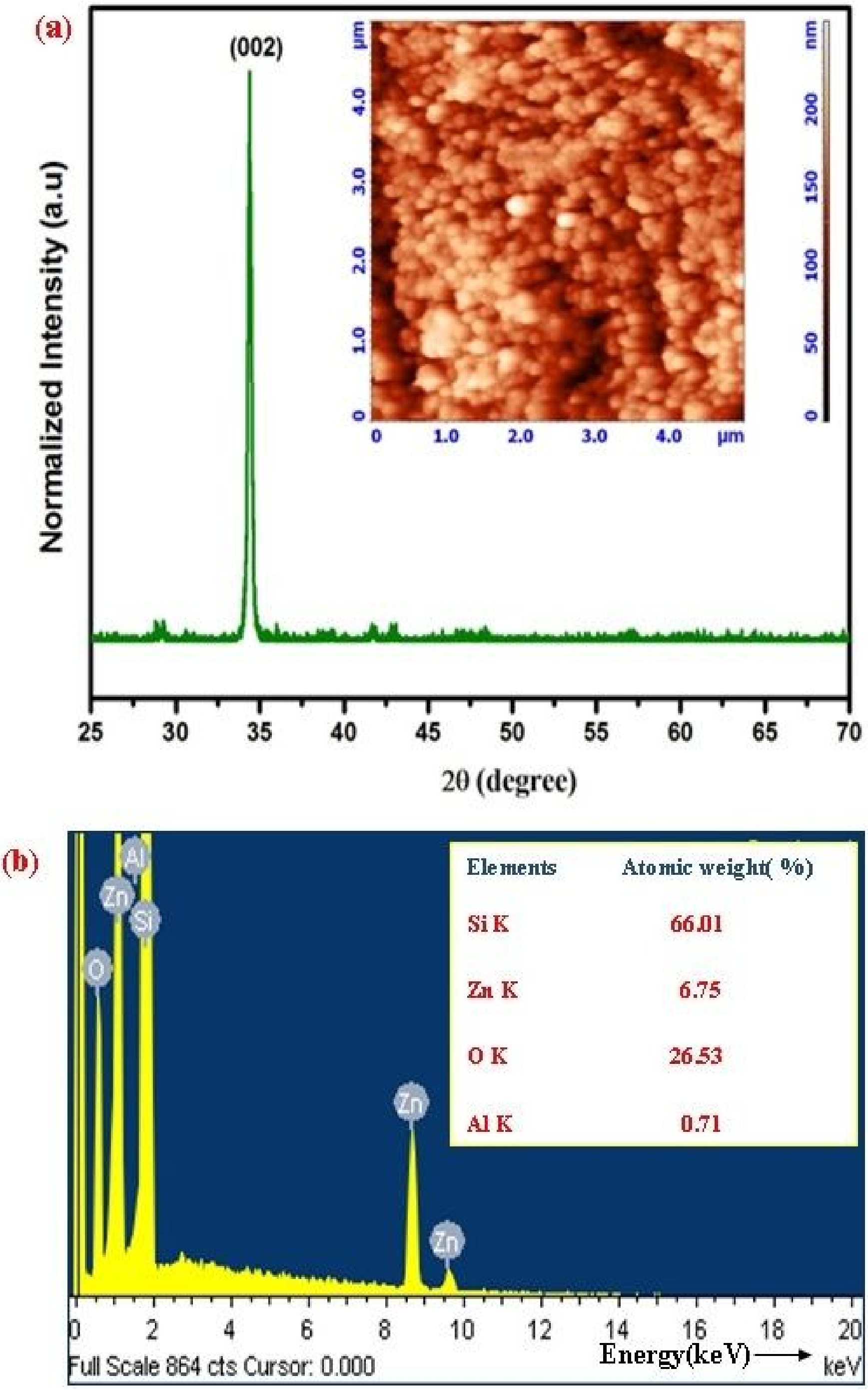

Elements	Atomic weight(%)
Si K	66.01
Zn K	6.75
O K	26.53
Al K	0.71

Fig.6.2. (a) XRD spectra of ZnO thin film (inset shows two-dimensional view AFM image of ZnO on Si), (b) EDX spectra for ZnO thin film (inset shows elements by corresponding atomic wt. % for ZnO/Si heterojunction).

6.3.2 Temperature Dependent Characteristics for n-ZnO/p-Si Heterojunction

Figure 6.3 shows the experimentally measured I-V characteristics for n-ZnO/p-Si heterojunction diode and confirms the rectifying nature of the contact. The turn-on voltage of the n-ZnO/p-Si heterojunction is estimated to be 0.8 V at room temperature. Conventional thermionic emission model has been used for the analysis of the temperature dependent I–V characteristics of n-ZnO/p-Si heterojunction to extract the diode parameters. Using standard thermionic emission equation for ZnO/Si heterojunction, the relation between voltage and current can be expressed as:

$$I = I_0\left[\exp\left(\frac{qV}{\eta kT}\right) - 1\right] \tag{6.1}$$

where q represents charge of electron, V is biasing voltage, k is Boltzmann constant, I_0 reverse saturation current and η is the ideality factor described as [149]:

$$\eta = \left[\frac{q}{kT}\frac{\partial V}{\partial \ln(I)}\right] \tag{6.2}$$

where $(\partial \ln(I))/\partial V)$ can be obtained from the linear region slop of $\ln(I) - V$ plot, A is contact area which is ~ 0.785×10^{-2} cm^2 in our case, A^* is Richardson constant (A^*= 32 Acm^{-2}k^{-2}) and $\phi_{B,eff}$ is the effective barrier height at zero bias described as:

$$\phi_{B,eff} = \frac{kT}{q} ln\left(\frac{AA^*T^2}{I_o}\right) \tag{6.3}$$

The proportionality of reverse current with temperature (refer Eq. (6.3)) clearly shows that reverse current is highly temperature dependent. Temperature dependent I-V curve shown in Fig. 6.3 also confirms this phenomenon. It is also observed in Fig. 6.3 that the reverse current is slightly non-saturating with the reverse bias voltage. This non-saturation of current with applied reverse bias is due to spatial inhomogeneity of barrier height explained by Yıldız *et al.* [222]. However, the saturated downward curvature in the temperature dependent I-V-T characteristics at forward bias region can be attributed to the large surface state density near the bottom of the conduction band and the series resistance of the device. Aydogan *et al.* [223] reported that series resistance is one of the reasons for non linear region I-V characteristics. The method introduced by Cheung *et al.* [224], verified by Altindal *et al.* [225] and Werner *et al.* [226] have been used to analyze the temperature dependence of series resistance for I-V characteristics. Series resistance for given n-ZnO/p-Si heterojunction diode can be described as [223]:

$$\frac{dV}{d(\ln(I))} = \frac{\eta kT}{q} + R_S I \tag{6.4}$$

Series resistance has been derived from the slop of $dV/\ d(\ln(I))$ vs I plot (not shown here) over the temperature range of 25^0C to 120^0C.

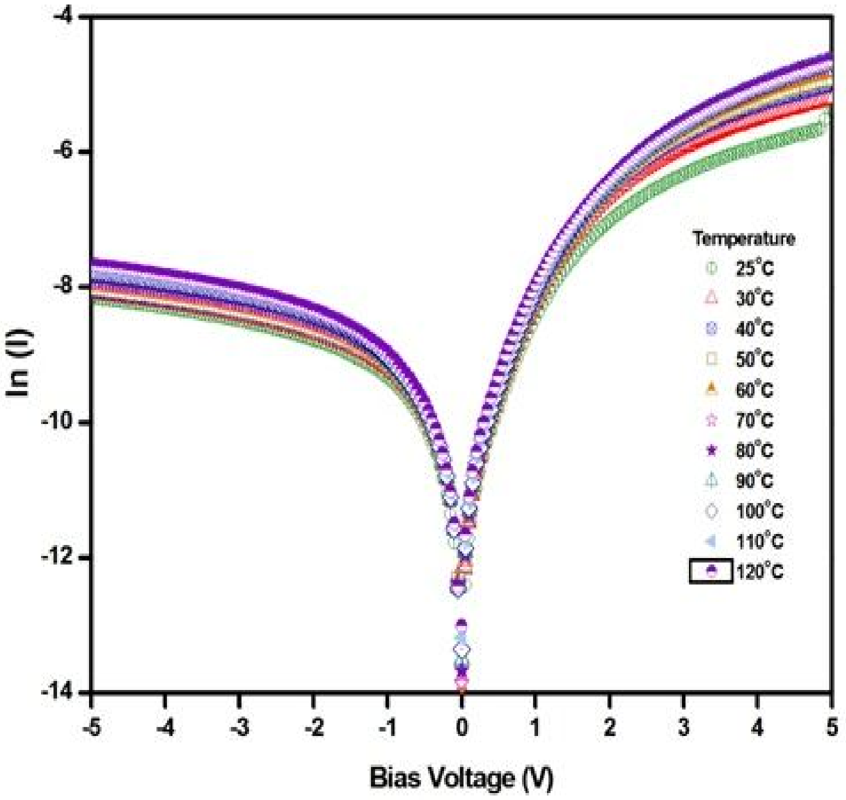

Fig.6.3 Experimental ln I-V characteristics of n-ZnO/p-Si heterojunction for different temperature ranges.

Fig.6.4 shows the variation of series resistance with temperature. It can be seen from the graph that as temperature increases from 25^0C to 120^0C, series resistance has reduced from ~ 933 Ω to ~ 481 Ω. The values of I_o, $\phi_{B,eff}$ and η estimated from the I–V-T characteristics over 25^0C to 120^0C operating temperatures are shown in Table I. Results confirm good temperature stability of n-ZnO/p-Si heterojunction diodes. It can be seen from Table. 6.1 that reverse saturation current, barrier height and ideality factor all are temperature dependent. As operating temperature increases from 25^0C to 120^0C, reverse saturation current and barrier height increases whereas ideality factor decreases with temperature rise. The value of ideality factor greater than its ideal value of unity is attributed to the inhomogeneity at n-ZnO/p-Si interface [227-231].

Difference between thermal expansion coefficient of Si and ZnO and lattice mismatch is the probable reason for this deviation from its ideal value. Lattice mismatch may cause strain in the film due to edge dislocations at the junction [152, 220]. The ideality factor of greater than 1 for n-ZnO/p-Si heterojunction diode indicates that thermionic emission and diffusion are not the only dominating current transport mechanism. Temperature dependence of ideality factor implies that diffusion, thermionic emission, tunnelling and space charge region recombination can be the possible current transport mechanisms for n-ZnO/p-Si heterostructure diodes. Fig. 6.5 shows a linear relationship between barrier heights and ideality factor over a given temperature range. According to Schmitsdorf *et al.*, this linear relationship between ideality factor and barrier height attributes to barrier irregularity and lateral inhomogeneities of barrier heights [232].

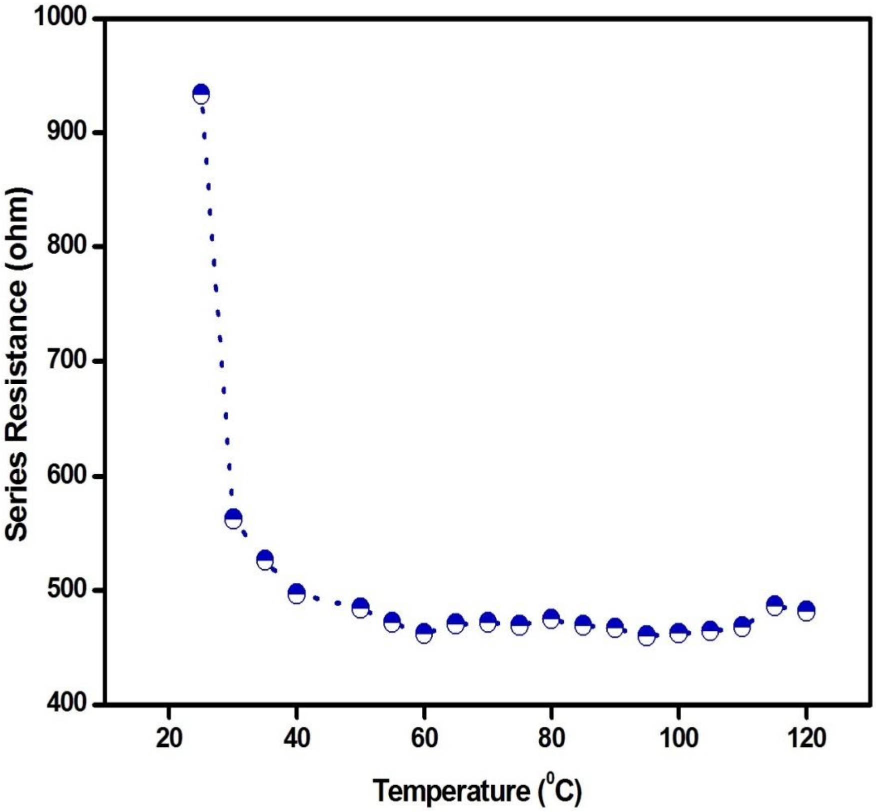

Fig.6.4. Series resistance vs temperature plot for n-ZnO/p-Si heterojunction diode.

Table 6.1. Variation of reverse saturation current, barrier height and ideality factor with temperature for n-ZnO/p-Si heterojunction diode.

Temperature (^{0}C)	**Reverse Saturation Current (A)**	**Barrier Height (eV)**	**Ideality Factor**
25	$1.25 x10^{-7}$	0.665299	3.50
30	$2.50 x10^{-7}$	0.659232	3.51
35	$3.43 x10^{-7}$	0.662585	3.48
40	$4.76 x10^{-7}$	0.665372	3.47
45	$5.60 x10^{-7}$	0.683857	3.40
50	$6.68 x10^{-7}$	0.690327	3.38
55	$7.62 x10^{-7}$	0.69794	3.37
60	$8.41 x10^{-7}$	0.706415	3.35
65	$9.56 x10^{-7}$	0.713944	3.34
70	$1.07 x10^{-6}$	0.717349	3.36
75	$1.10 x10^{-6}$	0.721012	3.33
80	$1.16 x10^{-6}$	0.730624	3.31
85	$1.23 x10^{-6}$	0.740033	3.28
90	$1.36 x10^{-6}$	0.748093	3.27
95	$1.47 x10^{-6}$	0.756799	3.26
100	$1.58 x10^{-6}$	0.765629	3.23
105	$1.65 x10^{-6}$	0.775348	3.20
110	$1.88 x10^{-6}$	0.782164	3.16
115	$2.03 x10^{-6}$	0.790676	3.15
120	$2.24 x10^{-6}$	0.798399	3.14

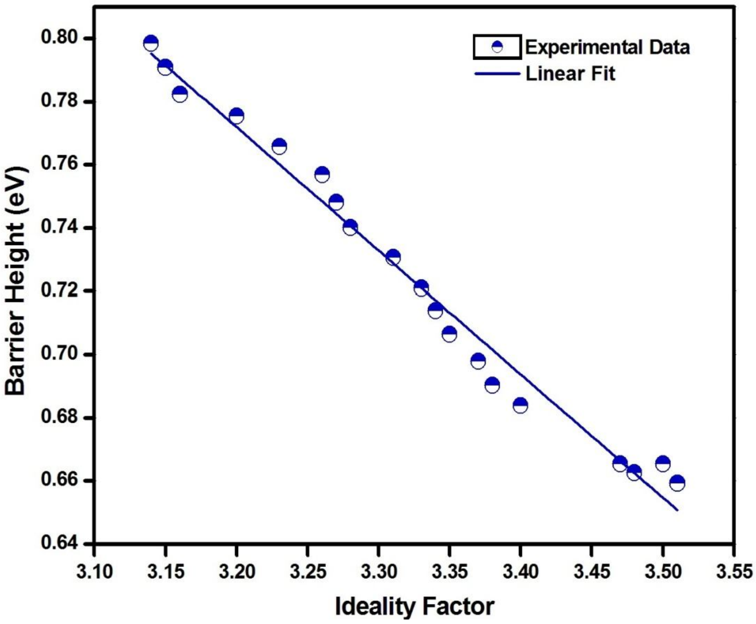

Fig.6.5. Barrier height vs ideality factor plot over the temperature range of 25^0C to 120^0C.

Equation 6.3 can be rearranged as Eq. (6.5) to obtain relationship between $ln(I_0/T^2)$ vs q/kT. Fig. 6.6 shows $ln(I_0/T^2)$ vs q/kT plot which gives barrier height of 194 meV and Richardson constant of 6.61×10^{-7} Acm^{-2}K^{-2} from slope and intercept respectively.

$$\ln\left(\frac{I_0}{T^2}\right) = \ln(AA^*) - \frac{q\phi_{B0}}{kT} \tag{6.5}$$

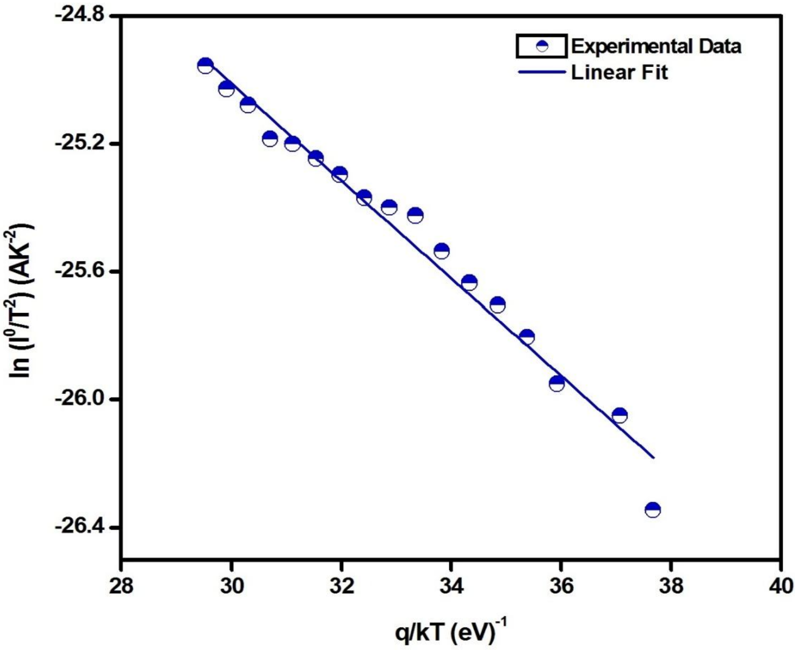

Fig.6.6. Richardson's plot of ln(I_0/T^2) vs q/kT for barrier height and Richardson constant calculation.

This significant deviation of Richardson constant from its theoretical value i.e. 32 Acm^{-2}K^{-2} is due to barrier inhomogeneities at the interface. This barrier imhomogeneity have been analyzed and corrected to obtain modified Richardson constant which is very close to the standard theoretical value of Richardson constant (32 Acm^{-2}K^{-2}) for ZnO. Tung [233] explained that the low barrier height region surrounded by high barrier height region should lead to "pinch off" of conduction path due to the interaction between the patches, and the change in barrier height may occur at very small scale as compared to depletion region width.

To solve the problem of inhomogeneous contacts, Gaussian distribution function with standard deviation of σ_0 around the mean barrier height has been used. Barrier height and ideality factor while implementing the Gaussian distribution can be described as [234, 235].

$$\emptyset_{B,eff}(T) = \emptyset_{B0,m}(T = 0) - \frac{q\sigma_0^2}{2kT} \tag{6.6}$$

$$\left(\frac{1}{\eta(T)} - 1\right) = \rho_1 - \frac{q\rho_2}{2kT} \tag{6.7}$$

$$\emptyset_{B,m}(V) = \emptyset_{B0,m} + \rho_1 V \tag{6.8}$$

$$\sigma^2(V) = \sigma_0^2 + \rho_2 V \tag{6.9}$$

where $\eta(T)$ is temperature dependent ideality factor, $\emptyset_{B,m}(V)$ is bias dependent mean barrier height, ρ_1 and ρ_2 are voltage coefficients which may depend upon temperature, $\sigma(V)$ is bias dependent standard deviation.

Fig. 6.7 shows the plot between barrier height vs q/2kT. Linear fit equation (shown in Fig. 6.7) obtained from the slope and the intercept of the given experimental data when compared with Eq. (6.6) gives $\emptyset_{B,0m}(T = 0)$ = 1.24 eV and σ_0=0.176 V. Similarly linear fit obtained from η^{-1}-1 vs q/2kT plot (Fig. 6.8) when compared with Eq. (6.7) gives $\rho_1 = 0.577\,V$ and ρ_2= 0.007 V. Temperature dependence of ideality factor can be calculated from equation (6.7) by using $\rho_1$and ρ_2 values derived from Fig.6.8. Bias dependent mean barrier height and standard deviation can be calculated from Eq. (6.8 and 6.9) using values of $\emptyset_{B0,m}(T = 0)$, ρ_1 and ρ_2. By considering barrier inhomogeneities, modified Richardson constant can be written as [234, 235]:

$$\ln\left(\frac{I_0}{T^2}\right) - \left(\frac{q^2\sigma_0^2}{2(kT)^2}\right) = \ln(AA^*) - \frac{q\emptyset_{B0,m}(T = 0)}{kT} \tag{6.10}$$

The plot between ln(I_0/T^2)- $q^2\sigma_0^2/2(kT)^2$ versus q/kT is a straight line where slope gives mean barrier height and intercept gives modified Richardson constant. Value of mean barrier height and modified Richardson constant obtained from Fig. 6.9 is 1.25 eV and 39.18 $Acm^{-2}K^{-2}$ respectively. Consideration of barrier height inhomogeneities phenomenon has shown significant improvement for modified Richardson constant which is very close to the actual theoretical value of Richardson constant i.e. 32 $Acm^{-2}K^{-2}$. This modified value of Richardson constant is better than reported by others. [234, 235].

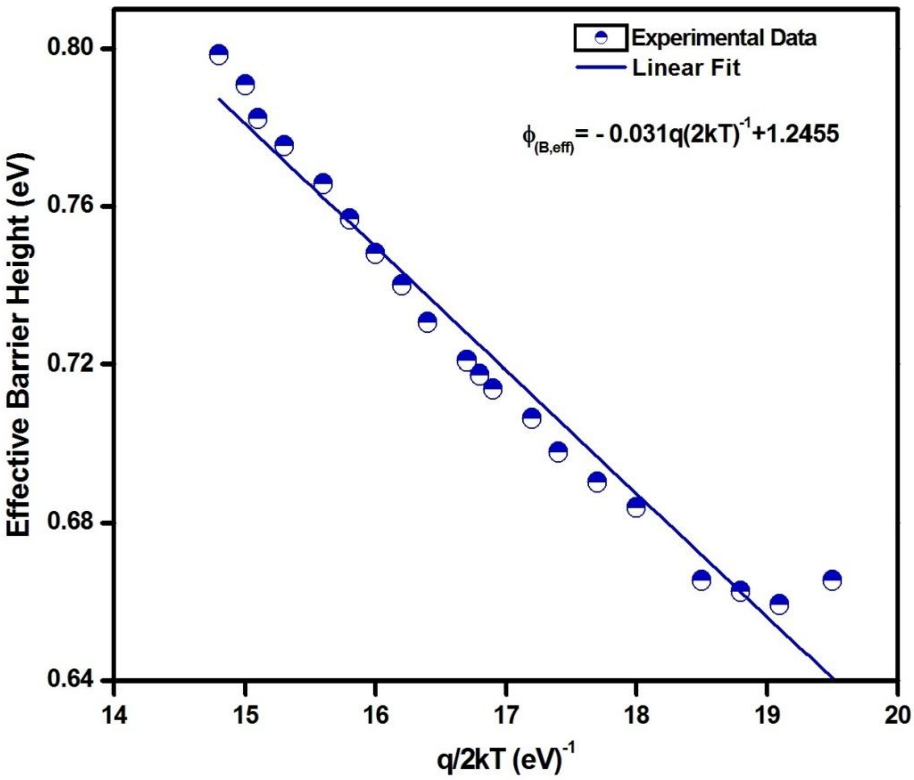

Fig.6.7. Effective barrier height as a function of q/2kT.

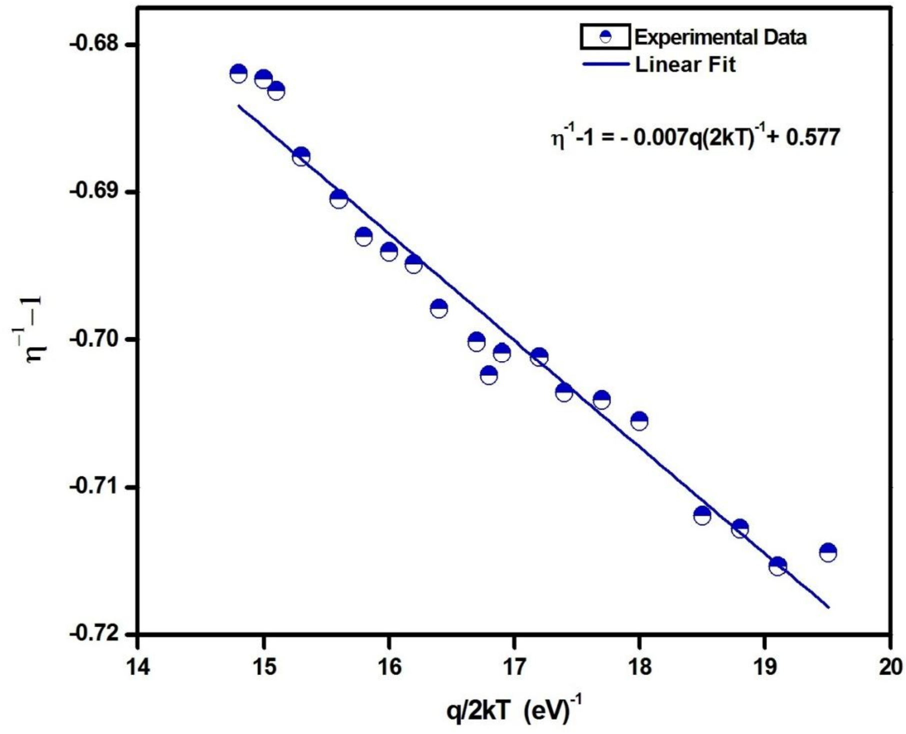

Fig.6.8. η^{-1}-1 Vs q/2kT plot for calculation of different parameters.

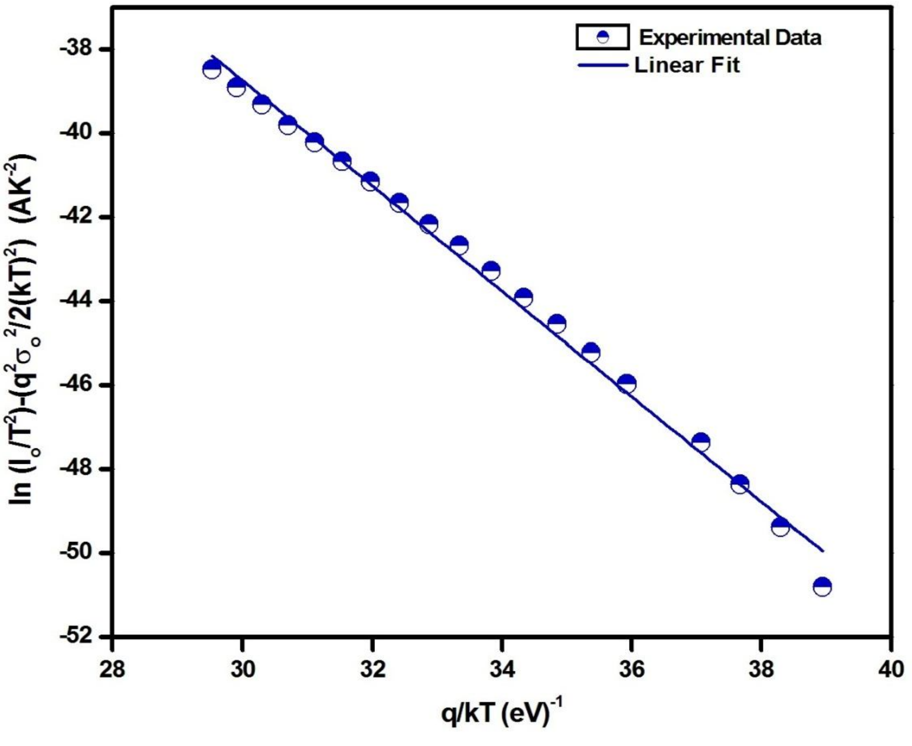

Fig.6.9. Modified Richardson plot for calculation of barrier height and Richardson constant by considering Gaussian distribution of barrier height.

6.4. Conclusion

In this chapter, fabrication and temperature dependent electrical characteristics of n-ZnO/p-Si heterojunction diode have been studied. Temperature variation of 25^0C to 120^0C for n-ZnO/p-Si heterojunction diode has shown good thermal stability. Effect of temperature variation on series resistance of n-ZnO/p-Si heterojunction diode has also been evaluated. It has been observed that as temperature increases barrier height and reverse saturation current increases whereas ideality factor decreases. The estimated value of Richardson constant obtained from $\ln{(I_0/T^2)}$ vs q/kT plot is 6.61×10^{-7} $Acm^{-2}K^{-2}$ which was very less than the theoretical value of Richardson constant for ZnO. It has been observed that the barrier inhomogeneity at the interface of ZnO/Si is the probable reason for deviation of Richardson constant. So by implementing the Gaussian distribution of barrier height to TE model, modified Richardson constant of 39.18 $Acm^{-2}K^{-2}$ is obtained which is very close to the actual theoretical value of Richardson constant i.e. 32 $Acm^{-2}K^{-2}$.

CHAPTER 7

Nancrystalline n-ZnO/p-Si Heterojunction Based Ultraviolet Detector

This chapter presents ultraviolet light detection properties of n-ZnO/p-Si heterojunction diodes. The structural and surface morphological properties of the deposited films were studied using XRD, AFM, SEM, TEM and Raman spectroscopy. The junction properties of ZnO/Si heterojunction diodes were investigated using current-voltage and capacitance-voltage measurements. Various other parameters such as built-in potential, donor concentration and depletion width have also been evaluated. The fabricated diodes show a very good response towards UV light.

7.1. Introduction

In last decade, ZnO has emerged as a promising candidate for wide variety of nanoelectronic and optoelectronic device applications. It’s cheap cost, wide bandgap, high exciton binding energy, high chemical stability and strong radiation hardness make ZnO a potential choice over other wide band gap materials. ZnO nanostructure based heterojunctions have proved their potentiality in many advanced applications which include sensors, actuators, light emitting diodes, solar cells and piezoelectric nanogenerators [236-238].

In recent years, ZnO has drawn a substantial attention of researchers for UV detection applications. Large and direct bandgap, high surface to volume ratio and other superior properties of ZnO has made it a promising choice for ultra violet light detection with high selectivity and sensitivity. ZnO based UV detectors can also be very useful in variety applications such as flame sensing, space to space communication, UV astronomy, and environmental monitoring. Different ZnO based UV photodetectors such as metal-semiconductor-metal photodiode, schottky photodiode and p-n heterojunction photodiode have been reported by researchers in past [11, 101, 239]. Among these, p-n heterojunction based photodiode is simple to fabricate with a very high UV detection capabilities.

While some reports on p-ZnO based optoelectronic devices are available in the literature, in general it is difficult to obtain high quality p-doped ZnO films with good repeatability and reproducibility. Studies on n-ZnO based heterojunctions with various p-type substrates such as AlGaN [240], GaN [157], SiC [182] and Si [241] have been reported in past. Among these, n-ZnO films deposited over p-Si substrates have attracted special interest because silicon technology is very well matured in industry. Many deposition techniques such as metal organic CVD [242], pulsed laser deposition (PLD) [185], sol-gel [168], radio frequency (RF) sputtering) [243] and thermal vapor deposition [219] have been used in past to grow ZnO thin films. Among these, RF sputtering provides high quality ZnO thin films with a precise control over different process parameters such as substrate temperature, sputtering power, gas flow rate and deposition pressure.

This chapter presents structural, electrical and UV detection properties of n-ZnO/p-Si heterojunction diodes. n-ZnO thin films were deposited over p-Si (100) substrate using RF sputtering. In order to investigate the quality of the deposited films, structural and surface morphological properties were studied using XRD, AFM, SEM, TEM and Raman spectroscopy. The effect of temperature on various electrical parameters (ideality factor, barrier height) was investigated using current (I) – voltage (V) measurements. Capacitance (C) – voltage (V) measurement were done to evaluate built-in potential, donor concentration and depletion width of the fabricated structures. The response of the fabricated n-ZnO/p-Si heterojunction diodes towards UV light was also tested and various other parameters such as responsivity and detectivity which are necessary to analyze the performance of n-ZnO/p-Si UV detectors have also been evaluated.

7.2 Experimental Details

The ZnO thin films were grown onto p-type Si (100) substrates (resistivity: 8^{-10} Ωcm, boron doping concentration: ~7×10^{15} cm^{-3}) using RF sputtering. All the process parameters such as sputtering power, deposition pressure and gas flow rate were optimized prior to the actual deposition, so that high quality films can be obtained. The deposition pressure, sputtering power and argon flow rate were maintained at 4-6×10^{-3} mbar, 100 W and 10 sccm respectively during the deposition. Deposition was done at room temperature and deposition rate was found to be in the range of 0.2-0.4 Å/sec. ZnO film thickness for device fabrication was ~350 nm. Post deposition samples were annealed for 1 hour at 400°C in argon ambient. RF sputter deposition with shadow masking was used to realize aluminium contacts on Si and ZnO. The thickness of aluminium dots was ~125 nm.

The crystallographic, structural and surface morphological properties of the deposited films were studied using XRD (PANalytical X'Pert Pro - 18 kW Cu X-ray diffractometer with Cu Kα radiation (λ = 1.542 Å)), AFM (Multimode 8 SPM, Bruker) and SEM (Nova Nano FE-SEM 450) respectively. In order to elucidate local morphology and structure of the ZnO nanocrystals, TEM was performed on ZnO films (~20 nm thickness) which were sputter deposited under the same conditions as the thicker device films onto 5 nm SiN TEM windows (Simpore, SN100A05Q00). TEM (Philips CM200) with electron acceleration voltage of 150 kV was employed to obtain complementary bright field, selected area electron diffraction (SAED) and dark field information. The obtained SAED patterns were phase identified by comparison to the Inorganic Crystal Structure Database (ICSD) entry 31052 (ZnO; P63mc Wurtzite structure). A Raman Spectrometer (NT MDT Ntegra Spectra) with 473 nm excitation laser was employed to investigate deposited ZnO thin film. Electrical characterization of fabricated n-ZnO/p-Si heterojunction diodes was been done using a Semiconductor Parameter Analyzer (Agilent-B1500A). A 365nm wavelength UV lamp from ORANGE, India (PVU365) was used to investigate UV detection capabilities of the fabricated n-ZnO/p-Si diodes.

7.3 Results and Discussion

7.3.1 Structural and Surface Morphology Study:

Fig. 7.1 shows the XRD pattern of the deposited ZnO thin films. The nature of the film was found to be polycrystalline with a dominating (002) crystallographic orientation. Some additional low intensity peaks with (101), (102) and (103) orientations has also been observed. The average crystalline size obtained from Scherrer formula [197] was found to be 55.2 nm for (002) crystallographic orientation. The value obtained for lattice parameters (a,b,c) from the diffraction pattern was recorded as a=b=3.013 Å and c=5.2202 Å which compares well with the standard JCPDS Card (No.-36-1451 [197]). The slight variation in lattice constants from bulk ZnO is usually expected in low dimensional growth of ZnO thin films. The values obtained for dislocation density, stress and strain [197, 198] were found to be

0.32×10^{-3} nm^{-2}, -0.635 GPa and 2.2×10^{-3} respectively. The negative sign in the stress value confirms that the nature of the stress was compressive.

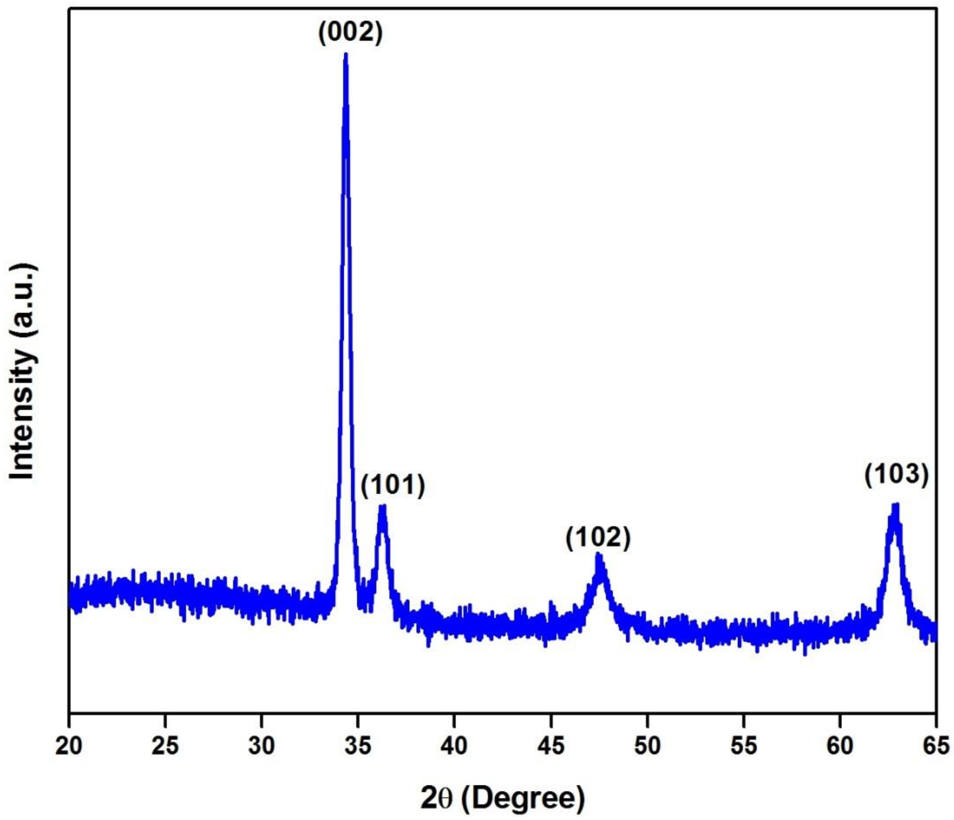

Fig.7.1. X-Ray diffraction pattern of deposited ZnO thin film over Si substrate.

Fig. 7.2 shows AFM images of the ZnO film surface. It is evident from the images that the surface of the deposited film is reasonably smooth. The roughness was found to be 5.4 nm over an area of 3×3 μm^2. The three dimensionally plotted AFM image also reveals the dense growth of grains with a highly homogenous distribution. Fig. 7.3 shows corresponding SEM micrograph of the deposited ZnO film. It is clear from the SEM image that the grains are uniformly distributed over the substrate with good adhesion. The size of the grains was found to be in the range of 45-100 nm. Energy dispersive X-Ray (EDX) spectroscopy confirms that only zinc and oxygen are present in the deposited film.

Fig. 7.4 shows TEM characterization of the sputter deposited ZnO films. The bright field TEM images in Fig. 7.4 (a) confirm the nanostructured morphology of the deposited film which is consistent with the SEM and AFM data. The selective area electron diffraction data in Fig. 7.4 (b) is consistent with ZnO of polycrystalline wurtzite structure ($P6_3mc$). The dark field TEM in Fig. 7.4 (c) shows the only crystals which diffract into the marked diffraction spot indicated in 7.4 (b), thus allowing to directly measure the crystallite size of separated nanocrystals. This reveals that the ZnO film is composed of nanocrystals with crystallite sizes of 10 nm to 30 nm. The somewhat smaller crystallite size obtained from TEM (ZnO film thickness: ~20 nm) compared to XRD/SEM (ZnO film thickness: ~350 nm) data can be correlated with film thickness.

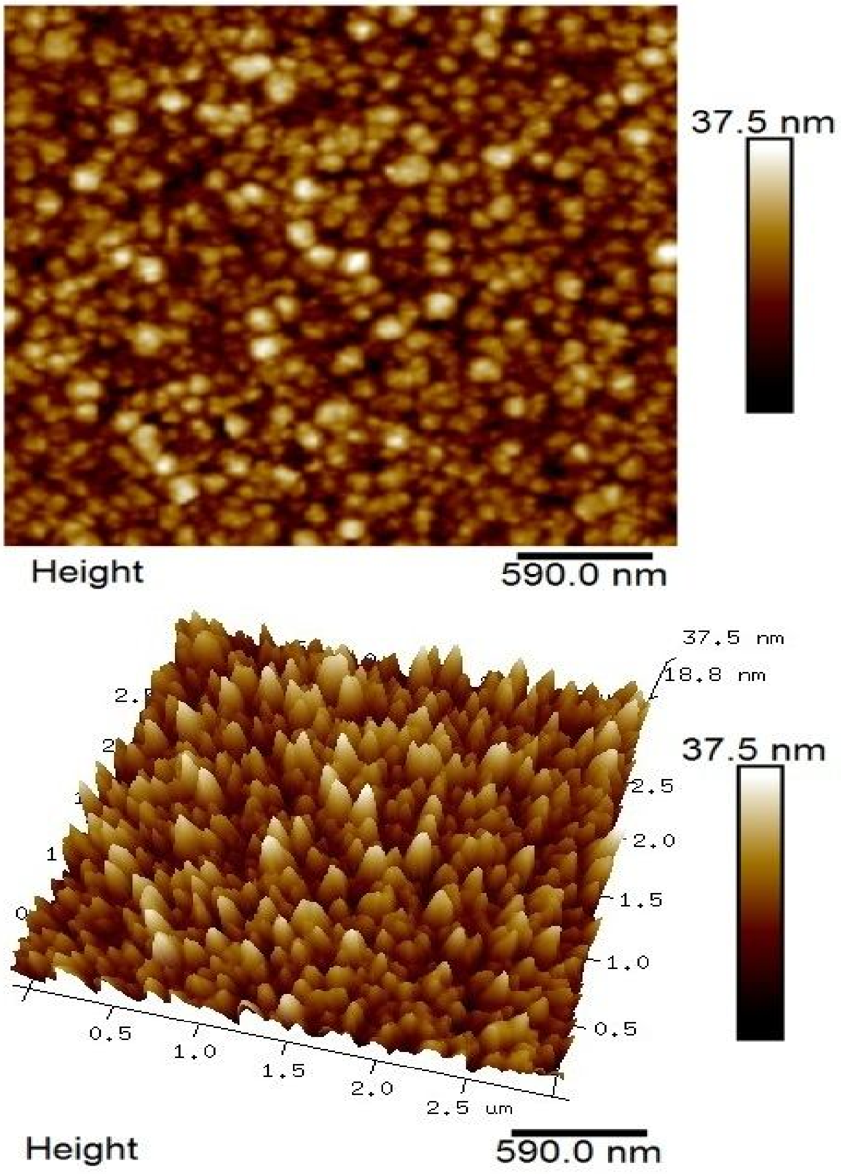

Fig.7.2. Two and three dimensional atomic force microscopy images of deposited ZnO thin films over 3 μm × 3 μm area.

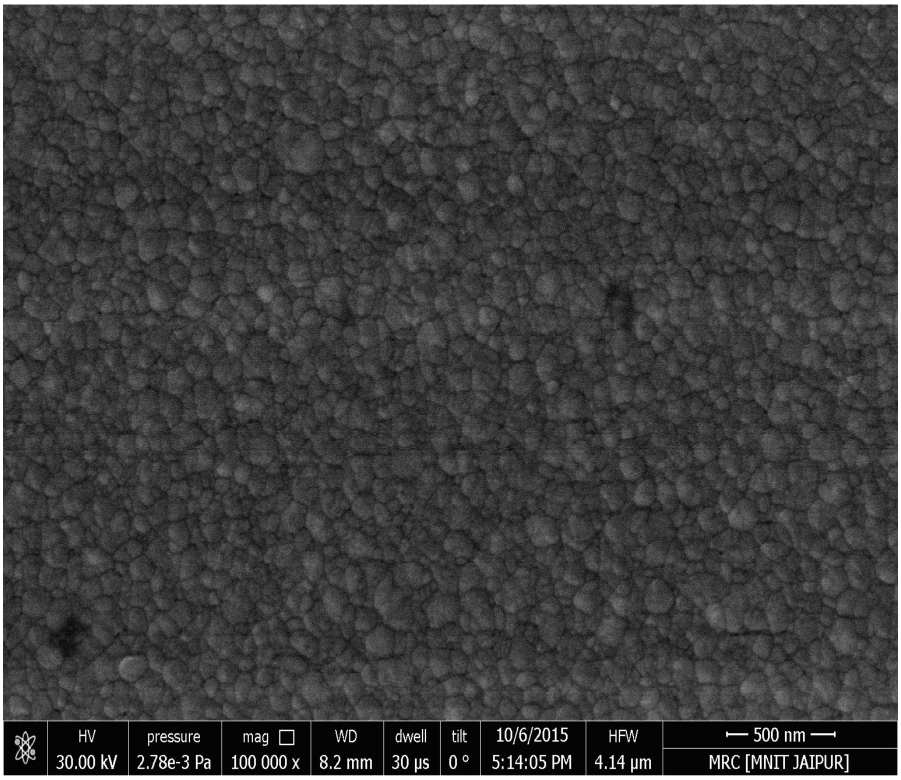

Fig. 7.3. Scanning electron microscopy images of deposited ZnO thin films.

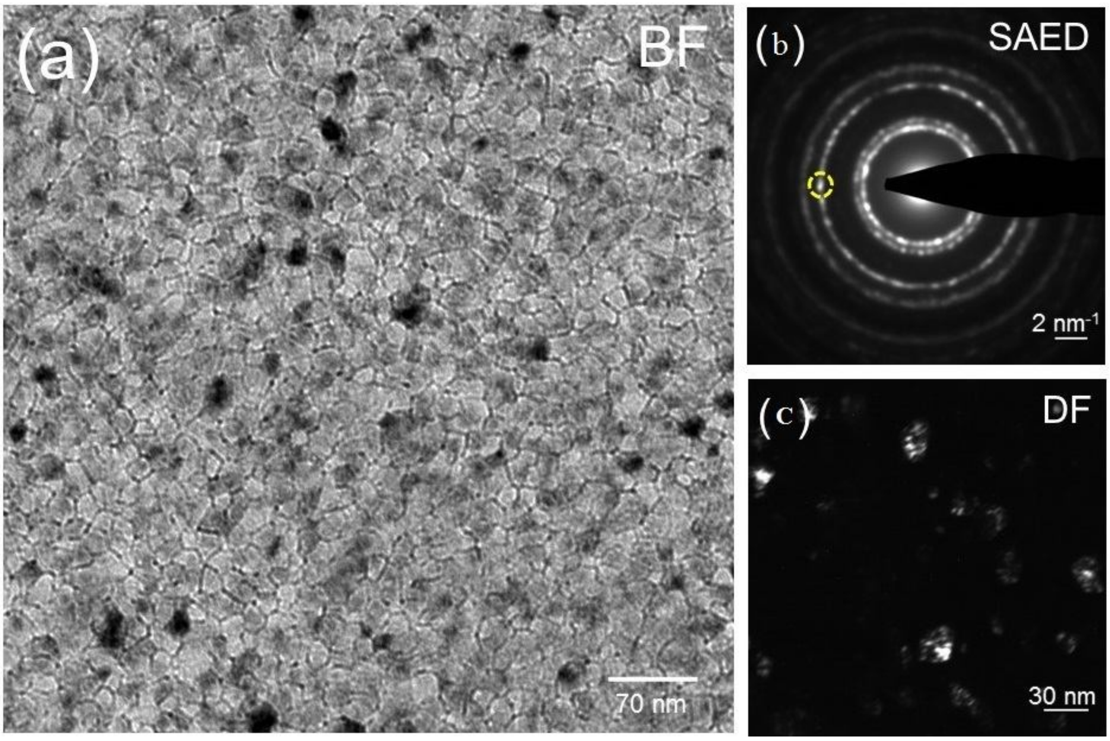

Fig.7.4. (a) Nanostructured morphology of deposited ZnO thin film (~20nm). (b). Selected area electron diffraction (SAED) of ZnO thin film. (c) Dark field (DF) image

of only crystals which diffract into the marked diffraction spot highlighted in image (b).

Raman Spectroscopy has also been used to confirm the lattice structure and crystalline quality of the ZnO thin films. Our measurements in Fig. 7.5 clearly reveal that two Raman peaks associated with ZnO can be observed in our films (while the other peaks are related to the Si substrate): One peak is observed at ~436 cm^{-1} and another peak is located at ~576 cm^{-1}, as a shoulder to a Si related peak. The former peak is related to E_2 (High) vibrations and the latter peak is located in the region between the A_1 (LO) and E_1 (LO) vibrations. The appearance of both these peaks is in good agreement with previous studies on nanostructured ZnO [244]. We note that the E_2 (high) peak is shifted by 3 cm^{-1} compared to its bulk value i.e. 439 cm^{-1}. Alim *et al.* suggested that that laser induced heating in the nanostructure, phonon localization defects and phonon confinement by quantum dot boundaries could be the probable reasons for this shift in E_2 (High) peak [244].

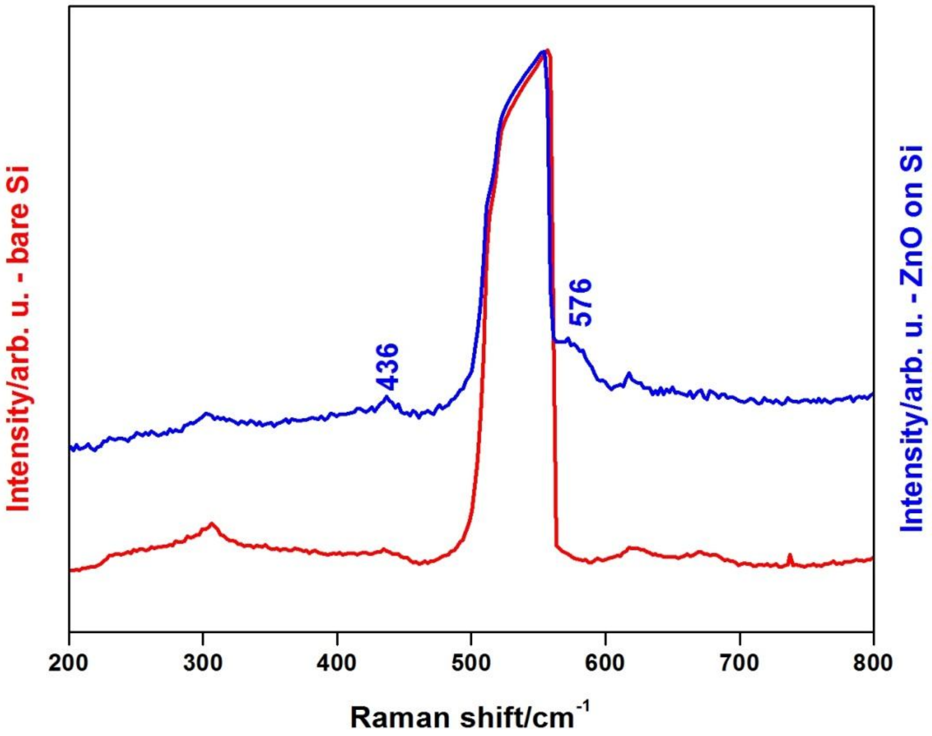

Fig.7.5. Raman spectra of deposited ZnO thin film deposited over p-Si substrate.

7.3.2 Electrical Characterization of n-ZnO/p-Si Diode:

Fig. 7.6 shows the schematic diagram of our fabricated n-ZnO/p-Si heterojunction photodiodes. The ohmic nature of the Al/Si/Al and the Al/ZnO/Al contacts was confirmed by current-voltage measurements as shown in the inset of Fig. 7.7. The I-V plot of a fabricated ZnO/Si heterojunction photodiode in forward and reverse bias conditions is shown in Fig. 7.7. The fabricated structure exhibits excellent rectification of ~840 at ±5 V. The current transport mechanism of the fabricated structure can be understood from I-V characteristics of the fabricated structure. The behaviour of forward current with applied bias can be divided in three distinct regions (X, Y and Z). For region X ($V < 1$ V), the relation between current and biasing voltage was found to be linear which is probably due to the domination of tunneling mechanism. In region II ($1 \text{ V} \leq V < 3.3$ V), an exponential increase in current with biasing voltage is observed which is mainly due to tunneling caused by recombination mechanism [178]. In region Z ($3.3 \text{ V} < V < 5.0$ V), the nature of the I-V characteristics deviates from ideal thermionic emission and exhibits a $I \sim V^2$ relation. This behaviour of current in $V \geq 3.3$V region is attributed to space charge limited current conduction which is a common phenomenon in large bandgap materials [245].

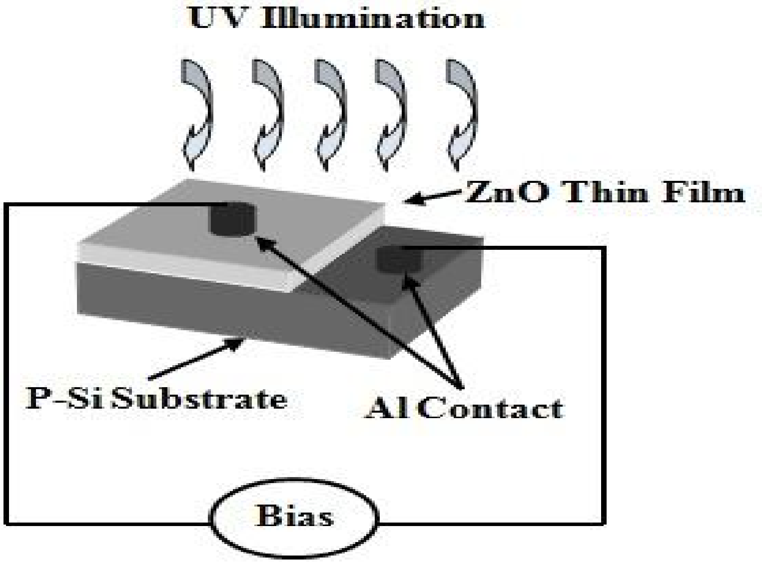

Fig.7.6. Schematic diagram of fabricated n-ZnO/p-Si heterojunction diode.

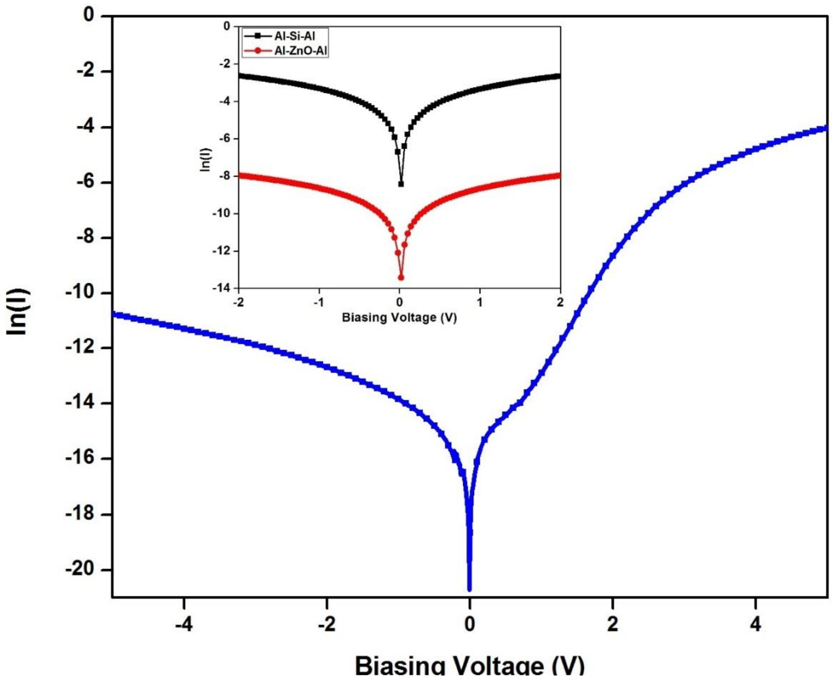

Fig.7.7. Current versus voltage plot of fabricated n-ZnO/p-Si diode (inset shows the ohmic nature of Al-Si-Al and Al-ZnO-Al contacts).

Fig. 7.8 shows temperature dependent I-V characteristics. The temperature has been varied from 303-403 K and effect of temperature on ideality factor and barrier height has been investigated. It is observed that the reverse saturation current increases with increase in temperature. The increase of thermally generated minority carriers in the depletion region of the p-n junction is the probable reason for this increased reverse saturation current at higher temperature ranges.

The typical current transport mechanism for such heterojunctions by assuming commonly used thermionic emission theory can be written as follows:

$$I = I_0\left(\exp(\frac{qV}{\eta kT}) - 1\right)$$

(7.1)

Where I_0, q, η, k and T are reverse saturation current, electronic charge, ideality factor, Boltzmann constant and operating temperature respectively. For $V >> kT/q$, the ideality factor derived from Eq.(7.1) can be expressed as follows [149]:

$$\eta = \frac{q}{kT}\left(\frac{dV}{d(\ln(I))}\right) \tag{7.2}$$

The effective barrier height for the fabricated n-ZnO/p-Si heterojunction can be obtained as [246]:

$$\phi_{B,eff} = \frac{kT}{q}\ln\left(\frac{AA^{*}T^{2}}{I_0}\right) \tag{7.3}$$

Where A and A^{*} are effective contact area and Richardson constant (32 Acm^{-2}K^{-2}) respectively. Fig. 7.9 shows the variation of ideality factor and barrier height with temperature. It is clearly seen from the plot that the ideality factor decreases from 3.2 to 1.7 whereas the barrier height increases from 0.74 eV to 0.96 eV as temperature has increased from 303 K to 403 K.

The spatial barrier inhomogeneties which may appear due to considerable mismatch in lattice constants and thermal expansion coefficients of ZnO and Si, or a thin native SiO_2 interfacial layer at ZnO/Si interface could be the probable reason for this enhancement in barrier height with temperature [178, 235]. At low temperature, low kinetic energy of carriers can surmount only spatial regions of lower barrier heights to contribute the current which results in large ideality factor and low barrier height at lower temperature. However, as the operating temperature increases, the kinetic energy of current carriers increases to surmount regions with higher barrier heights which results in reduced ideality factor and enhanced barrier height at high temperature ranges.

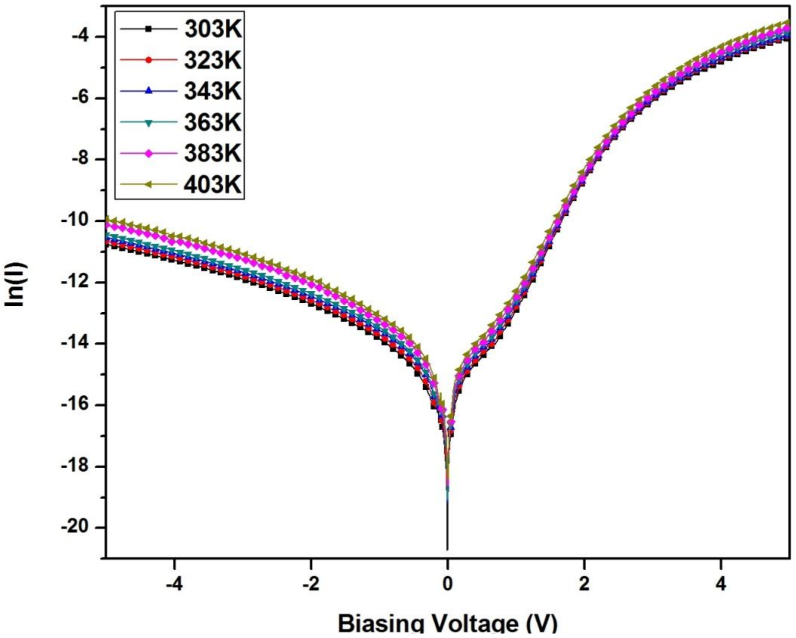

Fig.7.8. Temperature dependent current versus voltage curve of fabricated n-ZnO/p-Si diode for a temperature range of 303-403K.

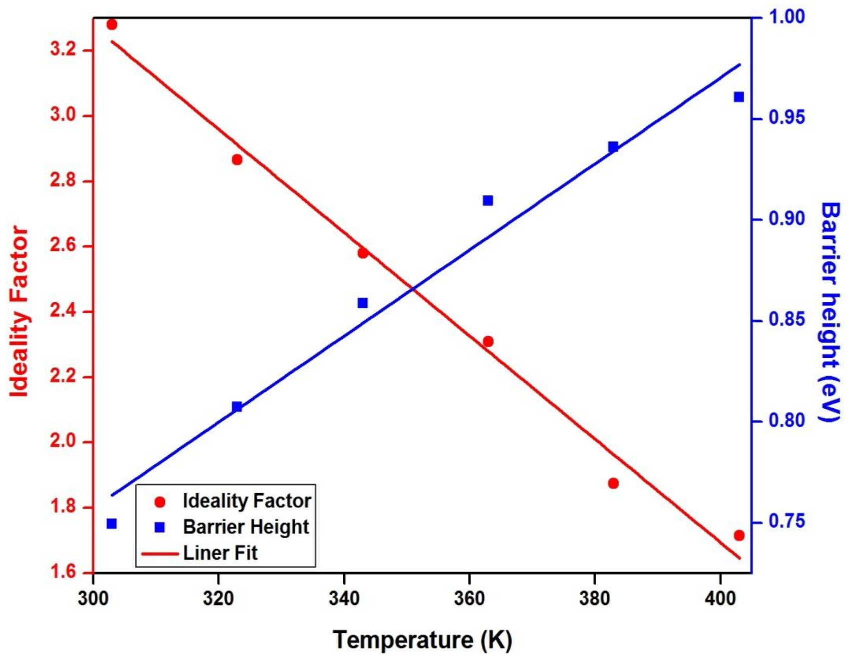

Fig.7.9. Variation of ideality factor and barrier height with temperature for n-ZnO/p-Si heterojunction diode..

Capacitance versus voltage measurement have been done to investigate charge carrier concentration, barrier height and depletion width of the fabricated p-n structure. Inset of Fig. 7.10 shows capacitance versus biasing voltage characteristic of n-ZnO/p-Si heterojunction diode at 1 MHz operating frequency. Considering $V >> kT/q$ and $N_A >> N_D$, the relation between capacitance and voltage in conventional heterojunction theory can be expressed as [108, 151]:

$$\frac{A^2}{C^2} = \frac{2(V_{bi} - V)}{q\varepsilon_s N_D} \tag{7.4}$$

Where A, V_{bi}, V, ε_s and N_D represents junction area, built-in-potential, basing voltage, permittivity of ZnO and donor concentration respectively. Fig. 7.10 shows A^2/C^2 versus V plot where the linear region intercept along the x-axis gives built in potential and the slope can be used to derive donor concentration using following equation:

$$N_D = \frac{2}{q\varepsilon_s \times slope} \tag{7.5}$$

The value obtained for the built-in potential and donor concentration (N_D) were found to be 0.58 V and 4.02×10^{15} cm^{-3} respectively. The barrier height of the p-n heterojunction can also be evaluated from C-V plot using following equation:

$$\phi = V_{d0} + \frac{kT}{q}\ln(\frac{N_C}{N_D}) \qquad (7.6)$$

Where N_C and V_{d0} represents effective density of states in conduction band (3.55×10^{18} cm^{-3} [151]) and diffusion voltage at zero bias that can be obtained as $V_{d0} = V_{bi} + (kT/q)$. The estimated value of barrier height obtained from Eq. (7.6) was found to be 0.78 eV. The slight variation of barrier height obtained from C-V curve as compared to barrier height obtained from I-V curve is probably due to the effect of image forces, barrier inhomogenities and surface impurities in the fabricated structure. The depletion width of the fabricated p-n junction can be obtained as [152]:

$$W_{Dep.} = \sqrt{\frac{\varepsilon_0 \varepsilon_s (V_{bi} - V)}{qN_D}} \qquad (7.7)$$

The value obtained for depletion width was found to be 0.43 μm.

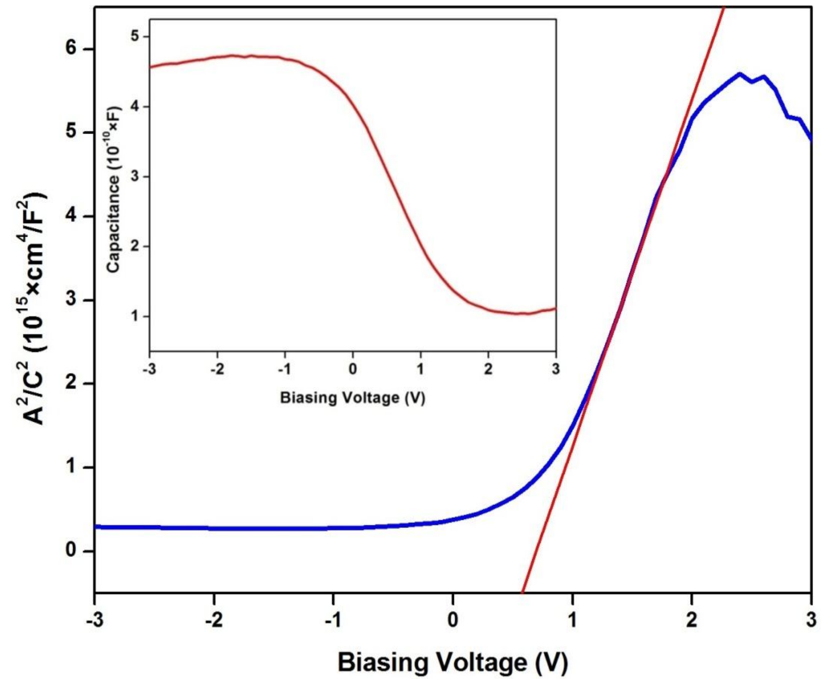

Fig.7.10. A^2/C^2 versus biasing voltage characteristics (inset shows capacitance versus voltage characteristics for n-ZnO/p-Si heterojunction diode)

7.3.3 Ultraviolet Detection Properties of n-ZnO/p-Si Diode:

Fig. 7.11 shows the response of our n-ZnO/p-Si heterojunction diodes to ultraviolet light of 365 nm wavelength. It is clearly seen from the I-V plot that the presence of UV light results in a significant variation in photocurrent under reverse bias condition. The contrast ratio that can be defined as the ratio of current under UV illumination to the current in dark, was found to be ~19 at -5 V. This high contrast ratio may be due to the oxygen related hole trap states present at the surface of the film that prevents the charge carrier recombination and results in increased lifetime of the holes. In fact, the short transit time and long lifetime of charge carriers, is combined responsible for high sensitivity of fabricated photodetector under UV illumination. This also confirms the potentiality of n-ZnO/p-Si heterojunction diodes for a variety of UV detection applications. The photoconduction mechanism of fabricated structure under UV illumination is shown in Fig. 7.12. This proposed model follows previous work by Zhang [247] (although we note that alternative models have also been put forward [248, 249]). When ZnO thin film comes in contact with atmospheric oxygen under dark condition, oxygen molecules get adsorbed on the ZnO surface by capturing free electrons from the conduction band of the ZnO layer. The above process under dark conditions can be written as follows:

$$O_2(g)+e^- = O_2^-(ad) \tag{7.8}$$

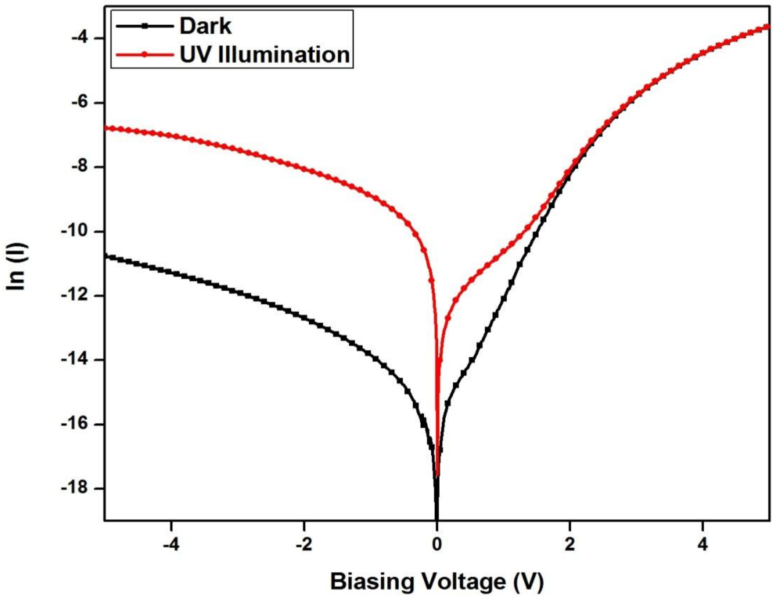

Fig.7.11. Current versus voltage curve of n-ZnO/p-Si diode under dark and UV illumination (365nm wavelength).

This adsorption of O_2 molecules over the ZnO surface creates a depletion layer over the ZnO which results in reduced conductivity of the ZnO film. When ZnO/Si heterojunction is exposed to UV lamp of 365 nm wavelength, the absorbed photons in the ZnO layer results in the generation of electron hole pairs:

$$h\upsilon = e^- + h^+ \tag{7.9}$$

Where e^- and h^+ are electrons and holes respectively. The photo-generated holes move towards the surface due to the electric field in the direction of the field extending in the depletion region. These holes neutralize the adsorbed oxygen atoms and hence the oxygen atoms get desorbed near the surface (Fig. 7.12 (c)). This process can be explained as follows:

$$O_2^-(ad) + h^+ = O_2(g) \tag{7.10}$$

Since desorption is a reverse process of adsorption, it increases the electron concentration in conduction band which results in increased photoconductivity of the detector. In addition to desorption of oxygen atoms, the photo-generated electrons under UV illumination also enhance the conductivity significantly. The trapping process involved in adsorption and desorption of oxygen molecules makes ZnO a potential candidate for UV detection applications.

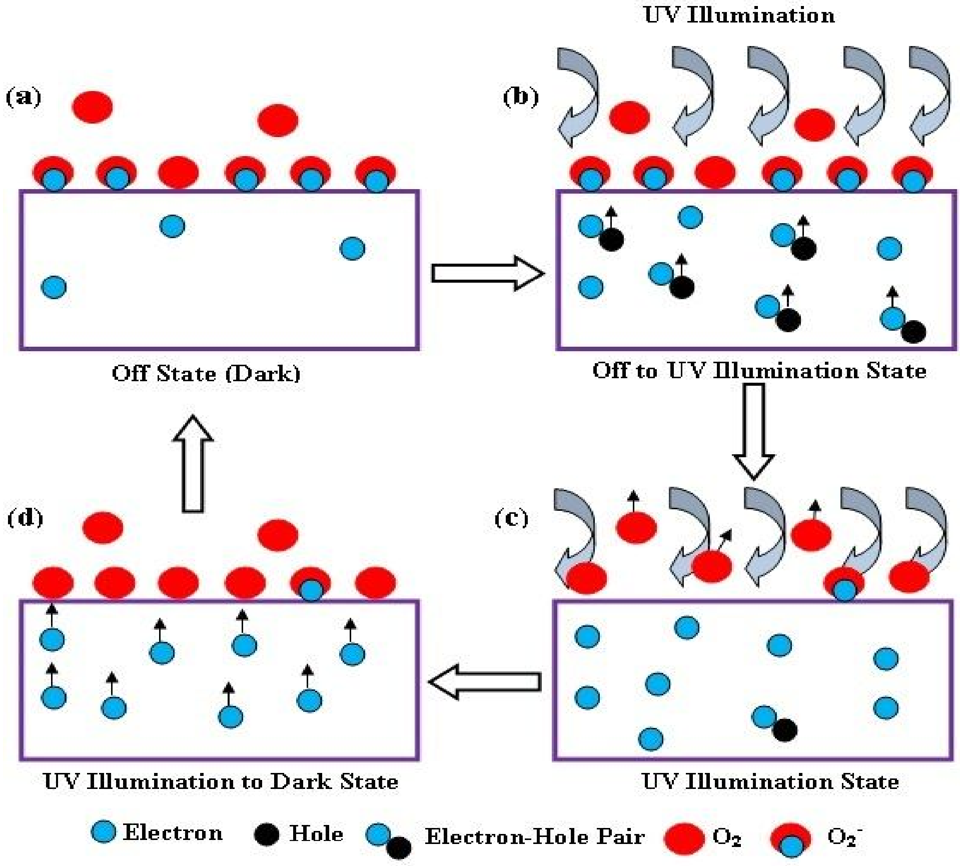

Fig.7.12. Schematic diagram for the UV detection mechanism of n-ZnO/p-Si diode .

The responsivity (R) of the fabricated p-n heterojunction photodiode can be obtained using following equation:

$$R = \frac{I_P}{P_{opt}} \tag{7.11}$$

Where I_P and P_{opt} represents photocurrent and incident optical power respectively. The value of responsivity for fabricated photodetector was found to be ~0.35 A/W.

Since the value of responsivity in most of the previously reported UV photodetectors lies in the range of 0.1-0.2 A/W [19, 250-253], the measured value of responsivity for the fabricated p-n heterojuction diode is considerably promising towards use in practical applications. The detectivity of our photodiode can be derived from following relation [261].

$$D = \left(\frac{R_0 A}{4kT} \right)^{1/2} \times \frac{\lambda \eta q}{hc} \tag{7.12}$$

Where k, T, λ, η, q, h and c represents Boltzmann constant, lattice temperature, illumination wavelength (365 nm), quantum efficiency ($\eta = R \times (hc / q\lambda)$), electronic charge, Plank's constant and velocity of light respectively. Zero bias resistance area product ($R_0 A$) can be obtained as follows:

$$R_0 A = \left(\frac{dJ}{dV} \right)^{-1} \tag{7.13}$$

The value of zero bias resistance area product was found to be 2.22 Ω.m^2. The detectivity value computed from Eq. (7.12) was found to be 4.16×10^9 mHz$^{1/2}$W^{-1}. Finally, Table 7.1 compares various performance parameters of the fabricated photodetector with other ZnO thin films based UV photodetector structures reported in past. It is clearly evident from the comparison that the fabricated photodetector has exhibited superior performance compared previously available reports and our device can be a potential candidate for future optoelectronic and Si photonic applications.

Table 7.1 Comparison of ZnO thin film based different UV photodetectors

Parameters	Our Work	p-n [254]	Schottky [255]	Schottky [176]	MSM [239]
Rectification Ratio	840	127	-	-	-
Barrier Height [eV]	0.74	0.76	0.70	0.73	0.74
Ideality Factor	3.2	2.72	4.0	6.7	8
Contrast Ratio	19	-	7	8	12
Responsivity [A/W]	0.35	0.075	0.17	0.21	.056
Detectivity [10^9×mHz$^{1/2}$W^{-1}]	4.16	6.44	-	1.45	1.28

7.4 Conclusion

In summary, n-ZnO/p-Si heterojunction diodes have been fabricated using RF sputtering technique. XRD, AFM, SEM TEM and Raman measurements were carried out to investigate the structural and surface morphological properties of deposited ZnO thin films. Results confirmed the highly c-axis oriented growth of ZnO nanocrystalline films with good homogeneity of grains over the entire substrate. The current-voltage measurements have shown a high rectification of ~840 for the fabricated structure. The temperature dependent I-V study has confirmed the good thermal stability of fabricated diode over a temperature range of 303-403 K. It has been observed that the ideality factor decreases whereas barrier height increases when temperature varies from 303-403 K. The capacitance versus voltage characteristics for the n-ZnO/p-Si heterojunction diode has also been studied. Current versus voltage measurements in dark and illumination conditions has confirmed the potential for UV detection of our fabricated structure. The values of responsivity and detectivity were found to be 0.35 A/W and 4.16×10^{9} $mHz^{1/2}W^{-1}$ respectively. Results conclude that n-ZnO/p-Si heterojunction based photodiode for UV detection can be very useful in variety of applications.

CHAPTER 8

Conclusion and Future Work

This chapter presents some major findings and outcomes of the thesis. It summarizes all the results presented in Chapter 4-7 of the thesis. Finally, the future scope of the work is outlined in the end.

8.1 Conclusion

Development of high quality ZnO thin films have opened up the new and existing applications in the field of optoelectronic and nanoelectronic devices. ZnO thin films have ensured their potentiality in active device applications which requires transparency of films in visible region such as detectors, solar cells and thin film transistors etc. In this thesis, a systematic study starting from simulation of ZnO based devices to actual device fabrication have been presented. First, the various electrical and optical parameters for ZnO/Si heterojunction based ultraviolet detectors have been simulated using ATLAS simulator from Silvaco International. In best of our knowledge, it was the first time that the simulation study of ZnO based UV detectors have been reported using TCAD tool. These kinds of studies can be very helpful to optimize the various device parameters over the tool itself which can reduce the fabrication cost and efforts significantly. After completing tool based study, we moved towards actual fabrication of high quality ZnO thin films with their applications in ultra violet light detection. ZnO thin films were deposited over p-Si (100) and glass substrates using RF sputtering technique. In order to ensure the high quality of deposited ZnO thin films, various physical and growth parameters such as film thickness, annealing temperature, sputtering power and gas flow rates have been optimized. A systematic investigation on how all these parameters affects structural and optical properties of ZnO thin films have been presented in detail. Thermal stability of fabricated devices is also an important concern which is required to be addressed. So a detailed investigation on temperature dependent electrical characteristics of n-ZnO/p-Si heterojunction diodes has also been done. Effect of temperature on various electrical parameters such as ideality factor, barrier height and Richardson constant has been investigated. The results confirmed the high thermal stability of the fabricated diodes. The current-voltage measurements suggested that n-ZnO/p-Si heterojunctions obey the theory of thermionic emission with Gaussian distribution. Finally, the potentiality of n-ZnO/p-Si heterojunction diodes for ultraviolet light detection application has been tested. Results confirmed the UV detection capabilities of ZnO/Si heterojunction diodes that can be very useful in variety of civil and military applications. Some of the major conclusions of this study are as follows:

In Chapter 4, simulation study and performance analysis of ZnO/Si heterojunction based UV-Visible photodetector have been presented. Different electrical and optical parameters such as energy band diagram, electric field profile, dark current, quantum efficiency, responsivity, detectivity and noise equivalent power of ZnO/Si heterojunction based photodetector have been simulated as a function of device thickness, operating wavelength and applied reverse bias voltage. The simulation software ATLAS™ in SILVACO package is used to describe the effect of ZnO/Si interface properties on its photodetection. The value obtained for external quantum efficiency, responsivity and specific detectivity for ZnO/Si heterojunction based photodetector were ~93%, 0.36 A/W and 7.2×10^{10} cmHz^{½}W^{-1} respectively. The estimated values for dark current and noise equivalent power were of the order of 10^{-14} A and 10^{-11} W respectively.

Chapter 5 is devoted to the preparation, characterization and optimization of nanocrystalline ZnO thin films using RF sputtering technique. High quality ZnO thin films were grown over Si (100) and glass substrates by RF magnetron sputtering technique. Effect of various physical and growth parameters such as thickness, annealing temperature, sputtering power and gas flow rate on structural and optical properties of ZnO thin films have been studied. Surface morphology, structural properties and quality of thin film have been studied using X-Ray Diffraction (XRD), Atomic Force Microscopy (AFM), Scanned Electron Microscopy (SEM) and Energy-Dispersive X-ray (EDX). Optical properties such as transmittance, reflectance, absorption coefficient, refractive index and dielectric constant for a spectral range of 300 nm to 800 nm have been evaluated. Photoluminescence (PL) spectra for ZnO thin films have also been studied. Some important conclusion that comes out from this study are as follows:

- In thickness dependent study of ZnO thin films, all samples have shown a hexagonal wurtzite structure with preferential growth along the c-axis perpendicular to the surface. It has been observed that structural disorder, stress and strain in the film decreases with thickness whereas crystalline quality of deposited ZnO thin films increases with increased thickness. Optical characterization of deposited films has been done using UV–visible spectrophotometer, ellipsometer and photoluminescence (PL) spectroscope. Transmittance spectra of all ZnO thin film samples (190 nm - 342 nm) have exhibited a high transmittance over 85% in the visible region, and refractive index has got varied between 0.85-3.1 in UV-Visible wavelength region. The optical band gap has increased from 3.22 eV to 3.26 eV when thickness varies from 190 nm to 342 nm.
- In annealing temperature dependent study of ZnO thin films, the annealing temperature has been varied from 300°C to 600°C in steps of 100. An increase in optical bandgap of deposited ZnO thin films with increasing annealing temperature has been observed. The average optical transmittance was found to be more than 85% for all deposited films. Photoluminiscense spectra (PL) suggested that the crystalline quality of deposited film has increased at higher annealing temperature.
- In RF power dependent study, four set of ZnO thin film samples with different sputtering powers (80-140 watt) were deposited over p-Si <100> and glass substrate using RF sputtering technique. Results confirms that sputtering power do have a considerable influence over deposition rate, crystallinity and surface morphology of deposited films. Diffraction angle, grain size and surface roughness of deposited films have increased with sputtering power whereas dislocation density, stress and strain of the films has decreased with sputtering power. ZnO thin film deposited at 120 watt sputtering power have shown best crystallinity, surface morphology and optical properties.
- In gas flow rate dependent study, ZnO thin films with varying argon gas flow rate were deposited using RF sputtering technique. It has been observed that the peak intensity at higher gas flow rates has reduced due to reduced plasma density. A high optical transmittance of 85-98% in visible region has been observed for all deposited samples. Films deposited at 20 sccm have exhibited

high quality results and it has been observed that as argon gas flow rate increases from 20 scccm to 40 scccm, the plasma density degrades which reduces the deposition rate drastically.

In Chapter 6, temperature dependent I-V characteristics of n-ZnO/p-Si heterojunction diode, fabricated using thermal evaporation method have been studied. Temperature variation of 25°C to 120°C for n-ZnO/p-Si heterojunction diode has shown good thermal stability. It has been observed that as temperature increases, barrier height and reverse saturation current increases whereas ideality factor decreases. The estimated value of Richardson constant obtained from $\ln(I_0/T^2)$ vs q/kT plot is $6.61\text{x}10^{-7}\text{Acm}^{-2}\text{K}^{-2}$ which was very less than the theoretical value of Richardson constant for ZnO. It has been observed that barrier inhomogeneity at the interface of ZnO/Si is the probable reason for the deviation of Richardson constant. So by implementing the Gaussian distribution of barrier height to TE model, modified Richardson constant of 39.18 $\text{Acm}^{-2}\text{K}^{-2}$ is obtained which is very close to the actual theoretical value of Richardson constant i.e. 32 $\text{Acm}^{-2}\text{K}^{-2}$.

In Chapter 7, ultraviolet light detection properties of n-ZnO/p-Si heterojunction diodes have been investigated. XRD, AFM, SEM, TEM and Raman measurements were carried out to investigate the structural and surface morphological properties of the deposited ZnO thin films. Results confirmed the highly c-axis oriented growth of ZnO nanocrystalline films with good homogeneity of grains over the entire substrate. The fabricated diodes exhibit a high rectification ratio of ~840 at ±5 V. The ideality factor of the fabricated diodes was found to decrease from 3.2 to 1.7 when measurement temperature was increased from 303 K to 403 K, whereas the barrier height increased from 0.74 eV to 0.96 eV in the same temperature range. Various other parameters such as built-in potential, donor concentration and depletion width have also been evaluated. The UV detection properties of our fabricated structures were investigated using an UV lamp of 365 nm wavelength. The fabricated diodes show a very good response towards UV light. The values of responsivity and detectivity were found to be 0.35 A/W and 4.16×10^9 $\text{mHz}^{1/2}\text{W}^{-1}$ respectively. The values obtained for responsivity and detectivity from experimental data (0.35 A/W and 4.16×10^9 $\text{mHz}^{1/2}\text{W}^{-1}$) has also shown good relevance with simulation data (0.36 A/W and 7.2×10^{10} $\text{cmHz}^{½}\text{W}^{-1}$) of ZnO/Si heterojunction based ultraviolet detectors.

8.2 Future Work

- The synthesis of different ZnO nanostructures is still a challenging task. Different parameters of ZnO nanostructures such as shape, diameter, density, orientation and crystallization plays a crucial role in the performance of the photodetectors. So some additional efforts are needed to investigate the relation between ZnO nanostructure parameters and device performance so that high efficiency of all these devices can be achieved.
- Larger lattice mismatch between ZnO and Si can introduce defect densities at ZnO/Si interface which can degrade the performance of the ZnO heterojunction based devices. To overcome these drawbacks, very thin layers of different seed layers of suitable materials can be introduced between ZnO and Si which can improve the interface qualities of ZnO-Si heterojunctions. These seed layers can minimize the lattice mismatch and can provide perfect nucleation cites for the growth of high quality ZnO nanostructures. The seed layers will also minimize the undesired oxidation of Si which will also help to improve the crystalline quality of grown films. The effect of these seed layers on the performance of ZnO based devices also needs to be studied in future.
- Transparent and semi-transparent metal contacts can significantly improve the performance of ZnO based photodetectors. A systematic study to investigate the impact of transparent contacts on the performance of the photodetectors is needed.

Finally, we conclude the thesis with a hope that we will be able to see the commercialization of ZnO nanostructure based devices in near future. We believe that the efforts to grow p-doped ZnO thin films and advancement in thin film technology will make this material more and more promising for next generation optoelectronic and nanoelectronic device applications. It is desirable to see the commercial manufacturing of ZnO thin film based devices in next 5-10 years.

Bibliography

[1]. I. M. Ross, “The invention of the transistor”, *Proceedings of the IEEE*, vol. 86, no. 1, pp. 7-28, 1998.

[2]. A. Janotti and C. G. V. Walle, “Fundamentals of zinc oxide as a semiconductor”, *Rep. Prog. Phys.*, vol. 72, pp. 126501-29, 2009.

[3]. A. Teke, U. Ozgur, S. Dogan, X. Gu, and H. Morkoc, “Excitonic fine structure and recombination dynamics in single-crystalline ZnO”, *Physical Review B*, vol. 70, pp. 195207-10, 2004.

[4]. H. Chen, K. Liu, L. Hu, A. A. A. Ghamdi and X. Fang, “New concept ultraviolet photodetectors”, *Materials Today*, vol. 18, no. 9, pp. 493-502, 2015.

[5]. Z. Fan and J. G. Lu, “Zinc oxide nanostructures: synthesis and properties”, J Nanosci Nanotechnol., vol. 5, no. 10, pp. 1561-73, 2005.

[6]. C. Jagadish and S. Pearton, “Basic Properties and Applications of ZnO”, in Zinc Oxide Bulk, Thin Films and Nanostructures: Processing, Properties, and Applications, 1st Ed., *Elsevier New York*, 2006, pp. 1-20.

[7]. W. J. Lee, J. Kang, and K. J. Chang, “p-Type doping and compensation in ZnO”, *Journal of the Korean Society*, vol. 53, no. 1, pp. 196-201, 2008.

[8]. U. Ozgur, D. Hofstetter, and H. Morkoc, “ZnO devices and applications: a review of current status and future prospects”, *Proceedings of the IEEE*, vol. 98, no.7, pp. 1255-1268, 2010.

[9]. Z. Xin-Yu, C. Zhou-Wen, Q. Yan-Peng, F. Yan, Z. Liang, Q. Li, M. Ming-Zhen, L. Ri-Ping and W . Wen-Kui, “Ab Initio Comparative Study of Zincblende and Wurtzite ZnO”, *Chinese Physics Letters*, vol. 24, no. 4, pp. 1032-1034, 2006.

[10]. H. Morkoc and U. Ozgur, “General Properties of ZnO”, in Zinc Oxide: Fundamentals, Materials and Device Technology, *Wiley*, NJ, 2009, pp. 1-76.

[11]. L. J. Brillson, and Y. Lu, “ZnO Schottky barriers and ohmic contacts”, *Journal of Applied Physics*, vol. 109, pp. 121301-31, 2011.

[12]. S. M. Sze and K. K. Ng, Physics of Semiconductor Devices, *Wiley*, NJ, 2007.

[13]. C. A. Mead, Ohmic Contacts to Semiconductors, edited by B. Schwartz, *Electrochem. Soc., NY,* 1969.

[14]. F. Leonard, A. Alec Talin, B. S. Swartzentruber, and S. T. Picraux, "Diameter-dependent electronic transport properties of Au-catalyst/Ge-nanowire Schottky diodes", *Phys. Rev. Lett.,* vol. 102, pp. 106805, 2009.

[15]. *C. A. Mead*, "Surface barriers on ZnSe and ZnO", *Phys. Lett.*, vol. 18, pp. 218, 1965.

[16]. D. Yan, H. Wang, B. Du, "Introduction to organic semiconductor heterojunctions", *Wiley*, NJ, 2010.

[17]. R. L. Anderson, "Germanium-gallium arsenide heterojunctions", *IBM Journal of Research and Development*, vol. 4, no. 3, pp. 283 – 287, 1960.

[18]. L. J. Brillson, "Surfaces and Interfaces of Electronic Materials", *Wiley*, NJ, 2012.

[19]. K. Liu , M. Sakurai and M. Aono, "ZnO-Based Ultraviolet Photodetectors", *Sensors*, vol. 10, pp. 8604-8634, 2010.

[20]. Mollow, E. Proceedings of the Photoconductivity Conference; Breckenridge, RG, Ed.; Wiley: New York, NY, USA, 1954; p. 509.

[21]. Y. Lee, T. Lu, H. Kuo, and S. Wang," High brightness GaN-based light-emitting diodes", *Journal Of Display Technology*, vol. 3, no. 2, pp. 118-125, 2007.

[22]. G. Rong-feng, T. Da-lei, W.Xing, and Z. Wen-qing, "Thermal, mechanical and optical analysis of SiC-based LED", *10th Electronics Packaging Technology Conference*, pp. 939-944, 2008.

[23]. Y. Choi, J. Kang, D. Hwang, and S. Park, "Recent advances in ZnO-based light-emitting diodes", *IEEE Transactions on Electron Devices*, vol. 57, no. 1, 2010.

[24]. H. Huang, G. Fang, X. Mo, H. Long, L. Yuan, B. Dong, X. Meng, and X. Zhao," ZnO-based fairly pure ultraviolet light-emitting diodes with a low operation voltage", *IEEE Electron Device Letters*, vol. 30, no. 10, pp. 1063-1065, 2009.

[25]. M. A. Abbasi, Z. H. Ibupoto, M. Hussain, O. Nur and M. Willander, "The fabrication of white light-emitting diodes using the n-ZnO/NiO/p-GaN heterojunction with enhanced luminescence", *Nanoscale Research Letters*, vol. 8, pp. 1-6, 2013.

[26]. J. Benz, S. Eisermann, P. J. Klar, B. K. Meyer, T. Detchprohm and C. Wetzel, “GaN/ZnO and AlGaN/ZnO heterostructure LEDs: growth, fabrication, optical and electrical characterization”, *MRS Proceedings*, vol. 1201, pp. 1-8, 2010

[27]. K. Nomura, H. Ohta, K. Ueda, T. Kamiya, M. Hirano, and H. Hosono, “Thin-film transistor fabricated in single-crystalline transparent oxide semiconductor”, *Science*, vol. 300, pp. 1269-72, 2003.

[28]. R. L. Hoffman, B. J. Norris and J. F. Wager, “ZnO-based transparent thin-film transistors”, *Appl. Phys. Lett.*, vol. 82, pp. 733, 2003.

[29]. J. H. Kim, B. D. Ahn, C. H. Lee, K. A. Jeon, H. S. Kang, and S. Y. Lee, “Characteristics of transparent ZnO based thin film transistors with amorphous HfO_2 gate insulators and Ga doped ZnO electrodes”, *Thin Solid Films*, vol. 516, no. 7, pp. 1529–1532, 2008.

[30]. E. M. C. Fortunato, P. M. C. Barquinha, A. C. M. B. G. Pimentel, A. M. F. Gonçalves, A. J. S. Marques, R. F. P. Martins and L. M. N. Pereira, “Wide-bandgap high-mobility ZnO thin-film transistors produced at room temperature”, *Appl. Phys. Lett.*, vol. 85, pp. 2541, 2004.

[31]. Z. L. Wang and J. Song, “Piezoelectric Nanogenerators Based on Zinc Oxide Nanowire Arrays”, *Scienc*e, vol. 32, pp. 242-246, 2006.

[32]. P. Bhattacharyyaa, P. K. Basub, B. Mondalb, and H. Saha, “A low power MEMS gas sensor based on nanocrystalline ZnO thin films for sensing methane”, *Microelectronics Reliability*, vol. 48, no. 11–12, pp. 1772–1779, 2008.

[33]. O. Lupan, G. Chaic, and L. Chow, “Novel hydrogen gas sensor based on single ZnO nanorod”, *Microelectronic Engineering*, vol. 85, no. 11, pp. 2220–2225, 2008.

[34]. C. Lu, S. Chang, S. Chang, T. Hsueh, C. Hsu, Y. Chiou, and I. Chen, “ZnO nanowire-based oxygen gas sensor”, *IEEE Sensors Journal*, vol. 9, no. 4, pp. 485-489, 2009.

[35]. N. Koshizaki, and T. Oyama, “Sensing characteristics of ZnO-based NOx sensor”, *Sensors and Actuators B: Chemical*, vol. 66, no. 1–3, pp. 119–121, 2000.

[36]. M. Hjiria, R. Dhahria, K. Omria, L. El Mira, S.G. Leonardic, N. Donatoc, and G. Neric, “Effect of indium doping on ZnO based-gas sensor for CO”, *Materials Science in Semiconductor Processing*, vol. 27, pp. 319–325, 2014.

[37]. M. Smirnov, C. Baban, and G.I. Rusu, “Structural and optical characteristics of spin-coated ZnO thin films”, *Applied Surface Science*, vol. 256, pp. 2405–2408, 2010.

[38]. C. Y. Tsay, H. C. Cheng, Y. T. Tung, W. H. Tuan, and C. K. Lin, “Effect of Sn-doped on microstructural and optical properties of ZnO thin films deposited by sol–gel method”, *Thin Solid Film*s, vol. 517, pp. 1032–1036, 2008.

[39]. S. Brien, L. H. K. Koh, and G. M. Crean, “ZnO thin films prepared by a single step sol–gel process”, *Thin Solid Films*, vol. 516, pp. 1391–1395, 2008.

[40]. G. Srinivasan, N. Gopalakrishnan, Y. S. Yu, R. Kesavamoorthy, and J. Kumar, “Influence of post-deposition annealing on the structural and optical properties of ZnO thin films prepared by sol–gel and spin-coating method”, *Superlattices and Microstructures*, vol. 43, pp. 112–119, 2008.

[41]. Y. S. Kim, W. P. Tai, and S. J. Shu, “Effect of preheating temperature on structural and optical properties of ZnO thin films by sol–gel process”, *Thin Solid Films*, vol. 491, pp. 153 – 160, 2005.

[42]. P. Gondoni, M. Ghidelli, F. Di Fonzo, V. Russo, P. Bruno, J. Martí-Rujas, C.E. Bottani, A. Li Bassi, and C. S. Casari, “Structural and functional properties of Al:ZnO thinfilms grown by pulsed laser deposition at room temperature”, *Thin Solid Films*, vol. 520, pp. 4707–4711, 2012.

[43]. Q. A. Drmoshb, S. G. Rao, Z. H. Yamani, and M. A. Gondal, “Crystalline nanostructured Cu doped ZnO thin films grown at room temperature by pulsed laser deposition technique and their characterization”, *Applied Surface Science*, pp. 270, pp. 104– 108, 2013.

[44]. J. Jiang, L. Zhu, Y. Li, Y. Guo, W. Zhou, L. Cao, H. He, Z. Ye, “Band gap modulation of ZnCdO alloy thin films with different Cd contents grown by pulsed laser deposition”, *Journal of Alloys and Compounds*, vol. 547, pp. 59–62, 2013.

[45]. V. Craciun, J. Elders, J. G. E. Gardeniers, and Ian W. Boyd, “Characteristics of high quality ZnO thin films deposited by pulsed laser deposition”, *Appl. Phys. Lett.*, vol. 65, no. 23,pp. 2963-2965, 1994.

[46]. W. Zhaoyanga, S. Liyuan, and H. Lizhong, “Effect of laser repetition frequency on the structural and optical properties of ZnO thinfilms by PLD”, *Vacuum*, vol. 85, pp. 397-399, 2010.

[47]. S. Y. Ting, P. J. Chen, and H. C. Wang, "Crystallinity improvement of ZnO thin film on different buffer layers grown by MBE", *Journal of Nanomaterials,* vol. 2012, pp. 1-7, 2012.

[48]. K. Iwata, P. Fons, A. Yamada, K. Matsubara, and S. Niki, "Nitrogen-induced defects in ZnO: N grown on sapphire substrate by gas source MBE", *Journal of Crystal Growth*, vol. 209, no. 2–3, pp. 526-531, 2000.

[49]. M. Chen, Q. Zhang, L. Su, Y. Su, J. Cao, Y. Zhu, T. Wu, X. Gui, C. Yang, R. Xiang, and Z. Tang, "ZnO film with ultra-low background electron concentration grown by plasma-assisted MBE using Mg film as the buffer layer", *Materials Research Bulletin*, vol. 47, no. 9, pp. 2673-2675, 2012.

[50]. F. J. Liu, Z. F. Hu, J. Sun, Z. J. Li, H. Q. Huang, J. W. Zhao, X. Q. Zhang, and Y. S. Wang, "Ultraviolet photoresistors based on ZnO thin films grown by P-MBE", *Solid State Electronics*, vol. 68, pp.90-92, 2012.

[51]. E. Przezdziecka, K. Goscinski, M. Stachowicz, D. Dobosz, E. Zielony, J. M. Sajkowski, M. A. Pietrzyk, E. Płaczek Popko, and A. Kozanecki, "Spectrum selective UV detectors from an p-ZnO:As/n-GaN diodes grown by molecular beam epitaxy", *Sensors and Actuators A: Physical*, vol. 195, pp. 27-31, 2013.

[52]. M. A. Pietrzyka, E. Zielony, M. Stachowicz, A. Reszka, E. Płaczek-Popko, A. Wierzbicka, E. Przezdziecka, A. Droba, and A. Kozanecki, "Electro-optical characterization of ZnO/ZnMgO structure grown on p-type Si (1 1 1) by PA-MBE method", *Journal of Alloys and Compounds,* vol. 587, pp. 724–728, 2014.

[53]. M. Asghar, K. Mahmood, F. Malik and M. A. Hasan, "Growth and interface properties of Au schottky contact on ZnO grown by molecular beam epitaxy", *Journal of Physics: Conference Series*, vol. 439, pp. 012031, 2013.

[54]. Z. Q. Wang, R. P. Ge, J. F. Gong, S. L. Gu, S. G. Yang, "Synthesis, characterization and optical properties of ZnS nanobelt/ZnO nanoparticle heterostructures", *Materials Letters*, vol. 82, no. 1, pp. 29-32, 2012.

[55]. P. Biswas, S. Kundu, P. Banerji, and S. Bhunia, "Super rapid response of humidity sensor based on MOCVD grown ZnO nanotips array", *Sensors and Actuators B: Chemical*, vol. 178, pp. 331-338, 2013.

[56]. H. Wang, Y. Zhao, C. Wu, X. Dong, B. Zhang, G. Wu, Y. Ma, and G. Du, "Ultraviolet electroluminescence from n-ZnO/NiO/p-GaN light-emitting diode fabricated by MOCVD", *Journal of Luminescence*, vol. 158, pp.6-10, 2015.

[57]. Y. Lei, J. Xu, K. Zhu, M. He, J. Zhou, Y. Gao, L. Zhang, and Y. Chen, “A GaN-Based LED with perpendicular structure fabricated on a ZnO dubstrate by MOCVD”, *Journal of Display Technology*, vol. 9, no. 5, pp. 377-381, 2013.

[58]. J. P. Biethan, V. P. Sirkeli, L. Considine, D. D. Nedeoglo, D. Pavlidis, and H.L. Hartnagel, “Photoluminescence study of ZnO nanostructures grown on silicon by MOCVD”, *Materials Science and Engineering: B*, vol. 177, no. 8, pp. 594-599, 2012.

[59]. M. L. Addonizio, and L. Fusco, “Preparation method of double-textured ZnO:B films deposited by MOCVD on plasma etched polymer buffer”, *Journal of Alloys and Compounds*, vol. 622, pp. 851-858, 2015.

[60]. D. C. Kim, W. S. Han, B. H. Kong, H. K. Cho, and C. H. Hong, “Fabrication of the hybrid ZnO LED structure grown on p-type GaN by metal organic chemical vapor deposition”, *Physica B: Condensed Matter*, vol. 401–402, pp. 386-390, 2007.

[61]. W. L. Dang, Y. Q. Fu, J. K. Luo, A. J. Flewitt, and W.I. Milne, “Deposition and characterization of sputtered ZnO films”, *Superlattices and Microstructures*, vol. 42, no. 1–6, pp. 89-93, 2007.

[62]. Y. Kumar, J. E. Garcia, F. Singh, S. F. Mendez, V. V. Sivakumar, D. Kanjilal, and V. Agarwal, “Influence of mesoporous substrate morphology on the structural, optical and electrical properties of RF sputtered ZnO layer deposited over porous silicon nanostructure”, *Applied Surface Science*, vol. 258, no. 7, pp. 2283-2288, 2012.

[63]. N. H. Al-Hardan, M. J. Abdullah, H. Ahmad, A. Abdul Aziz, and L. Y. Low, “Investigation on UV photodetector behavior of RF-sputtered ZnO by impedance spectroscopy”, *Solid State Electronics*, vol. 55, no. 1, pp. 59-63, 2011.

[64]. V. Bhavanasi, C. B. Singh, D. Datta, V. Singh, K. Shahi, and S. Kumar, “Structural, optical and light scattering properties of post etched RF sputtered ZnO: Al thin films deposited at various substrate temperature”, *Optical Materials*, vol. 35, no.7, pp. 1352-1359, 2013.

[65]. Y. Jouane, S. Colis, G. Schmerber, A. Dinia, P. Leveque, T. Heiser, and Y. A. Chapuis, “Influence of flexible substrates on inverted organic solar cells using sputtered ZnO as cathode interfacial layer”, *Organic Electronics*, vol. 14, no. 7, pp.1861-1868, 2013

[66]. A. Tamvakos, D. Calestani, D. Tamvakos, R. Mosca, D. Pullini, and A. Pruna,” Effect of grain-size on the ethanol vapor sensing properties of room-temperature sputtered ZnO thin films”, Microchim Acta., vol. 182, pp. 1991-1999, 2015.

[67]. L. Duan, X. Yu, L. Ni, and Z. Wang, “ZnO:Ag film growth on Si substrate with ZnO buffer layer by RF sputtering”, *Applied Surface Science*, vol. 257, no. 8, pp. 3463-3467, 2011.

[68]. P. Liu, Y. Li, Y. Guo, and Z. Zhang, “Growth of catalyst-free high-quality ZnO nanowires by thermal evaporation under air ambient”, *Nanoscale Research Letters*, vol. 7, no. 1, pp. 1-3, 2012.

[69]. H. I. Abdulgafour, Z. Hassan, F. K. Yam, K. AL-Heuseen, and Y. Yusof, “Enhancing photoresponse time of low cost Pd/ZnO nanorods prepared by thermal evaporation techniques for UV detection”, *Applied Surface Science,* vol. 258, no. 1, pp. 461-465, 2011.

[70]. T. Nguyen, N. T. Tuan, V. D. Nguyen, N. D. Cuong, N. D. T. Kien, P..T. Huy, V. H. Nguyen, and D. H. Nguyen, “Near-infrared emission from ZnO nanorods grown by thermal evaporation”, *Journal of Luminescence*, vol. 156, pp. 199-204, 2014.

[71]. L. Feng, A. Liu, M. Liu, Y. Ma, J. Wei, and B. Man, “Synthesis, characterization and optical properties of flower-like ZnO nanorods by non-catalytic thermal evaporation”, *Journal of Alloys and Compounds*, vol. 492, no. 1–2, pp. 427-432, 2010.

[72]. A. Zaier, A. Meftah, A. Y. Jaber, A. A. Abdelaziz, and M. S. Aida, “Annealing effects on the structural, electrical and optical properties of ZnO thin films prepared by thermal evaporation technique”, *Journal of King Saud University - Science*, vol. 27, no. 4, pp. 356-360, 2015.

[73]. S. Singh and P. Chakrabarti, “Optical characterization of ZnO thin films grown by thermal oxidation of metallic zinc”, *Advanced Science, Engineering and Medicine*, vol. 5, no. 7, pp. 677-682, 2013.

[74]. N. F. Ahmad, K. Yasui, A. M. Hashim,” Seed/catalyst-free growth of zinc oxide on graphene by thermal evaporation: effects of substrate inclination angles and graphene thicknesses” *Nanoscale Research Letters* , vol. 10, no. 10, pp. 1-9, 2015.

[75]. C. Periasamy and P. Chakrabarti, “Time-dependent degradation of Pt/ZnO nanoneedle rectifying contact based piezoelectric nanogenerator”, *Journal of Applied Physics*, vol. 109, pp. 054306, 2011.

[76]. J. Wang, S. Li, Y. Zhang, “A sensitive DNA biosensor fabricated from gold nanoparticles, carbon nanotubes, and zinc oxide nanowires on a glassy carbon electrode”, *Electrochimica Acta*, vol. 55, pp. 4436–4440, 2010.

[77]. Y. Lei, X. Yan, N. Luo, Y. Song, and Y. Zhang, “ZnO nanotetrapod network as the adsorption layer for the improvement of glucose detection via multiterminal electron-exchange”, Colloids *Surf. A: Physicochem. Eng. Aspects*, vol. 361, pp. 169-173, 2010.

[78]. M. Ahmad, C. Pan, J. Iqbal, L. Gan, and J. Zhu, “Bulk synthesis route of the oriented arrays of tip-shape ZnO nanowires and an investigation of their sensing capabilities”, *Chemical Physics Letters*, vol. 480, pp. 105–109, 2009.

[79]. J. S. Jeong and J. Y. Lee, “Investigation of initial growth of ZnO nanowires and their growth mechanism”, *Nanotechnology*, vol. 21, pp. 475603-5, 2010.

[80]. T. J. Hsueh, C. L. Hsu, “Fabrication of gas sensing devices with ZnO nanostructure by the low-temperature oxidation of zinc particles”, *Sensors and Actuators B*, vol. 131, pp. 572–576, 2008.

[81]. L. Chen, B. Gu, G. Zhu, Y. Wu, S. Liu, C. Xu, “Electron transfer properties and electrocatalytic behavior of tyrosinase on ZnO nanorod”, *Journal of Electroanalytical Chemistry* , vol. 617, pp. 7-13, 2008.

[82]. P. I. Reyes, C. Ku, Z. Duan, Y. Lu, A. Solanki, and K. Lee, “ZnO thin film transistor immunosensor with high sensitivity and selectivity”, *Applied Physics Letters*, vol. 98 , pp. 173702-3, 2011

[83]. Y. Wang, L. Yu, Z. Zhu, J. Zhang, J. Zhu, C. Fan, “Improved enzyme immobilization for enhanced bioelectrocatalytic activity of glucose sensor”, *Sensors and Actuators B*, vol. 136, pp. 332–337, 2009.

[84]. Y. T. Wang, L. Yu, J. Wang, L. Lou, W. J. Du, Z. Q. Zhu, H. Peng, J. Z. Zhu, “A novel L-lactate sensor based on enzyme electrode modified with ZnO nanoparticles and multiwall carbon nanotubes”, *Journal of Electroanalytical Chemistry*, vol. 661, pp. 8–12, 2011.

[85]. Z. Zhang, N. W. Emanetoglu, G. Saraf, Y. Chen, P. Wu, J. Zhong, Y. Lu, J . Chen, O. Mirochnitchenko, M. Inouye”, *IEEE Trans Ultrason Ferroelectr Freq Control.* , vol. 53, no. 4, pp. 786-92, 2006.

[86]. O. Taratula, E. Galoppini, R. Mendelsohn, P.I. Reyes, Z. Zhang, Z. Duan, J. Zhong, and Y. Lu, "Stepwise Functionalization of ZnO Nanotips with DNA" *Langmuir,* vol. 25, pp. 2107 -2113, 2009.

[87]. P. I. Reyes, Z. Zheng, C. Hanhong, D. Ziqing, Z. Jian, G. Saraf, L. Yicheng, O. Taratula, E. Galoppini, and N.N. Boustany, "A ZnO nanostructure-based quartz crystal microbalance device for biochemical sensing", *Sens. J. IEEE,* vol. 9, pp. 1302-1307, 2009.

[88]. H. Cheng, J. Cheng, Y. Zhang, Q. M. Wang, "Large-scale fabrication of ZnO micro-and nano-structures by microwave thermal evaporation deposition", *J. Cryst. Growth* , vol. 299, pp. 34-40, 2007.

[89]. S. Jit, A. Chatterjee, "Three Classes of FDEs Amenable to Approximation Using a Galerkin Technique", in Advances in Fractional Calculus, *Springer Netherlands*, 2007, pp. 3-14.

[90]. S. Saha and V. Gupta, "Influence of surface defects in ZnO thin films on its biosensing response characteristic", *J. Appl. Phys.*, vol. 110, pp. 064904, 2011.

[91]. O. Takai, M. Futsuhara, G. Shimizu, C.P. Lungu, J. Nozue, "Nanostructure of ZnO thin films prepared by reactive RF magnetron sputtering", *Thin Solid Films,* vol. 318, pp. 117–119, 1998.

[92]. S. Venkatachalam, Y. Kanno, "Preparation and characterization of nano and microcrystalline ZnO thin films by PLD", *Curr. Appl. Phys.* , vol. 9, pp. 1232-1236, 2009.

[93]. X. Wang , C. J. Summers , and Z. L. Wang , "Large-scale hexagonal-patterned growth of aligned ZnO nanorods for nano-optoelectronics and nanosensor arrays", *Nano Letters*, vol. 4, no. 3, pp. 423–426, 2004.

[94]. J. X. Wang, X. W. Sun, A. Wei, Y. Lei, X. P. Cai, C. M. Li, and Z. L. Dong," Zinc oxide nanocomb biosensor for glucose detection", *Appl. Phys. Lett.*, vol. 88, pp. 233106, 2006.

[95]. S. S. Lina, I. C. Chenb, J. Yangc, T. J. Hsuehd, C. L. Hsue, H. E. Leea and T. Y. Shieh, "A study on one-step immobilization of horse immunoglobulin with vertically grown ZnO nanorods substrates", *J. Electrochem. Soc.*, vol. 158, no. 4, pp. 107-111, 2011.

[96]. Q. Wan, K. Yu, T. H. Wang, and C. L. Lin, "Low-field electron emission from tetrapod-like ZnO nanostructures synthesized by rapid evaporation", *Appl. Phys. Lett.*, vol. 83, pp. 2253, 2003.

[97]. S. H. Huang, Z. Chen, X.C. Shen, Z. Q. Zhu, K. Yu, “Raman scattering of single tetrapod-like ZnO nanostructure synthesized by catalyst-free rapid evaporation”, *Solid State Communications*, vol. 145, pp. 418–422, 2008.

[98]. J. Weber, S. Jeedigunta, A. Kumar, "Fabrication and characterization of ZnO nanowire arrays with an investigation into electrochemical sensing capabilities", *Journal of Nanomaterials*, vol. 2008, pp. 1-5, 2008.

[99]. S. G. Cho, D. Uk Lee, S. W. Pak, T. Nahm, E. K. Kim, “Fabrication of a n-ZnO/p-Si heterojunction diode by ultra-high vacuum magnetron sputtering”, *Thin Solid Films*, vol. 520, pp. 5997–6000, 2012.

[100]. S. Aksoy, and Y. Caglar, “Effect of ambient temperature on electrical properties of nanostructure n-ZnO/p-Si heterojunction diode”, *Superlattices and Microstructures*, vol. 51, pp. 613–625, 2012.

[101]. J. Y. Lee, Y. S. Choi, J. H. Kim, M. O. Park, and S. Im, “Optimizing n-ZnO/p-Si heterojunctions for photodiode applications”, *Thin Solid Films*, vol. 403 – 404, pp. 553–557, 2002.

[102]. H. Y. Kim, J. H. Kim, Y. J. Kim, K. H. Chae, C. N. Whang, J. H. Song, and S. Im, “Photoresponse of Si detector based on n-ZnO/p-Si and n-ZnO/n-Si structures ”, *Optical Materials*, vol. 17, pp. 141-144, 2001.

[103]. M. Soylun, and O. Savas, “Electrical and optical properties of ZnO/Si heterojunctions as a function of the Mg dopant content”, *Materials Science in Semiconductor Processing*, vol. 29 pp. 76–82, 2015.

[104]. Z. N. Urgessa, S. R. Dobson, K. Talla, D. M. Murape, A. Venter, and J. R. Botha, “Optical and electrical characteristics of ZnO/Si heterojunction”, *Physica B*, vol. 439, pp. 149–152, 2014.

[105]. Y. Zhang, J. Xu, B. Lin, Z. Fu, S. Zhong, C. Liu, Z. Zhang, “Fabrication and electrical characterization of nanocrystalline ZnO/Si heterojunctions”, *Applied Surface Science*, vol. 252, pp. 3449–3453, 2006.

[106]. W. Wang, C. Chen, G. Zhang, T. Wang, H. Wu, Y. Liu and C. Liu, “The function of a 60-nm-thick AlN buffer layer in n-ZnO/AlN/p-Si(111)”, *Nanoscale Research Letters*, vol. 10, pp. 1-7, 2015.

[107]. H. Lu,Y. Gu, Y. Zhang, X. Liu, P. Wang, Q. Sun, S. Ding, and D. W. Zhang, “Improved photoelectrical properties of n-ZnO/p-Si heterojunction by inserting an optimized thin Al_2O_3 buffer layer”, *Optics Express*, vol. 22, no. 18, pp. 22184-22189, 2014.

[108]. P. Hazra and S. Jit, “A p-silicon nanowire/n-ZnO thin film heterojunction diode prepared by thermal evaporation”, *Journal of Semiconductors*, vol. 35, no. 1, 2014.

[109]. R. Romero, M.C. Lopez, D. Leinen, F. Martin, J.R. Ramos-Barrado, “Electrical properties of the n-ZnO/c-Si heterojunction prepared by chemical spray pyrolysis”, *Materials Science and Engineering B,* vol. 110, pp. 87–93, 2004.

[110]. X. D. Chen, C. C. Ling, S. Fung, and C. D. Beling, “Current transport studies of ZnO/p-Si heterostructures grown by plasma immersion ion implantation and deposition”, *Applied Physics Letters*, vol. 88, pp. 132104, 2006.

[111]. W. Zhang, Q. Meng, B. Lin, and Z. Fu, “Influence of growth conditions on photovoltaic effect of ZnO/Si heterojunction”, Solar Energy Materials & Solar Cells, vol. 92, pp. 949– 952, 28.

[112]. N. H. Al-Hardan, A. Jalar, M. A. A. Hamidb, L. K. Keng, N. M. Ahmed, and R. Shamsudin,” A wide-band UV photodiode based on n-ZnO/p-Si heterojunctions”, *Sensors and Actuators A*, vol. 207, pp. 61– 66, 2014.

[113]. K. Keramatnejad, F. Khorramshahi, S. Khatami, and E. Asl-Soleimani, “Optimizing UV detection properties of n-ZnO nanowire/p-Si heterojunction photodetectors by using a porous substrate”, *Opt. Quant. Electron*, vol. 47, pp. 1739–1749, 2015.

[114]. J. D. Hwang, D. H. Wu, and S. B. Hwang,” Enhanced Ultraviolet Response of p-Si/SiO$_x$/i-ZnO/n-ZnO Photodetectors”, *IEEE Photonics Technology Letters,* vol. 26, no. 11, pp. 1081-1084, 2014.

[115]. T. C. Zhang, Y. Guo, Z. X. Mei, C. Z. Gu, and X. L. Du, “Visible-blind ultraviolet photodetector based on double heterojunction of n-ZnO/insulator-MgO/p-Si”, *Applied Physics Letters*, vol. 94, pp. 113508-3, 2009.

[116]. Z. Xu, H. Deng, Y. Li and Y. Li, “Photoconductive UV detectors based on ZnO films prepared by Sol-Gel method”, *Journal of Sol-Gel Science and Technology*, vol. 36, pp. 223–226, 2005.

[117]. A. Vasudevan, S. Jung, and T. Ji,” On the responsivity of UV detectors based on selectively grown ZnO nanorods”, *IEEE Sensors Journal*, vol. 12, no. 5, pp. 1317-1325, 2012.

[118]. L. Guoa, H. Zhang, D. Zhao, B. Li, Z. Zhang, M. Jiang, and D. Shen, “High responsivity ZnO nanowires based UV detector fabricated by the

dielectrophoresis method", *Sensors and Actuators B*, vol. 166-167, pp. 12-16, 2012.

[119]. D. Somvanshi and S. Jit, "Pd/ZnO nanoparticles based schottky ultraviolet photodiodes grown on Sn-Coated n-Si substrates by thermal evaporation method", *IEEE Journal of Selected Topics in Quantum Electronics*, vol. 20, no. 6, pp. 3803106-6, 2014.

[120]. S. Alkis, B. Tekcan, A. Nayfeh and A. K. Okyay, "UV/vis range photodetectors based on thin film ALD grown ZnO/Si heterojunction diodes", *J. Opt.*, vol. 15, pp. 105002-5, 2013.

[121]. Y. H. Ko, G. Nagaraju, and J. S. Yu, "Fabrication and optimization of vertically aligned ZnO nanorod array-based UV photodetectors via selective hydrothermal synthesis", *Nanoscale Research Letters*, vol. 10, pp. 1-7, 2015.

[122]. H. Zhang, A. V. Babichev, G. Jacopin, P. Lavenus, F. H. Julien, A. Yu. Egorov, J. Zhang, T. Pauport and M. Tchernycheva, "Characterization and modeling of a ZnO nanowire ultraviolet photodetector with graphene transparent contact", *Journal of Applied Physics*, vol.114, pp. 234505-9, 2013.

[123]. A. Baltakesmez, S. Tekmen, P. Koc¸ S. T. Uzemen, and K. Meral, "UV-visible detector and LED based n-ZnO/p-Si heterojunction formed by electrodeposition", *AIP Advances*, vol. 3, pp. 032125, 2013.

[124]. L. Chen and C. Pan, "P-ZnO/n-Si photodiodes prepared by ultrasonic spraying pyrolysis method", *The Open Crystallography Journal*, vol. 1, pp. 10-13, 2008.

[125]. S. Shichen, Y. Xiaodong and H. Candong, "Fabrication of ZnO nanowall-network ultraviolet photodetector on Si substrates", *Journal of Semiconductors*, vol. 32, no. 7, pp. 074008-3, 2011.

[126]. H. Zhu, C. X. Shan, B. Yao, B. H. Li, J. Y. Zhang, D. X. Zhao, D. Z. Shen, and X. W. Fan, "High spectrum selectivity ultraviolet photodetector fabricated from an n-ZnO/p-GaN heterojunction", *J. Phys. Chem. C*, vol. 112, pp. 20546–20548, 2008.

[127]. K. Wang and Y. Vygranenko, "ZnO-based p-i-n and n-i-p heterostructure ultraviolet sensors: A comparative study", *J. Appl. Phys.*, vol. 101, pp. 114508, 2007.

[128]. L. A. Kosyachenko, G. V. Lashkarev, V. M. Sklyarchuk, A. I. Levtushenko, O. F. Sklyarchuk, V. I. Lazorenko, and A. Ulyashin, "ZnO-based photodetector

with internal photocurrent gain", *Phys. Status Solidi A*, vol. 207, no. 8, pp. 1972-1977, 2010.

[129]. Y. I. Alivov, U. Ozgur, S. Dogan, D. Johnstone, V. Avrutin, N. Onojima, C. Liu, J. Xie, Q. Fan, H. Morkoç, " Photoresponse of n-ZnO/p-SiC heterojunction diodes grown by plasma-assisted molecular-beam epitaxy", *Appl. Phys. Lett.*, vol. 86, pp. 241108, 2005.

[130]. C. H. Park, I. S. Jeong, J. H. Kim, S. Im, "Spectral responsivity and quantum efficiency of n-ZnO/p-Si photodiode fully isolated by ion-beam treatment", *Appl. Phys. Lett.*, vol. 82, pp. 3973-3975, 2003.

[131]. S. Mridha, and D. Basak, "Ultraviolet and visible photoresponse properties of n-ZnO/p-Si heterojunction", *J. Appl. Phys.*, vol. 101, pp. 083102, 2007.

[132]. C. P. Chen, P. H. Lin, L. Y. Chen, M. Y. Ke, Y. W. Cheng, J. J. Huang, "Nanoparticle-coated n-ZnO/p-Si photodiodes with improved photoresponsivities and acceptance angles for potential solar cell applications", *Nanotechnology,* vol. 20, pp. 245204, 2009.

[133]. B. Gupta, A. Jain, and R. M. Mehra, "Development and characterization of Sol-gel derived Al doped ZnO/p-Si Photodiode", *J. Mater. Sci. Technol.*, vol. 26, pp. 223-227, 2010.

[134]. L. C. Chen, and C.N. Pan, "Photoresponsivity enhancementof ZnO/Si photodiodes through use of an ultrathin oxide interlayer", *Eur. Phys. J. Appl. Phys.*, vol. 44, pp. 43-46, 2008.

[135]. T. C. Zhang, Y. Guo, Z. X.Mei, C. Z. Gu, and X. L. Du, "Visible-blind ultraviolet Photodetector based on double heterojunction of n-ZnO/insulator-MgO/p-Si", *Appl. Phys. Lett.*, vol. 94, pp. 113508, 2009.

[136]. I. S. Jeong, J. H. Kim, and S. Lm, "Ultraviolet-enhanced photodiode employing n-ZnO/p-Si structure" *Appl. Phys. Lett.*, vol. 83, pp. 2946-2948,2003.

[137]. I. S. Jeong, J. H. Kim, H. H. Park, and S. Im, " n-ZnO/p-Si UV photodetectors employing AlO_x films for antireflection", *Thin Solid Films*, vol. 447-448, pp. 111-114,2004.

[138]. Y. S. Choi, J. Y. Lee, S. Im, and S. J. Lee, " Dynamic and static photo-responses of n-ZnO/p-Si photodiodes.", *J. Appl. Phys.* , vol. 44, pp. 1560-1562, 2003.

[139]. Y. S. Choi, J. Y. Lee, S. Im, S. J. Lee, “Photoresponse characteristics of n-ZnO/p-Si heterojunction photodiodes” *J. Vac. Sci. Technol. B* , vol. 20, pp. 2384-2387, 2002.

[140]. M. Birkholz, “Principles of X-ray diffraction”, in thin film analysis by X-Ray scattering, *Wiley*, NJ, 2006.

[141]. S. K. Singh, P. Hazra, S. Tripathi, and P. Chakrabarti, “Fabrication and experimental characterization of a sol–gel derived nanostructured n-ZnO/p-Si heterojunction diode”, *J Mater Sci: Mater Electron*, vol. 26, pp. 7829–7836, 2015.

[142]. J. Goldstein, D. E. Newbury, P. Echlin, D. C. Joy, A. D. Romig Jr., C. E. Lyman, C. Fiori, E. Lifshin, “scanning eectron microscopy and X-Ray microanalysis: A text for biologists, materials scientists, and geologists”, *Plenum,* New York, 1992.

[143]. N. Jalili, and K. Laxminarayana, “A review of atomic force microscopy imaging systems: application to molecular metrology and biological sciences”, *Mechatronics*, vol. 14, no. 8, pp. 907–945, 2004.

[144]. D. B. Williams, and C. Barry Carter,” Transmission Electron Microscopy: A Textbook for Materials Science”, *Springer*, US, 2009.

[145]. P. Vandenabeele, “Practical Raman Spectroscopy: An Introduction”, *Wiley*, NJ, 2013.

[146]. H. A. Wahab, A. A. Salama, A. A. El-Saeid, O. Nur, M. Willander, and I.K. Battisha, “Optical, structural and morphological studies of (ZnO) nano-rod thin films for biosensor applications using sol gel technique”, *Results in Physics,* vol. 3, pp. 46–51, 2013.

[147]. S. Kim, G. Nam, H. Yoon, H. Park, H. Choi, J. S. Kim, J. S. Kim, D. Y. Kim, S. Kim, and J. Leem,” Structural, optical, and electrical properties of ZnO thin films deposited by sol-gel dip-coating process at low temperature”, *Electron. Mater. Lett.*, vol. 10, no. 4, pp. 869-878, 2014.

[148]. P. B. Taunk, R. Das, D. P. Bisen, R. K. Tamrakar, and N. Rathor,” Synthesis and optical properties of chemical bath deposited ZnO thin film”, *Karbala International Journal of Modern Science*, vol. 1, no. 3, pp. 159–165, 2015.

[149]. M. Yilmaz , Z. Caldiran, A. R. Deniz, S. Aydogan , R. Gunturkun, and A. Turut, “Preparation and characterization of sol–gel-derived n-ZnO thin film for

schottky diode application", *Applied Physics A*, vol. 119, no. 2, pp. 547-552, 2015.

[150]. P. Hazra and S. Jit, "A p-silicon nanowire/n-ZnO thin film heterojunction diode prepared by thermal evaporation", *Journal of Semiconductors*, vol. 35, no. 1, pp. 014001-5, 2014.

[151]. S. Chirakkara, and S. B. Krupanidhi, "Study of n-ZnO/p-Si (100) thin film heterojunctions by pulsed laser deposition without buffer layer", *Thin Solid Films*, vol. 520, pp. 5894-5899, 2012.

[152]. S. Majumdar and P. Banerji, "Temperature dependent electrical transport in p-ZnO/n-Si heterojunction formed by pulsed laser deposition", *Journal of Applied Physics*, vol. 105, pp. 043704-4, Feb. 2009.

[153]. R. Hradaynath," Materials for Opto-Electronics", *IETE Technical Review*, vol. 2, pp. 123-137, 1985.

[154]. M. M. Mandhare, S. A. Gangal and R. N. Karekar, "Effect of thick film and bulk ZnO overlays on Ag thick film microstrip rejection filter", *IETE Technical Review* , vol. 6, pp. 490-491, 1989.

[155]. T. J. Bukowski, K. McCarthy, F. McCarthy, G. Teowee, T. P. Alexander, D. R. Uhlmann, J. T. Dawley and B. J. J. Zelinski, "Piezoelectric properties of sol-gel derived ZnO thin films", *Integrated Ferroelectrics*, vol. 17, pp. 339-347, Aug. 1997.

[156]. H. Ohta, K. Kawamura, M. Orita, M. Hirano, N. Sarukura and H. Hosono, "Current injection emission from a transparent p–n junction composed of p-$SrCu_2O_2$/n-ZnO", *Appl. Phys. Lett.* , vol.77, pp. 475-477, 2000.

[157]. Y. I. Alivov, J. E. Van Nostrand, D. C. Look, M. V. Chukichev and B. M. Ataev, "Observation of 430 nm electroluminescence from ZnO/GaN heterojunction light-emitting diodes", *Appl. Phys. Lett.*, vol. 83, pp. 2943-2945, 2003.

[158]. B. L. Sharma and R. K. Purohit, Semiconductor Heterojunctions, *Pergamon Press*, New York 1974.

[159]. ATLAS User's manual Version 5.10.0.R, SILVACO International, Santa Clara, CA 95054 2005.

[160]. C. Periasamy, and P. Chakrabarti, "Effect of temperature on the electrical characteristics of nanostructured n-ZnO/p-Si heterojunction diode", *Science of Advanced Materials*, vol. 5, pp. 1384-1391, Oct. 2013

[161]. A.D.D. Dwivedi, A. Mittal, A. Agrawal and P. Chakrabarti," Analytical modeling and ATLAS simulation of N+-InP/n0-In0.53Ga0.47As/p+-In0.53Ga0.47 as p-i-n photodetector for optical fiber communication", *Infrared Physics & Technology*, vol. 53, pp. 236–245, 2010.

[162]. R. K. Lal and P. Chakrabarti," An analytical model of P^+-InAsSbP/n^{0-}InAs/n^+-InAs single heterojunction photodetector for 2.4–3.5μm region", *Optical and Quantum Electronics*, vol. 36, pp. 935–947, 2004.

[163]. P. Chakrabarti, A. Krier, and A. F. Morgan," Analysis and simulation of a mid-infrared P^+-$InAs_{0.55}Sb_{0.15}P_{0.30}$/$n^0$-$InAs_{0.89}Sb_{0.11}$/$N^+$-$InAs_{0.55}Sb_{0.15}P_{0.30}$ double heterojunction photodetector grown by LPE", *IEEE Transactions on Electron Devices*, vol.50, pp. 2049-2058, 2003.

[164]. "ZnO based LED: A Performance Optimization through TCAD Simulation," *Simulation Standard*, vol. 22, pp. 7-10, 2012.

[165]. L. J. Mandalapu, Z. Yang, S. Chu, and J. L. Liu, "Ultraviolet emission from Sb-doped p-type ZnO based heterojunction light-emitting diodes" *Applied Physics Letters*, vol. 92, pp. 122101-3, 2008.

[166]. V. Kabra, L. Aamir and M. M. Malik," Low cost, p-ZnO/n-Si, rectifying, nano heterojunction diode: fabrication and electrical characterization", *Beilstein J. Nanotechnol.* vol.5, pp. 2216–2221, 2014,

[167]. K. Liu , M. Sakurai and M.Aono," ZnO based ultraviolet photodetectors", *Sensors*, vol. 10, pp. 8604-8634, 2010.

[168]. S. Mridha and D. Basak," Ultraviolet and visible photoresponse properties of n-ZnO/p-Si heterojunction", *Journal of Applied Physics*, vol. 101, pp. 083102-5, 2007.

[169]. I. S. Jeong, J. H. Kim and S. Im," Ultraviolet-enhanced photodiode employing n-ZnO/p-Si structure", *Applied Physics Letters*, vol.83, pp. 2946-2948, 2003.

[170]. M. S. P. Reddy, B. Kim, and J. Jang," Dual detection of ultraviolet and visible lights using a DNA-CTMA/GaN photodiode with electrically different polarity", *Optics Express*, vol. 22, pp. 908-915, 2014.

[171]. L. C. Chen ,"Si-based ZnO ultraviolet photodiodes", in Photodiodes - From Fundamentals to Applications, *InTech*, Croatia, European Union, 2012, pp. 195-213.

[172]. P. K. Saxena and P. Chakrabarti, “Computer modeling of MWIR single heterojunction photodetector based on mercury cadmium telluride,” *Infrared Physics & Technology,* vol. 52, pp. 196-203, 2009.

[173]. R. K. Lal, M. Jain, S. Gupta and P. Chakrabarti, An analytical model of a double-heterostructure mid-infrared photodetector, *Infrared Phys. Technol.* vol. 44, pp. 125-132, 2003.

[174]. A. D. D. Dwivedi,” Analytical modeling and numerical simulation of P^+-Hg $_{0.69}$Cd $_{0.31}$Te/ n-Hg $_{0.78}$Cd$_{0.22}$Te/ CdZnTe hetero junction photodetector for a long-wavelength infrared free space optical communication system”, *Journal of Applied Physics,* vol. 110, pp. 043101-10, 2011.

[175]. C. H. Park, I. S. Jeong, J. H. Kim, and Seongil Im,” Spectral responsivity and quantum efficiency of n-ZnO/p-Si photodiode fully isolated by ion-beam treatment”, *Applied Physics Letters,* vol. 82, pp. 3973-3975, 2003.

[176]. G. M. Ali and P. Chakrabarti, Performance of ZnO-based ultraviolet photodetectors under varying thermal treatment”, *IEEE Photonics Journal*, vol. 2, 784-793, 2010.

[177]. S. Mridha, M. Dutta and D. Basak, “Photoresponse of n-ZnO/p-Si heterojunction towards ultraviolet/visible lights: thickness dependent behaviour”, *J. Mater. Sci-Mater. El.*, vol. 20, pp. 376-379, 2009.

[178]. R. Ghosh and D. Basak,” Electrical and ultraviolet photoresponse properties of quasialigned ZnO nanowires/p-Si heterojunction”, *Applied Physics Letters,* vol.90, no.24, pp. 243106-3, 2007.

[179]. J. L. Deschanvres, P. Rey, G. Delabouglise, M. Labeau, J.C. Joubert,” Characterization of piezoelectric properties of zinc oxide thin films deposited on silicon for sensors applications”, *Sensors and Actuators A: Physical*, vol. 33, no. 1–2, pp. 43–45, 1992.

[180]. R. Singh, M. Kumar, S. Chandra,” Growth and characterization of high resistivity c-axis oriented ZnO films on different substrates by RF magnetron sputtering for MEMS applications”, *Journal of Materials Science*, vol. 42, no. 12, pp. 4675-4683, 2007.

[181]. X. Wei, R. Zhao, M. Shao, X. Xu and J. Huang, “Fabrication and properties of ZnO/GaN heterostructure nanocolumnar thin film on Si (111) substrate”, *Nanoscale Research Letters*, vol. 8, pp.112-7, 2013.

[182]. A. El-Shaer, A. Bakin, E. Schlenker, A.C. Mofor, G. Wagner, S.A. Reshanov and A. Waag, “Growth of wide band gap wurtzite ZnMgO layers on (0001) Al_2O_3 by radical-source molecular beam epitaxy”, *Superlattices and Microstructures*, vol. 42, pp. 129-133, 2007.

[183]. S. Sharma and C Periasamy, Superlattices and Microstructures 73, 12(2014).

[184]. L. Xu, X. Li, Y. Chen and F. Xu,” Structural and optical properties of ZnO thin films prepared by sol–gel method with different thickness”, *Applied Surface Science*, vol. 257, pp. 4031-4037, 2011.

[185]. R. Kumar, G. Kumar, and A. Umar , “Pulse laser deposited nanostructured ZnO thin films: A review” *J Nanosci Nanotechnol.*, vol. 14, pp. 1911-30, 2014.

[186]. J. B. Lee,” Physical properties of RF-sputtered ZnO thin films: effects of two-step deposition” *Journal of the Korean Physical Society*, vol. 50, pp. 1073-1078, 2007.

[187]. S. Sharma and C. Periasamy, Superlattices and Microstructures 73 (2014) 12-21.

[188]. A. Ashour, M. A. Kaid, N. Z. El-Sayed and A. A. Ibrahim,” Physical properties of ZnO thin films deposited by spray pyrolysis technique” *Applied Surface Science*, vol. 252, pp. 7844-7848, 2006.

[189]. S. Mridha and D. Basak, “Effect of thickness on the structural, electrical and optical properties of ZnO films”, *Materials Research Bulletin*, vol. 42, pp. 875-882, 2007.

[190]. S. S. Lin and J. L. Huang, “Effect of thickness on the structural and optical properties of ZnO films by RF magnetron sputtering”, *Surface & Coatings Technology*, vol. 185, pp. 222-227, 2004.

[191]. S. S. Shariffudin, M. Salina, and S. H. Herman, “Effect of film thickness on structural, electrical, and optical properties of Sol-Gel deposited layer-by-layer ZnO nanoparticles” *Transactions on Electrical and Electronic Materials*, vol. 13, 102-105, 2012.

[192]. O. Lupan, T. Pauporte , L. Chow, B. Viana, F. Pelle , L.K. Ono, B. Roldan Cuenya and H. Heinrich, “Effects of annealing on properties of ZnO thin films prepared by electrochemical deposition in chloride medium”, *Applied Surface Science* , vol. 256, pp. 1895-1907, 2010.

[193]. A. Umar, Y.B. Hahn, A. Al-Hajry and M. Abaker, “Low-temperature growth of aligned ZnO nanorods: effect of annealing gases on the structural and optical

properties" *Journal of Nanoscience and Nanotechnology*, vol. 14, pp. 4564-9, 2014.

[194]. C. Periasamy and P. Chakrabarti, "Effect of annealing on the characteristics of nanocrystalline ZnO thin films", *Science of Advanced Materials*, vol. 3, pp. 73-79, 2011.

[195]. J. Husna, M. M. Aliyu, M. A. Islam, P. Chelvanathan, N. Radhwa Hamzah, M. Sharafat Hossain, M.R. Karim and N. Amin, "Influence of annealing temperature on the properties of ZnO thin films grown by sputtering" *Energy Procedia*, vol. 25, pp. 55-61, 2012.

[196]. S. S. Lin and J. L. Huang, "Effect of thickness on the structural and optical properties of ZnO films by RF magnetron sputtering" *Surface & Coatings Technology*, vol. 185, pp. 222-227, 2004.

[197]. B. D. Cullity, and S. Rstock, Elements of X-Ray Diffraction, Prentice Hall, New Jersey, USA, 2001.

[198]. V. Bilgin, S. Kose, F. Atay, and I. Akyuz," The effect of substrate temperature on the structural and some physical properties of ultrasonically sprayed CdS films", *Mater. Chem. Phys.*, vol. 94, pp. 103–108, 2005.

[199]. R. S. Reddy, A. Sreedhar, A. Sivasankar Reddy and S. Uthanna, "Effect of film thickness on the structural morphological and optical properties of nanocrystalline ZnO films formed by RF magnetron sputtering", *Adv. Mat. Lett.*, vol. 3, pp. 239-245, 2012.

[200]. A. A. Mosquera, D. Horwat, A. Rashkovskiy, A. Kovalev, P. Miska, D. Wainstein, J. M. Albella and J. L. Endrino, "Exciton and core-level electron confinement effects in transparent ZnO thin films", *Scientific Reports*, vol. 3, pp. 1-6, 2013.

[201]. S. Aydogu, O. Sendil, and M. B. Coban, "The optical and structural properties of ZnO thin films deposited by the spray pyrolysis technique", *Chinese Journal of Physics*, vol. 50, no. 89-100, 2012.

[202]. J. Tauc, Amorphous and Liquid Semiconductors, *Plenum*, London, UK, 1974.

[203]. A. Jain, P. Sagar and R. M. Mehra, "Changes of structural, optical and electrical properties of sol-gel derived ZnO films with their thickness", *Materials Science – Poland*, vol. 25, pp. 233-242, 2007.

[204]. F. Urbach," The long-wavelength edge of photographic sensitivity and of the electronic Absorption of Solids", *Phys. Rev.*, vol. 92, pp. 1324, 1953.

[205]. A. S. Gadallah, and M. M. El-Nahass, "Structural, optical constants and photoluminescence of ZnO thin films grown by Sol-Gel spin coating", *Advances in Condensed Matter Physics*, vol. 2013, pp. 1-11, 2013.

[206]. M. Di Giulio, G. Miccci, R. Rella, P. Siciliano, and A. Tepore, "Optical absorption of tellurium suboxide thin films", *Physica Status Solidi A*, vol. 136, K101-K104, 1993.

[207]. T. S. Moss, G.J. Burrell, and B. Ellis, "Semiconductor Opto-Electronics", *Wiley*, New York, 1973.

[208]. M. S. Kim, K. G. Yim, J. Leem, S. Kim, G. Nam, D. Lee, J. S. Kim and J. S. Kim, "Effects of annealing temperature on the structural and the optical properties of ZnO thin films grown on porous silicon by using plasma-assisted molecular beam epitaxy", *Journal of the Korean Physical Society*, vol. 59, pp. 2354-2361, 2011.

[209]. J. M. Myoung, W. H. Yoon, D. H. Lee, I. Yun, S. H. Bae and S. Y. Lee, "Effects of thickness variation on properties of ZnO thin films grown by pulsed laser deposition", *Jpn. J. Appl. Phys.*, vol. 41, pp. 28-31, 2002.

[210]. T. Singh, T. Lehnen, T. Leuning, D. Sahu and S. Mathura, "Thickness dependence of optoelectronic properties in ALD grown ZnO thin films", *Applied Surface Science*, vol. 289, pp. 27-32, 2014.

[211]. S. W. Xue, X. T. Zu, W. L. Zhou, H. X. Deng, X. Xiang, L. Zhang and H. Deng, "Effects of post-thermal annealing on the optical constants of ZnO thin film", *Journal of Alloys and Compounds*, vol. 448, pp. 21-26, 2008.

[212]. J. Lim, K. Shin, H. W. Kim and C. Lee, "Effect of annealing on the photoluminescence characteristics of ZnO thin films grown on the sapphire substrate by atomic layer epitaxy", *Materials Science and Engineering B*, vol. 107, pp. 301-304, 2004.

[213]. S. Youssef, P. Combette, J. Podlecki, R. Al Asmar and A. Foucaran, "Structural and optical characterization of ZnO thin films deposited by reactive RF magnetron sputtering", *Cryst. Growth Des.*, vol. 9, no. 1088-1094, 2009.

[214]. J.Y. Lee, Y.S. Choi, J.H. Kim, M.O. Park, S. Im, "Optimizing n-ZnO/p-Si heterojunctions for photodiode applications", *Thin Solid Films*, vol. 403 – 404, pp. 553-557, 2002.

[215]. J. D. Lee, C.Y. Park, H.S. Kim, J.J. Lee and Y.G. Choo, "A study of conduction of ZnO film/p-Si heterojunction fabricated by photoinduced

electrodeposition under illumination", *J. Phys. D: Appl. Phys.*, vol. 43, pp. 365403, 2010.

[216]. H. Ohta, H. Mizoguchi, M. Hirano, S. Narushima, T. Kamiya, H. Hosono, "Fabrication and characterization of heteroepitaxial p-n junction diode composed of wide-gap oxide semiconductors p-$ZnRh_2O_4$/n-ZnO", *Appl. Phys. Lett.*, vol. 82, 823-825, 2003.

[217]. H. Ohta, M. Kamiya, T. Kamiya, M. Hirano, H. Hosono, "UV-detector based on pn-heterojunction diode composed of transparent oxide semiconductors, p-NiO/n-ZnO", *Thin Solid Films*, vol. 445, pp**.** 317-321, 2003.

[218]. R. S. Ajimsha, M. K. Jayaraj, and L. M. Kukreja, "Electrical characteristics of n-ZnO/p-Si heterojunction diodes grown by pulsed laser deposition at different oxygen pressures" *J. Electron. Mater.*, vol. 37, pp. 770-775, 2008.

[219]. C. Periasamy and P. Chakrabarti, "Large-area and nanoscale n-ZnO/p-Si heterojunction photodetectors", *J. Vac. Sci. Technol. B*, vol. 29, pp. 051206-6, 2011.

[220]. S. Al-Heniti, Ahmad Umar, R. I. Badran, H. M. Zaki, A. Al-Hajry, "N-ZnO based nanostructure/p-silicon substrate based efficient p-n heterojunction diode", *Sci. Adv. Mater.*, vol. 5, 301-307, 2013.

[221]. H. Asil, Kubra Cinar, Emre Gur, Cevdet Coskun, Sebahattin Tuzemen, "Temperature dependent current-voltage characteristics of electrodeposited p-ZnO/n-Si heterojunction" *Int. J. Phys. Sci.*, vol. 8, pp. 371-379, 2013.

[222]. D. E. Yıldız, S. Altındal , H. Kanbur, "Gaussian distribution of inhomogeneous barrier height in Al/SiO2/p-Si Schottky diodes", *J. Appl. Phys.*, vol. 103, 124502-7, 2008.

[223]. S. Aydogan, K.Cinar, H. Asil, C. Coskun, A. Turut , "Electrical characterization of Au/n-ZnO Schottky contacts on n-Si" *Journal of Alloys and Compounds*, vol. 476, pp. 913-918, 2009.

[224]. S. K. Cheung, N. W. Cheung, "Extraction of Schottky diode parameters from forward current-voltage characteristics", *Appl. Phys. Lett.*, vol. 49, pp. 85-87, 1986.

[225]. S. Altindal, S. Karadeniz, N. Tugluoglu, A. Tataroglu," The role of interface states and series resistance on the I-V and C-V characteristics in Al/SnO_2/p-Si Schottky diodes", *Solid State Electronics*, vol. 47, pp. 1847-1854, 2003.

[226]. J. H. Werner, “Schottky barrier and pn-junction I/V plots - Small signal evaluation”, *Appl. Phys. A*, vol. 47, 291-300, 1988.

[227]. D. Somvanshi, and S. Jit, “Mean barrier height and richardson constant for Pd/ZnO Thin film-based Schottky Diodes grown on n-Si substrates by thermal evaporation method”, *IEEE Electron Device Letters*, vol. 34, pp. 1238-1240, 2013.

[228]. S. Al-Heniti, R. I. Badran, A. A. Al-Ghamedi, and F. A. Al-Age,” Electrical properties of p-Si/n-ZnO nanowires heterojunction devices”, *Adv. Sci. Lett.*, vol. 4, pp. 24-28, 2011.

[229]. S. Al-Heniti, R. I. Badran, A. Umar, A. Al-Ghamdi, S. H. Kim, F. AlMarzouki, A. Al-Hajry, S. A. Al-Sayari, and T. Al-Harbi, “Temperature dependant structural and electrical properties of ZnO nanowire networks”, *J. Nanosci. Nanotechnol.*, vol. 12, pp. 68-74, 2012.

[230]. W. Monch, “Barrier heights of real Schottky contacts explained by metal-induced gap states and lateral inhomogeneities”, *J. Vac. Sci. Technol. B*, vol. 17, 1867-1876, 1999.

[231]. J. H. Werner, and H. H. Gijttler, “Barrier inhomogeneities at Schottky contacts” *J. Appl. Phys.*, vol. 69, pp. 1522-1533, 1991.

[232]. R. F. Schmitsdorf, T. U. Kampen, and W. Monch, “Explanation of the linear correlation between barrier heights and ideality factors of real metal-semiconductor contacts by laterally nonuniform Schottky barriers”, *J. Vac. Sci. Technol. B*, vol. 15, pp. 1221-1226, 1997.

[233]. R. T. Tung, “Electron transport at metal-semiconductor interfaces: General theory”, *Phys. Rev. B*, vol. 45, pp. 13509-13523, 1992.

[234]. E. Bacaksiz, G. C. Ankayab, I. Polata, S. Yılmaza, C. Duranc, and M. Altunbas, , “Structural and electrical characterization of ZnO-based homojunctions”, *J. Alloy Compd.*, vol. 496, pp. 560-565, 2010.

[235]. W. Mtangi, F. D. Auret, C. Nyamhere, P. J. J. Rensburg, M. Diale, and A. Chawanda,” Analysis of temperature dependent I^2V measurements on Pd/ZnO Schottkybarrier diodes and the determination of the Richardson constant” , *Physica B*, vol. 404, pp. 1092-1096, 2009.

[236]. J. D. Ye, S. L. Gu, S. M. Zhu, W. Liu, S. M. Liu, R. Zhang, Y. Shi and Y. D. Zheng, “Electroluminescent and transport mechanisms of n-ZnO/p-Si heterojunctions”, *Applied Physics Letters*, vol. 88, pp. 182112, 2006.

[237]. H. C. Chen, M. J. Chen, Y. H. Huang, W. C. Sun, W. C. Li, J. R. Yang, H. Kuan, and M. Shiojiri," White-light electroluminescence from n-ZnO/p-GaN heterojunction light-emitting diodes at reverse breakdown bias", *IEEE Transactions on Electron Devices*, vol. 58, no. 11, pp. 3970-3975, 2011.

[238]. N.F. Wang, Y.Z. Tsai, and F. H. Hsu, "Effect of surface texture on Al–Y codoped ZnO/n-Si heterojunction solar ce.lls", *IEEE Transactions on Electron Devices*, vol. 60, no. 12, pp. 4073-4078, 2013.

[239]. G.M. Ali and P. Chakrabarti," ZnO-based interdigitated MSM and MISIM ultraviolet photodetectors", *J. Phys. D: Appl. Phys.*, vol. 43, no. 41, pp. 415103-8, 2010.

[240]. X. Tang, G. Li, and S. Zhou, "Ultraviolet electroluminescence of light-emitting diodes based on single n-ZnO/p-AlGaN heterojunction nanowires", *Nano Lett.*, vol. 13, no. 11, pp. 5046-5050, 2013.

[241]. J.Y. Lee, Y.S. Choi, W.H. Choi, H.W. Yeom, Y.K. Yoon, J.H. Kim and S. Im, "Characterization of films and interfaces in n-ZnO/p-Si photodiodes", *Thin Solid Film*, vol. 420–421, pp. 112–116, 2002.

[242]. K. Haga, T. Suzuki, Y. Kashiwaba, H. Watanabe, B.P. Zhang, Y. Segawa, "High-quality ZnO films prepared on Si wafers by low-pressure MO-CVD", *Thin Solid Films*, vol. 433, no. 1–2, pp. 131-134, 2003.

[243]. F. Chaabouni, M. Abaab and B. Rezig, "Characterization of n-ZnO/p-Si films grown by magnetron sputtering", *Superlattices and Microstructures*, vol. 39, no. 1–4, pp. 171-178, 2006.

[244]. K. A. Alim, V.A. Fonoberov, M. Shamsa, and A. A. Balandin, "Micro-Raman investigation of optical phonons in ZnO nanocrystals", *Journal of Applied Physics*, vol. 97, pp. 124313-5, 2005.

[245]. S. Ranwa, P. Kumar Kulriya,V. Dixit, and M. Kumar, "Temperature dependent electrical transport studies of self-aligned ZnO nanorods/Si heterostructures deposited by sputtering", *Journal of Applied Physics*, vol. 115, pp. 233706-6, 2014.

[246]. A. B. Yadav, A. Pandey, D. Somvanshi, and S. Jit , "Sol-Gel-based highly sensitive Pd/n-ZnO thin film/n-Si schottky ultraviolet photodiodes", *IEEE Transactions on Electron Devices*, vol. 62, no. 6 , pp. 1879-1884, 2015.

[247]. D.H. Zhang, “Adsorption and photodesorption of oxygen on the surface and crystallite interfaces of sputtered ZnO films”, *Materials Chemistry and Physics*, vol. 45, no. 3, pp. 248-252, 1996.

[248]. S. Lany and A. Zunger, “Anion vacancies as a source of persistent photoconductivity in II-VI and chalcopyrite semiconductors”, *Phys. Rev. B*, vol. 72, pp. 035215, 2005.

[249]. I. Beinik, M. Kratzer, A. Wachauer, L. Wang, Y. P. Piryatinski, G. Brauer, X. Y. Chen, Y. F. Hsu, A. B. Djurišić and C. Teichert, “Photoresponse from single upright-standing ZnO nanorods explored by photoconductive AFM”, *Beilstein J. Nanotechnol.* , vol. 4, pp. 208–217, 2013.

[250]. U. Ozgur, Y. I. Alivov, C. Liu, A. Teke, M. A. Reshchikov, S. Dogan, V. Avrutin, S. J. Cho and H. Morkoc, “A comprehensive review of ZnO materials and devices,” *J. Appl. Phys.*, vol. 98, no. 4, pp. 041301, 2005.

[251]. Y.Jin, J.Wang, B.Sun, J.C.Blakesley, and N.C.Greenham, “Solution -processed ultraviolet photodetectors based on colloidal ZnO nanoparticles,” *Nano Lett.*, vol. 8, no. 6, pp. 1649–1653, 2008.

[252]. C. Soci, A. Zhang , B. Xiang , S. A. Dayeh , D. P. R. Aplin , J. Park , X. Y. Bao , Y. H. Lo , and D. Wang, “ZnO nanowire UV photodetectors with high internal gain,” *Nano Lett.*, vol. 7, no. 4, pp. 1003–1009, 2007.

[253]. Y. K. Su, S. M. Peng, L. W. Ji, C. Z. Wu, W. B. Cheng, and C. H. Liu, “Ultraviolet ZnO nanorod photosensors,” *Langmuir*, vol. 26, no. 1, pp. 603–606, 2010.

[254]. P. Hazra, S. K. Singh and S. Jit, “Ultraviolet photodetection properties of ZnO/Si heterojunction diodes fabricated by ALD technique without using a buffer layer”, *Journal of Semconductor Technology and Science,* vol. 14, no. 1, pp. 117-122, 2014.

[255]. G. M. Ali and P. Chakrabarti, “Fabrication and characterization of thin film ZnO Schottky contacts based UVphotodetectors: A comparative study,” *J. Vac. Sci. Technol. B*, vol. 30, no. 3, pp. 031206-7, 2012.

List of Publications

Journals

[1]. **Shashikant Sharma**, Bernhard C. Bayer, Viera Skakalova, Ghanshyam Singh and C. Periasamy, “Structural, Electrical and UV Detection Properties of ZnO/Si Heterojunction Diodes” ***IEEE Transaction on Electron Devices***, Vol. 63, no. 5, pp. 1949-1956, 2016. (SCI Indexed, Impact Factor: 2.47).

[2]. **Shashikant Sharma**, A. Sumathi and C. Periasamy, "Photodetection Properties of ZnO/Si Heterojunction Diode: A Simulation Study", ***IETE Technical Review (Taylor & Francis),*** vol. 33, no. 2, pp. 1-8, 2016. (SCI Indexed, Impact Factor: 1.30).

[3]. **Shashikant Sharma** and C Periasamy ,"A Study on the Electrical Characteristic of n-ZnO/p-Si Heterojunction Diode Prepared by Vacuum Coating Technique", ***Superlattices and Microstructures (Elsevier)***, Vol 73, pp. 12-21,201*4*. (SCI Indexed, Impact Factor: 2.09).

[4]. **Shashikant Sharma**, C. Periasamy and P. Chakrabarti ,"Thickness Dependent Study of RF Sputtered ZnO Thin Films for Optoelectronic Device Applications", ***Electronic Materials Letters (Springer),*** Vol. 11, No.6, pp. 1093-1101, 2015**.** (SCI Indexed, Impact Factor: 2.0).

[5]. **Shashikant Sharma**, Sumit Vyas, C. Periasamy and P. Chakrabarti ,"Structural and Optical Characterization of ZnO Thin Films for Optoelectronic Device Applications by RF Sputtering Technique" , ***Superlattices and Microstructures (Elsevier)**, Vol 75, pp. 378-389,2014.* (SCI Indexed, Impact Factor: 2.09).

[6]. **Shashikant Sharma**, Tarun Varma , K. Asokan , C. Periasamy, Dharmendar Boolchandani ,"Annealing Temperature Dependent Structural and Optical Properties of RF Sputtered ZnO Thin Films ", ***Journal of Nanoscience and Nanotechnology (ASP)***, 2016. (In Press, SCI Indexed, Impact Factor: 1.33)

[7]. **Shashikant Sharma** and C. Periasamy," Effect of Sputtering Power on Structural and Optical Properties of ZnO Thin Films Grown by RF

Sputtering Technique, ***Journal of Nanoelectronics & Optoelectronics (ASP)***, Vol.10, pp. 205-210, 2015. (SCI Indexed, Impact Factor: 0.67)

[8]. **Shashikant Sharma** and C. Periasamy, "Study of ZnO Thin Films Deposited at Different Argon Gas Flow Rates Using RF Sputtering", ***Advanced Science, Engineering and Medicine (ASP)***, Vol. 7, No. 10, pp. 855-858, 2015.

[9]. **Shashikant Sharma** and C. Periasamy," Simulation Study and Performance Analysis of n-ZnO/p-Si Heterojunction Photodetector", ***Journal of Electron Devices***, Vol. 19, pp. 1633-1636, 2014.

Brief CV

Shashi Kant Sharma
Ph.D. Scholar (VLSI Design)
Dept. of Electronics & Comm. Engg.
Malaviya National Institute of Technology
Jaipur, Rajasthan, India
Email – shashkant@gmail.com
Mobile No. - +91-9414780222

EDUCATION PROFILE:

Examination	Institute	University	Year	CGPA/%
Ph.D. (Doctor of Philosophy)	Malaviya National Institute of Technology (MNIT) , Jaipur, India	Institute of Ministry of HRD, Govt. of India	Pursuing	9.66
Post Graduation (M.Tech - VLSI Design)	Indian Institute of Information Technology & Management , Gwalior, India (An Autonomous Institute of Ministry of HRD, Govt. of India)	Institute of Ministry of HRD, Govt. of India	2012	8.21
Bachelor of Engineering (Electronics & Communication with HONS)	M.L.V. Govt. Textile and Engineering College, Bhilwara, Rajasthan, India (An autonomous college of Govt. of Rajasthan)	University of Rajasthan	2009	74.99
Senior Secondary	K.V. – 2, Jaipur	C.B.S.E.	2004	68.00
Secondary	N.K. Public Sr. Sec. School, Jaipur	Rajasthan Board	2002	84.17

TECHNICAL SKILLS :

Deposition Techniques	Thermal Vapor & E-Beam Deposition, RF Sputtering, Spin Coating
Characterization Techniques	XRD, AFM, SEM, TEM, Ellipometry, PL, UV-Visible, SPA
Design Tools	Silvaco ,TANNER, SPICE, Xilinx , Modelsim
Languages	VHDL, C, C++ , SystemC (Basic), Assembly language (8085, 8086).
Platforms	Linux, Windows

WORK EXPERIENCE:

- Worked as Assistant Professor from May, 2012 to December, 2012 in Department of Electronics & Communication Engineering, IMS Engineering College, Ghaziabad, India.
- Worked as Visiting Scholar at University of Vienna, Austria with Dr. Viera Skakalova and Dr. Bernhard C. Bayer, Faculty of Physics, University of Vienna, Austria in June, 2016.

RESEARCH & CONSULTANCY PROJECTS:

- "Design and Development of Nanostructured ZnO Film Based Piezoelectric Devices for Energy Harvesting Applications" Sponsored By Department of Science and Technology (Indo-Austrian (DST-BMWF) Joint Research Program), No. INT/AUA/BMWF/P-24/2015. Duration: 2 Years (May-2015 to May-2017).

ACADEMIC PROJECTS/RESEARCH WORK:

Ph.D. Work **(Supervisors: Dr. C. Periasamy)** **Jan’13-Present**

PhD. Topic: “Investigations on Nanocrystalline ZnO Thin Film Based Heterojunctions for Electronic and Photonic Device Applications”

M.Tech Thesis **May’11-May’12**

M.Tech. Dissertation Topic: “Leakage Current and Ground bounce Noise Aware MTCMOS Techniques.”

B.Tech Projects **June’08-June’09**

- Automatic Communication system using ARM7TDMI-S Processor.
- Multitouch display design and applications using D.S.P. and IMAGE PROCESSING.
- An RTOS based project using ARM7TDMI-S Processor (LPC2106/2103 Board).

PUBLICATION SUMMARY

Total Publications : 17					
Journals		**International/National Conferences**	**Book**	**Others Details**	
SCI Indexed	08	04	01	**Total Impact Points:**	12.35
				H-Index:	04
Other	04			**Citations:**	64

CONFERENCES/WORKSHOPS/INTERNS/SHORT TERM COURSES ATTENDED:

Short Term Courses/ Workshops	**National/International Conferences**	**Interns**
05	04	02

PERSONAL INFORMATION

Gender :	Male
Date of Birth:	20th August 1987
Language known:	English, Hindi, Marwari
Permanent Address:	Gha-85, Bhawani Nagar, Murlipura, Sikar Road Jaipur, Rajasthan, India, Pin - 302023.

I hereby declared that the information given above is true to the best of my knowledge.

Date **Shashi Kant Sharma**